The Thesis committee for Emily Allen McDowell
Certifies that this is the approved version of the following thesis:

An Evaluation of Quartz-Inclusion Barometry by Laser Raman Microspectrometry: A Case Study from the Llano Uplift of Central Texas

APPROVED BY
SUPERVISING COMMITTEE:

Supervisor: ______________________
William D. Carlson

____
Sharon Mosher

____
Richard A. Ketcham

An Evaluation of Quartz-Inclusion Barometry by Laser Raman Microspectrometry: A Case Study from the Llano Uplift of Central Texas

by

Emily Allen McDowell, B.S.

Thesis

Presented to the Faculty of the Graduate School
of the University of Texas at Austin
in Partial Fulfillment
of the Requirements
for the Degree of

Master of Science in Geological Sciences

The University of Texas at Austin
August 2010

ACKNOWLEDGEMENTS

The completion of this study would not have been possible without the help and support of many during my time at the Jackson School of Geosciences.

The biggest thank you goes to Dr. Bill Carlson, my advisor, for teaching me so much about so many topics: metamorphism, Llano Uplift, diffusion, etc. The best lesson was not the end result, but the process of getting there. It's amazing that it actually happened!

Thank you to Drs. Sharon Mosher and Rich Ketcham for serving on my committee. Your comments and insights into this study were much appreciated.

Thank you to the Center for Electrochemistry, Dr. Alan Campion and Jaclyn Wiggins-Camacho for all of your assistance during the course of my study.

Thank you to the Garnet Club! From day one, I knew it would not be the same without you all. I could go on and on about our three years together but to keep this thesis under 210 pages, I will practice my new skills in brevity: Thanks to Eric Kelly a.k.a. Bosley for your friendship, mentoring and advice. To Stephanie Moore and Elizabeth Hatley: among other things, it was so great to be Carlson's Angels with y'all! Thanks also to all the other garnet club members: Martin Robyr, Ed Lane, Wes Crawford, Josh Garber, Steven Arauza, Casey Corbin, and Ted Cross. I learned something from all of you, especially on Friday afternoons.

An Evaluation of Quartz-Inclusion Barometry by Laser Raman Microspectrometry: A Case Study from the Llano Uplift of Central Texas

by

Emily Allen McDowell, M.S. Geo. Sci.
The University of Texas at Austin, 2010
SUPERVISOR: William D. Carlson

A new barometric technique measuring stored stress in quartz inclusions via laser Raman microspectrometry was employed in an attempt to elucidate the extent of high-pressure (HP) metamorphism in the Llano Uplift of central Texas. Rare lithologies within the Llano Uplift contain mineralogical evidence of HP metamorphism (pressures from 1.4 to 2.4 GPa at temperatures from 650 to 775°C), but much of the uplift is composed of felsic gneisses lacking any HP signature; these felsic gneisses may never have transformed to HP assemblages, or they may have been thoroughly overprinted by later low-pressure events. Barometry via laser Raman microspectrometry computes entrapment pressure for a quartz inclusion in garnet from measurement of the displacements of its Raman peak positions from those of a quartz standard at atmospheric pressure. Quartz inclusions in garnets that grew in felsic gneisses under HP conditions should retain HP signatures, despite later overprinting. Application of the Raman microspectrometry technique should therefore allow barometry of previously uncharacterizable rocks.

For two localities in the Llano Uplift, entrapment pressures from Raman barometry (0.6-0.7 GPa and 0.2-0.3 GPa) were substantially lower than pressures expected based on conventional barometers (1.4 GPa and 1.6-2.4 GPa). This absence of any HP signatures in the Llano rocks contrasts with more successful applications of the Raman technique by previous workers in high P/T blueschist-facies rocks. A key difference in the Llano rocks is that they reached peak temperatures at which intracrystalline diffusion in garnet, driven by compositional gradients produced during growth, had noticeable effects: complete homogenization of growth zoning had occurred in the locality that produced the greatest discrepancies between Raman and conventional pressures, and modest relaxation of zoning occurred in the locality with the smaller discrepancies. The failure of the Raman technique to recover pressures consistent with conventional barometry in the Llano Uplift is therefore attributed to relaxation of stress on the quartz inclusions as the result of intracrystalline diffusion within the garnet. This conclusion suggests that use of the Raman barometric technique must be restricted to rocks whose time-temperature histories produce only very limited intracrystalline diffusion in garnet, typically those rocks whose peak metamorphic temperatures fall at or below upper amphibolite-facies conditions.

TABLE OF CONTENTS

LIST OF FIGURES

LIST OF TABLES

INTRODUCTION

An active pursuit within the metamorphic and tectonic research communities is the search for evidence of continental-margin subduction to great depths, in the form of orogens recording high-pressure (HP) and ultrahigh-pressure (UHP) metamorphic conditions (HP = 1.0-2.5 GPa; UHP >2.5 GPa; Ernst and Liou, 2008). Most recognized UHP terranes are thin slabs of intensely deformed crust in which mineral assemblages that can be unambiguously recognized as forming at UHP conditions are rare, or are largely restricted to particular lithologies, such as mafic boudins within quartzofeldspathic gneisses (Ernst, 2001). The rarity of (U)HP assemblages is commonly attributed either to subsequent overprinting by lower-pressure assemblages (Ernst, 2001), or to failure of some lithologies to transform to (U)HP assemblages during subduction (Peterman et al., 2009). The first alternative implies that most or all of the crust underwent densification (conversion to high-pressure assemblages) during subduction; the second alternative implies that much of the crust did not convert to higher-density assemblages. Because crustal densification greatly reduces the buoyancy forces available to drive gravitational uplift of subducted continental materials, differentiating between these alternatives is vital to understanding the processes responsible for return of (U)HP terranes to the surface in the course of subduction-to-collision orogenesis.

The scarcity of mineralogic evidence for or against substantial densification of subducted crust has led to the development of unconventional techniques to determine pressure conditions during subduction and exhumation. This study seeks to address the densification question via a new barometric technique whose results may elucidate pressure conditions during garnet growth.

Crustal Densification

A traditional model for continental collision at subduction zones presumes that low-density materials making up the continental margin and attached to a downgoing high-density oceanic slab are recrystallized during subduction to assemblages of denser minerals. Then, during exhumation, the bulk of the continental material retrogresses back to lower-pressure, lower-density mineral assemblages (Ernst, 2001). This model is based on the fact that most recognized UHP terranes are composed primarily of quartzofeldspathic gneisses (Ernst, 2001). Evidence for (U)HP metamorphic conditions within the gneisses is usually restricted to either: (1) a limited volume percent of high-density rock types that bear mineralogical evidence of having formed at great pressures, such as mafic eclogites or garnet peridotites; or (2) mineral inclusions in garnet or zircon that are known to be stable only at UHP conditions, such as coesite or diamond. Ernst (2001) suggests that in most lithologies, the assemblages stable at UHP conditions back-reacted during exhumation.

Recent research into the densification process has led to a different scenario, in which only portions of the subducted crust are actually transformed to higher-density assemblages. Peterman et al. (2009) investigated the P-T history of assemblage transformations during a subduction event that formed the Western Gneiss Region of Norway. The study linked Sm-Nd geochronology that dated garnet growth in quartzofeldspathic gneisses to models of compositional zoning patterns that constrained the P-T history during garnet growth. They found that the majority of the Western Gneiss Region quartzofeldspathic gneiss was subducted and exhumed without ever transforming into higher-density eclogite-facies minerals.

A Test Case: Applying a New Barometric Technique in the Llano Uplift

The Llano Uplift of central Texas is an excellent candidate for exploring the issue of densification. During Grenville-aged orogenesis, the region experienced subduction followed by continent-continent collision. Resulting metamorphism can be broken down into three main phases (Carlson et al., 2007). *P-T* conditions during the earliest phase, a high-pressure event, have been estimated from mineral assemblages in mafic eclogites; across the various eclogite bodies in the uplift, peak conditions range from ~1.4 GPa at ~650 °C to ~2.4 GPa at ~775 °C. Two later phases of metamorphism produced ubiquitous overprinting by Barrovian assemblages at ~0.7 GPa and ~700 °C, and largely static recrystallization at ~0.3 GPa and ~575 °C.

Eclogite bodies are found as partially retrogressed boudins encased by felsic gneisses. Much of the omphacitic pyroxene in the eclogite assemblage has retrogressed to symplectites of sodian augite + oligoclase, or in more advanced stages, to amphibole and plagioclase (Carlson et al., 2007). Because the felsic gneisses lack any HP minerals, possibly due to the intense overprint that also affected eclogites, conventional barometric methods cannot be used to estimate pressure conditions during metamorphism. Carlson and Schwarze (1997) suggest that the similarity of garnet zoning profiles in both felsic gneisses and eclogites from the western part of the uplift indicate that felsic gneisses did transform, but that all of them retrogressed. A barometric technique that does not rely on mineral assemblages is therefore required to further elucidate the pressure history of the quartzofeldspathic gneisses.

A new method developed by Enami et al. (2007) uses laser Raman microspectrometry to measure pressures retained in quartz inclusions within garnet. An elastic model relates the measured quartz-inclusion pressure to the pressure at the depth at which the quartz inclusion was trapped. The usefulness of the Raman method is that it allows pressure estimates to be made for rocks lacking HP assemblages but containing garnets with quartz inclusions.

The initial goal for this study was to test the accuracy of the Raman barometric technique by comparing pressure values for eclogitic garnets obtained from conventional thermobarometry on mineral assemblages to those obtained from Raman inclusion barometry. After verification of the technique, the next intended goal was to use the method on other, non-eclogitic garnetiferous rocks, to determine the geographic extent in the uplift of rocks containing garnet that grew under HP conditions. This in turn would indicate the proportion of crustal materials in the Llano Uplift that underwent densification during subduction.

This study did not accomplish the above goals, because it encountered previously unrecognized shortcomings of Raman barometry that make the technique unsuitable for analysis of inclusions in garnets whose growth culminated at high temperatures. Enami et al. (2007) studied low-temperature rocks (470-570 °C, 470-635 °C and 660-710 °C), whereas those from the Llano Uplift experienced much higher metamorphic temperatures (650-775°C). In this study, it was found that garnets that have undergone high-temperature diffusional homogenization no longer record geologically reasonable pressures. This limitation restricts the applicability of Raman barometry to rocks in which only limited intracrystalline diffusion has taken place in garnet.

GEOLOGY OF THE LLANO UPLIFT

A complete tectonic history for the Llano Uplift appears in Mosher (1998) and Mosher et al. (2008). Carlson et al. (2007) provides a review of the relevant metamorphic history. Included below is a brief overview of the Precambrian evolution of the Llano Uplift, focusing on relevant information for this locality as a test case for quartz-inclusion barometry.

The Llano Uplift is a ~9000 km^2 complex of metamorphosed igneous and sedimentary rocks intruded by granite plutons. Evidence from the orogenic belt suggests that the entire region experienced a polymetamorphic history due to Mesoproterozoic subduction of the southern margin of Laurentia beneath an unknown continent (Carlson et al., 2007; Mosher et al., 2008). The overall timing of the continent-continent collision coincides with other Grenville-aged orogenic events in the eastern United States. The southwestern portions of the uplift were subducted more deeply than the northeastern portions, so rock types and *P-T* conditions vary across the uplift.

Polyphase Metamorphism

Metamorphism in the Llano Uplift has been grouped into three main phases: an early, high-pressure phase; an intermediate, moderate-pressure phase; and a late, low-pressure phase.

Direct evidence for the initial high-pressure metamorphism is limited to boudinaged eclogite bodies surrounded by quartzofeldspathic gneisses. Several eclogite pods crop out across the uplift (Fig. 1), though the bodies are generally restricted to a few meters or tens of meters in size (Anderson, 2001). Thermobarometry for these eclogite bodies yields estimates

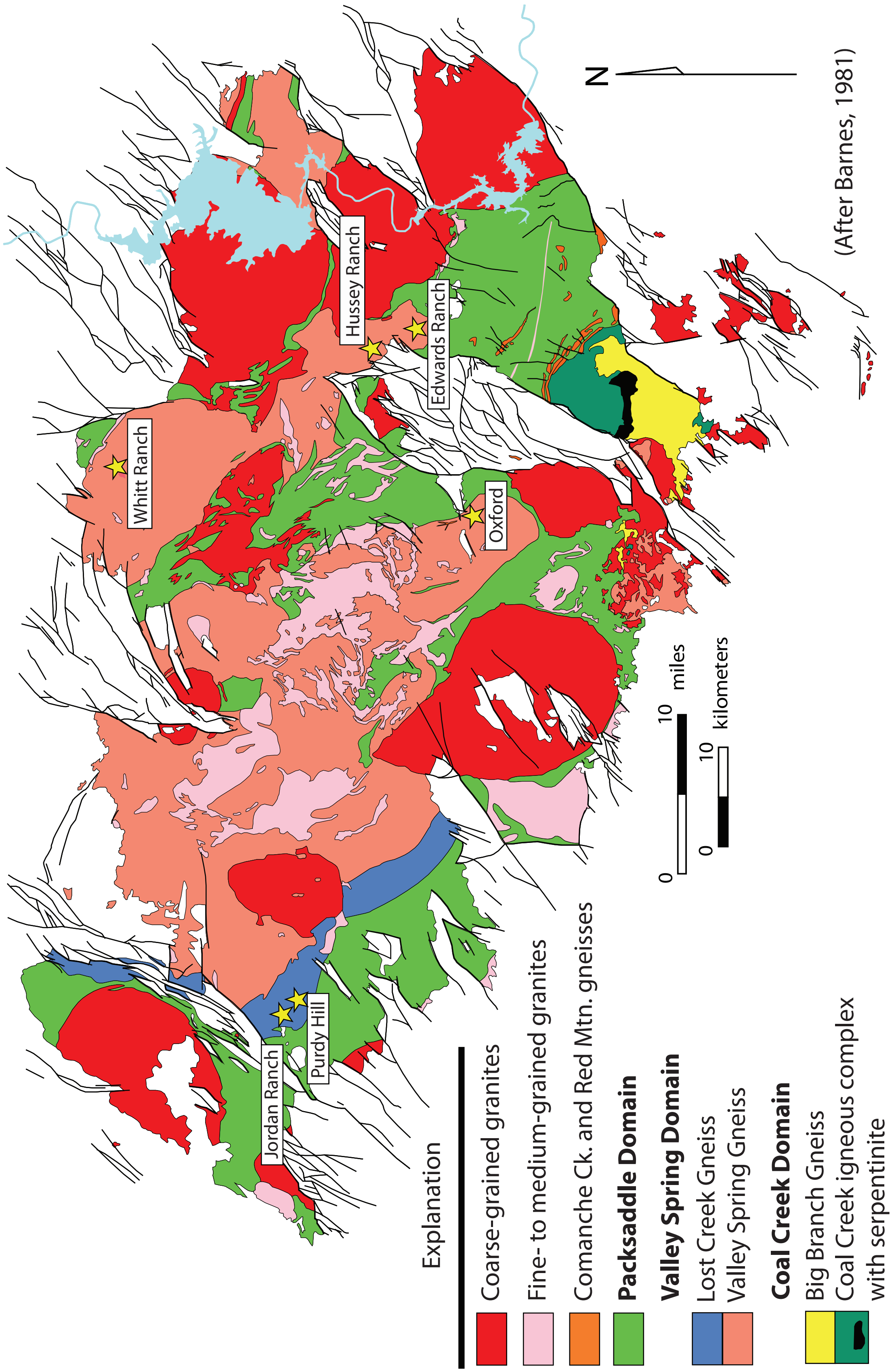

Figure 1: Geologic map of the Llano uplift, modified from Mosher (1998), after Barnes (1981). Eclogite localities are indicated by a star and labeled by name.

for pressures and temperatures within Ernst and Liou's (2008) field of "HP metamorphism," ranging from 1.4 to 2.4 GPa and from 650 to 775 °C (Carlson et al., 2007). Felsic gneisses encasing eclogite pods do not have remnants of HP mineral assemblages. However, eclogitic and gneissic garnets from the western part of the uplift have similar, diffusionally homogenized zoning profiles, suggesting that these garnets experienced similar metamorphic histories (Carlson and Schwarze, 1997). Figure 2 shows the garnet zoning profiles from several garnets across the entire uplift.

The intermediate metamorphism was a Barrovian-type retrogression event, at mid- to upper-amphibolite facies, in conjunction with intense deformation. Eclogites must have been present as discrete layers before the widespread deformation that accompanied the second phase of metamorphism, because boudins have foliated, amphibolitized margins and in some cases contain an internal foliation at an angle to the external foliation. Assemblages suitable for thermobarometry of this second metamorphic phase are scarce, due to intense overprinting by the final event. *P-T* conditions of ~700 °C and ~0.7 GPa are constrained by phase equilibria in pelites and in a strongly foliated ultramafic body, and by recrystallization mechanisms of quartz and feldspar in the felsic gneisses (Carlson et al., 2007).

The final metamorphism was a low-pressure, largely static event. At 525-625 °C and 0.3 GPa, this event occurred simultaneously with granitic plutonism (Bebout and Carlson, 1986). Buchan-series mineral assemblages are found to overgrow all earlier foliations, and static textures such as reaction coronas are present around garnets in the eclogite bodies. Additionally, secondary amphibole + plagioclase assemblages overprint the primary eclogite assemblage of garnet, sodic clinopyroxene, low-Al orthopyroxene, pargasitic amphibole and rutile (Carlson et al., 2007).

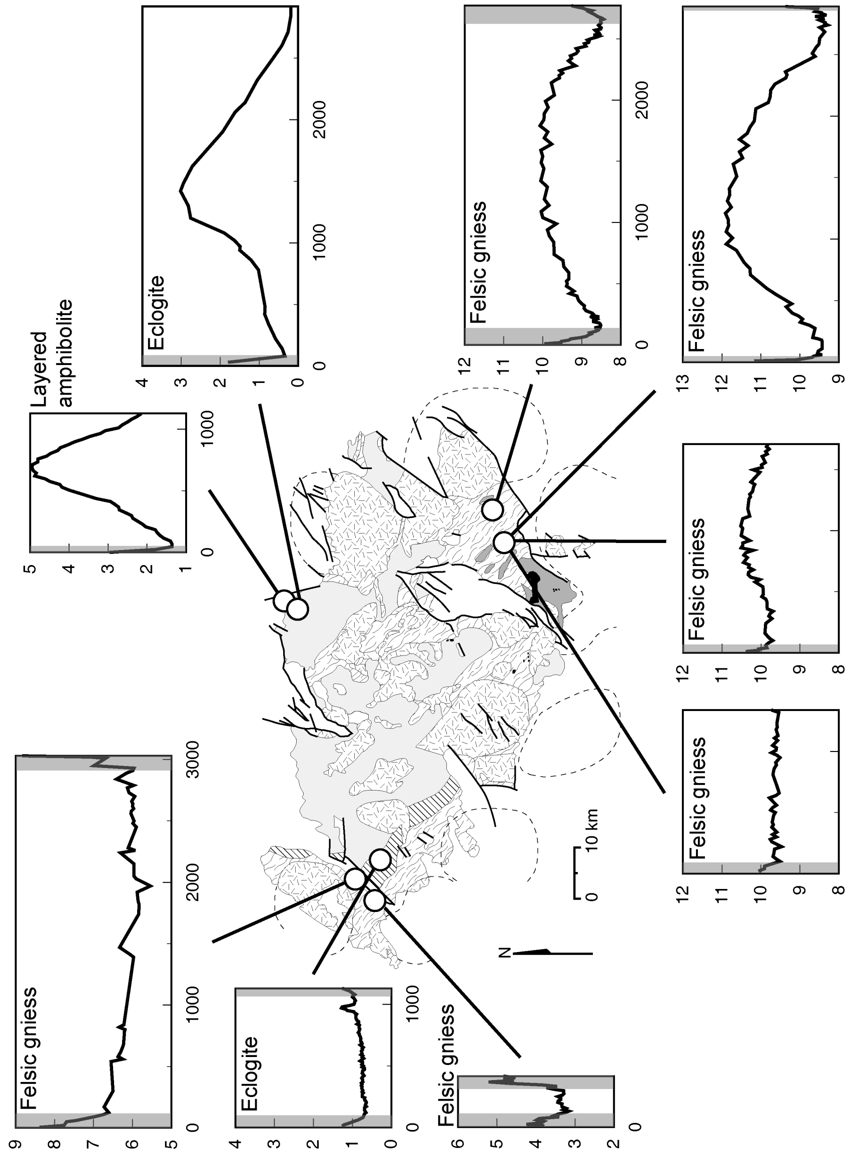

Figure 2: Garnet zoning profiles by locality, showing MnO wt % from EPMA traverses. Figure from Carlson et al. (2007), after data published by Carlson and Schwarze (1997).

The complex metamorphic history presents an obvious problem: little mineralogical evidence remains to establish the geographic extent of HP conditions. In the expectation that Raman barometry might reveal HP histories in overprinted rocks, this new technique was first applied to localities in the Llano Uplift for which conventional thermobarometry yielded unambiguous evidence of HP conditions during garnet growth, so that pressures from Raman barometry could be compared to results of conventional barometry.

Localities for This Study

Two localities were chosen for this study, with the intent for expansion to other localities once the method was verified: if the new barometer retrieved pressures in agreement with conventional pressures, the method could be applied to all garnetiferous rocks throughout the Llano Uplift. The first locality, Whitt Ranch, is in the northern part of the eastern half of the uplift. Only eclogites were analyzed from this locality. The second locality, Purdy Hill, is in the western half of the uplift. Purdy Hill exposures include both eclogites and garnetiferous felsic gneisses.

Whitt Ranch Eclogites

The Whitt Ranch locality is the largest exposure of retrogressed eclogite in the Llano Uplift; it is a mafic body approximately 0.5 km in diameter, with an elliptical shape elongate in the direction of the local foliation. The outer portions of the eclogite body, up to thirty meters in thickness but typically thinner, are extensively retrogressed to a biotite amphibolite with a strong foliation parallel to the edges of the eclogite body. The interior features local compositional layering, and less retrogression. This body has been the focus of several previous studies (Carlson and Johnson, 1991; Carlson and Schwarze, 1997; Carlson et al., 2007), including one that found inclusions of omphacitic pyroxene within garnet rims. The matrix of omphacitic clinopyroxene has been replaced by a vermicular intergrowth of sodian augite and oligoclase (Fig. 3), in which regions of optical continuity reveal a coarser-grained protolith, if the vermicular intergrowth has not already been replaced by coarse amphibole. Crawford (2004) demonstrated that garnet crystallization began under amphibolite-facies conditions and ended under eclogite-facies conditions, based on a transition in the garnet inclusion suite. In their interiors, garnets feature inclusions of quartz, andesine, epidote/clinozoisite, tschermakitic amphibole, and ilmenite, whereas garnet rims feature inclusions of rutile and occasionally omphacite, lack ilmenite and plagioclase, and rarely contain epidote and amphibole. Significant amounts of garnet resorption have occurred in most rocks, which erased much of the evidence at garnet edges of growth at higher-pressure conditions. Resorbed Whitt Ranch garnets have coronas of symplectitic hornblende, orthopyroxene and plagioclase, edged by magnetite (Carlson and Johnson, 1991). Additionally, garnets from Whitt Ranch retain steep zoning profiles, indicating that peak temperatures were not high enough or of sufficiently long duration to produce homogenization by intracrystalline diffusion (Carlson and Schwarze, 1997). Representative core compositions are $Alm_{52}Grs_{26}Sps_{10}Pyp_8And_4$, and rim compositions are $Alm_{57}Grs_{29}Pyp_{13}Sps_1$ (Carlson et al., 2007).

Conventional thermobarometry for Whitt Ranch eclogites estimates primary-stage metamorphic P-T conditions at ~1.4 GPa and ~650 °C (Carlson et al., 2007). Barometry was based on the garnet-rutile-ilmenite-plagioclase-quartz (GRIPS) equilibrium, and used inclusions at the transition between assemblages, so metamorphic pressures during rim

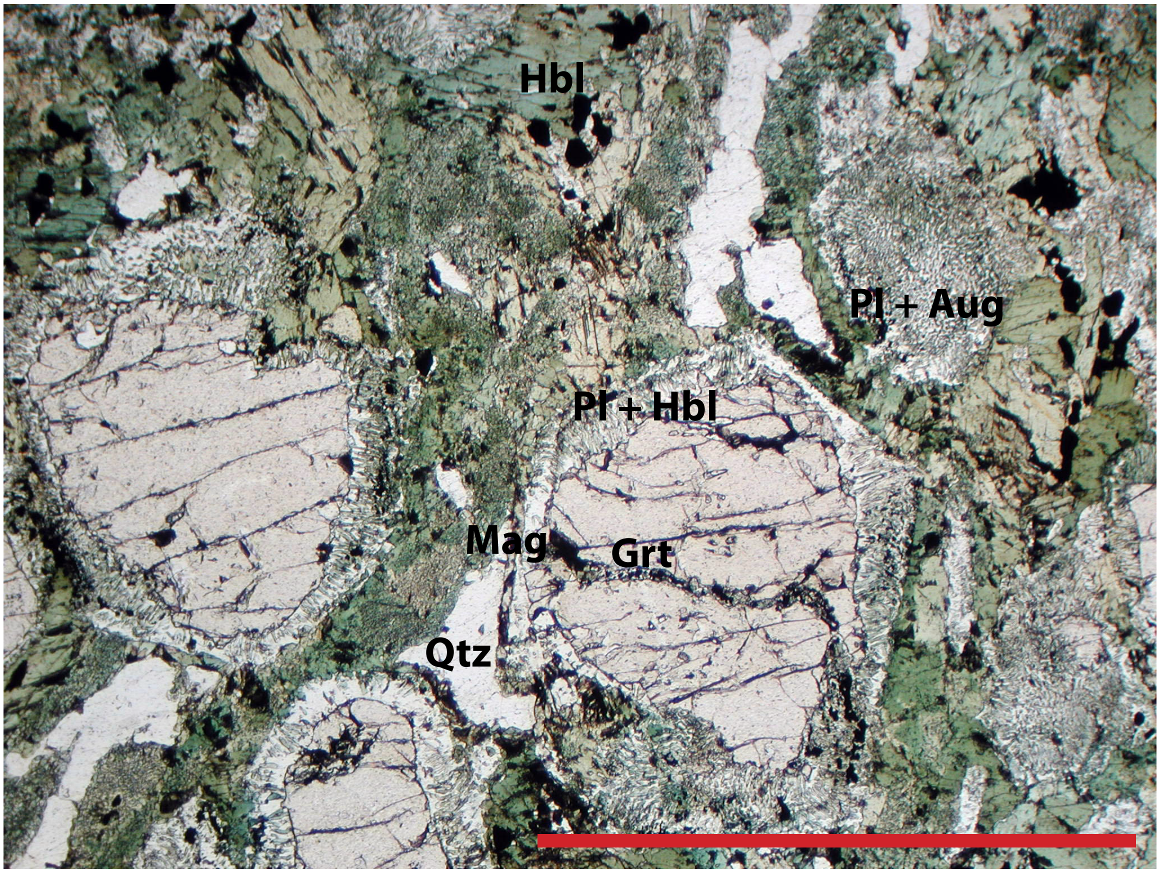

Figure 3: Photomicrograph of Whitt Ranch thin section WRMG 60. Light colored minerals are garnet (Grt) and quartz (Qtz). Coronas around garnet are hornblende, magnetite (Mag), and a symplectite zone of hornblende (Hbl) + oligoclase (Pl). Outside of garnet rim, retrogression of primary omphacite produced the fine grained symplectite of oligoclase (Pl) + sodian augite (Aug), which is often replaced by coarse amphibole (Hbl). Scale bar represents 2.0 mm. Abbreviations after Kretz (1983).

growth were likely higher but cannot be quantified. Temperature estimates from Fe-Mg exchange are 611 ± 24 °C for garnet-clinopyroxene and 693 ± 25 °C for garnet-amphibole. For elastic-model calculations that will be explained below, a median temperature of 650 °C was used for Whitt Ranch.

Purdy Hill Eclogites

The Purdy Hill eclogite exposure crops out as multiple lenses of tens-of-meter-long bodies that are elongate in the direction of the surrounding foliation. Many of these bodies are associated with quartz masses that discontinuously line the margins of the eclogite occurrences and occupy spaces between them. Mapping by Anderson (2001) indicates that these mafic bodies crop out in patterns that trace structural trends evident in the surrounding quartzofeldspathic gneiss. The Purdy Hill eclogites are generally the better preserved of the two eclogites studied: they are less retrogressed, so original textures and mineralogy are more easily identified. Primary minerals present in Purdy Hill eclogites are garnet, sodian augite, low-Al enstatite, pargasite, and rutile (Fig. 4). The typical inclusion suite matches the mineralogy of the matrix phases, plus quartz, but with little orthopyroxene; these inclusions indicate that garnet growth occurred under eclogite-facies conditions. Garnet zoning profiles in these garnets are relatively flat, indicating homogenization by intracrystalline diffusion at peak temperature (Carlson and Schwarze, 1997). Compositions of garnets in the Purdy Hill eclogites are near $Alm_{59}Pyp_{19}Grs_{14}Sps_4And_4$ (Anderson, 2001, Appendix B-1). Amphibolite-facies retrogression produced overprint textures similar to those at Whitt Ranch.

Extensive thermobarometry has been undertaken to accurately assess the equilibration conditions for the Purdy Hill eclogites (Carlson et al., 2007). Pressures were

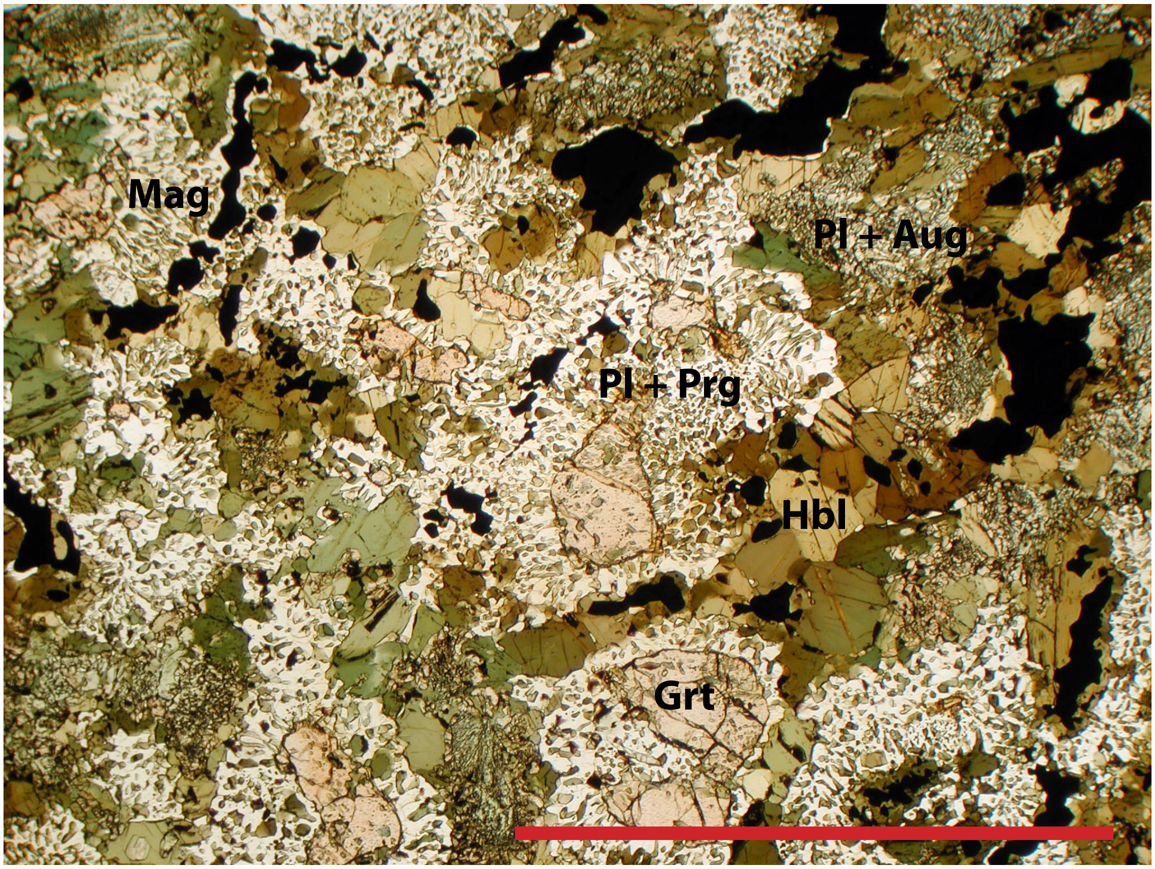

Figure 4: Photomicrograph of Purdy Hill eclogite thin section PH 97-63b. Pinkish mineral is garnet (Grt). Coronas around garnet are a symplectite zone of pargasite (Prg) + oligoclase (Pl). Within Purdy Hill eclogites, magnetite (Mag) and some primary clinopyroxene are found outside of garnet reaction rims. Retrogression of omphacite produced the fine grained symplectite of oligoclase (Pl) + sodian augite (Aug), which is often replaced by coarse amphibole (Hbl). Scale bar represents 2.0 mm. Abbreviations after Kretz (1983).

obtained from aluminum-in-orthopyroxene barometry. Cores were estimated to have grown at 2.2 GPa, whereas rims grew at 1.6 GPa; continuous Al zoning between these limits implies a continuous decrease in pressure during garnet growth. Temperatures obtained from Fe-Mg exchange thermometry between garnet and clinopyroxene, garnet and orthopyroxene, and garnet and amphibole range from 738 to 867 °C. The accepted P-T conditions for the Purdy Hill eclogites are 2.2 to 1.6 GPa and 775°C.

Purdy Hill Felsic Gneisses

Field relations at Purdy Hill show that eclogite boudins are elongated and partially foliated in the same orientation as the overall foliation within the surrounding gneisses, indicating that the boudins were discrete layers within the gneiss prior to the deformation. This physical relationship suggests the gneisses and eclogites share a common history. Garnets from both rocks also share flat zoning profiles (Carlson and Schwarze, 1997), meaning that both sets of garnets reached peak temperatures sufficient to drive diffusional homogenization. Garnet compositions in the gneisses (E. Lane, unpublished data) are close to $Alm_{79}Pyp_{13}Grs_4Sps_4$. Other minerals present are quartz + plagioclase + biotite ± sillimanite + tourmaline (Fig. 5). The presence of sillimanite rather than kyanite indicates equilibration at lower pressures than those attained by the included eclogite pods. Sillimanite was apparent in the matrix of three of the four samples from this area that were used in this study, and was found as rod-like inclusions in the rims of some garnets. Garnet cores were free of sillimanite inclusions. Inclusions were typically quartz, although some opaque minerals were also present as inclusions. Thermobarometry for the quartzofeldspathic gneisses at Purdy Hill cannot be done via conventional methods, for lack of appropriate assemblages.

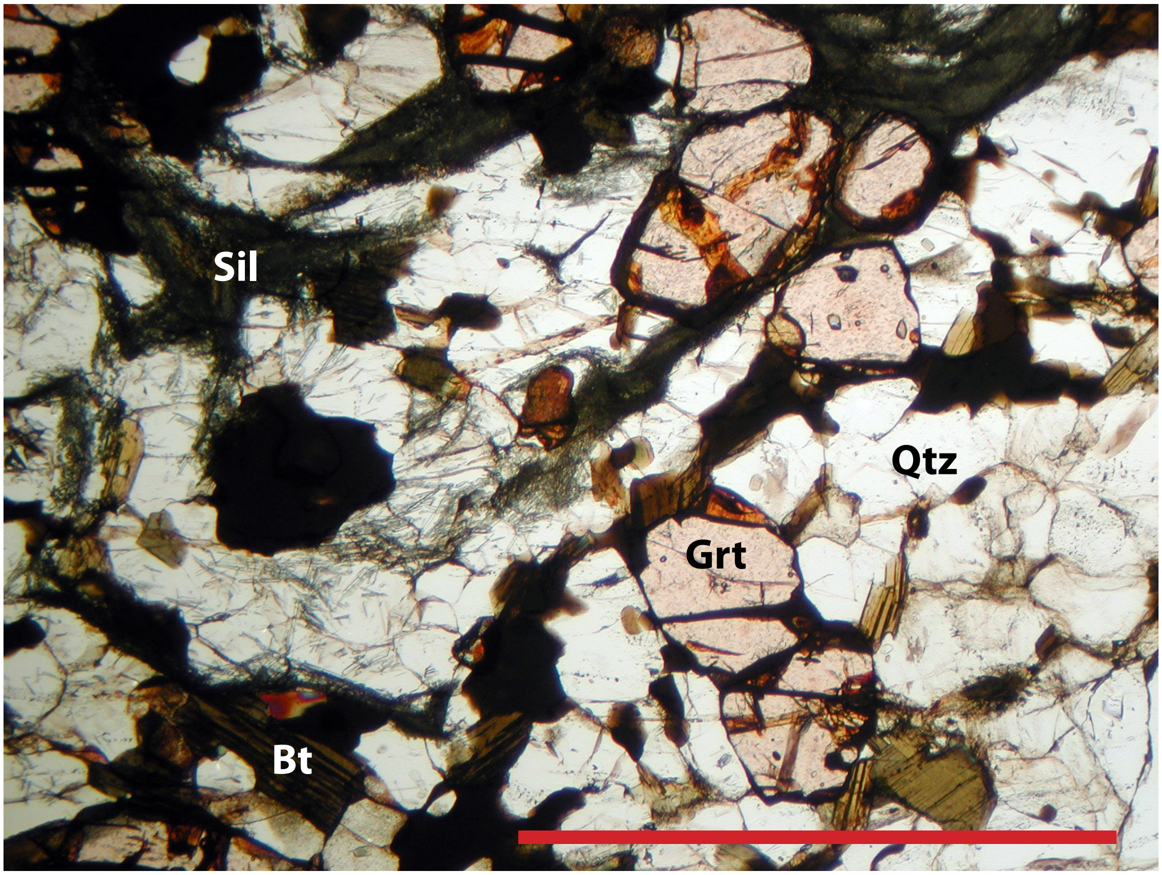

Figure 5: Photomicrograph of Purdy Hill felsic gneiss thin section LU 02-9. Pinkish mineral is garnet (Grt). Other minerals include quartz (Qtz), biotite (Bt), and sillimanite (Sil). Scale bar represents 2.0 mm. Abbreviations after Kretz (1983).

Geological evidence to constrain the metamorphic history for Llano's quartzofeldspathic gneisses is sparse, and is split between two competing theories. On one hand, garnet zoning and field relationships suggest a shared HP history with the eclogites, but original mineral assemblages may have been heavily overprinted by later events. On the other hand, the presence of sillimanite and the lack of HP mineral assemblages in the gneisses suggest that the gneisses might not have experienced the HP metamorphism at all. If any of the garnet in these gneisses preserves a HP signature in the form of high residual pressures on included quartz crystals, this question can be resolved. Thus the new barometric method of Raman microspectrometry of quartz inclusions in garnet provides a promising opportunity to determine the pressures at which garnet grew, despite any overprinting that has occurred.

BACKGROUND

Theory from Previous Work

The quartz-inclusion barometer was first applied by Enami et al. (2007) to investigate the areal extent of rocks experiencing high-P/T conditions in the Sanbagawa metamorphic belt of Japan. This belt features eclogite-facies rocks typical of any high-P/T metamorphic belt, but as in the Llano region, the occurrence of HP assemblages is sparse. Enami et al. (2007) hypothesized that during exhumation, many of the HP assemblages had been recrystallized to amphibolite-facies or lower-grade mineral assemblages. In order to see through this overprint, they devised a method for determining the entrapment pressure of a quartz inclusion in garnet.

The basic concept behind this new barometer is that quartz crystals included within garnet retain, after exposure at the surface, a measurable pressure (the *residual pressure*) that can be related to the pressure at which the inclusion was surrounded during garnet growth (the *entrapment pressure*). The residual pressure preserved in the quartz crystal after exhumation and cooling can be determined using a laser Raman microspectrometer together with a set of experimental calibrations of displacement of Raman peaks. The residual pressure can then be related quantitatively to the entrapment pressure through a calculation based on an elastic-strain model of the changes that occur during exhumation and cooling. These changes are illustrated in Figure 6.

Enami et al. (2007) reported several significant findings: (1) completely surrounded quartz inclusions in garnet had systematically different Raman shifts when garnets from eclogite and epidote-amphibolite host rocks were compared; (2) residual pressures

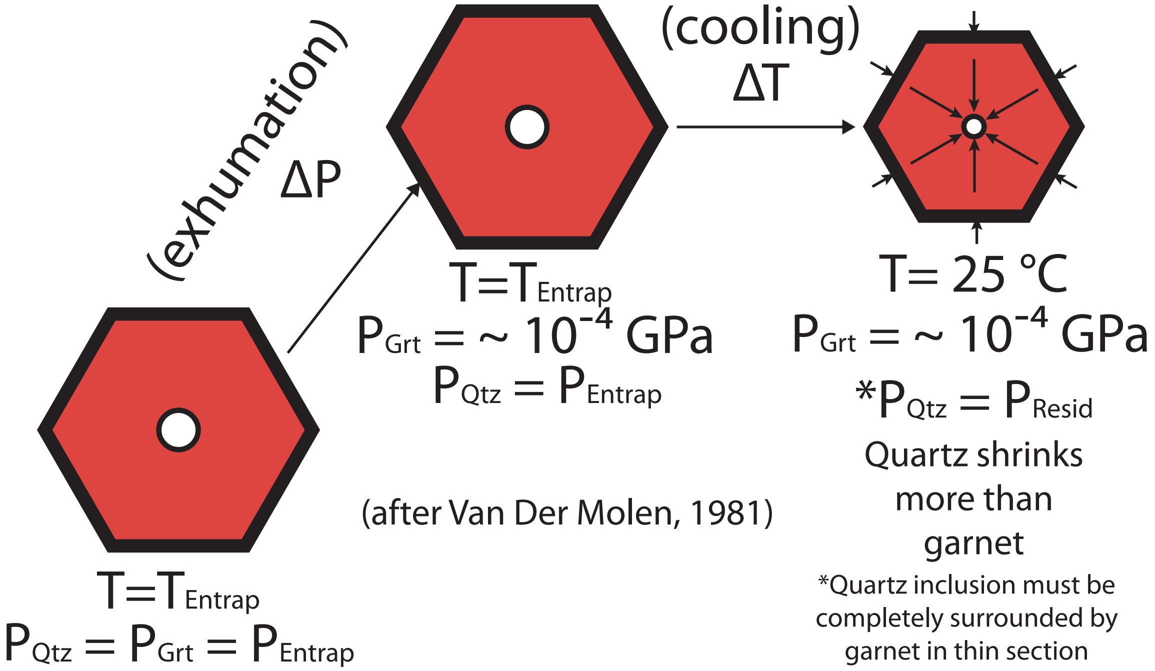

Figure 6: Schematic depiction of the exhumation and cooling process and its effects on a quartz inclusion in garnet, based on sphere-in-hole model of Van der Molen (1981). Although decompression and cooling occur simultaneously in nature, their effects are shown separately here to illustrate the approach taken by Van der Molen to calculate residual pressure.

back-calculated from conventional thermobarometry were consistent with Raman-measured residual pressures to within ± ~0.2 GPa; and (3) the areal extent of HP metamorphism based on Raman data was considerably larger than the region in which petrologic evidence of HP metamorphism was preserved. The Raman-measured residual pressure results were split into two populations of data: one set representing inclusions in rocks that reached eclogite-facies conditions before being overprinted; the other representing inclusions in epidote-amphibolite rocks lacking an earlier HP history. A wide spread existed between the two populations, greater than the spread due to the value cited for accuracy of the method. In a second paper, Mouri and Enami (2008) proposed that this method had the potential for detecting high-pressure garnet growth in extensively retrogressed rocks. This innovative study held much promise for other polyphase metamorphic terranes in which HP assemblages are rare or absent due to overprinting by lower pressure assemblages.

Quartz Inclusion Barometry via Laser Raman Microspectrometry

Raman microspectrometry measures the scattering of monochromatic light upon interaction with a sample. When a sample is excited by photons from a light source with a specific frequency, most light is absorbed and reemitted at the same frequency. This is elastic Rayleigh scattering. However, a few of the photons (e.g. 1 in 10^5) are absorbed by the sample, interact with the molecules, and are reemitted at a frequency different from that of the incident photons. This inelastic scattering is the Raman effect; it produces a shift up or down in wavenumber from the original monochromatic frequency. The Raman effect is very weak, but it allows characterization of a material's molecular modes, including the vibrational and rotational modes.

A laser Raman microspectrometer has four crucial components: an excitation source (a laser); a sample illumination system and light collection optics (a specialized microscope); a wavelength selector to differentiate the elastically and inelastically scattered photons (a filter); and a detector to record the intensity and wavenumber of inelastically-scattered photons (typically a charge-coupled device, or CCD). The microspectrometer produces a spectrum from data collected by the detector showing the frequencies at which the weak inelastic scattering occurs. Intense scatter at a specific frequency produces a peak, and each mineral produces a pattern of peaks with different frequency shifts, which depend upon its unique bond energies.

Figure 7 shows the Raman spectra produced by garnet and by the common inclusion minerals feldspar and quartz. The spectrum of α-quartz has peaks near the Raman wavenumbers (ν_i) 464 cm^{-1}, 205 cm^{-1} and 128 cm^{-1} (Fig. 8). The 464 cm^{-1} peak is dominated by bending of the O-Si-O bond; the 205 cm^{-1} peak is likewise dominated by the O-Si-O bending vibrations, but is also affected by stretching and twisting of the Si-O bond; and the 128 cm^{-1} peak is primarily dominated by the Si-O-Si bond stretching, but also affected by the same bending as the other two bonds, and twisting of the Si-O bond (Etchepare et al., 1974). Pressure applied to a quartz crystal causes a movement of Raman peaks to wavenumbers higher than 464 cm^{-1}, 205 cm^{-1} and 128 cm^{-1}, as a result of increases in the vibrational frequencies of the O-Si-O bonds in quartz (Dean et al., 1982; Liu and Mernagh, 1992; Schmidt and Ziemann, 2000). These changes in peak position as a function of pressure have been calibrated in diamond-anvil-cell experiments (Liu and Mernagh, 1992;

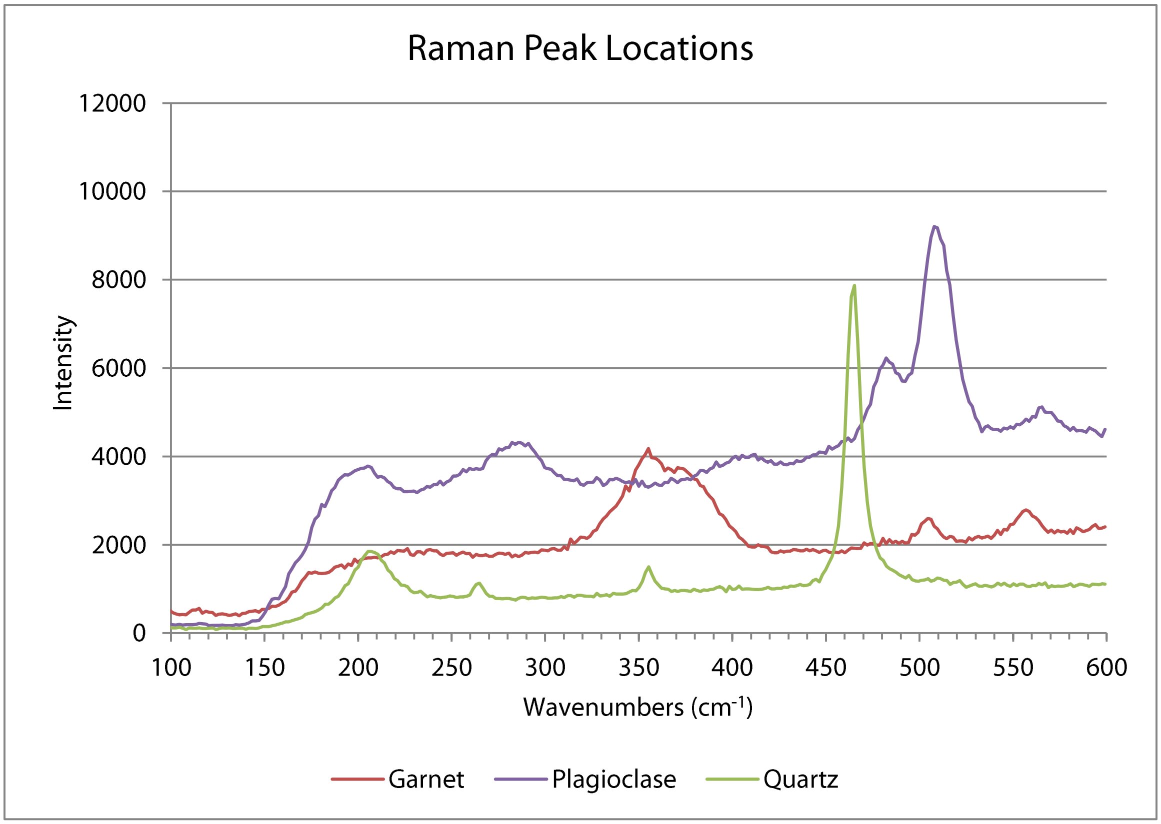

Figure 7: Raman spectra for garnet, plagioclase and quartz. These spectra were obtained using a lower-quality "notch" filter, preventing data collection below ~160 cm^{-1}. All data used for calculations was collected after the higher-quality "edge" filter was installed. The “edge” filter allows data collection between ~80 and 160 cm^{-1}.

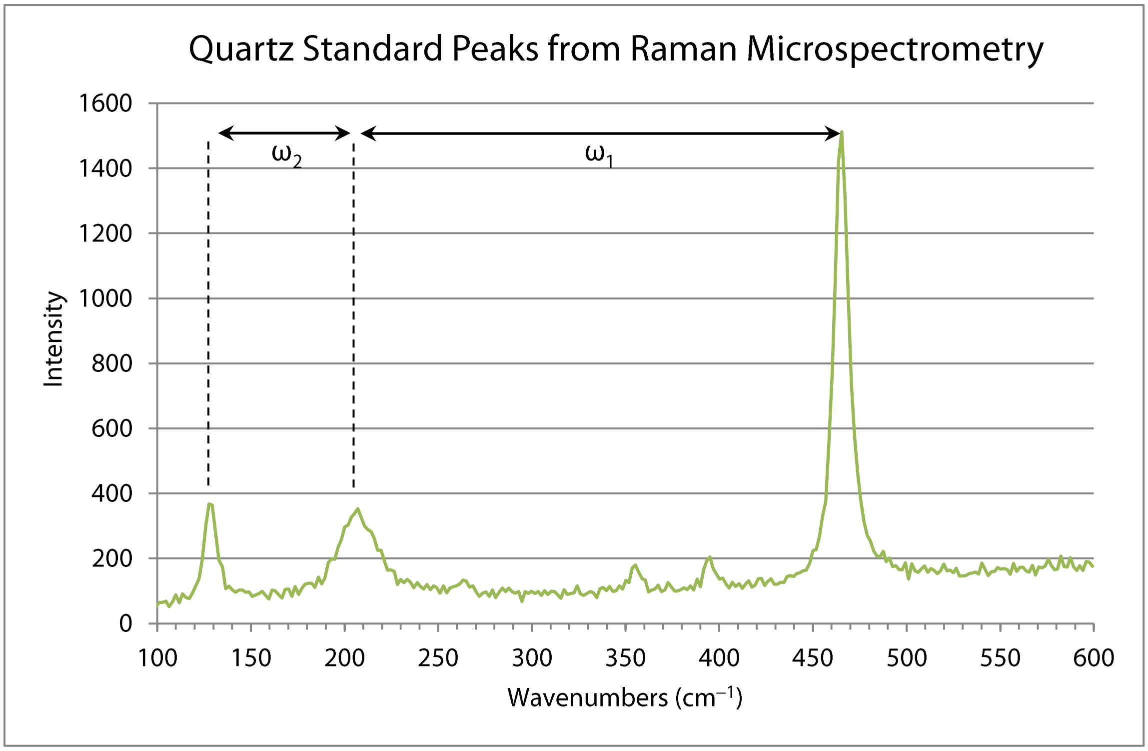

Figure 8: The ω_1 and ω_2 relationships are indicated on this unfitted spectrum indicating relative quartz standard peak locations.

Schmidt and Ziemann, 2000). With an appropriate laser, the microspectrometry is non-destructive, and the Raman spectrum of a quartz inclusion is easily measured.

By measuring changes in the Raman spectrum of a natural α-quartz inclusion relative to the spectrum of an α-quartz standard at atmospheric pressure, the residual pressure on the inclusion can be determined. To compare the standard to the sample, Enami et al. (2007) measured the difference between the positions of the 464 cm^{-1} peak and the 205 cm^{-1} peak, and also the difference between the 205 cm^{-1} peak and the 128 cm^{-1} peak. The relative wavenumber differences are defined by the following parameters: $\omega_1 = \nu_{464} - \nu_{205}$ and $\omega_2 = \nu_{205} - \nu_{128}$ (Fig. 8). The calculated ω values for the α-quartz standard and the sample can then be compared to determine the total wavenumber difference: $\Delta\omega_1 = \omega_1^{\text{standard}} - \omega_1^{\text{sample}}$ and $\Delta\omega_2 = \omega_2^{\text{sample}} - \omega_2^{\text{standard}}$. Enami et al. (2007) used these relative measures to correct for any fluctuations in the locations of quartz peaks due to changes in measurement conditions, such as instrument calibration or room temperature. They correlated the Raman shift to pressure on the inclusion using the experimental results of Liu and Mernagh (1992) and Schmidt and Ziemann (2000); Figure 9 illustrates these correlations as determined by Schmidt and Ziemann (2000).

To relate the residual pressure to the entrapment pressure, Enami et al. (2007) used the spherical-inclusion model of Van der Molen (1981) to approximate the normal stresses, or residual pressures, within and surrounding a spherical inclusion. This model assumes that an inclusion is completely surrounded by a confining medium to an infinite distance around the inclusion. The model accounts for changes in pressure and temperature during exhumation and cooling, but holds the elastic parameters of the minerals constant. Van der

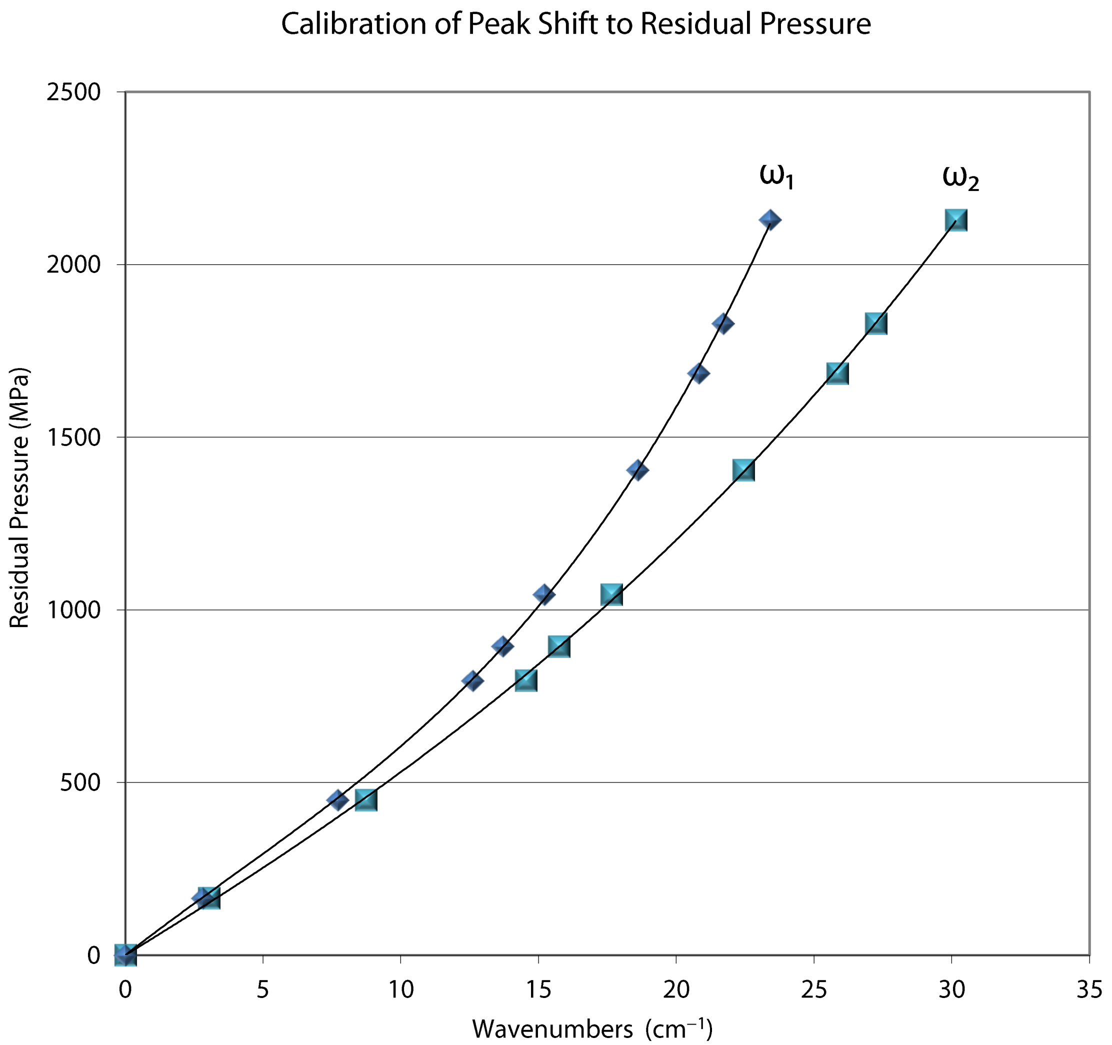

Figure 9: Calibration relating ω_1 and ω_2 to residual pressure (MPa), after data published by Schmidt and Ziemann (2000).

Molen's "sphere-in-hole" equation produces a value of pressure at the time of entrapment from the residual pressure value derived via Raman microspectrometry. The equation describes the residual pressure P_{Qtz} on a spherical inclusion in an isotropic matrix that was included at an entrapment pressure P_{Grt} and has experienced a change in temperature, $\Delta T = T_{\mathrm{Room}} - T_{\mathrm{Peak}}$ (in Kelvin):

$$P_{\mathrm{Qtz}} = \frac{\kappa_{\mathrm{Qtz}}}{\kappa_{\mathrm{Grt}}(3\kappa_{\mathrm{Qtz}}+4\mu_{\mathrm{Grt}})}\left\{P_{\mathrm{Grt}}(3\kappa_{\mathrm{Grt}}+4\mu_{\mathrm{Grt}}) - 4\kappa_{\mathrm{Grt}}\mu_{\mathrm{Grt}}\Delta T\Delta A\right\} \qquad \text{Eqn. 1}$$

The variables are the thermal expansion coefficients and the bulk and shear moduli, or elasticity parameters, for each mineral: the bulk modulus is symbolized by κ with units of GPa, and the shear modulus is symbolized by μ, also with units of GPa. The factor for the difference in the thermal expansivity parameters ΔA has units of K^{-1} and is defined as $\Delta A = A_{\mathrm{Grt}} - A_{\mathrm{Qtz}}$. Values for these parameters come from data (Table 1) that was compiled by Enami et al. (2007) from primary sources (Bass, 1995; Fei, 1995; Wang and Ji, 2001). The effects of variations in garnet composition are very small (Carlson et al., 2009); however, all calculations in this study used elastic parameters linearly interpolated among endmembers based on the average compositions.

Table 1: Bulk (κ) and shear (μ) moduli and thermal expansion parameters (*A*) at standard conditions (10^{-4} GPa and 298 K), after Enami et al. (2007).

Mineral	κ (GPa)	μ (GPa)	*A* (K^{-1})
Quartz	37.8*		2.38E−05‡
Almandine	175.1†	92.1†	1.57E−05‡
Pyrope	170.1†	90.2†	1.98E−05‡
Grossular	166.3†	98.1†	1.63E−05‡
Spessartine	171.8†	93.3†	1.71E−05‡

* Bass (1995).

† Wang and Ji (2001).

‡ Fei (1995).

METHODS FOR THIS STUDY

Laser Raman microspectrometry is straightforward but the complexity of natural rock samples requires careful development of analytical methods. Methods for this study were based on those developed by Enami et al. (2007) and are detailed below. In addition, protocols for depth profiling were added to help account for potential sources of error.

The instrument used for this study is housed in the University of Texas at Austin Center for Electrochemistry. Raman spectra produced by a 514-nm Ar laser at 50 mW were acquired using a Renishaw inVia RM 2000 Raman spectrometer. To focus on the sample, the spectrometer was coupled to a Leica INM200 optical microscope, using a Leica 100X objective. The entire instrument was interfaced with a computer-controlled XYZ-stage (Prior Scientific). The Raman spectrometer was equipped with a thermoelectrically cooled charge-coupled detector (CCD) camera (Wright Instruments, Ltd.) for spectral acquisition, while the optical microscope was fitted with a Sony DXC-970MD color CCD camera for general sample viewing. The microspectrometer's confocal setup allowed spectral acquisition at selected depths within the thin section. The confocal mode of the instrument essentially focuses the laser beam on a specific level in the thin section and permits only light scattered from that level to reach the CCD. Use of the confocal mode is required for several reasons: (1) it permits measuring spectra for a quartz inclusion below the surface of the thin section; (2) it permits evaluation of whether a quartz grain is completely enclosed by garnet; and (3) it permits spectra to be gathered that originate from scatter entirely within quartz. Horizontal spatial resolution was ~1 μm; vertical spatial resolution from the confocal setup was ~2 μm. The high spatial resolution means that spectra can be collected from small inclusions; however, better results come from either larger inclusions or longer measurement times.

Prior to Raman microspectrometry, individual inclusions were carefully examined on the petrographic microscope to evaluate their suitability. Standard-thickness (30 μm), polished, uncovered thin sections were used for most samples. Two thin sections of Purdy Hill gneiss (LU 02-6, LU 02-9) were thicker than normal (~65 μm). Due to the small size of the inclusions, careful petrography was required to select inclusions that were of quartz rather than another phase, such as plagioclase. Discrimination of quartz was based on its colorless appearance, near-spherical habit, and extremely low birefringence (lower than typical standard quartz in thin section). The identity of all inclusions was verified via Raman microspectrometry. Suitable inclusions must be completely surrounded by garnet, must be as equant as possible to accord with the assumptions in the elastic model, and must not be located along a grain boundary or crack within the garnet.

During Raman measurements, several steps were taken to maximize precision and accuracy. First, the instrument was calibrated by the lab manager using a silicon wafer with a strong peak at 520 cm^{-1}. Second, an α-quartz standard was measured for 180 seconds over a range between 100 and 600 cm^{-1}. The standard was an (0001) section of a euhedral α-quartz crystal from a Brazilian pegmatite. Spectra were measured at ~6 μm below the surface of the standard to generate intensities similar to those for completely surrounded inclusions below the surface. The analysis time was chosen as the shortest interval needed to produce a clean, low-noise spectrum. Third, depth profiles were made to locate the vertical center of each inclusion. Each depth profile was set up as an automated process in which the instrument acquired spectra at 2 μm intervals into the thin section (Fig. 10). Scan modes for

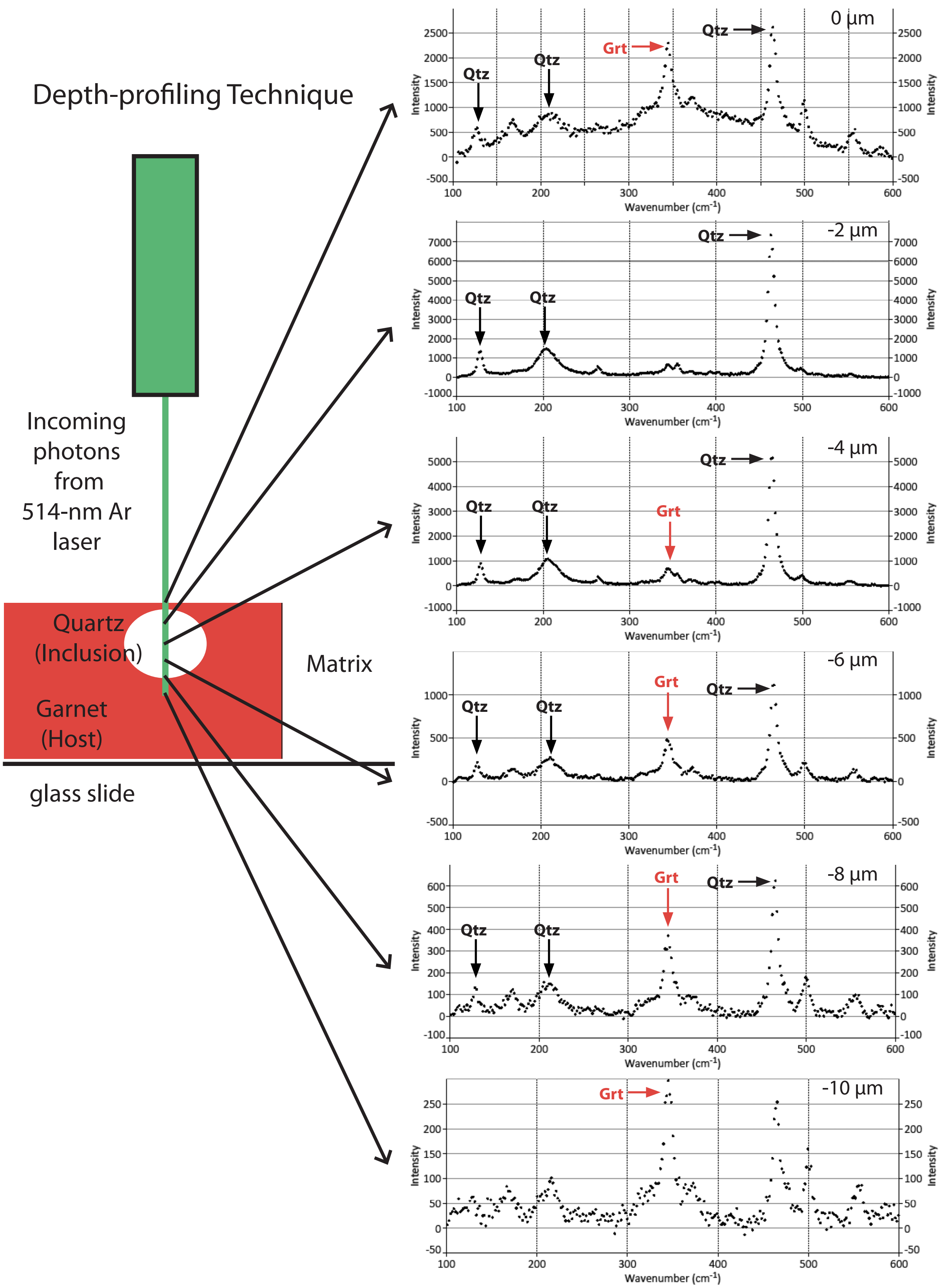

Figure 10: Raman spectra are collected in confocal mode at closely spaced depths (~2 µm intervals) within the thin section. The vertical center of the inclusion is identified by spectra with low or zero intensity garnet peaks and high intensity quartz peaks. Data collected by Casey Corbin (Corbin, 2010).

the depth profiles encompassed ~500 cm^{-1} on each side of 520 cm^{-1}, and this mode was the fastest way to verify the inclusion was surrounded by garnet. Measurement times during depth profiles were often as short as 60 seconds but could be as long as 600 seconds if spectra were noisy. After the depth profile was completed, a depth inside the thin section at the approximate center of the inclusion was chosen to ensure that peak positions would not be compromised by edge effects generated near the boundary between garnet and quartz. Edge effects are buildups in stress at the interface between garnet and quartz crystals. Enami et al. (2007) showed that regions of an inclusion within ~2-4 μm of the grain boundary were commonly subject to edge effects. Thus, the centers of large inclusions (e.g., 12 μm in diameter) are more likely to be unaffected than smaller inclusions (e.g., 5 μm in diameter). A final measurement, longer in time than those made during the depth profile, was made at the inclusion center to decrease background noise relative to peak intensities. Typical measurements were between 300 and 1200 seconds.

Once this final measurement was made, the raw data were exported into PeakFit v4.06 to determine peak centers. Linear fits to background were subtracted from all spectra. Outliers such as single "spike" data points clearly from cosmic rays, or data points near or below the edge filter at ~80 cm^{-1} were also eliminated. The three main quartz peaks were manually fitted using a combination of Gaussian and Lorentzian curves to account for each peak's unique shape.

Enami et al. (2007) determined residual pressures from both $\Delta\omega_1$ and $\Delta\omega_2$ (cf. Fig. 9). When all three peaks are present at high intensity, they can be fit without large errors and in these cases $\Delta\omega_1$ and $\Delta\omega_2$ should produce identical values for residual and entrapment pressures. For this study, because the goal was calculation of an entrapment pressure, the

$\Delta\omega_1$ values were used because the 464 cm^{-1} and 205 cm^{-1} peaks were more intense and easier to fit reliably than the lower-intensity 128 cm^{-1} peak. In addition to being low in intensity in some spectra, the 128 cm^{-1} peak was also occasionally masked by strong epoxy fluorescence at ~105 cm^{-1}. At times, the 205 cm^{-1} peak was broad and could not be fit reliably, so an idea in this study was to create a "$\Delta\omega_3$" calibration curve based on the relationship between the 464 and 128 cm^{-1} peaks. However, this curve is subject to relatively poor precision (small differences in "$\Delta\omega_3$" lead to large differences in inferred residual pressure), so it was not used beyond an initial investigation.

Error Prevention

Because this is an untested method, additional precautions were taken to prevent errors that may affect the data quality, and to assess uncertainties in the measurements. Prior to acquiring data for a particular inclusion, the following criteria were checked. Inclusions were as near-spherical as possible, to ensure that they could be modeled accurately. Inclusions along cracks or near garnet edges were not used, nor were inclusions that were possibly exposed to the top or bottom of the thin section, as release of stress is possible in these circumstances. Finally, the depth profiles were added to the method to ensure that the inclusion was completely surrounded, and to find the centers of inclusions.

The edge effects noted by Enami et al. (2007) could cause an increase in calculated residual pressure, so the final spectra were taken as near to the inclusion center as possible. Spectral acquisitions were as long as reasonably possible, to obtain measurements with low background noise relative to the signal intensity. At times during measurements longer than about 20 minutes or during long depth profiles, the mechanical stage would freeze or move slightly, moving the inclusion out of focus. In these situations the sample would have to be re-measured because the data were unreliable. Peakfitting is another potential source of error, insofar as ambiguity about the position of a peak affects the $\Delta\omega_1$ calculations, which consequently affects the estimates of residual and entrapment pressure. Spectra with low background noise were preferable because the peaks were easier to fit reliably.

One other step added to the methods in this study was to evaluate the reproducibility of the laser Raman microspectrometric technique. This was done by repeatedly measuring the Raman spectrum of a specific quartz inclusion, once during each session over a several-month period. The inclusion was measured at the same depth and for the same amount of time during each session. This test will define the reproducibility of measurements from the University of Texas at Austin laser Raman microspectrometer.

RESULTS

The results from the quartz standard and the reproducibility test will be presented first, to evaluate the precision of the technique. Results for the residual pressure and entrapment pressure from each of the three rock types will then be presented, and an example thin section and data specific to each thin section will be included. For both the reproducibility test and the locality results, all values for residual and entrapment pressure will be derived from the $\Delta\omega_1$ calculation. A list of all samples used in this study is included at the beginning of the Appendix, followed by detailed sample descriptions and calculation results for each of them. The full results for each inclusion are accompanied by thin section photomicrographs and plots of spectra from the quartz standard and the inclusion.

Quartz Standard

The quartz standard was measured 53 times, usually for 180 seconds. Figure 11 is a plot of the 464 cm^{-1} and 205 cm^{-1} peaks for quartz over the ~15 month period of this study. Table 2 lists the locations of the three major peaks for each measurement session. The most significant result from the repeated quartz-standard measurements is the presence of two discontinuities in peak position for the 464 cm^{-1} and 205 cm^{-1} peaks. Despite these abrupt changes, the ω_1 calculation is relatively consistent over the course of the study (Fig. 12), with an average value of 258.3 ± 0.4 cm^{-1}. Enami et al. (2007) report a standard deviation for ω_1 of $\pm$ 0.3 cm^{-1} for their measurements on a quartz standard.

Reproducibility Results

The sample chosen for reproducibility studies was from the Whitt Ranch locality, sample WRMG SR-3 (Fig. 13). Over about three months, the inclusion was measured 16

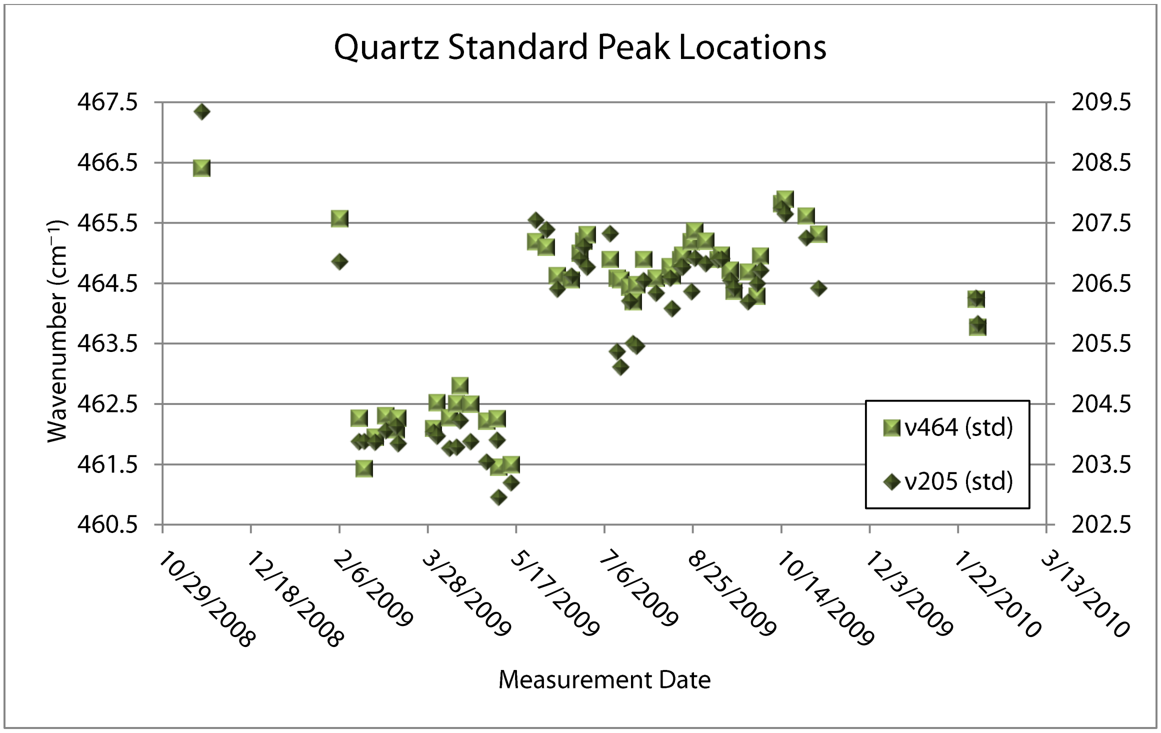

Figure 11: Measured Raman peak locations from the quartz standard after peak fitting.

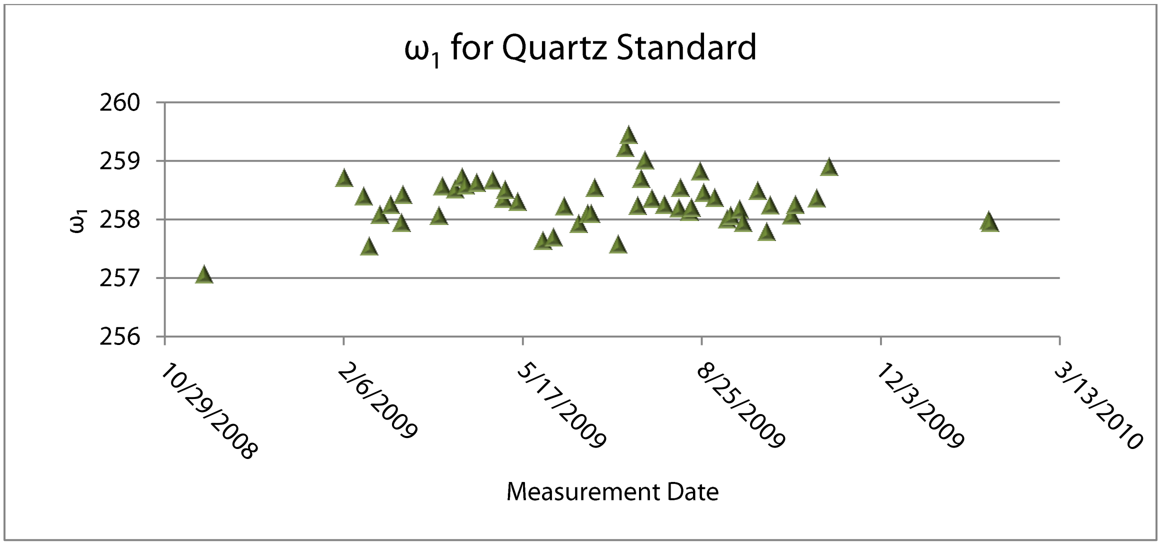

Figure 12: Calculated ω_1 for the quartz standard.

Table 2: Data from all quartz standard measurements.

Date of Measurement	ν128 (std)	ν205 (std)	ν464 (std)	ω_1	ω_2
11/20/2008	129.83	209.35	466.41	257.06	79.52
2/6/2009	128.92	206.87	465.58	258.71	77.95
2/17/2009	125.3	203.88	462.27	258.39	78.58
2/20/2009	124.52	203.89	461.43	257.54	79.37
2/26/2009	125.15	203.87	461.95	258.08	78.72
3/4/2009	125.19	204.06	462.31	258.25	78.87
3/10/2009	125.32	204.14	462.08	257.94	78.82
3/11/2009	125.56	203.85	462.27	258.42	78.29
3/31/2009	124.92	204.04	462.10	258.06	79.12
4/2/2009	125.29	203.97	462.53	258.56	78.68
4/9/2009	125.38	203.77	462.28	258.51	78.39
4/13/2009	125.41	203.79	462.51	258.72	78.38
4/15/2009	126.02	204.23	462.81	258.58	78.21
4/21/2009	125.36	203.88	462.5	258.62	78.52
4/30/2009	125.52	203.55	462.22	258.67	78.03
5/6/2009	125.1	203.91	462.26	258.35	78.81
5/7/2009	124.96	202.96	461.46	258.5	78
5/14/2009	124.8	203.2	461.5	258.3	78.4
5/28/2009	128.86	207.55	465.19	257.64	78.69
6/3/2009	128.47	207.4	465.1	257.7	78.93
6/9/2009	128.01	206.41	464.63	258.22	78.4
6/17/2009	127.85	206.63	464.56	257.93	78.78
6/22/2009	128.19	206.91	465	258.09	78.72
6/24/2009	128.59	207.11	465.2	258.09	78.52
6/26/2009	128.49	206.77	465.31	258.54	78.28
7/9/2009	128.36	207.33	464.9	257.57	78.97
7/13/2009	127.56	205.37	464.59	259.22	77.81
7/15/2009	127.55	205.12	464.56	259.44	77.57
7/20/2009	127.33	206.21	464.44	258.23	78.88
7/22/2009	127.35	205.51	464.2	258.69	78.16
7/24/2009	127.65	205.47	464.48	259.01	77.82
7/28/2009	128.2	206.55	464.9	258.35	78.35
8/4/2009	127.99	206.34	464.59	258.25	78.35
8/12/2009	128.23	206.59	464.78	258.19	78.36
8/13/2009	127.76	206.09	464.63	258.54	78.33
8/18/2009	128.21	206.77	464.9	258.13	78.56
8/19/2009	128.39	206.77	464.97	258.2	78.38

8/24/2009	128.79	206.37	465.19	258.82	77.58
8/26/2009	128.75	206.92	465.37	258.45	78.17
9/1/2009	128.43	206.83	465.2	258.37	78.4
9/8/2009	128.38	206.9	464.9	258	78.52
9/10/2009	128.32	206.91	464.97	258.06	78.59
9/15/2009	127.99	206.55	464.72	258.17	78.56
9/17/2009	127.62	206.43	464.37	257.94	78.81
9/25/2009	127.95	206.2	464.69	258.49	78.25
9/30/2009	127.76	206.5	464.29	257.79	78.74
10/2/2009	128.25	206.72	464.96	258.24	78.47
10/14/2009	129.46	207.75	465.82	258.07	78.29
10/16/2009	129.22	207.65	465.9	258.25	78.43
10/28/2009	129.26	207.26	465.62	258.36	78
11/4/2009	128.23	206.42	465.32	258.9	78.19
2/1/2010	127.23	206.26	464.24	257.98	79.03
2/2/2010	126.94	205.84	463.78	257.94	78.9
Average:	127.32	205.80	464.09	258.29	78.48
Std. Dev.:	1.49	1.48	1.37	0.42	0.40

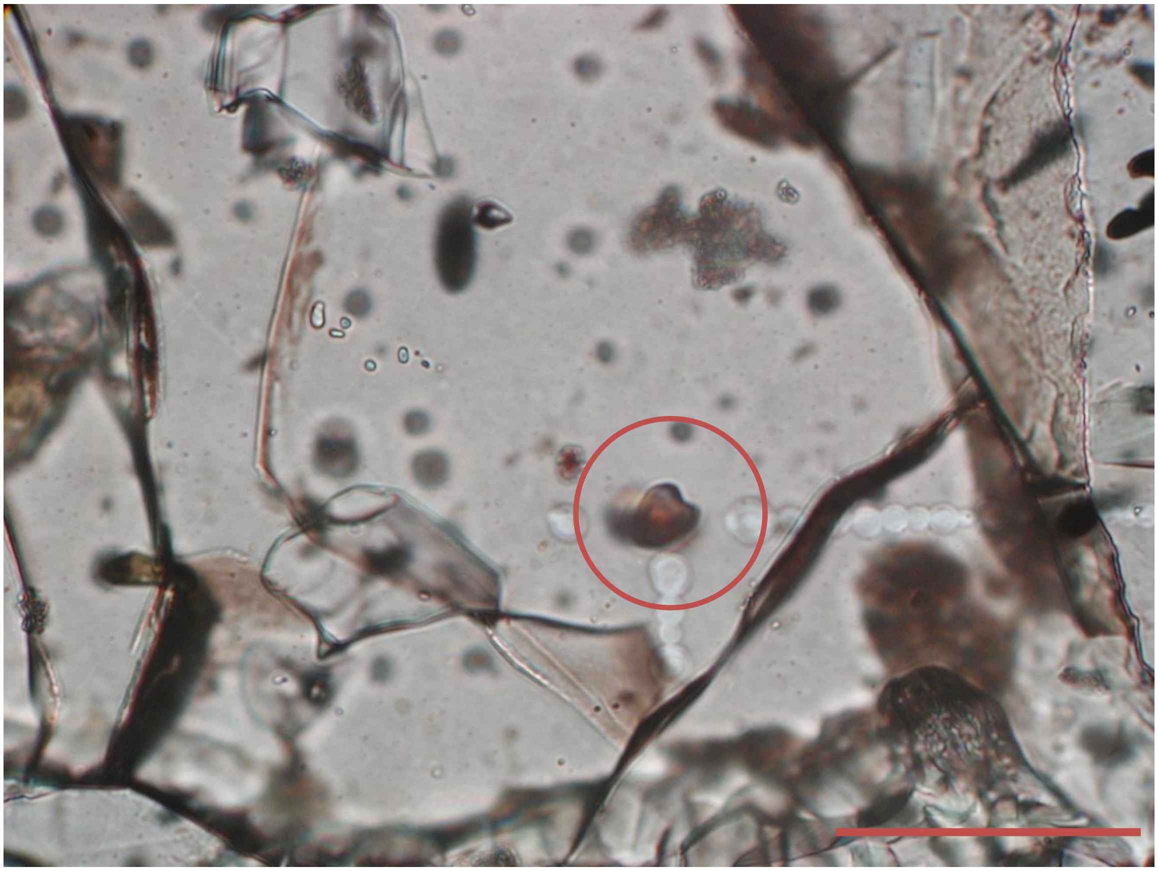

Figure 13: Inclusion from WRMG SR-3. Scale bar is approximately 50 μm.

times, generally for a time period of 300 seconds. In six instances this measurement time was increased due to background noise. Table 3 lists the positions of the three main peaks from those measurements, along with the value of $\Delta\omega_1$ and the calculated entrapment pressure for each of the measurements. A histogram of the $\Delta\omega_1$ values for the WRMG SR-3 inclusion reveals that the results vary over a range of ~6 cm^{-1} (Fig. 14). The average for $\Delta\omega_1$ is 3.7 ± 1.8 cm^{-1}. The standard deviation is more than four times larger than the level of reproducibility for ω_1 on the quartz standard reported above. The average residual pressure is 0.22 ± 0.11 GPa, and the average entrapment pressure is 0.86 ± 0.26 GPa. These levels of reproducibility cannot be referenced to any results from Enami et al. (2007), as they did not publish evidence that they performed comparable tests.

Each of the individual measurements of $\Delta\omega_1$, residual pressure, and entrapment pressure reported below is assigned uncertainties equal to the values obtained from this evaluation of reproducibility.

Localities

Whitt Ranch Eclogites

Twenty-six inclusions from seven Whitt Ranch thin sections were suitable for Raman spectral acquisition (Table 4). A representative inclusion for the Whitt Ranch is from thin section 61, garnet 1 (Fig. 15). The inclusion measured approximately 15.9 µm by 9.5 µm, with a vertical thickness of about 18 µm (Fig. 16). Measurements for this inclusion were made on April 15, 2009. Figure 17 shows the spectrum from the quartz standard on that day plotted at the top, and the spectrum from the inclusion plotted at the bottom. The inclusion was measured for 180 seconds at 6 µm below the surface. The $\Delta\omega_1$ value for this inclusion

Table 3: Data from repeated Raman microspectrometry measurements of WRMG SR-3.

Date of Measurement	Measurement Time (s)	$\Delta\omega_1$	P_{entrap} [$\Delta\omega_1$] (GPa)
6/9/2009	300	2.69	0.71
6/17/2009	1200	4.03	0.90
6/22/2009	600	2.23	0.64
6/24/2009	600	3.36	0.80
6/26/2009	300	4.39	0.95
7/13/2009	600	5.87	1.16
7/15/2009	300	3.28	0.79
7/20/2009	300	5.81	1.16
7/22/2009	600	5.76	1.15
7/24/2009	300	5.82	1.16
8/4/2009	300	1.28	0.50
8/13/2009	300	5.25	1.07
8/24/2009	300	3.32	0.80
8/26/2009	300	2.58	0.69
9/8/2009	300	4.54	0.97
9/10/2009	300	-0.29	0.26
	Average:	3.75	0.86
	Standard Deviation:	1.79	0.26

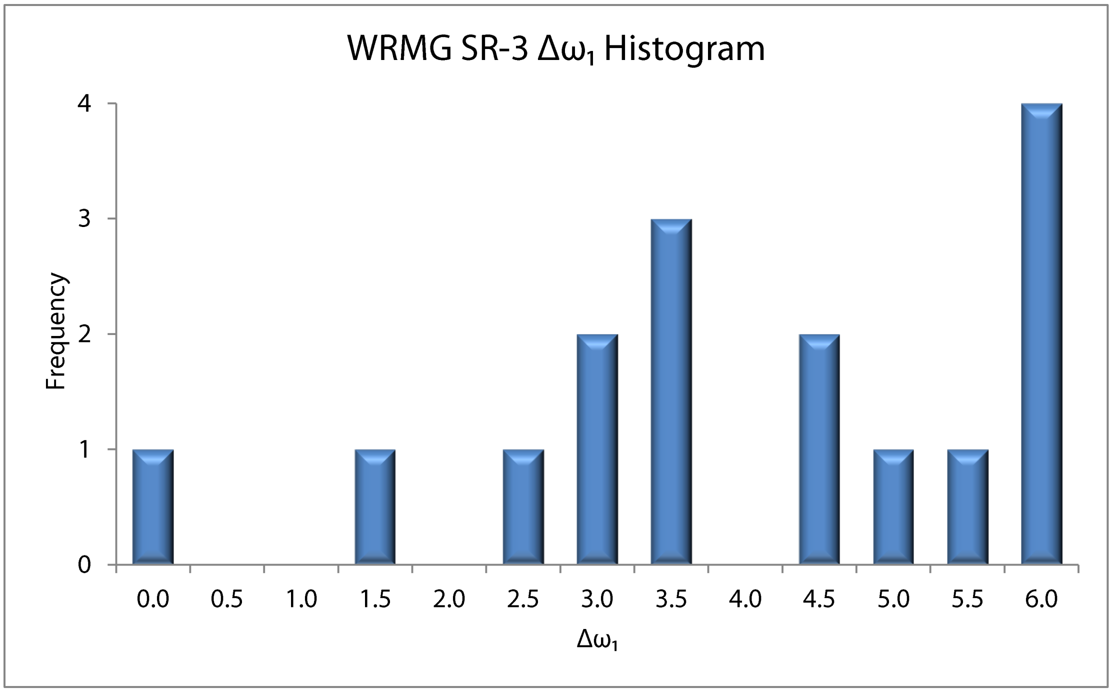

Figure 14: Histogram of $\Delta\omega_1$ values for WRMG SR-3 reproducibility tests. Average $\Delta\omega_1$ is 3.75 cm^{-1}.

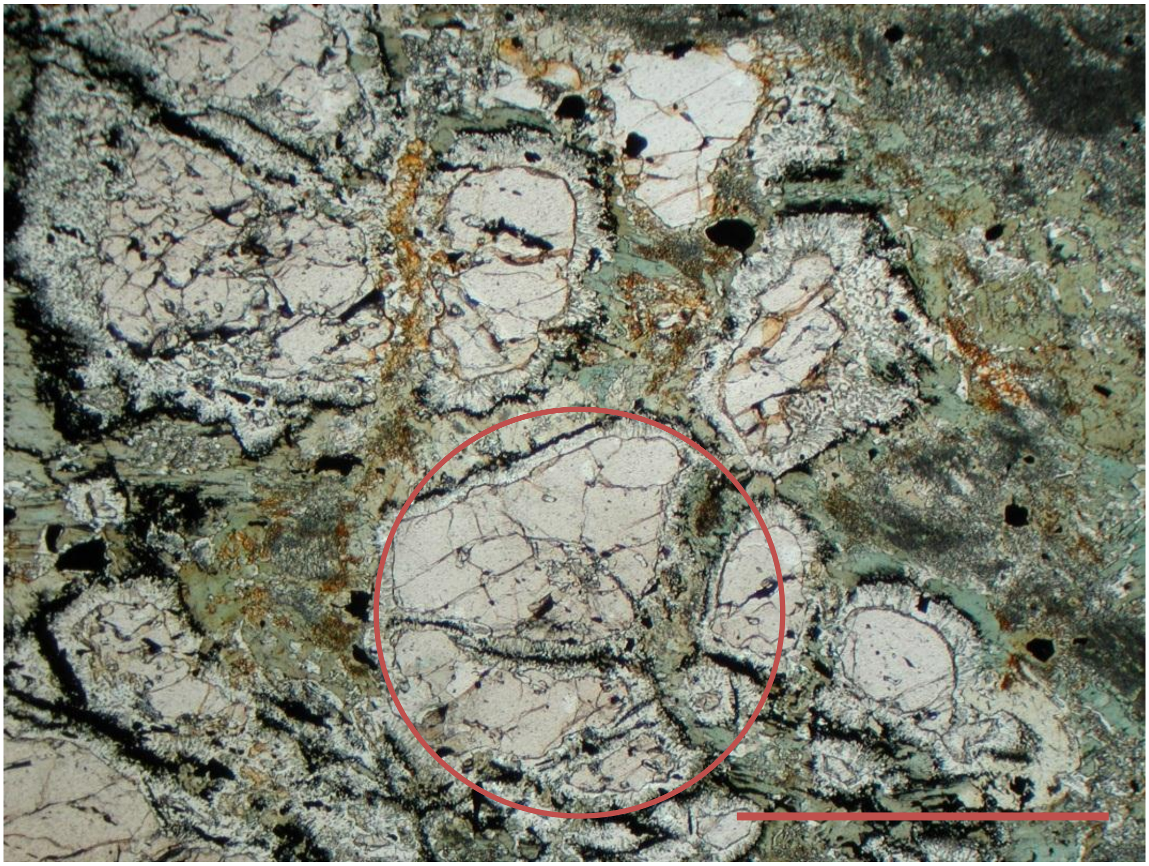

Figure 15: Whitt Ranch eclogite thin section WRMG 61, garnet 1. Scale bar is approximately 2.0 mm.

Table 4: Results from Raman microspectrometry measurements for Whitt Ranch eclogites.

	Thin Section	Garnet	Date of Measurement	Measurement Time (s)	$\Delta\omega_1$	P_{resid} [$\Delta\omega_1$] (MPa)	P_{entrap} [$\Delta\omega_1$] (GPa)
1	WRMG 2	2	4/13/2009	300	4.38	258	0.95
2	WRMG 2	3	8/19/2009	300	6.04	354	1.19
3	WRMG 2	4	8/19/2009	300	3.10	184	0.77
4	WRMG 2	5	8/19/2009	600	2.14	128	0.63
5	WRMG 2	6	8/24/2009	300	5.54	325	1.12
6	WRMG 2	7	8/24/2009	300	7.40	436	1.39
7	WRMG 2	9	8/24/2009	300	9.05	541	1.65
8	WRMG 56	1	4/21/2009	300	-0.96	-61	0.16
9	WRMG 56	2	7/13/2009	180	6.28	369	1.22
10	WRMG 56	3	7/15/2009	300	2.82	168	0.73
11	WRMG 56	4	7/15/2009	300	4.33	255	0.94
12	WRMG 56	6	7/15/2009	300	2.69	160	0.71
13	WRMG 56	7	7/15/2009	300	1.78	107	0.57
14	WRMG 60	1	6/3/2009	1200	-0.14	-9	0.29
15	WRMG 60	4	7/20/2009	300	0.13	8	0.33
16	WRMG 60	5	7/20/2009	300	5.00	294	1.04
17	WRMG 60	7	7/20/2009	300	0.83	51	0.43
18	WRMG 60	9	7/22/2009	600	9.67	582	1.76
19	WRMG 61	1	4/15/2009	180	2.27	136	0.65
20	WRMG 61	4	7/24/2009	300	2.26	135	0.64
21	WRMG 61	5	7/28/2009	300	1.26	77	0.50
22	WRMG 61	6	7/28/2009	300	-0.33	-21	0.26
23	WRMG 61	7	7/28/2009	300	-0.95	-60	0.16
24	WRMG 90	1	5/14/2009	300	-1.43	-92	0.08
25	WRMG 1036	2	4/2/2009	720	-2.49	-164	-0.10
26	WRMG SR-3	1	6/9/2009	300	2.69	160	0.71

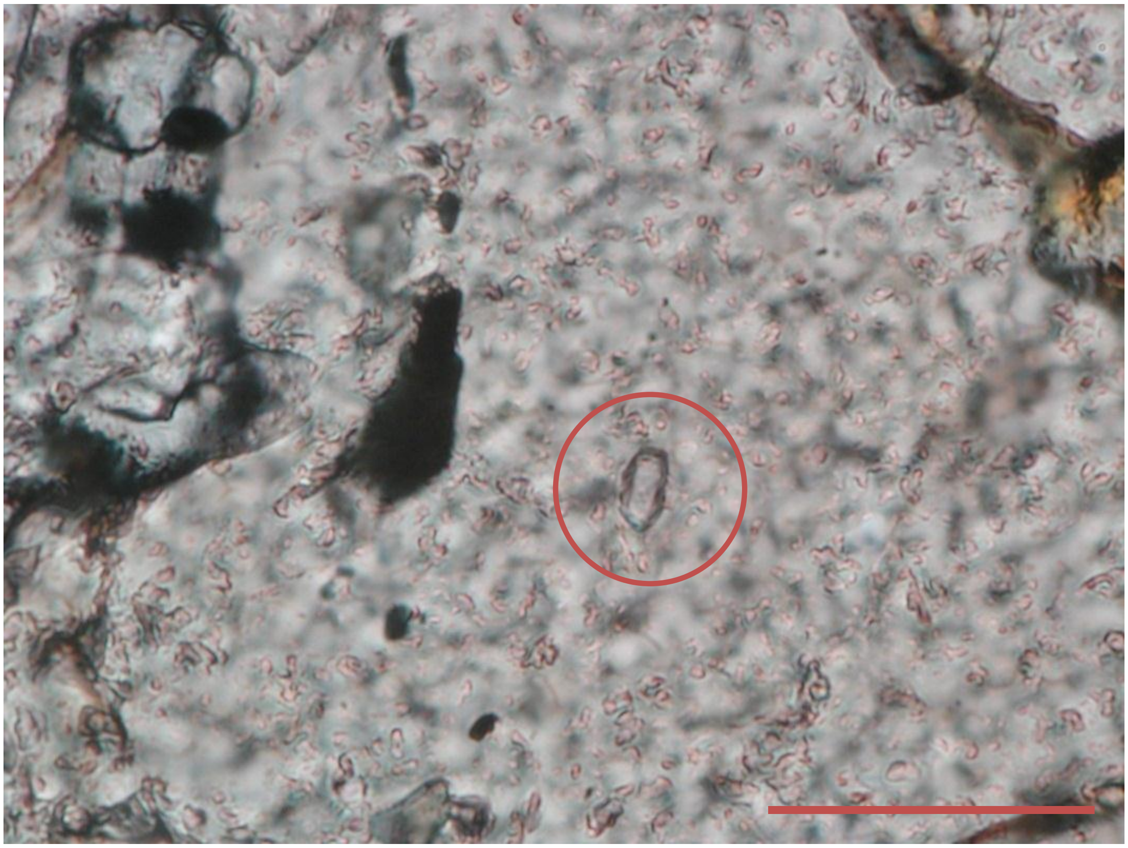

Figure 16: Quartz inclusion from WRMG 61, garnet 1 is circled. It measures 14.2 μm by 7.9 μm. Scale bar is approximately 50 μm.

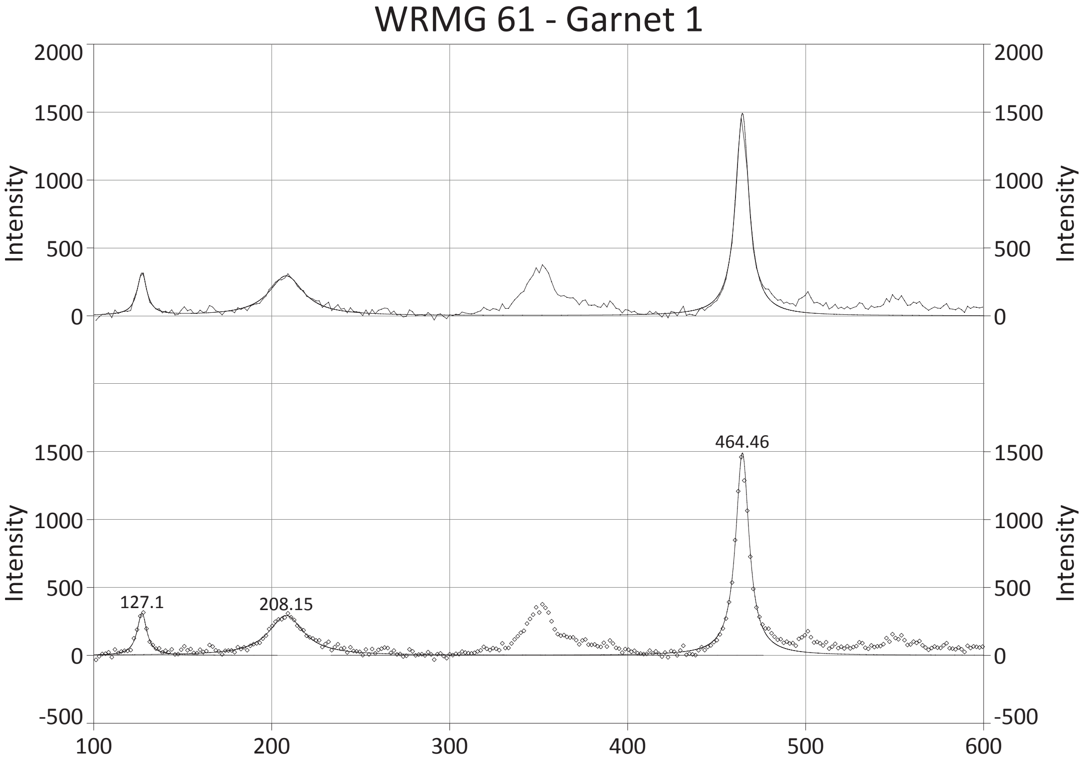

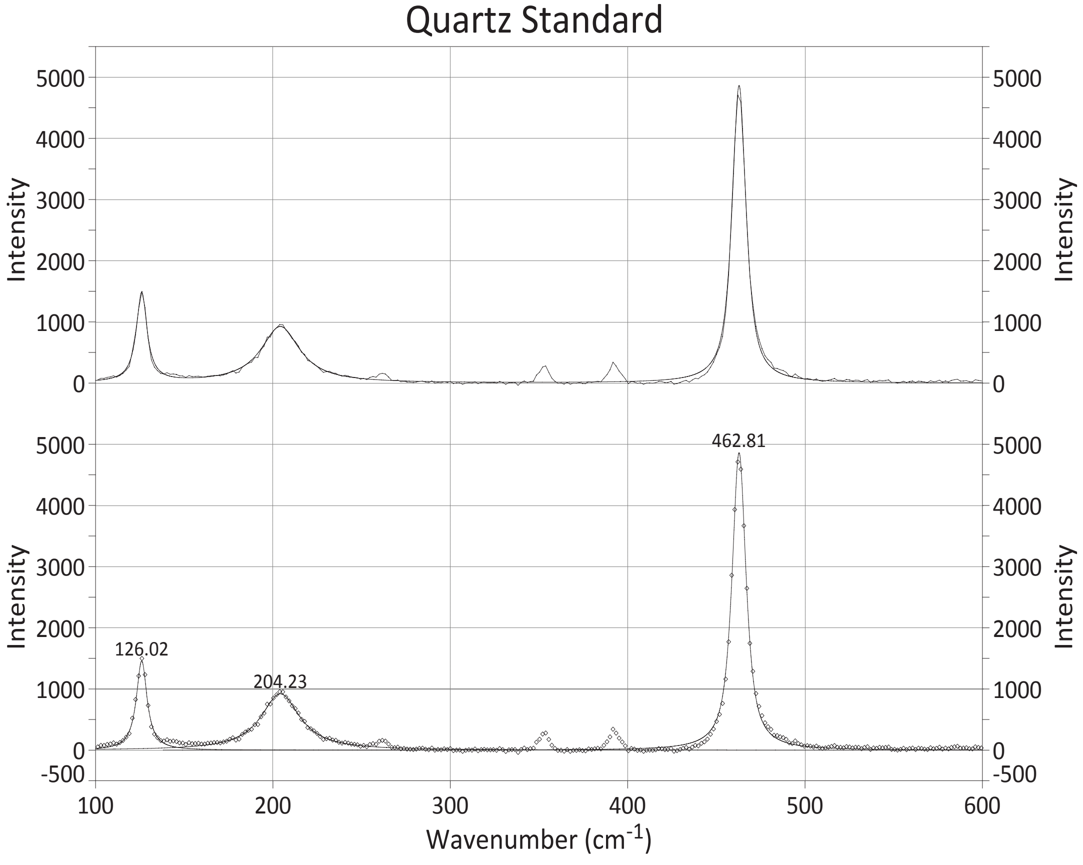

Figure 17: Measurements from April 15, 2009 of WRMG 61 garnet 1 and quartz standard.

was 2.3 ± 1.8 cm^{-1}. Using the calibration of Schmidt and Ziemann (2000), the residual pressure retained in the inclusion is 0.14 ± 0.11 GPa. From Van der Molen's (1981) elastic model, the entrapment pressure for the inclusion is 0.65 ± 0.26 GPa.

The entrapment pressure for this inclusion lies at the center of a histogram of all Whitt Ranch entrapment pressures (Fig. 18). The histogram shows that entrapment pressures for Whitt Ranch range between -0.1 GPa and 1.8 GPa, but cluster near 0.6-0.7 GPa. The expected entrapment pressure for Whitt Ranch is a minimum of 1.4 ± 0.1 GPa, based on GRIPS barometry. Only one Whitt Ranch inclusion had an entrapment pressure of 1.4 GPa, and 3 of the 26 inclusions were above 1.4 GPa. The majority of Whitt Ranch quartz inclusions are in a range of entrapment pressures that could be considered geologically reasonable, though grossly inconsistent with conventional barometry. However, 7 of 26 inclusions plot at or below 0.3 GPa, which is approximately the lowest pressure at which garnet should be stable in rocks of this bulk composition.

Purdy Hill Eclogites

A total of 18 suitable inclusions was found in four thin sections from the retrogressed Purdy Hill eclogite (Table 5). A representative sample is from thin section PH 97-29, garnet 1 (Fig. 19). This inclusion is 22.1 μm by 12.6 μm, and approximately 14 μm thick (Fig. 20). Measurements for this inclusion were made on August 26, 2009 for 300 seconds at 2 μm below the surface. Figure 21 includes the spectra for both the quartz standard and the inclusion. The $\Delta\omega_1$ value for this inclusion is -2.26 ± 1.8 cm^{-1}. The calculated residual pressure is -0.15 ± 0.11 GPa, and the calculated entrapment pressure is 0.01 ± 0.26 GPa.

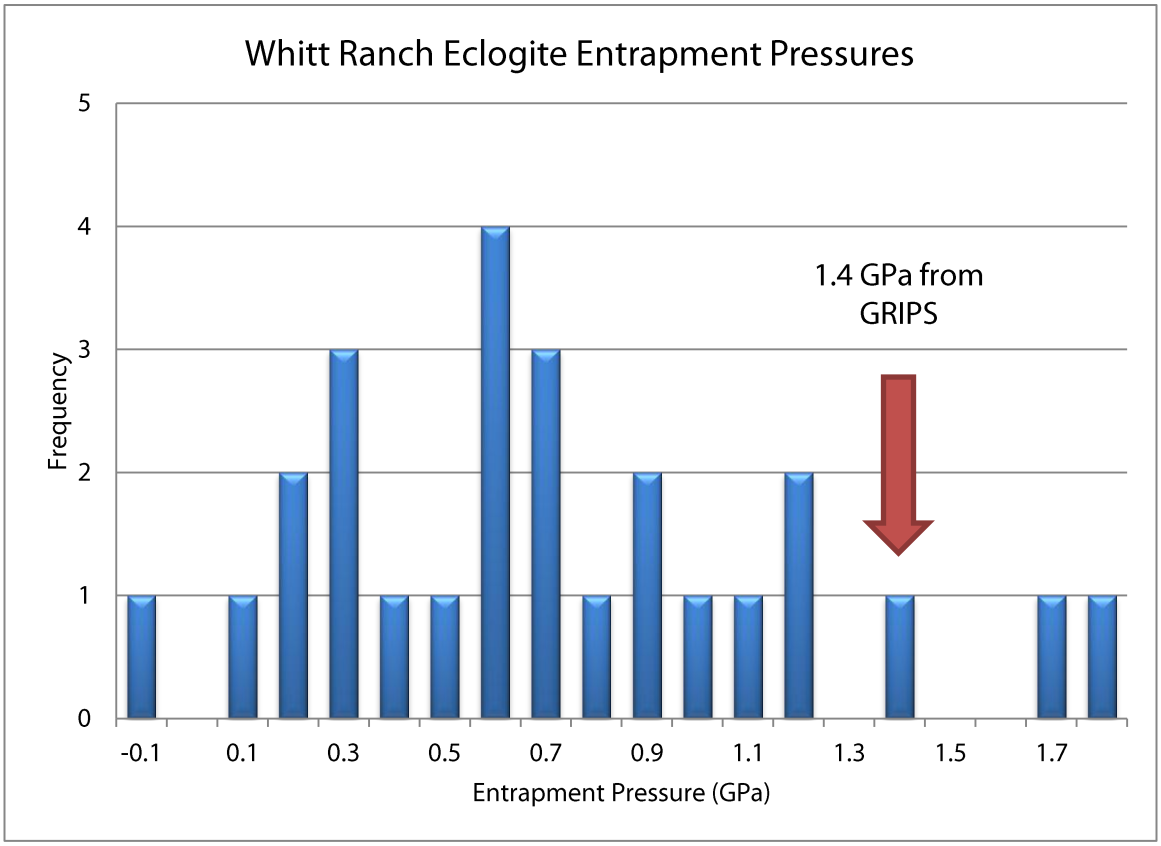

Figure 18: Histogram of entrapment pressures for all Whitt Ranch eclogites. Expected entrapment pressure based on GRIPS barometry is indicated by the arrow at 1.4 GPa.

Table 5: Results from Raman microspectrometry measurements for Purdy Hill eclogites.

	Thin Section	Garnet	Date of Measurement	Measurement Time (s)	$\Delta\omega_1$	P_{resid} [$\Delta\omega_1$] (MPa)	P_{entrap} [$\Delta\omega_1$] (GPa)
1	PH 97-29	1	8/26/2009	300	-2.28	-149	0.01
2	PH 97-29	2	9/1/2009	300	-2.26	-148	0.01
3	PH 97-29	3	9/1/2009	300	0.29	18	0.42
4	PH 97-29	4	9/1/2009	300	1.12	68	0.55
5	PH 97-29	5	9/8/2009	300	-1.17	-74	0.19
6	PH 97-33	1	9/10/2009	300	1.06	65	0.54
7	PH 97-33	2	9/15/2009	300	1.32	80	0.58
8	PH 97-33	3	9/15/2009	300	-0.92	-58	0.23
9	PH 97-33	4	9/15/2009	300	-1.78	-115	0.09
10	PH 97-33	5	9/17/2009	300	-1.71	-110	0.10
11	PH 97-62	2	9/17/2009	300	-5.77	-418	-0.64
12	PH 97-62	3	9/25/2009	300	-8.87	-716	-1.39
13	PH 97-62	4	9/30/2009	300	-2.08	-135	0.06
14	PH 97-62	5	10/2/2009	300	-6.74	-504	-0.86
15	PH 97-62	6	10/2/2009	300	-3.70	-251	-0.23
16	PH 97-62	7	10/2/2009	300	-6.91	-520	-0.90
17	PH 97-63b	1	9/17/2009	300	0.42	26	0.46
18	PH 97-63b	2	9/17/2009	300	-3.59	-243	-0.21

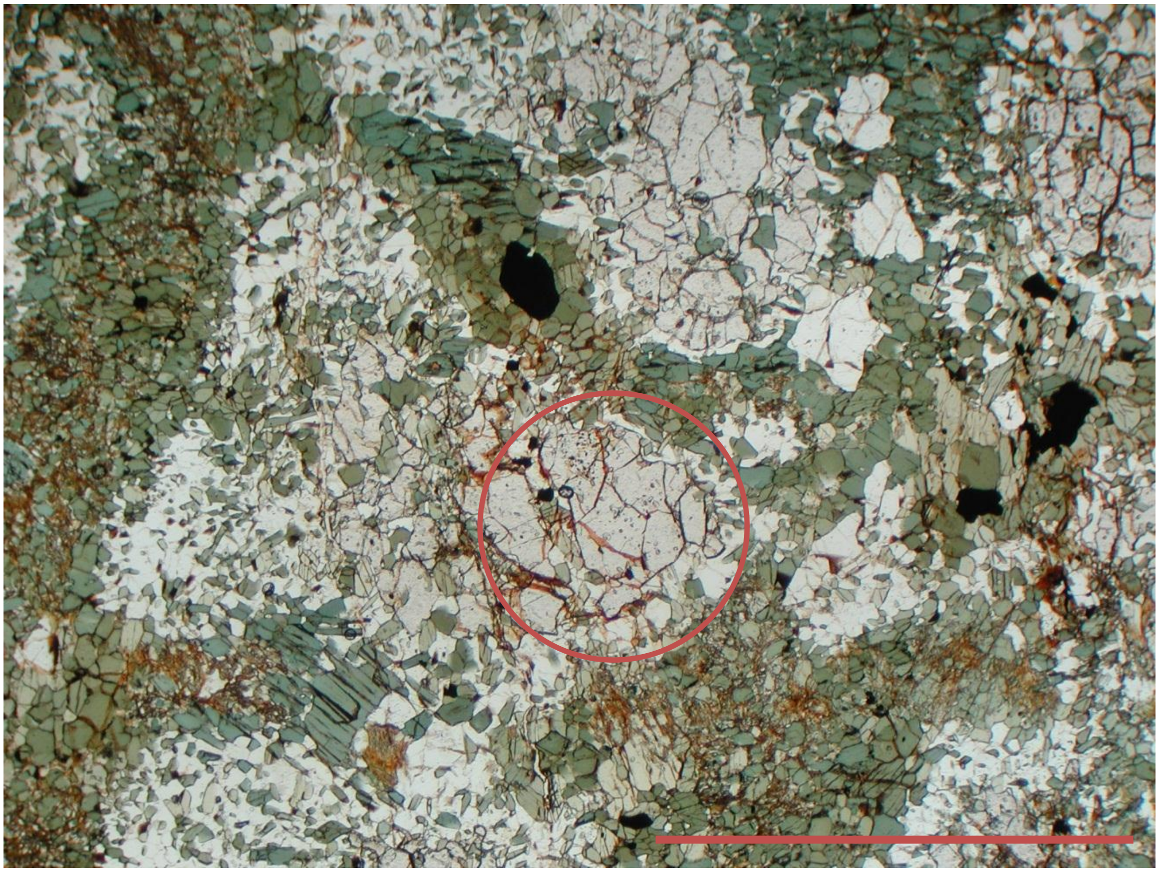

Figure 19: Garnet in Purdy Hill thin section 29, garnet 1. Scale bar represents approximately 2 mm.

Figure 20: Quartz inclusion from PH 97-29, garnet 1 (circled). It measures 22.1 μm by 12.6 μm. Scale bar represents approximately 50 μm.

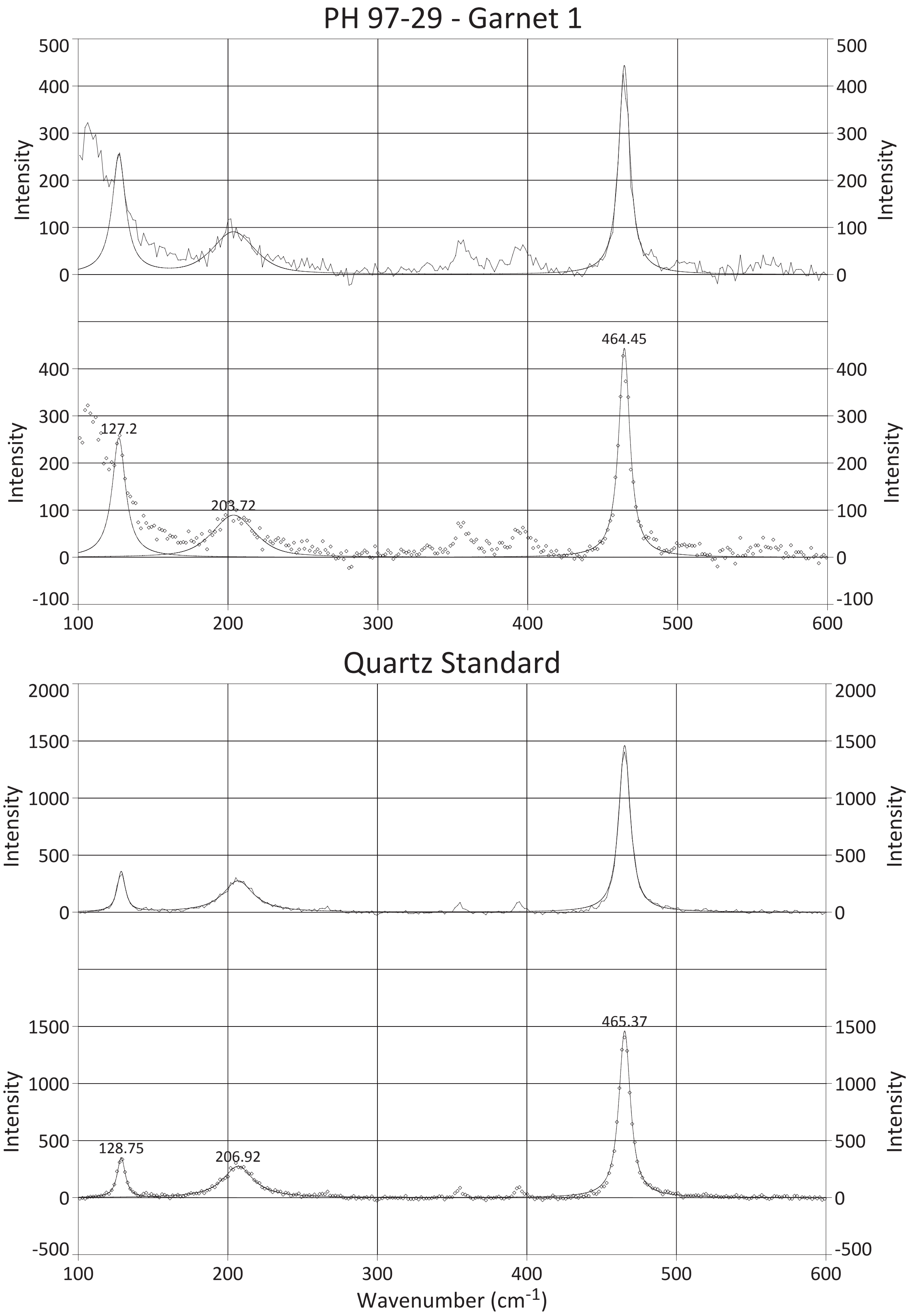

Figure 21: Measurements from August 26, 2009 of PH 97-29 garnet 1 and quartz standard.

This representative inclusion falls within a wide range of entrapment pressures for Purdy Hill eclogite garnets, from -1.4 GPa to 0.6 GPa (Fig. 22). The entrapment pressures are concentrated between 0.1 and 0.6 GPa without a clearly defined cluster of commonly encountered values. Expected entrapment pressures for Purdy Hill eclogitic garnets are between 1.6 and 2.4 GPa. No inclusion is calculated to have been trapped at pressures greater than 0.6 GPa. Of the 18 inclusions, 13 have entrapment pressures below the approximate minimum for garnet stability (~0.3 GPa).

Purdy Hill Felsic Gneisses

Four thin sections from the Purdy Hill felsic gneisses yielded 19 inclusions suitable for laser Raman microspectrometry (Table 6). A representative inclusion for the quartzofeldspathic gneisses is LU02-6, garnet K (Fig. 23). This sample is from a "thick" section and the inclusion is 28.4 by 23.7 μm, with a vertical thickness of 25 μm (Fig. 24). The inclusion was measured on June 24, 2009 for 300 seconds at 8 μm below the surface. Figure 25 is a plot of the spectra from both the quartz standard and inclusion. The $\Delta\omega_1$ value for this inclusion is -3.6 ± 1.8 cm^{-1}. The calculated residual pressure is 0.00 ± 0.11 GPa, and the entrapment pressure is 0.40 ± 0.26 GPa.

The histogram of entrapment pressures for Purdy Hill felsic gneisses is shown in Figure 26 and has a range from -1.2 to 0.9 GPa. Two groups are present, one centered near −0.2 GPa and one centered near 0.5-0.6 GPa. Only two of the inclusions do not have entrapment pressures within these groups.

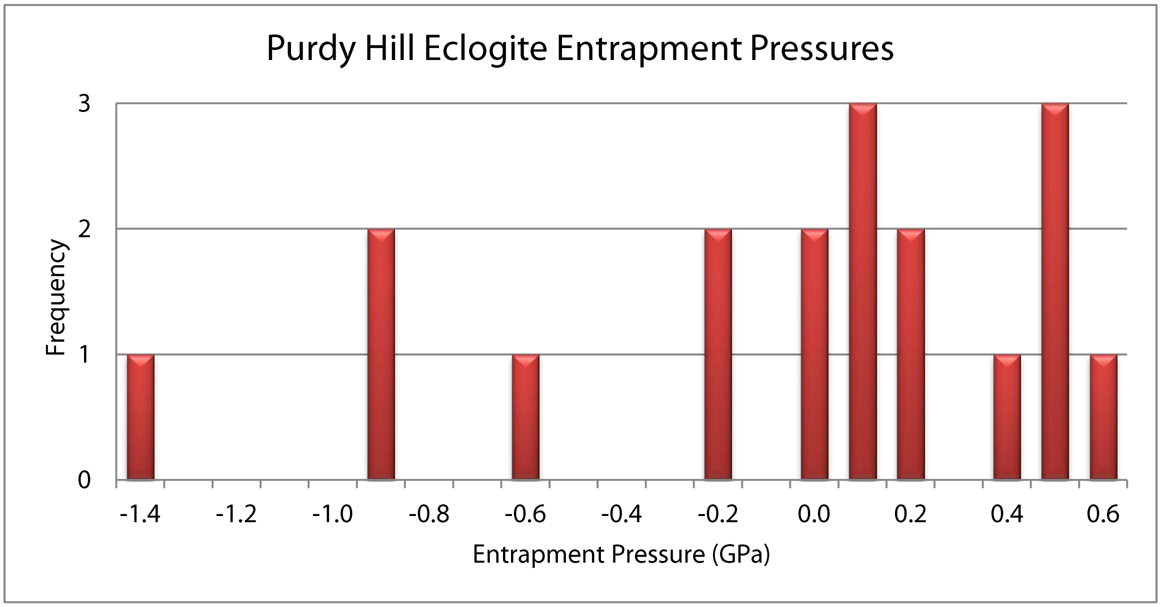

Figure 22: Entrapment pressure (GPa) histogram from Purdy Hill eclogites. Expected pressures should be between 1.6 and 2.4 GPa.

Table 6: Results from Raman microspectrometry measurements for Purdy Hill felsic gneisses.

	Thin Section	Garnet	Date of Measurement	Measurement Time (s)	$\Delta\omega_1$	P_{resid} [$\Delta\omega_1$] (MPa)	P_{entrap} [$\Delta\omega_1$] (GPa)
1	LU 02-6	E	11/4/2009	300	-2.72	-180	-0.04
2	LU 02-6	G	11/4/2009	300	1.52	92	0.63
3	LU 02-6	J	11/4/2009	600	-3.42	-230	-0.17
4	LU 02-6	K	6/24/2009	300	-0.01	-1	0.40
5	LU 02-6	X	10/28/2009	300	-3.02	-201	-0.10
6	LU 02-8	G	10/28/2009	300	-8.30	-656	-1.23
7	LU 02-8	H	8/4/2009	300	-4.75	-333	-0.42
8	LU 02-8	I	10/16/2009	300	1.01	62	0.56
9	LU 02-8	K	10/28/2009	300	0.18	11	0.43
10	LU 02-8	L	8/4/2009	300	-3.31	-222	-0.15
11	LU 02-9	D	6/22/2009	600	-3.56	-241	-0.19
12	LU 02-9	F	2/2/2010	360	1.74	105	0.67
13	LU 02-9	G	2/2/2010	300	1.45	88	0.62
14	LU 02-9	H	2/2/2010	300	-0.92	-58	0.26
15	LU 02-9	I	2/2/2010	300	3.20	190	0.88
16	LU 02-10	B	2/1/2010	300	2.23	134	0.74
17	LU 02-10	D	2/2/2010	1200	-4.22	-291	-0.32
18	LU 02-10	E	2/2/2010	300	-0.58	-36	0.32
19	LU 02-10	G	2/1/2010	300	-4.85	-341	-0.44

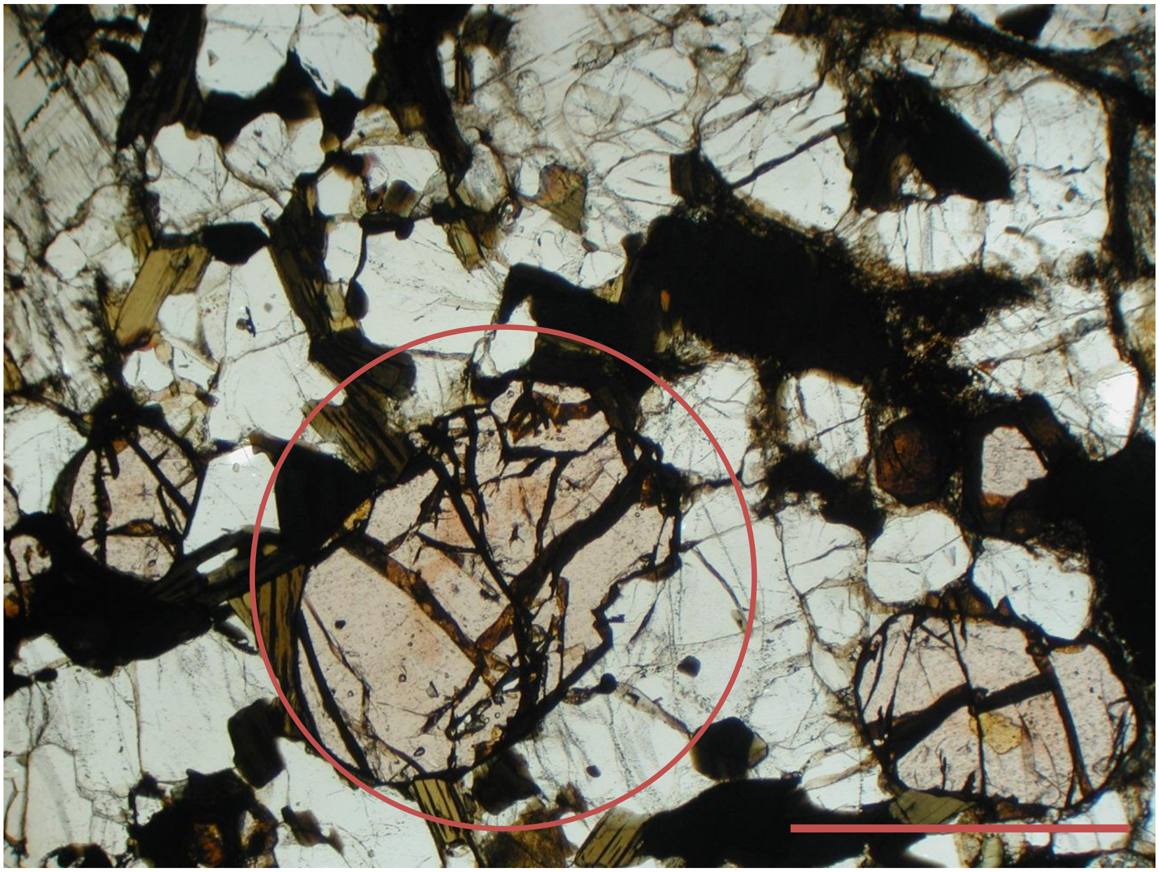

Figure 23: Photomicrograph of Purdy Hill felsic gneiss sample LU 02-6, garnet K. Scale bar represents approximately 2.0 mm.

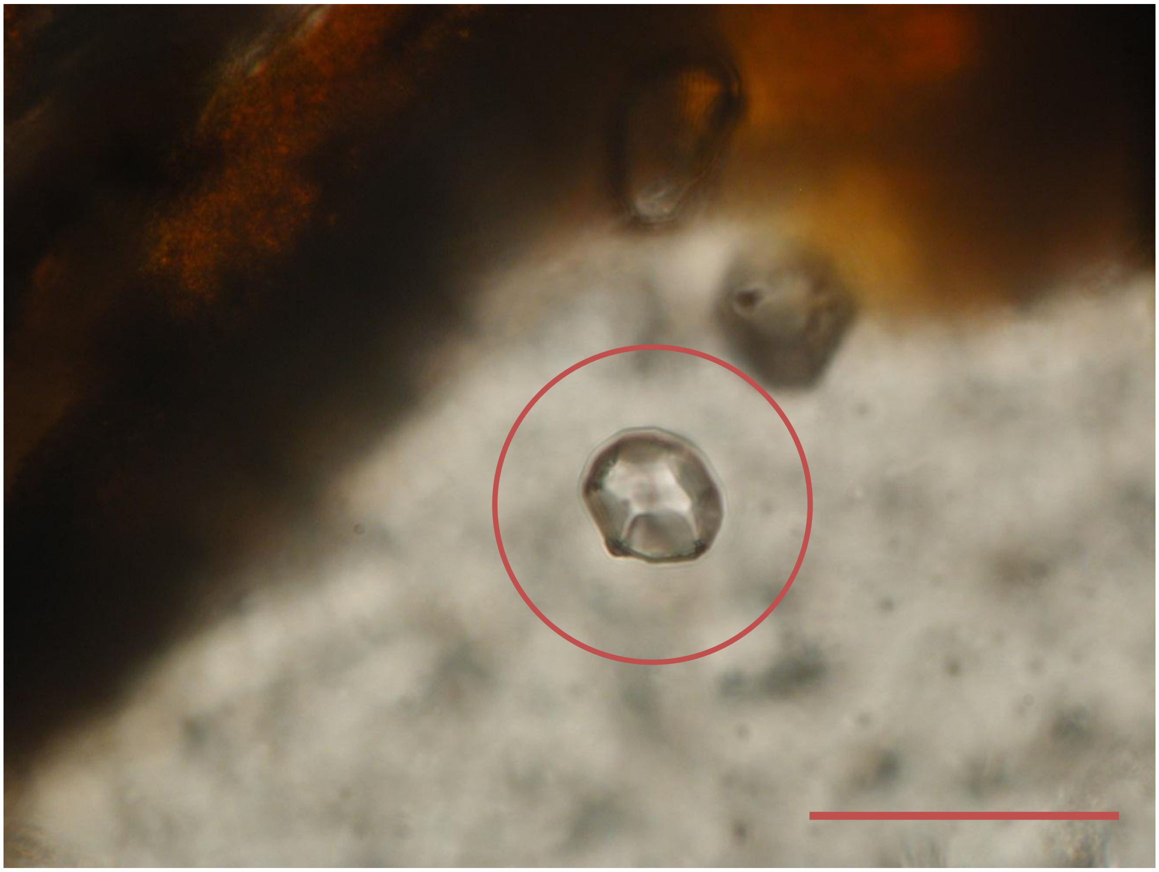

Figure 24: Photomicrograph of quartz inclusion from LU 02-6 garnet K (circled), 28.4 µm by 23.7 µm. This is a thicker-than-normal thin section, and scale bar represents approximately 50 µm.

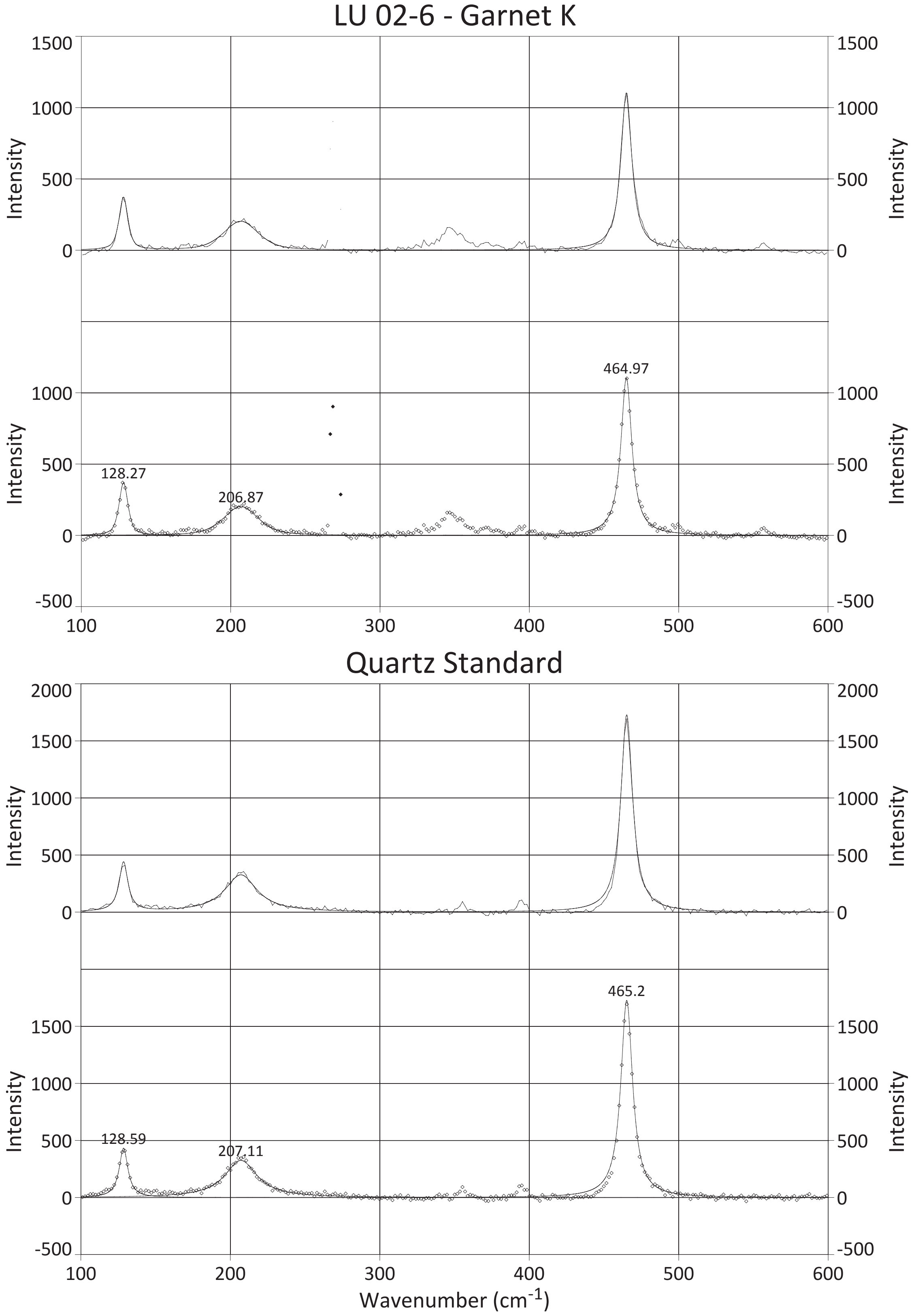

Figure 25: Measurements from June 24, 2009 of LU 02-6 garnet K and quartz standard.

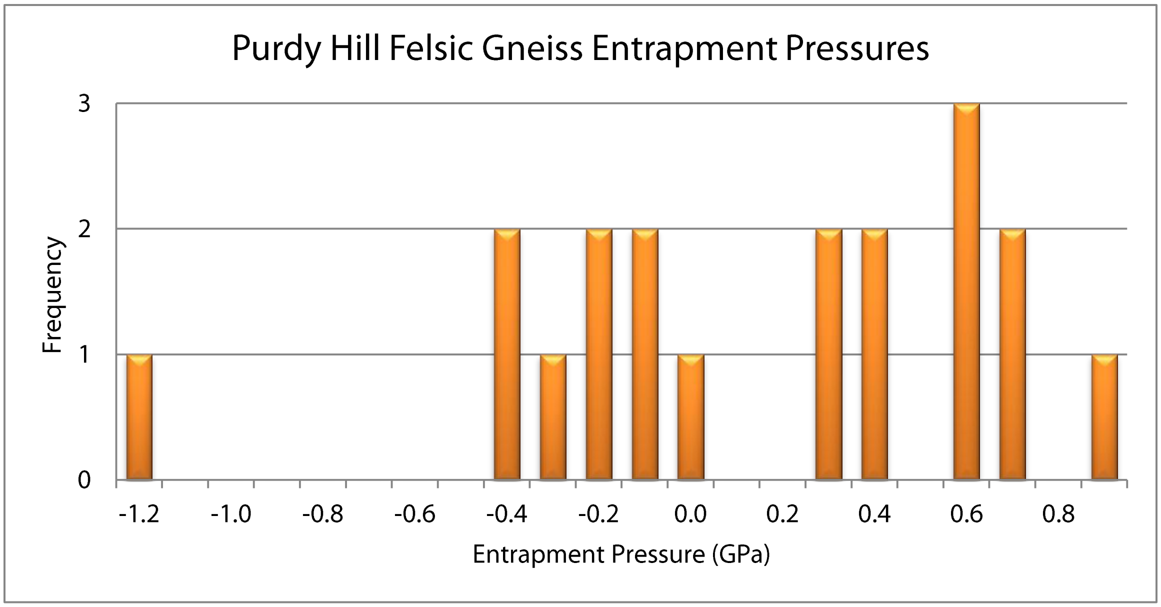

Figure 26: Histogram of entrapment pressures (GPa) for Purdy Hill gneisses. Expected pressures should range between 1.6 and 2.4 GPa, based on conventional barometry from Purdy Hill eclogites.

DISCUSSION

The results from the quartz standard, the reproducibility test, and from each locality will be discussed individually, followed by a comparison of the locality results and the implications for future work. Finally, the potential effects on residual or entrapment pressure from the elastic model or errors during measurement will be discussed.

Quartz Standard

Positions of peaks for the quartz standard varied significantly over the 15-month course of this study: the standard deviation of peak positions was 1.3-1.4 cm^{-1}. However, all peaks are offset by the same amount. The usefulness of the ω_1 calculation is made clear here because the standard deviation of the ω_1 value over the same 15 months is ± 0.4 cm^{-1}. The cause of the offset of the three quartz peak positions from one month to the next, although unknown, is relatively inconsequential because the equivalent offsets for the 464 cm^{-1} and 205 cm^{-1} peaks cancel in the ω_1 calculation. This small uncertainty in the ω_1 value is similar to that observed by Enami et al. (2007), who report a standard deviation of ± 0.3 cm^{-1}, implying that measurements from this study should be comparable in quality to those from the previous study.

Causes for the variation of peak positions for the quartz standard are unknown, but one potential cause is variability in air temperature due to heating or cooling throughout the year. The microspectrometry lab has a high-quality independent thermostat regulated to a specific temperature, so this should not be the reason for the change in peak location. Another cause could be instrumental. The method at the microspectrometry lab was carefully developed to prevent instrument errors; however, the instrument was part of a multi-user facility so alignment could potentially change over time. Alignment issues are regarded as the most likely cause of the variations in peak positions over time.

Reproducibility Test

No reproducibility test was reported by Enami et al., so the present results are the only evaluation of the precision of the technique. The $\Delta\omega_1$ values measured in the reproducibility test are spread over a wider range than those for the quartz standard, with a standard deviation of 1.8 cm^{-1}. Notably, the disparity of $\Delta\omega_1$ values cannot be linked to variations over time (Fig. 27). The precision of the technique is restricted to an uncertainty of ± 1.8 cm^{-1}, which corresponds to an uncertainty of ± 0.26 GPa for entrapment pressure.

Localities

Whitt Ranch Eclogites

The three major quartz peaks from all Whitt Ranch inclusions were all displaced to higher wavenumbers relative to the quartz standard, with the exception of one inclusion. A positive displacement is expected for inclusions under compression, whereas inclusions under tension have negative displacements. The implication is that there is a real residual pressure retained within the quartz inclusions from the Whitt Ranch locality.

However, results from the Whitt Ranch eclogites suggest the method, in this application, is not as reliable as the results of Enami et al. (2007) would indicate. The entrapment pressures measured via Raman microspectrometry do not come close to approximating pressures estimated by conventional barometry. The main cluster of entrapment pressures at 0.6 GPa is lower than the expected entrapment pressure of 1.4 GPa by an amount much greater than the 0.26 GPa uncertainty identified in the reproducibility

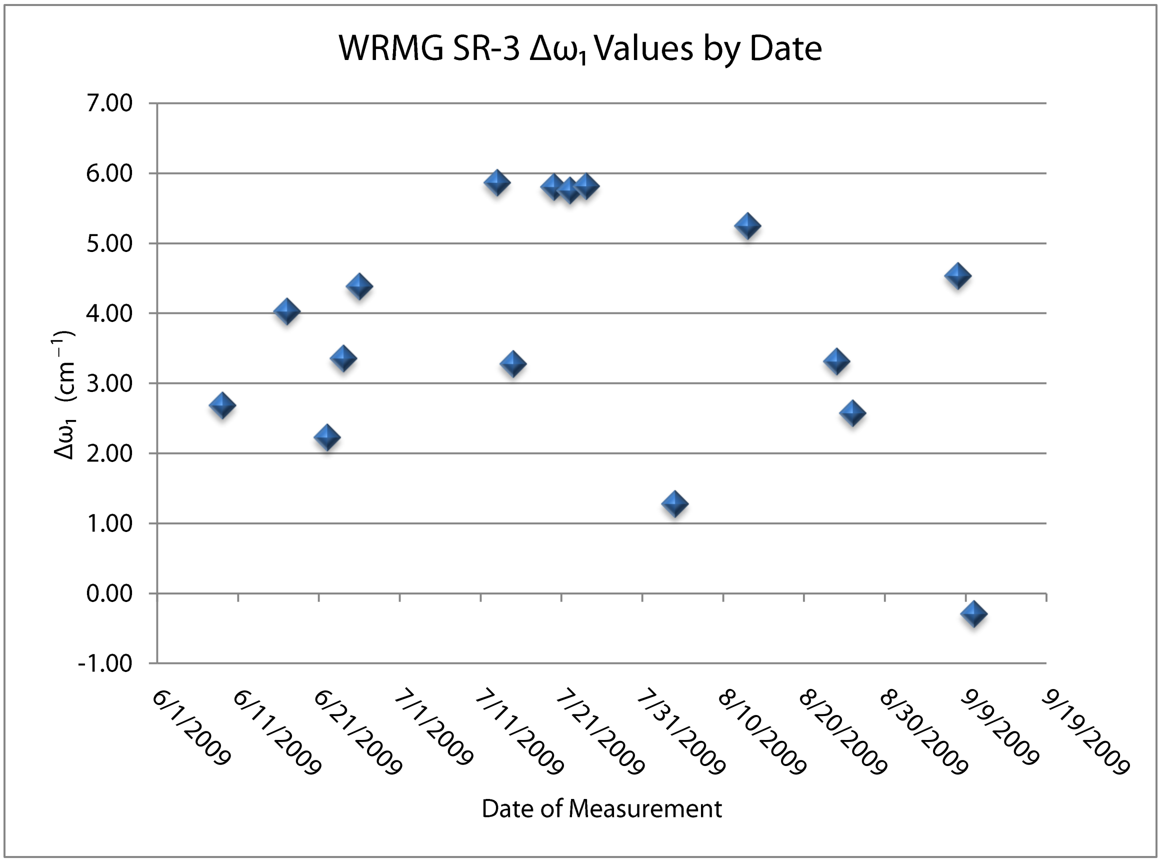

Figure 27: Plot of WRMG SR-3 $\Delta\omega_1$ values by date, showing that no correlation exists between date of measurement and $\Delta\omega_1$ value.

approximating pressures estimated by conventional barometry. The main cluster of entrapment pressures at 0.6 GPa is lower than the expected entrapment pressure of 1.4 GPa by an amount much greater than the 0.26 GPa uncertainty identified in the reproducibility test. In fact, only 5 of the 26 measured inclusions fall within ± 0.26 GPa of the expected entrapment pressure

An attempt was made to disregard "poor quality" data to see if this improved the distribution of entrapment pressures. Data quality was ranked qualitatively by examining signal-to-noise ratios in each inclusion's spectrum; inclusions with a high ratio were easy to fit and were given a rank of 5; inclusions with a low ratio were difficult to fit because the signal barely stood out from the noise, so these were given a rank of 1. Whitt Ranch entrapment pressures were replotted by rank (Fig. 28). There was no correlation between entrapment pressures and quality ranking: a good quality spectrum was just as likely to produce a low entrapment pressure as a poor quality spectrum.

Another source of erroneous entrapment-pressure data could be Raman measurements made on non-spherical inclusions. Internal stresses within these types of inclusions are not modeled accurately by Van der Molen's (1981) spherical-inclusion model. Though most natural quartz crystals are not spherical, it is possible that extremely oblong or ellipsoid inclusions would preserve consistently different pressures. This hypothesis was tested via a calculation of each inclusion's aspect ratio, comparing the maximum dimension to the minimum dimension, and plotting this ratio relative to the inclusion's entrapment pressure (Fig. 29). However, this figure clearly shows that no correlation exists between an inclusion's sphericity and its entrapment pressure.

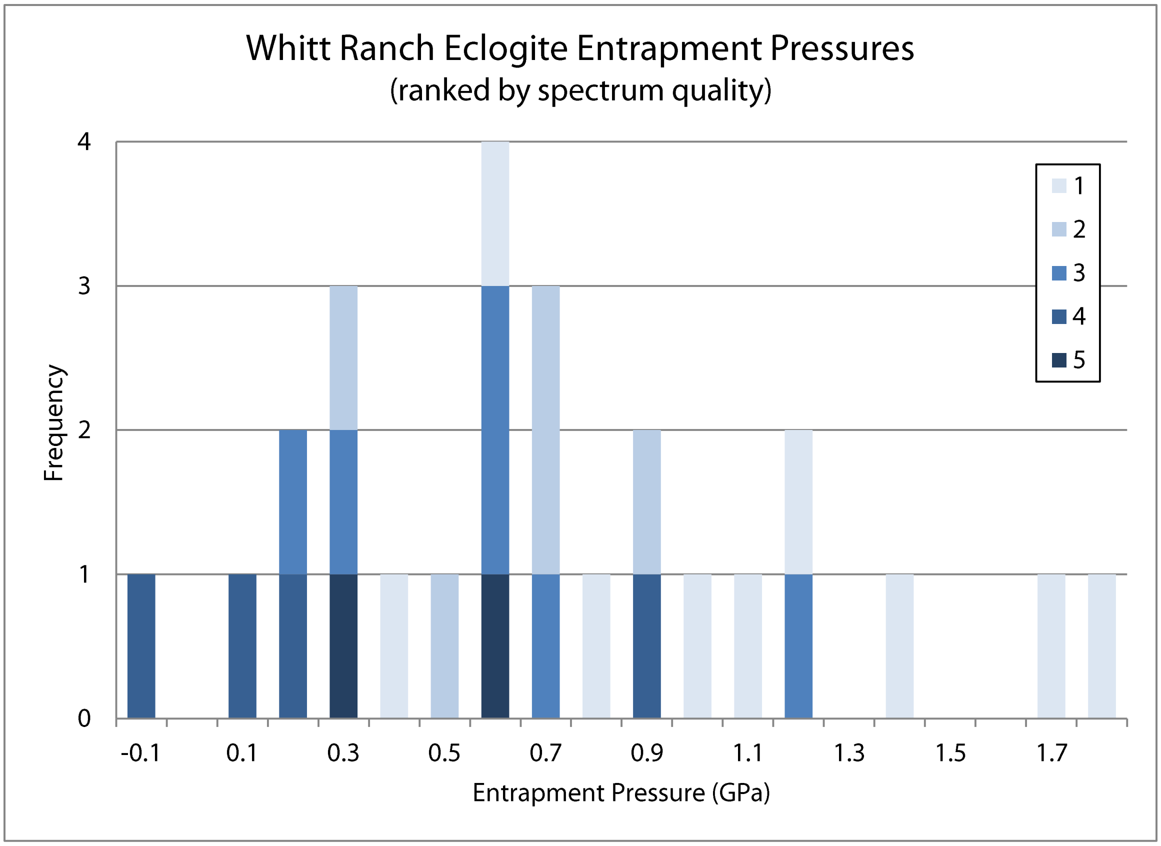

Figure 28: Histogram of ranked entrapment pressures for the Whitt Ranch eclogites. Low quality data are ranked (1) and high quality data are ranked (5).

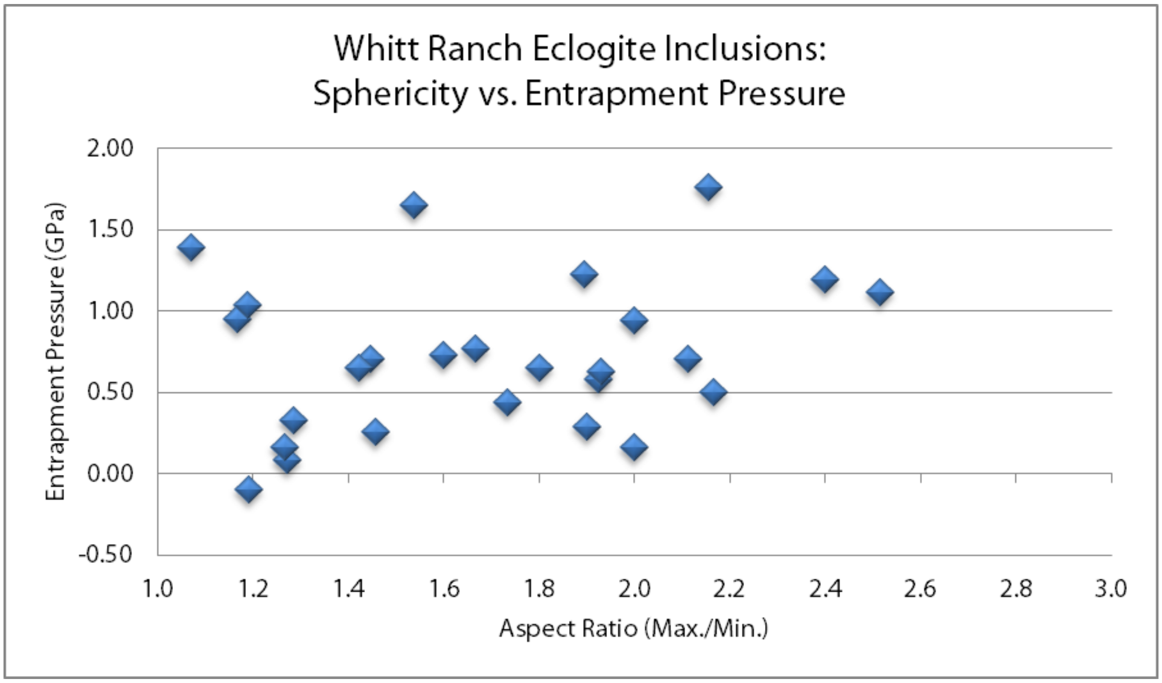

Figure 29: Comparison of aspect ratios with entrapment pressures for all Whitt Ranch eclogite inclusions, showing that no correlation exists between an inclusion's sphericity and its calculated entrapment pressure.

Purdy Hill Eclogites

The $\Delta\omega_1$ values for the Purdy Hill eclogites are predominately negative (cf. Table 5), suggesting the garnet-quartz relationship is tensional rather than compressional. The maximum pressure in the histogram is only 0.6 ± 0.26 GPa, well below the expected pressure range of 1.6 to 2.4 GPa from conventional barometry. The range of entrapment pressures measured from Purdy Hill eclogite inclusions is substantially wider than ±0.26 GPa, indicating the pressure spread is due to more than just instrumental imprecision. Only 10 of the 18 inclusions have entrapment pressures that fall above the rough minimum of garnet stability at 0.3 GPa, or within 0.26 GPa below that limit. Ranking the entrapment pressures by quality does not lead to any correlation between entrapment pressure and quality ranking (Fig. 30). Plotting the sphericity of each inclusion versus its entrapment pressure also yields no correlation (Fig. 31).

Purdy Hill Felsic Gneisses

Results from the Purdy Hill felsic gneisses are similar to the unreasonably low entrapment pressures from the Purdy Hill eclogites. No result suggests that these inclusions were entrapped at the expected 1.6 to 2.4 GPa pressures predicted by conventional barometry. The maximum entrapment pressure measured at this locality is 0.9 ± 0.26 GPa, which is still ~0.5 GPa lower than expected. Clearly, the range of entrapment pressures measured from the Purdy Hill felsic gneisses cannot be exclusively explained by instrumental imprecision. Only 10 of the 19 inclusions yield entrapment pressures above the garnet stability minimum at ~0.3 GPa, and 9 of the 19 yield negative entrapment pressures. One potential explanation for low entrapment pressures in the felsic gneisses could be linked

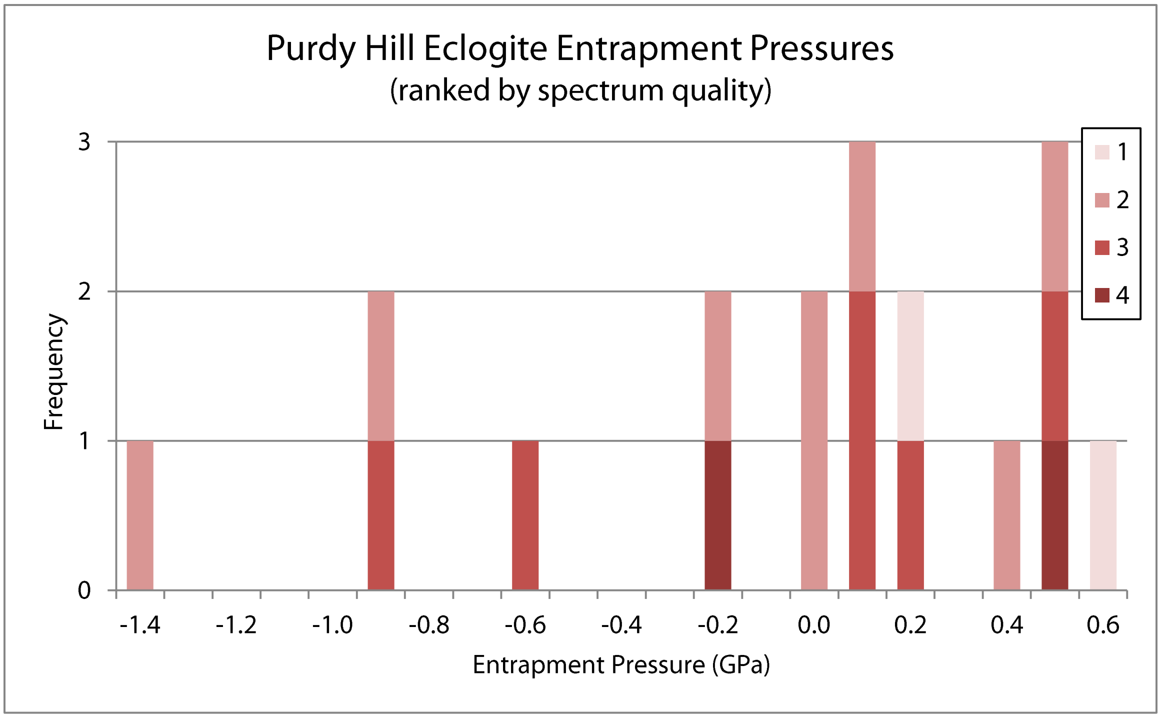

Figure 30: Histogram of ranked entrapment pressures for the Purdy Hill eclogites. Low quality data are ranked (1) and high quality data are ranked (5).

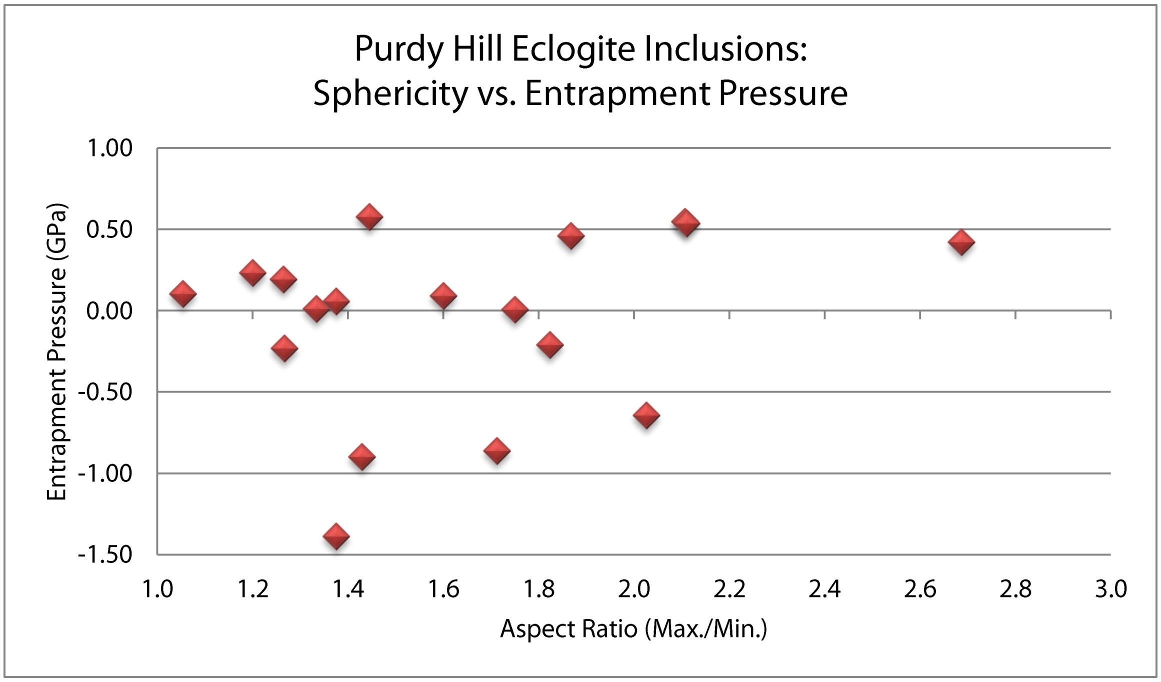

Figure 31: Comparison of aspect ratios with entrapment pressures for all Purdy Hill eclogites inclusions, showing that no correlation exists between an inclusion's sphericity and its calculated entrapment pressure.

to the occurrence of sillimanite in both garnet rims and the matrix in three of four thin sections. This mineral might suggest that the gneisses never reached HP conditions, at which sillimanite is unstable. Such a scenario that might explain the 10 inclusions that produce geologically reasonable but lower-than-expected entrapment pressures, but it cannot account for the 9 inclusions that produce negative entrapment pressures. Low pressures during garnet growth as suggested by sillimanite cannot account for tension rather than compression while quartz crystals were being trapped by garnet. As has been seen for the other localities, a plot of the ranked entrapment pressures for the felsic gneisses shows no correlation between entrapment pressure and quality ranking (Fig. 32). Likewise, a plot of sphericity versus entrapment pressure also shows no correlation (Fig. 33).

Comparison of Locality Results

The key observation from all three localities is that entrapment pressures are unreasonably low. In seeking an explanation for these low calculated entrapment pressures, it is helpful to take note of the differences between the Purdy Hill localities on one hand and the Whitt Ranch occurrence on the other. Figure 34 compares the $\Delta\omega_1$ values for each of the three sample sets; examination of values for $\Delta\omega_1$ has the advantage of allowing comparison of the fundamental measurements, unperturbed by later calculations. Plotting together the data from all three localities shows a clear disparity in $\Delta\omega_1$ values. Despite having similar assemblages, eclogites from both Whitt Ranch and Purdy Hill have radically different $\Delta\omega_1$ trends. Fifteen Whitt Ranch eclogites inclusions are characterized by $\Delta\omega_1$ values greater than 2 cm^{-1}. The other 11 inclusions values fall below 2 cm^{-1}, but with the exception of 6 inclusions, Whitt Ranch values can be described as positive. In comparison, all of the Purdy

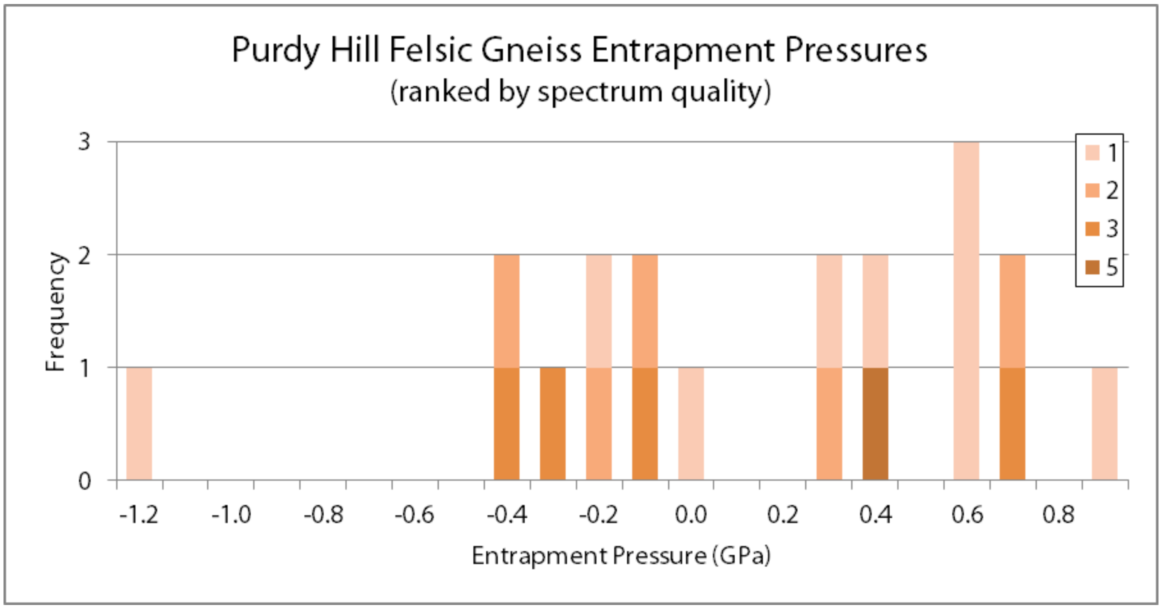

Figure 32: Plot of ranked entrapment pressures for Purdy Hill felsic gneisses. Low quality data are ranked (1) and high quality data are ranked (5).

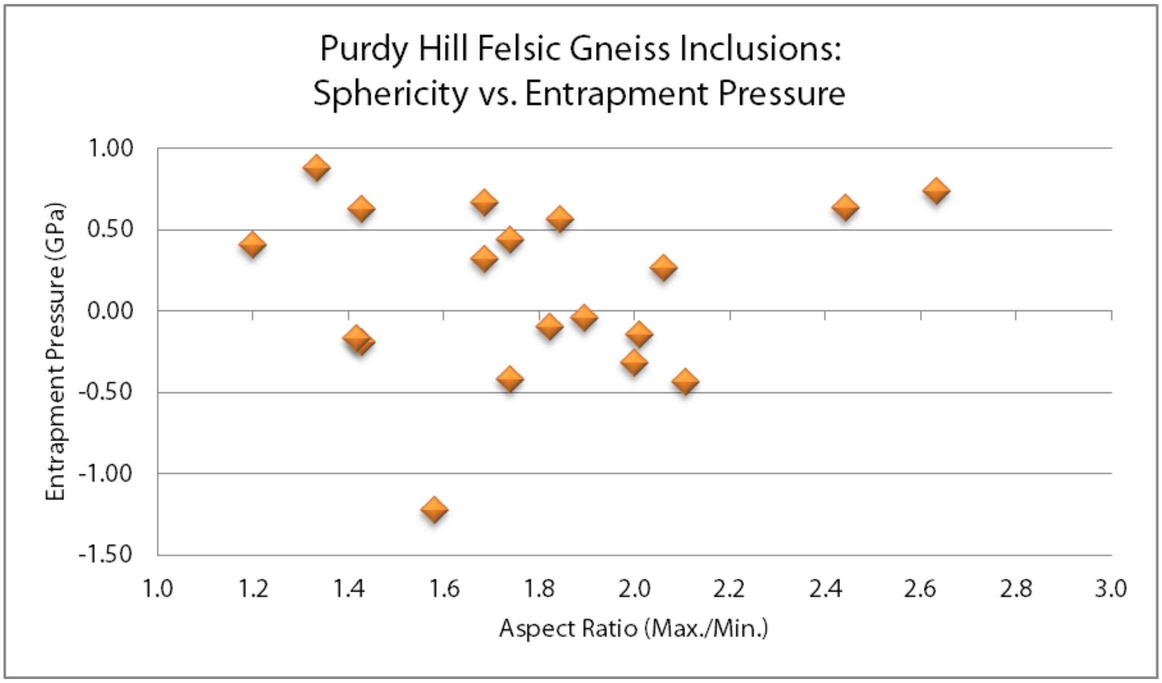

Figure 33: Comparison of aspect ratios with entrapment pressures for all Purdy Hill felsic gneiss inclusions, showing that no correlation exists between an inclusion's sphericity and its calculated entrapment pressure.

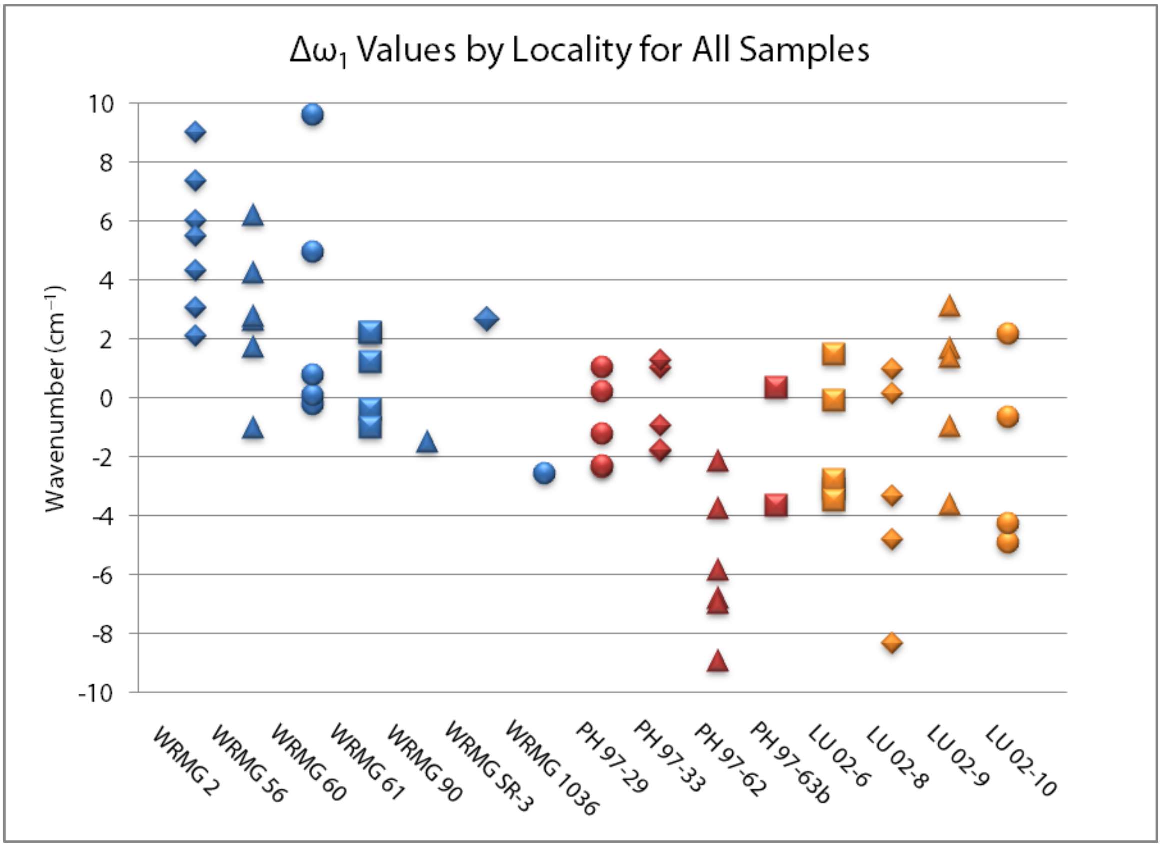

Figure 34: Comparison of $\Delta\omega_1$ values from quartz inclusions from all three localities shows the disparity between the Whitt Ranch and Purdy Hill eclogites and the similarity between the Purdy Hill eclogites and gneisses.

Hill eclogites range from low to negative $\Delta\omega_1$ values (~2 cm^{-1} and below). Like the Purdy Hill eclogites, almost all Purdy Hill gneisses also have low or negative $\Delta\omega_1$ values, indicating that in both lithologies quartz inclusions at Purdy Hill apparently preserved lower residual pressures than at Whitt Ranch. For all three sets of inclusions, approximately half of the $\Delta\omega_1$ values are distributed between −2 and 2 cm^{-1}, but outside of this zone the trend of Whitt Ranch is clearly positive, whereas the trend at Purdy Hill is clearly negative.

The fact that the ranges of calculated entrapment pressures for both rock types at Purdy Hill are so similar to each other yet distinctly different from the range of values at Whitt Ranch strongly suggests that the entrapment pressures retrieved by the Raman technique are controlled by geologic factors that differ between the two localities. The most conspicuous difference between the localities is seen in Figure 2, which illustrates that growth zoning profiles have been completely homogenized by intracrystalline diffusion in the Purdy Hill garnets, whereas the Whitt Ranch garnets retain steeper gradients in composition. Homogenization of growth zoning requires significant redistribution of material at length scales of hundreds of microns or more. An overall reduction in stored strain energy should occur if material is moved away from regions of higher stress to regions of lower stress (or equivalently, if vacancies diffuse into regions of higher stress); this would have the effect of reducing normal stresses on quartz inclusions in garnets that are subjected to appreciable intracrystalline diffusion while under compressive stress.

Normal clockwise *P-T* paths require that peak temperatures — at which most intracrystalline diffusion will occur — should be reached at pressures lower than the maximum pressure achieved along the prograde path that produces garnet growth. Under these conditions, inclusions trapped at or near peak pressures would be under compressive stress when diffusion occurs at or near peak temperatures. In addition, heating to peak temperatures after entrapment will produce a modest further increase in stress on the inclusion, because the thermal expansion coefficient for quartz is larger than that for garnet. Therefore, partial or even complete relaxation of stress differences between garnet and quartz inclusions should occur if peak temperatures reach ~650-700 °C or higher, and persist for millions of years, because appreciable intracrystalline diffusion in garnet should then take place (Carlson and Schwarze, 1997). As shown in the illustration of Van der Molen's elastic model (cf. Fig. 6), the quartz contracts more than garnet, so subsequent cooling during exhumation will produce further reductions in normal stresses on inclusions, and may even lead to tensional stresses on them. Such a mechanism would explain the very low and even negative entrapment pressures calculated for rocks from the Purdy Hill locality.

Reheating of both localities, during either the medium-pressure Barrovian event or subsequent low-pressure overprinting or both, produced modest intracrystalline diffusion; the latter was effective over distances of roughly 100 μm, as evidenced by the stranded diffusion profiles produced by resorption at the rims of garnets (shaded regions in Figure 2). These later diffusion events should also have reduced stresses on inclusions, but these effects are likely to have been much less pronounced than those occurring at peak temperature in the HP event, as the amounts of diffusion are considerably smaller.

Implications

The most significant difference between this study and that of Enami et al. (2007) is the disparity in peak temperatures experienced by rocks in each of the localities. The successful results in Enami et al. (2007) came from lower-temperature rocks that did not undergo diffusional homogenization; in fact, garnets described by Mouri and Enami (2008) had complex zoning that preserved two separate growth stages. In contrast, the Llano rocks experienced higher peak temperatures during metamorphism, and were thus subject to substantial intracrystalline diffusion. The implication is that use of the Raman quartz inclusion barometer must be restricted to rocks in which garnets have not been partially or wholly homogenized during or after growth.

Although diffusional effects are interpreted to be the dominant source of inaccuracy in the present results, this study also helps to identify other possible sources of error, because it quantifies the internal reproducibility of repeated measurements on an individual inclusion. Repeated measurements on the quartz standard were nearly as precise as those of Enami et al. (2007), indicating that the wide spreads in entrapment pressures arise from sources other than internal precision of the spectrometer itself or its operational protocols and environment.

As discussed above, the reproducibility of measurements on a natural quartz inclusion is poorer by a factor of four or more than the reproducibility of measurements on the quartz standard. This increase is attributed to sampling different states of stress within the inclusion; the stress will vary spatially due to edge effects and shape effects. However, this effect translates to uncertainties in entrapment pressures of ± 0.26 GPa, which is still substantially smaller than the range of variation seen in measured entrapment pressures from a single locality.

A likely source of further error is departures of reality from the idealized spherical inclusion model of Van der Molen (1981), which relies upon several simplifying assumptions. One main assumption is that the inclusion is perfectly spherical. A non-spherical inclusion will have a heterogeneous stress profile, because angular portions of the inclusion cause a wedging effect resulting in stress concentrations. Although near-spherical inclusions were chosen in this study, even ellipsoidal inclusions can still have concentrated regions of higher residual stress. This effect could explain the occasional occurrence of inclusions with measured entrapment pressures higher than expected from conventional barometry, despite the fact that inclusion aspect ratio — an oversimplified measure of non-sphericity — does not correlate with calculated entrapment pressures.

Another assumption in the elastic model is that the quartz inclusion is surrounded by a medium of infinite extent. Van der Molen (1981) suggests that only negligible differences exist between an infinite medium and one with a thickness that is a minimum of 5 times the radius *r* of the inclusion. However, a real section commonly has a thickness of garnet around quartz that is much less than the requisite 5*r* in the vertical dimension. Thus, cutting the thin section could result in elastic relaxation of the garnet around a quartz inclusion. This stress release would explain entrapment pressures lower than expected from conventional barometry.

The non-sphericity of quartz inclusions and relaxation of stress due to reduction in garnet thickness during thin section preparation — compounded, perhaps, by variability in the amount and effect of stress relaxation due to intracrystalline diffusion in garnet — are regarded as the most reasonable explanations for the wide spread of entrapment pressures measured in this study.

CONCLUSION

This study determined the level of internal precision of the Raman barometric method, and identified a key, but previously unrecognized, limitation on the applicability of the technique, namely its restriction to rocks in which garnet has not been subjected to appreciable intracrystalline diffusion. Because of this restriction, the attempt to identify HP signatures in the overprinted rocks of the Llano Uplift was unsuccessful.

The first major finding of this study is quantification of the internal precision of this technique by the reproducibility tests. Reproducibility on the quartz standard yielded an uncertainty for ω_1 of ±0.4 cm^{-1}, a value only slightly in excess of the value of ±0.3 cm^{-1} reported by Enami et al. (2007). Repeated measurements on a single inclusion yielded uncertainties of $\pm$ 1.8 cm^{-1} ($\Delta\omega_1$) = $\pm$ 0.11 GPa (P_{resid}) = $\pm$ 0.26 GPa (P_{entrap}), which defines for the first time the level of reproducibility to be expected from the technique in applications to natural samples. The significantly larger uncertainty for the inclusion compared to the standard is likely related to spatial variations of stress within the inclusion (edge effects, non-sphericity) that were sampled to varying degrees in different measurements, due to small differences in the horizontal position of the laser beam and/or the sampling depth as determined by the confocal mode of the instrument.

The second major finding from this study is a correlation between low or negative $\Delta\omega_1$ values and localities with greater intracrystalline diffusion. From this correlation, it is reasonable to conclude that relaxation due to intracrystalline diffusion in garnet can partially or completely relieve the compressive stress around a quartz inclusion. Both the eclogites and the felsic gneisses at the Purdy Hill locality, which were subjected to near-complete post-growth diffusional homogenization, yielded very low estimates of entrapment pressures, values that cannot have geological significance. The eclogites at Whitt Ranch, which were subjected to substantially less diffusional homogenization, were affected enough to yield entrapment pressures mostly lower than what would have been expected from conventional barometry. The implication is that application of the Raman quartz-inclusion barometer must be restricted to garnets in which post-entrapment diffusion is negligible.

APPENDIX

Part of each inclusion's description includes X-Y coordinates, which were determined using a Leitz mechanical microscope stage. The conventional method to properly orient the thin section is to insert the short, labeled side of a thin section into the right-angle holder on the stage. X coordinates are distinguished by values greater than 100, and Y coordinates are distinguished by values less than 100. When areas of the sample are blocked by limited stage movement, the thin section is reversed, so that the labeled edge of the thin section is away from the mounted holder. To indicate reversed thin sections, a negative sign is placed in front of the coordinate pair.

List of Thin Sections:

Samples from the Whitt Ranch locality:

Whitt Ranch Eclogite

Thin Section	Garnet
WRMG 2	2
	3
	4
	5
	6
	7
	9
WRMG 56	1
	2
	3
	4
	6
	7
WRMG 60	1
	4
	5
	7
	9
WRMG 61	1
	4
	5
	6
	7
WRMG 90	1
WRMG 1036	2
WRMG SR-3	1

Samples from the Purdy Hill locality:

Purdy Hill Eclogite

Thin Section	Garnet
PH 97-29	1
	2
	3
	4
	5
PH 97-33	1
	2
	3
	4
	5
PH 97-62	2
	3
	4
	5
	6
	7
PH 97-63b	1
	2

Purdy Hill Gneiss

Thin Section	Garnet
LU 02-6	E
	G
	J
	K
	X
LU 02-8	G
	H
	I
	K
	L
LU 02-9	D
	F
	G
	H
	I
LU 02-10	B
	D
	E
	G

WRMG 2

Garnet 2

Locality: Whitt Ranch
Collected by Susan Harris

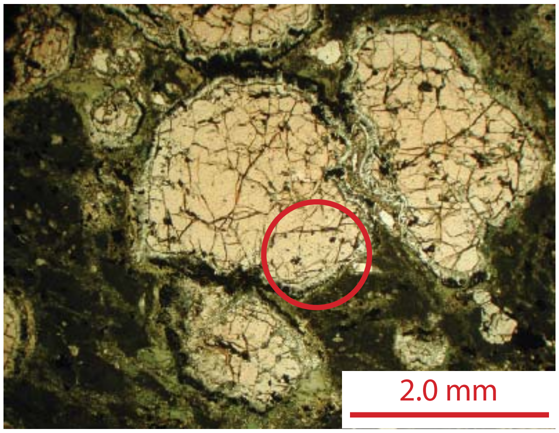

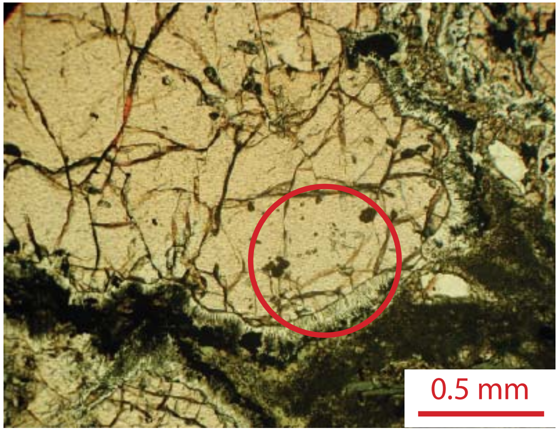

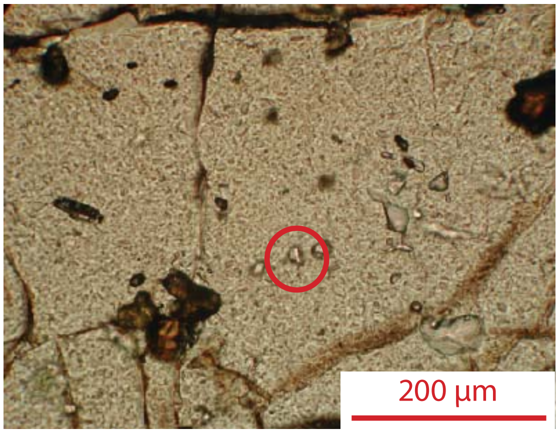

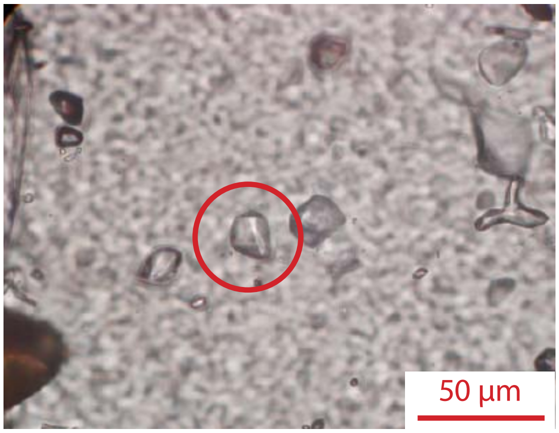

Inclusion Information

Maximum length (X-Y) (μm)	22.1
Minimum length (X-Y) (μm)	19.0
Inclusion thickness (Z) (μm)	21
Location (X-Y coordinates)	-(103.8,8.2)
Description of shape	Teardrop
Garnet composition	$Alm_{54.0}$, $Prp_{27.6}$, $Grs_{18.1}$, $Sps_{0.3}$

Data and Pressure Calculation Results

Depth of spectrum (μm)	-6
$\Delta\omega_1$ (cm^{-1})	4.38
$\Delta\omega_2$ (cm^{-1})	5.26
$P_{resid\ [\Delta\omega1]}$ (GPa)	0.258
$P_{resid\ [\Delta\omega2]}$ (GPa)	0.267
$P_{entrap\ [\Delta\omega1]}$ (GPa)	0.95
$P_{entrap\ [\Delta\omega2]}$ (GPa)	0.97

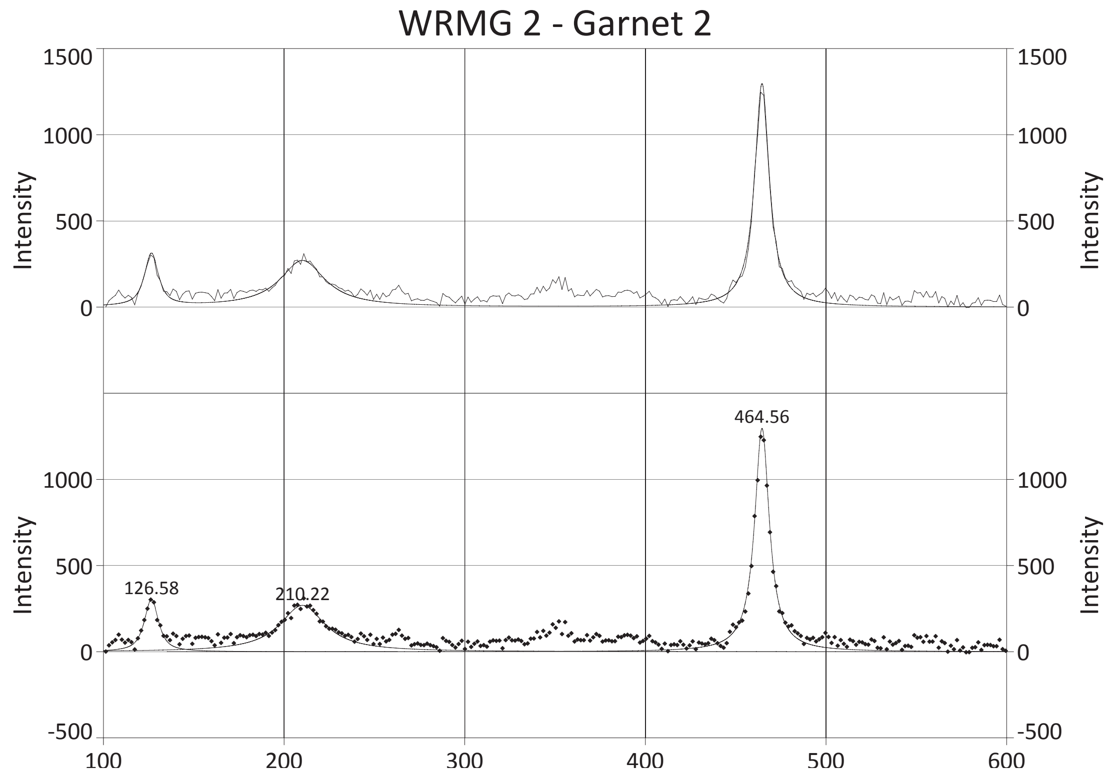
WRMG 2 - Garnet 2
1500
1000
500
0
Intensity
464.56
126.58
210.22
-500
100
200
300
400
500
600

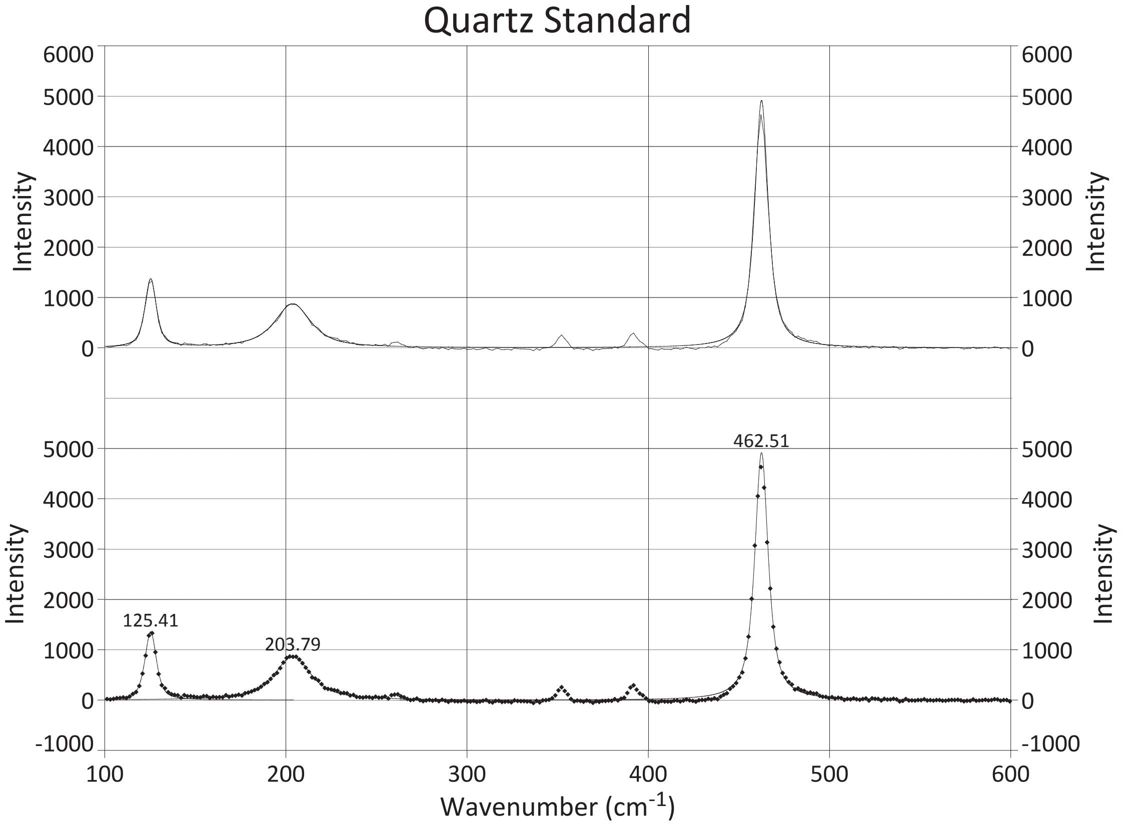
Quartz Standard
6000
5000
4000
3000
2000
1000
0
Intensity
462.51
125.41
203.79
-1000
100
200
300
400
500
600
Wavenumber (cm^{-1})

WRMG 2

Garnet 3

Locality: Whitt Ranch
Collected by Susan Harris

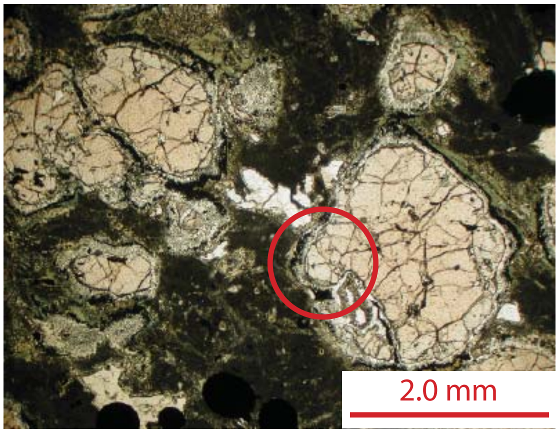

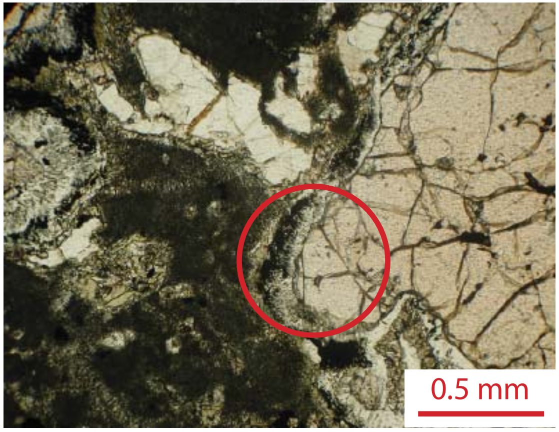

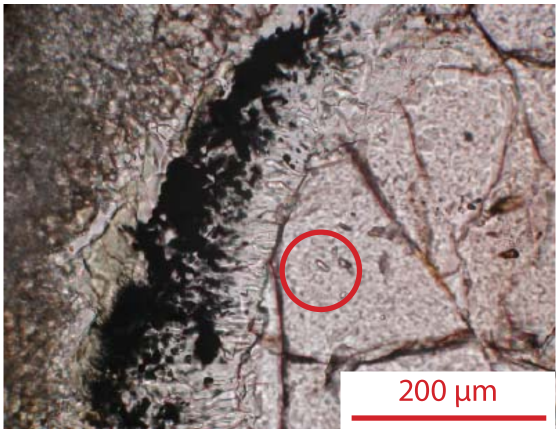

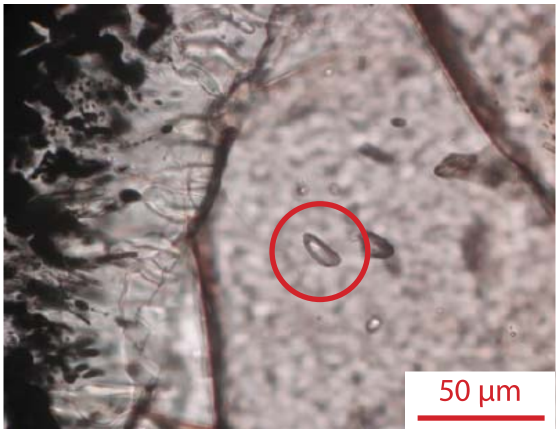

Inclusion Information

Maximum length (X-Y) (µm)	19.0
Minimum length (X-Y) (µm)	7.9
Inclusion thickness (Z) (µm)	15
Location (X-Y coordinates)	-(105.2,15.7)
Description of shape	Elongate
Garnet composition	Alm$_{54.0}$, Prp$_{27.6}$, Grs$_{18.1}$, Sps$_{0.3}$

Data and Pressure Calculation Results

Depth of spectrum (µm)	-2
$\Delta\omega_1$ (cm^{-1})	6.04
$\Delta\omega_2$ (cm^{-1})	7.21
$P_{\text{resid }[\Delta\omega 1]}$ (GPa)	0.354
$P_{\text{resid }[\Delta\omega 2]}$ (GPa)	0.372
$P_{\text{entrap }[\Delta\omega 1]}$ (GPa)	1.19
$P_{\text{entrap }[\Delta\omega 2]}$ (GPa)	1.23

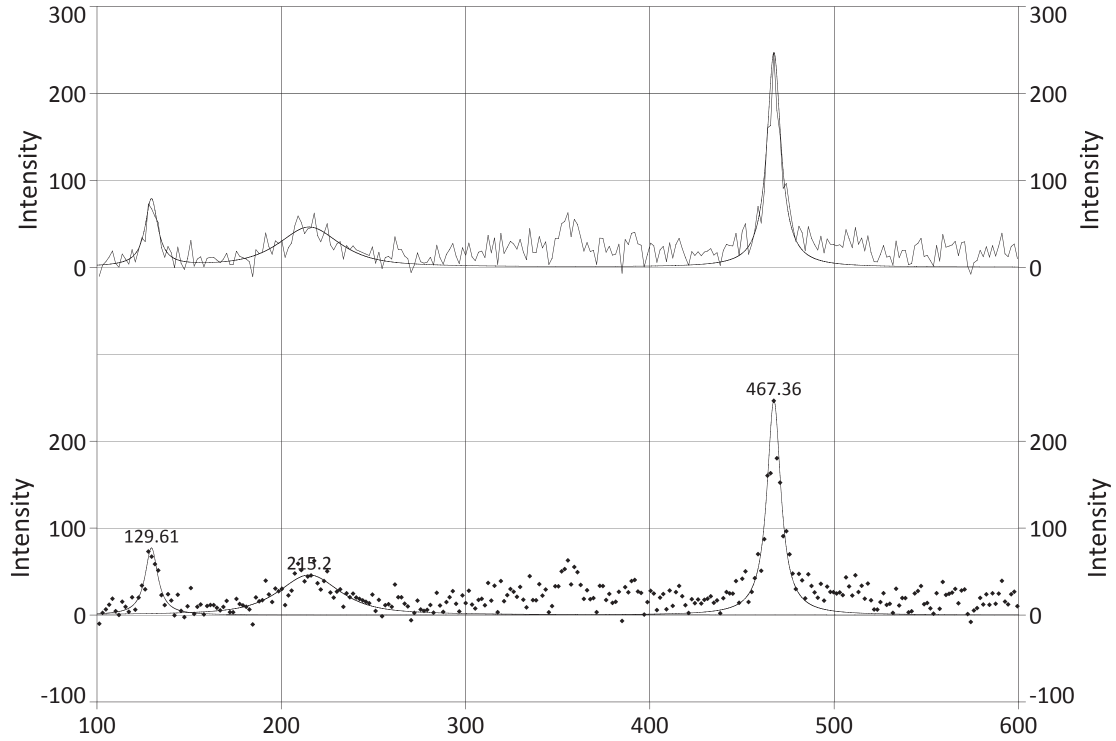
WRMG 2 - Garnet 3

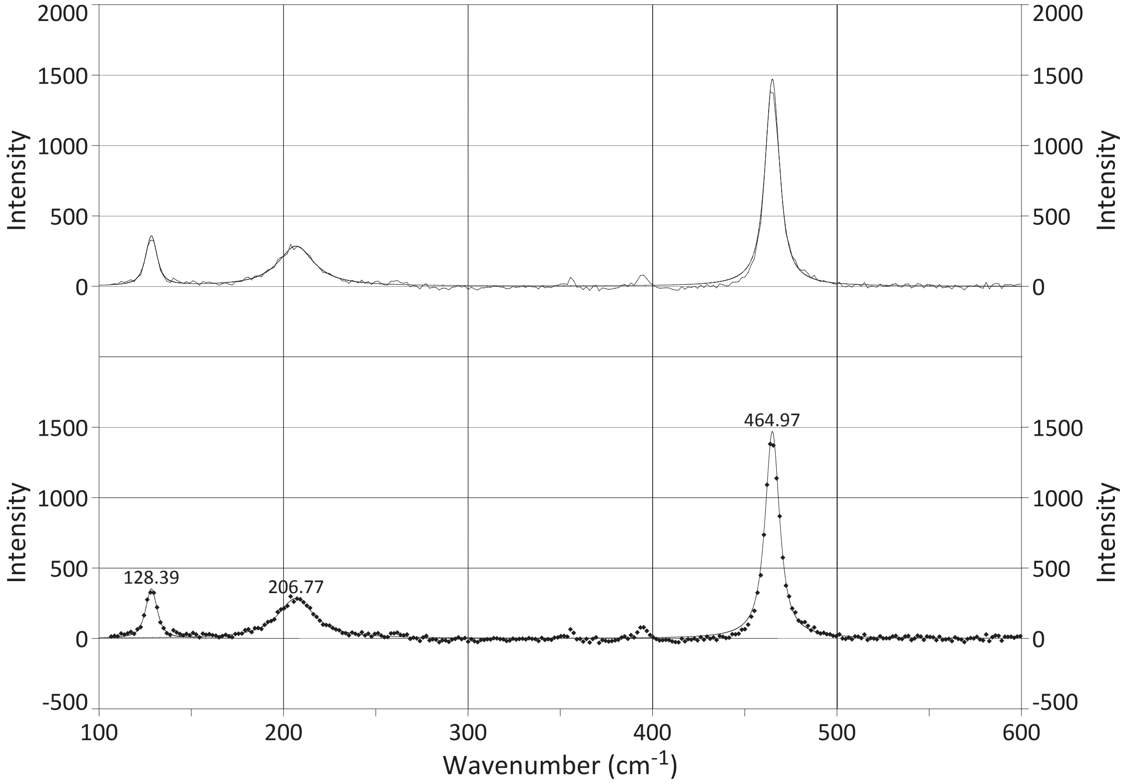
Quartz Standard

WRMG 2

Garnet 4

Locality: Whitt Ranch
Collected by Susan Harris

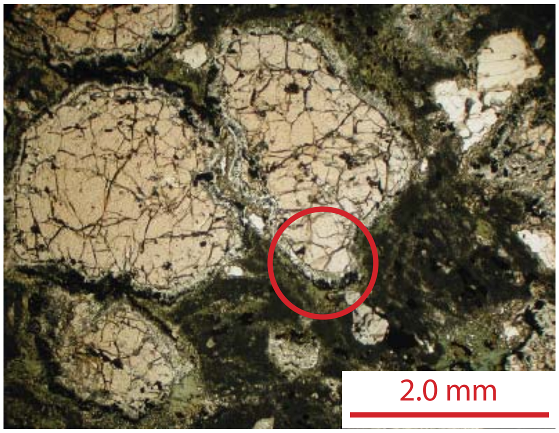

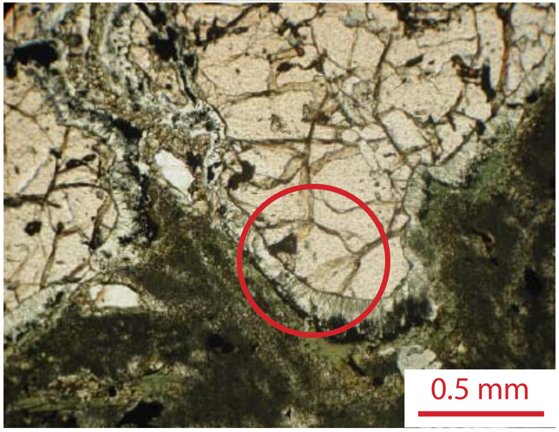

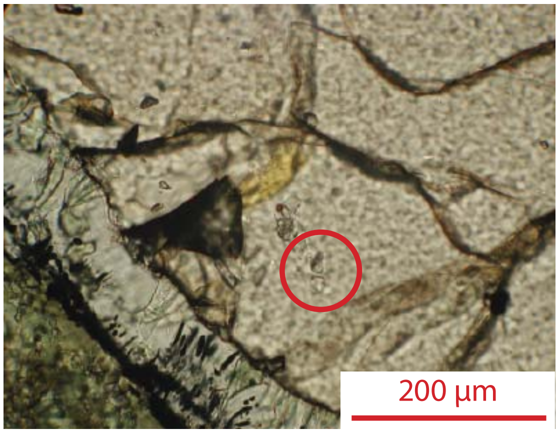

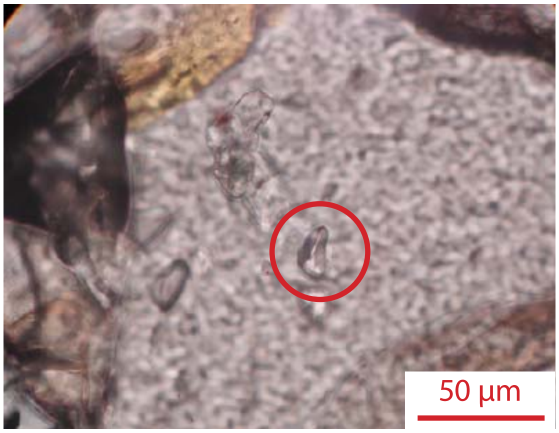

Inclusion Information

Maximum length (X-Y) (µm)	23.7
Minimum length (X-Y) (µm)	14.2
Inclusion thickness (Z) (µm)	16
Location (X-Y coordinates)	-(104.4, 8.5)
Description of shape	Triangular
Garnet composition	$Alm_{54.0}$, $Prp_{27.6}$, $Grs_{18.1}$, $Sps_{0.3}$

Data and Pressure Calculation Results

Depth of spectrum (µm)	-4
$\Delta\omega_1$ (cm^{-1})	3.10
$\Delta\omega_2$ (cm^{-1})	3.68
$P_{resid\ [\Delta\omega1]}$ (GPa)	0.184
$P_{resid\ [\Delta\omega2]}$ (GPa)	0.185
$P_{entrap\ [\Delta\omega1]}$ (GPa)	0.77
$P_{entrap\ [\Delta\omega2]}$ (GPa)	0.77

WRMG 2 - Garnet 4

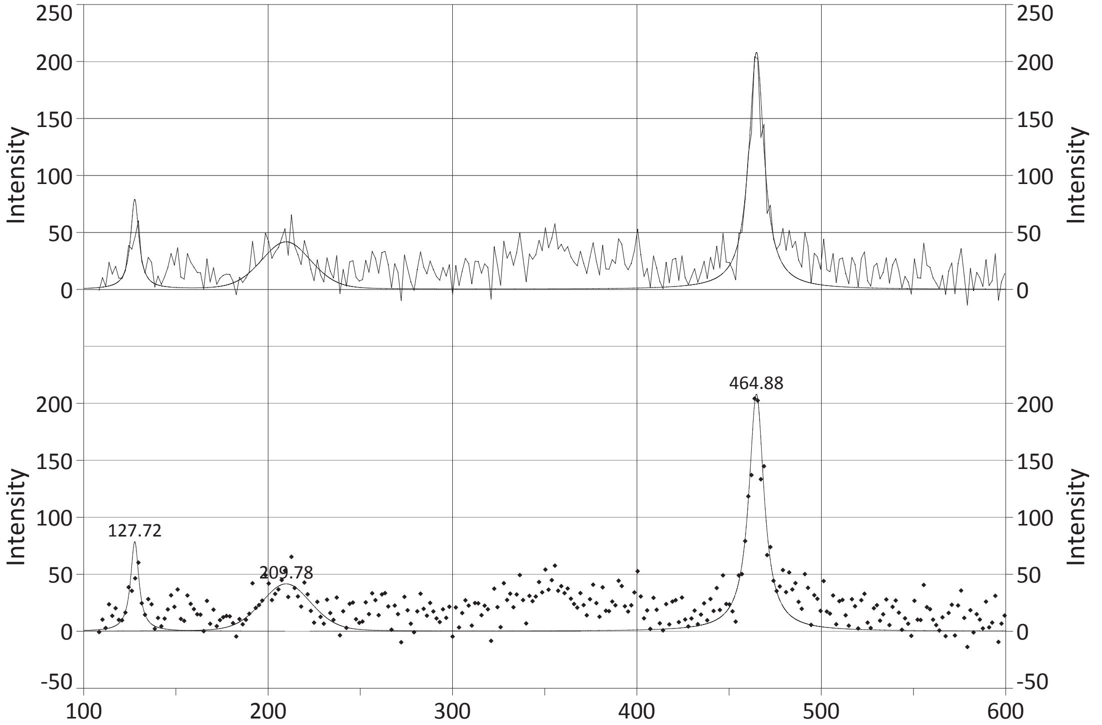

Quartz Standard

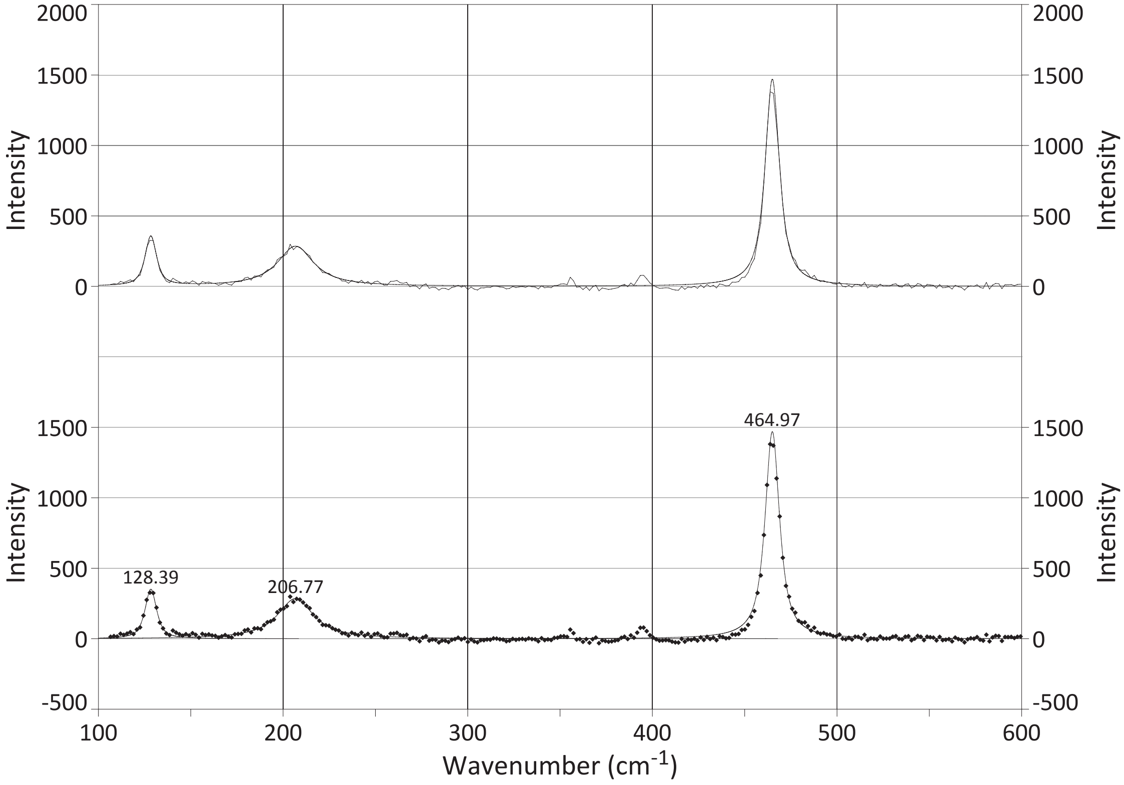

WRMG 2

Garnet 5

Locality: Whitt Ranch
Collected by Susan Harris

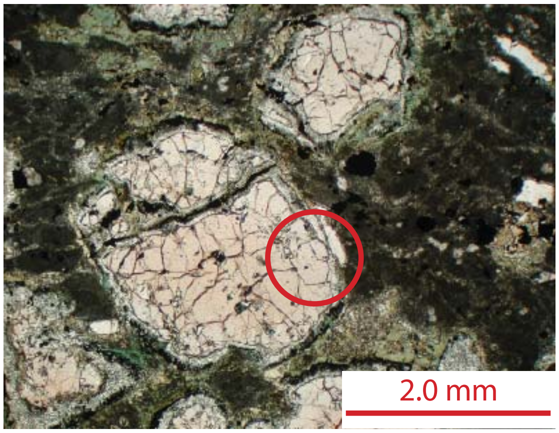

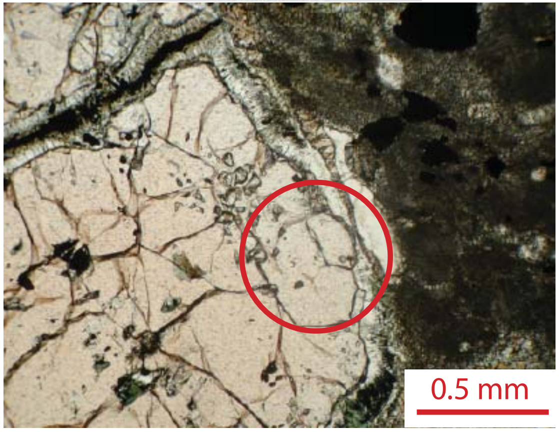

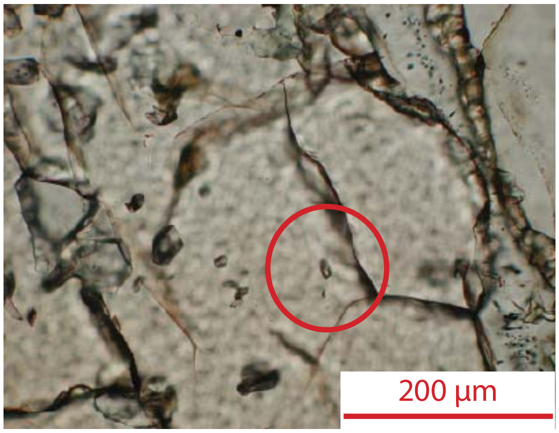

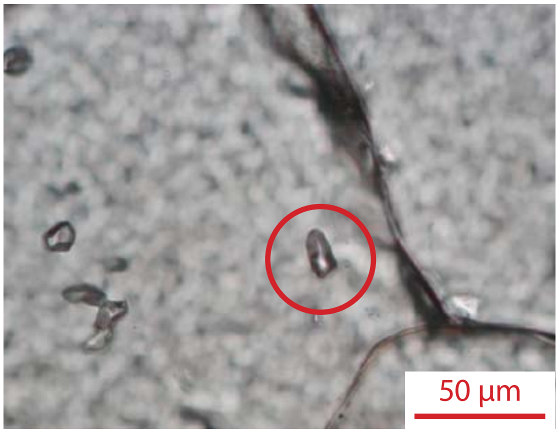

Inclusion Information

Maximum length (X-Y) (µm)	21.3
Minimum length (X-Y) (µm)	11.1
Inclusion thickness (Z) (µm)	21
Location (X-Y coordinates)	-(103.3, 11.0)
Description of shape	Elongate
Garnet composition	$Alm_{54.0}$, $Prp_{27.6}$, $Grs_{18.1}$, $Sps_{0.3}$

Data and Pressure Calculation Results

Depth of spectrum (µm)	-8
$\Delta\omega_1$ (cm^{-1})	2.14
$\Delta\omega_2$ (cm^{-1})	4.24
$P_{resid\ [\Delta\omega1]}$ (GPa)	0.128
$P_{resid\ [\Delta\omega2]}$ (GPa)	0.213
$P_{entrap\ [\Delta\omega1]}$ (GPa)	0.63
$P_{entrap\ [\Delta\omega2]}$ (GPa)	0.84

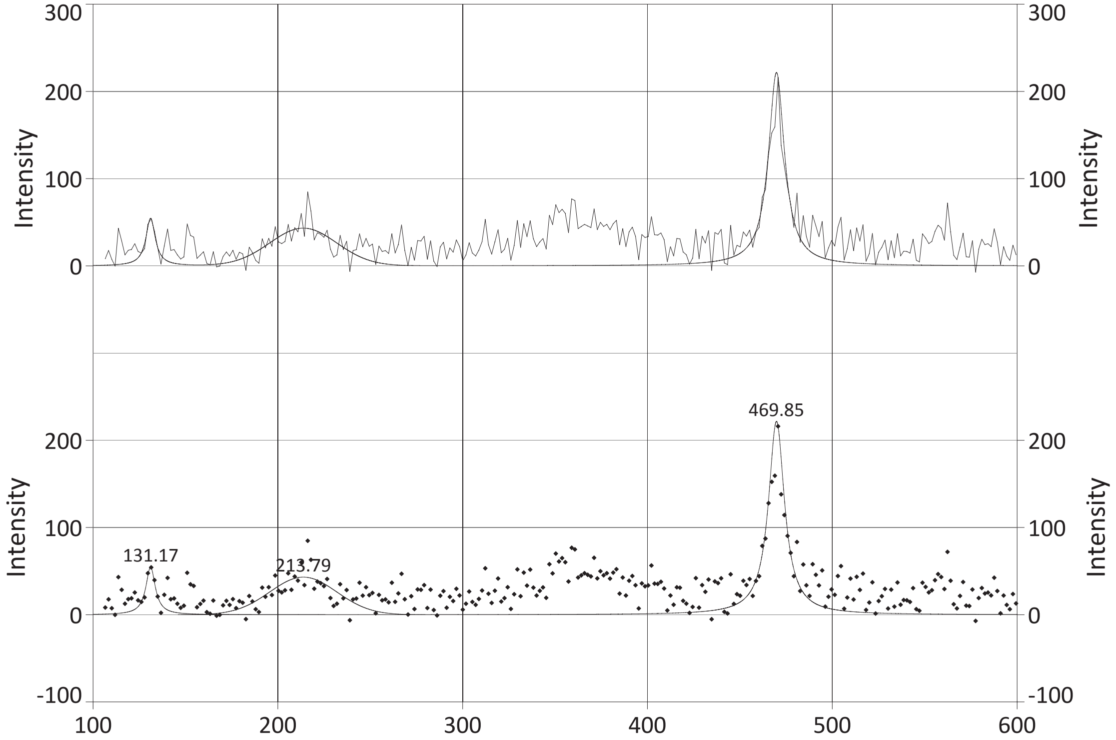
WRMG 2 - Garnet 5

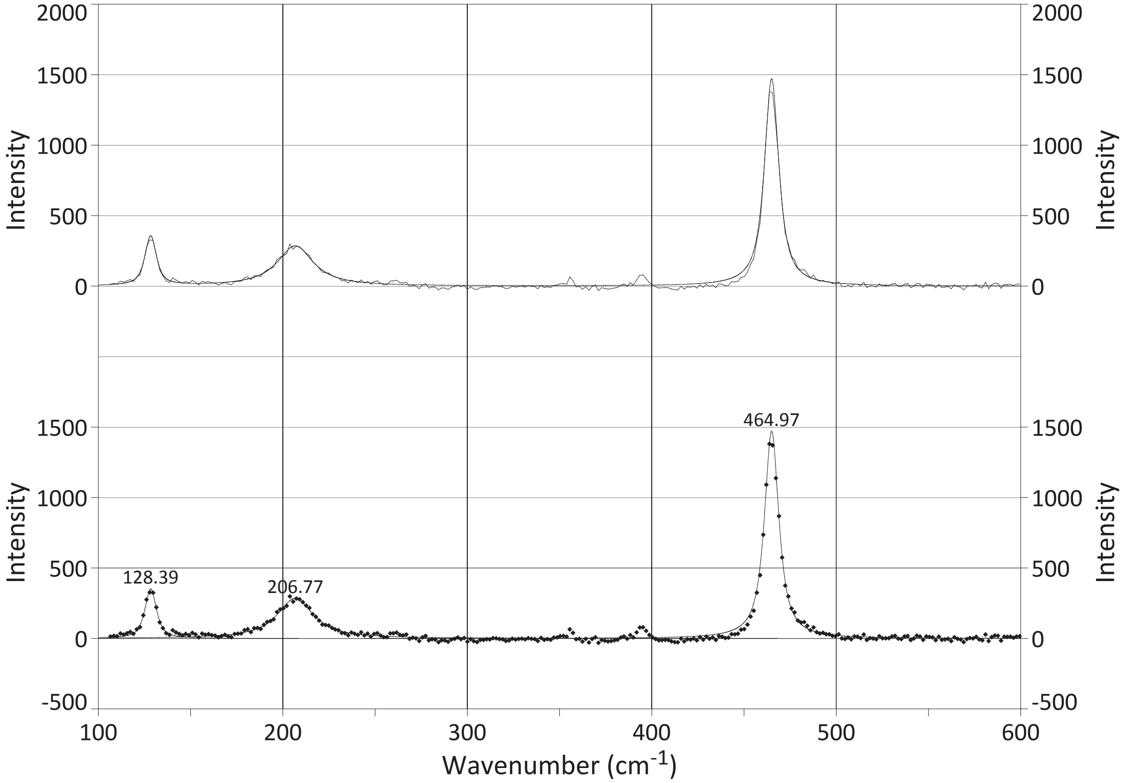
Quartz Standard

WRMG 2

Garnet 6

Locality: Whitt Ranch
Collected by Susan Harris

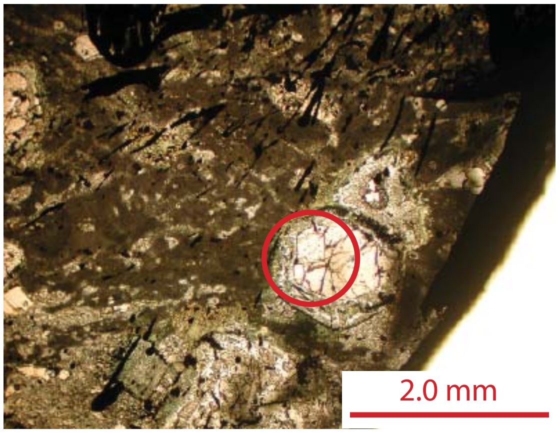

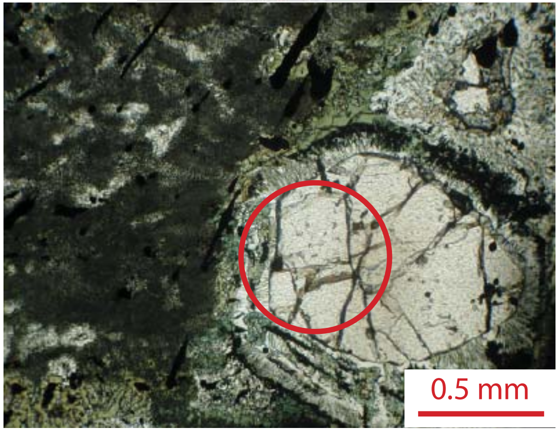

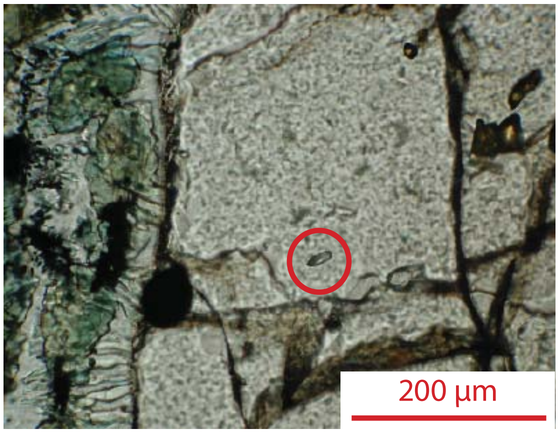

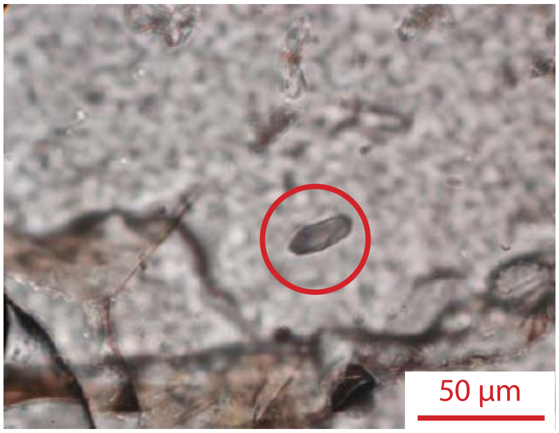

Inclusion Information

Maximum length (X-Y) (µm)	27.7
Minimum length (X-Y) (µm)	11.1
Inclusion thickness (Z) (µm)	11
Location (X-Y coordinates)	-(107.2, 16.3)
Description of shape	Elongate
Garnet composition	$Alm_{54.0}$, $Prp_{27.6}$, $Grs_{18.1}$, $Sps_{0.3}$

Data and Pressure Calculation Results

Depth of spectrum (µm)	-2
$\Delta\omega_1$ (cm^{-1})	5.54
$\Delta\omega_2$ (cm^{-1})	7.21
$P_{resid\ [\Delta\omega1]}$ (GPa)	0.325
$P_{resid\ [\Delta\omega2]}$ (GPa)	0.372
$P_{entrap\ [\Delta\omega1]}$ (GPa)	1.12
$P_{entrap\ [\Delta\omega2]}$ (GPa)	1.23

WRMG 2 - Garnet 6

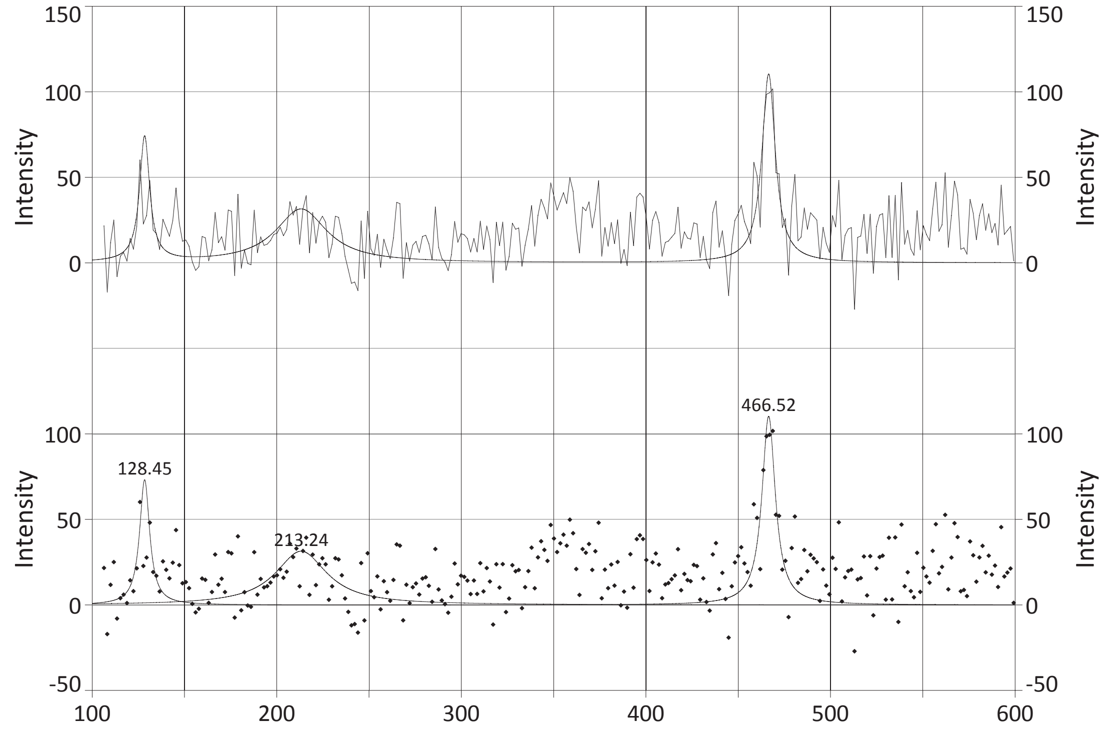

Quartz Standard

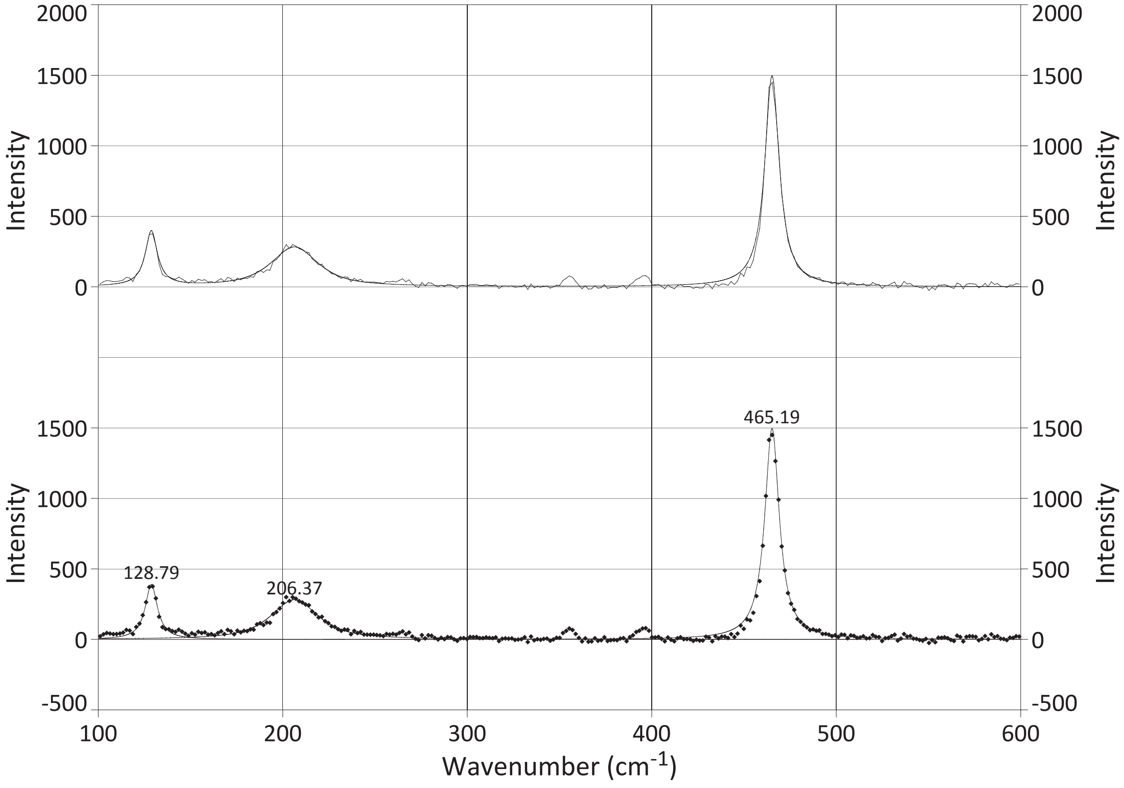

WRMG 2

Garnet 7

Locality: Whitt Ranch
Collected by Susan Harris

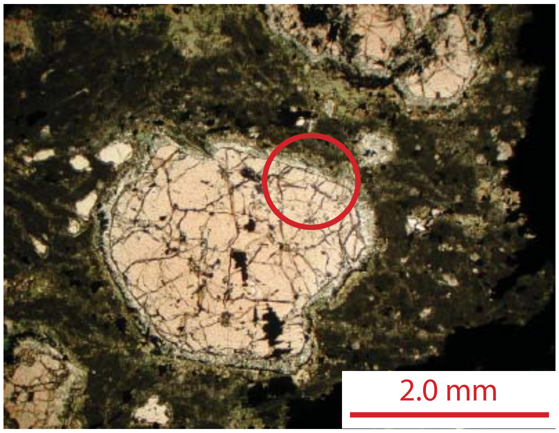

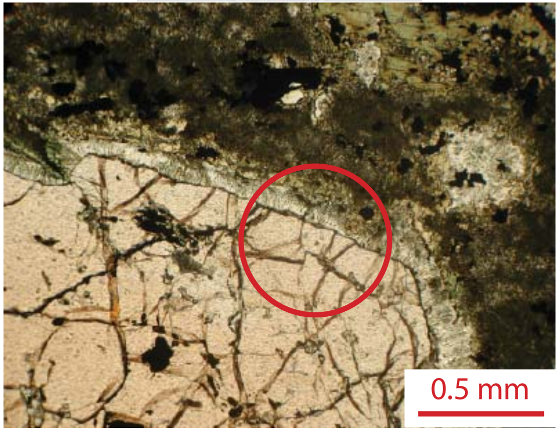

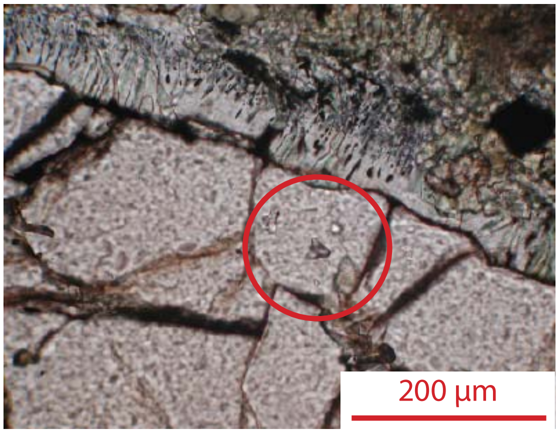

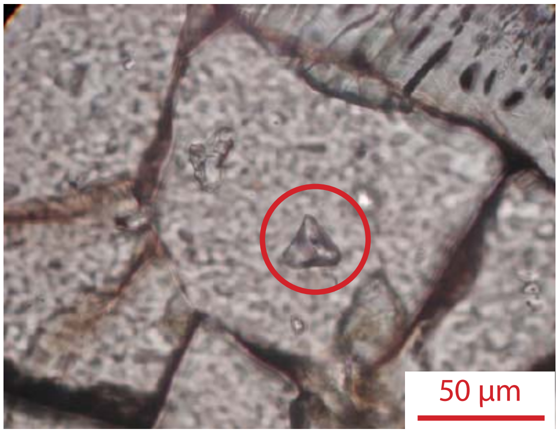

Inclusion Information

Maximum length (X-Y) (µm)	23.7
Minimum length (X-Y) (µm)	22.1
Inclusion thickness (Z) (µm)	13
Location (X-Y coordinates)	(106.5, 9.7)
Description of shape	Triangular
Garnet composition	$Alm_{54.0}$, $Prp_{27.6}$, $Grs_{18.1}$, $Sps_{0.3}$

Data and Pressure Calculation Results

Depth of spectrum (µm)	-6
$\Delta\omega_1$ (cm^{-1})	7.40
$\Delta\omega_2$ (cm^{-1})	9.70
$P_{resid\ [\Delta\omega1]}$ (GPa)	0.436
$P_{resid\ [\Delta\omega2]}$ (GPa)	0.513
$P_{entrap\ [\Delta\omega1]}$ (GPa)	1.39
$P_{entrap\ [\Delta\omega2]}$ (GPa)	1.58

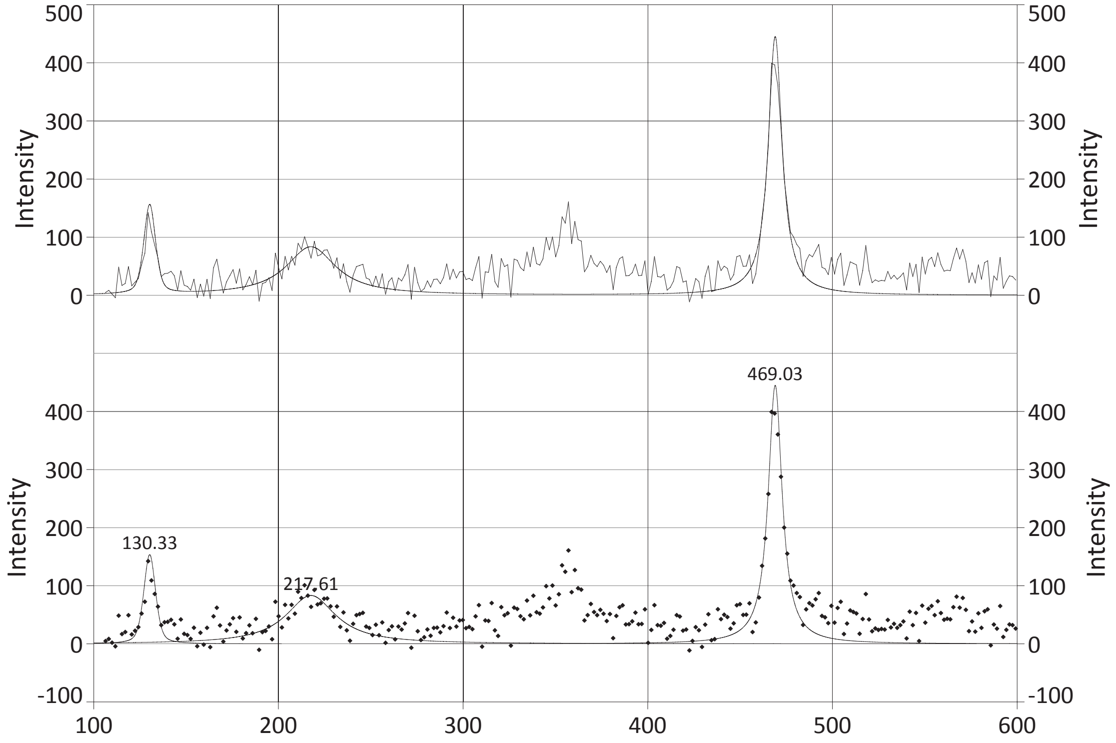

WRMG 2 - Garnet 7

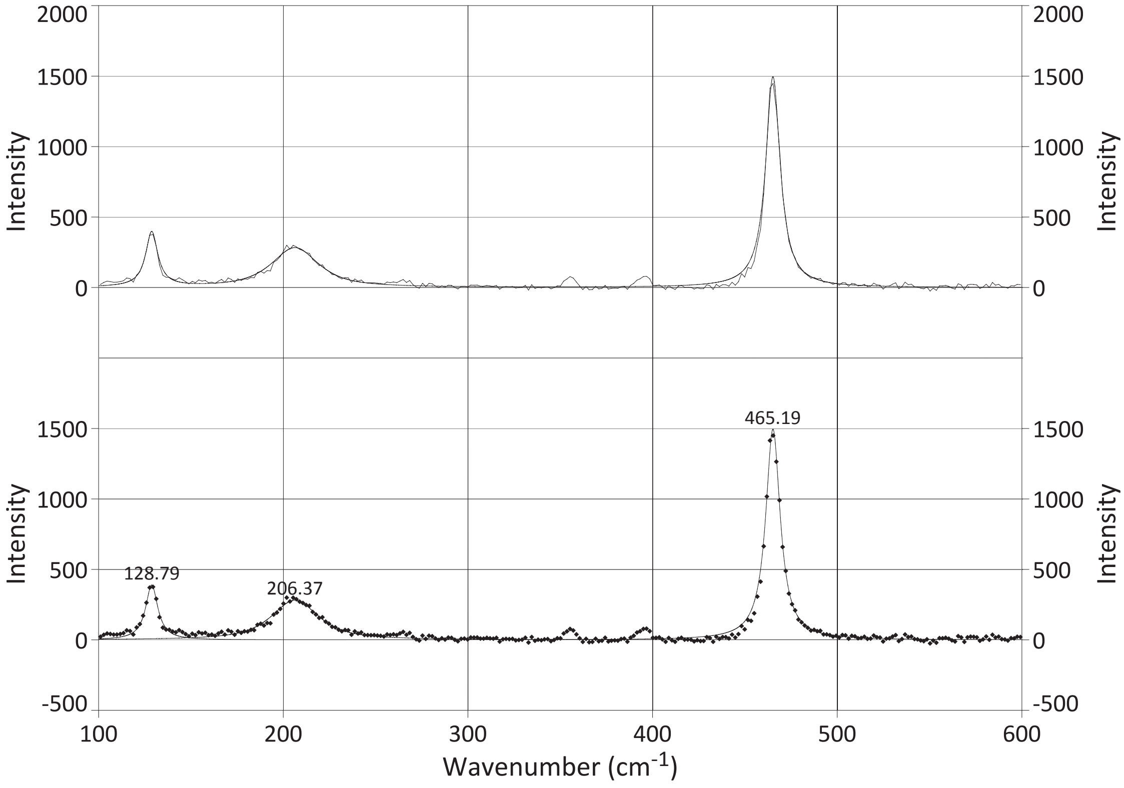

Quartz Standard

WRMG 2

Garnet 9

Locality: Whitt Ranch
Collected by Susan Harris

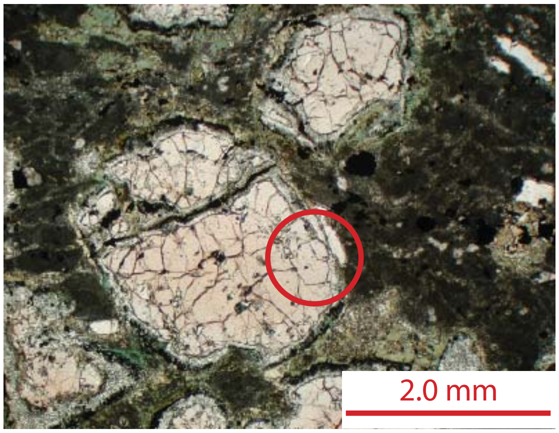

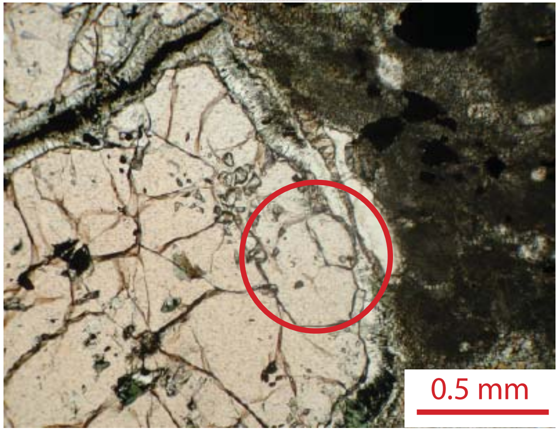

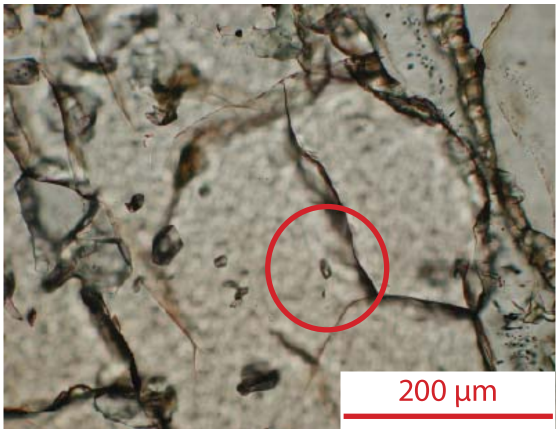

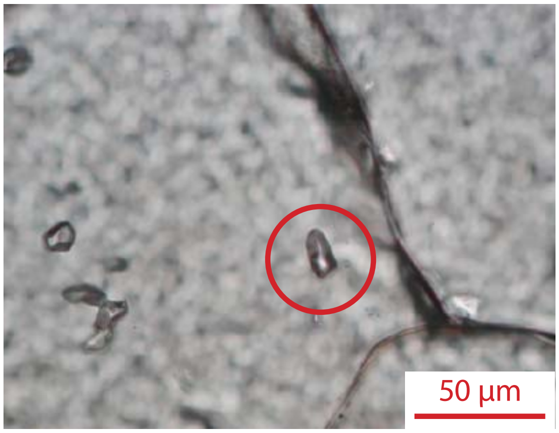

Inclusion Information

Maximum length (X-Y) (µm)	14.2
Minimum length (X-Y) (µm)	11.1
Inclusion thickness (Z) (µm)	17
Location (X-Y coordinates)	-(100.9, 4.6)
Description of shape	Elongate
Garnet composition	Alm$_{54.0}$, Prp$_{27.6}$, Grs$_{18.1}$, Sps$_{0.3}$

Data and Pressure Calculation Results

Depth of spectrum (µm)	-4
$\Delta\omega_1$ (cm^{-1})	9.05
$\Delta\omega_2$ (cm^{-1})	7.96
$P_{resid\ [\Delta\omega1]}$ (GPa)	0.541
$P_{resid\ [\Delta\omega2]}$ (GPa)	0.414
$P_{entrap\ [\Delta\omega1]}$ (GPa)	1.65
$P_{entrap\ [\Delta\omega2]}$ (GPa)	1.34

WRMG 2 - Garnet 9

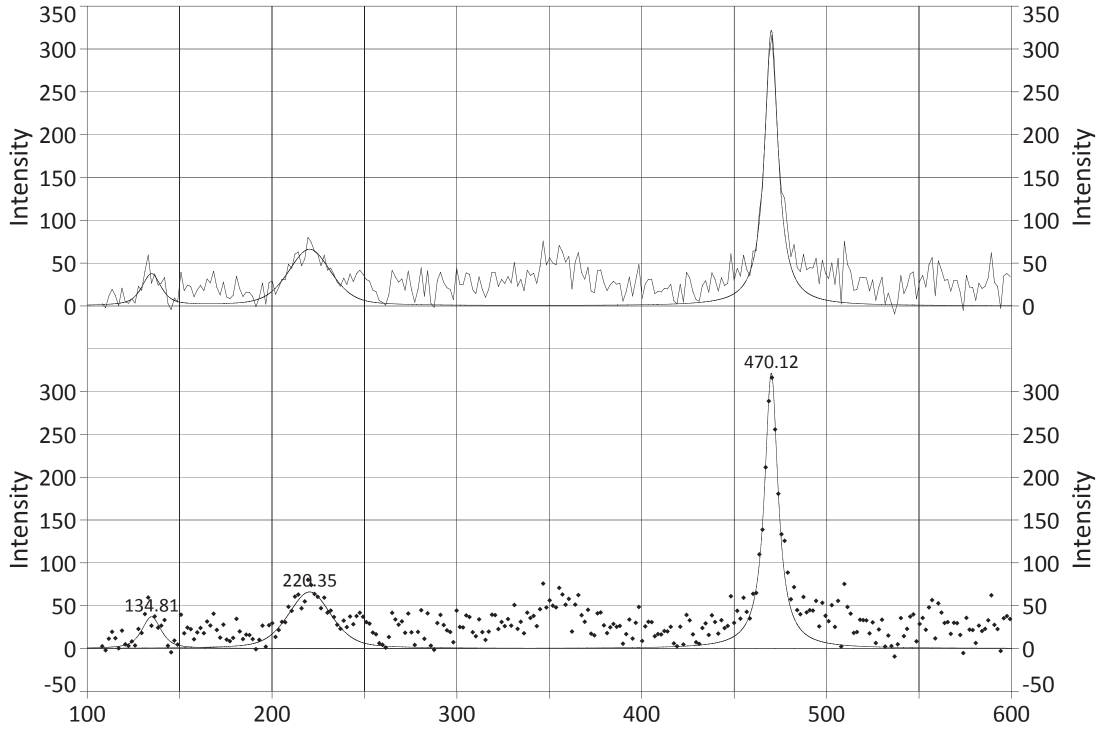

Quartz Standard

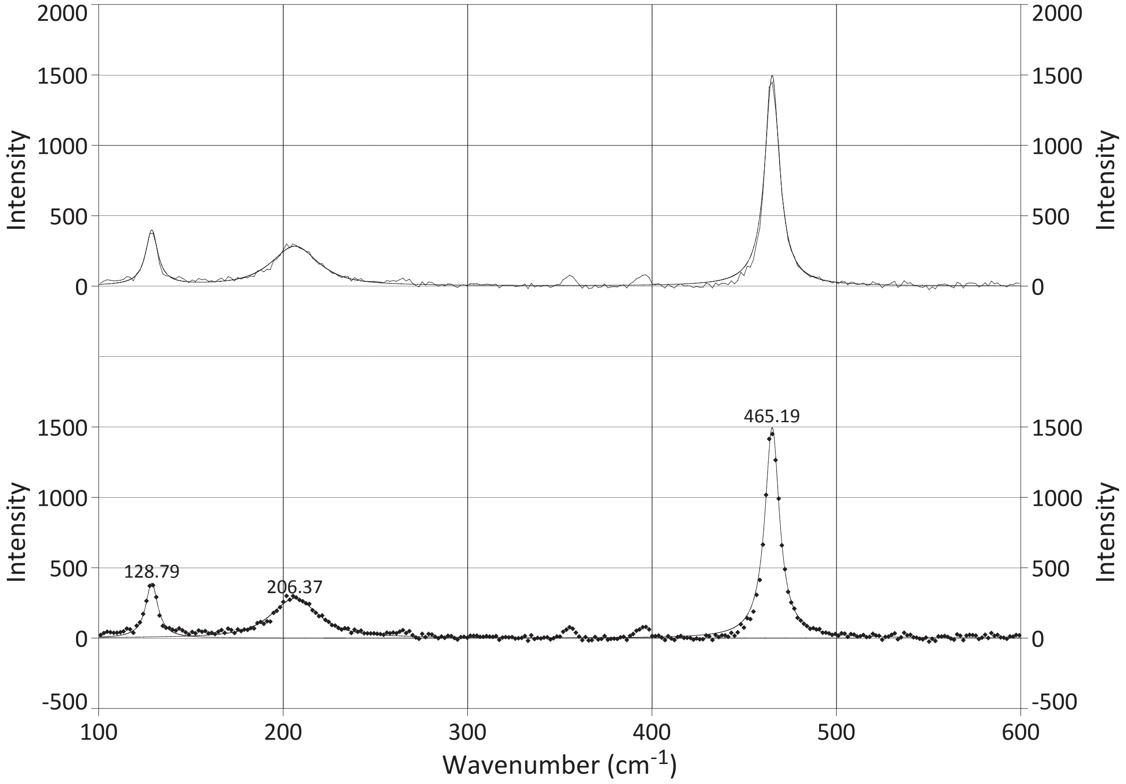

WRMG 56

Garnet 1

Locality: Whitt Ranch
Collected by Susan Harris

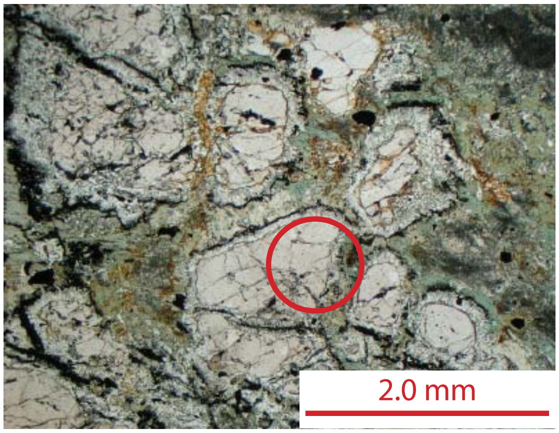

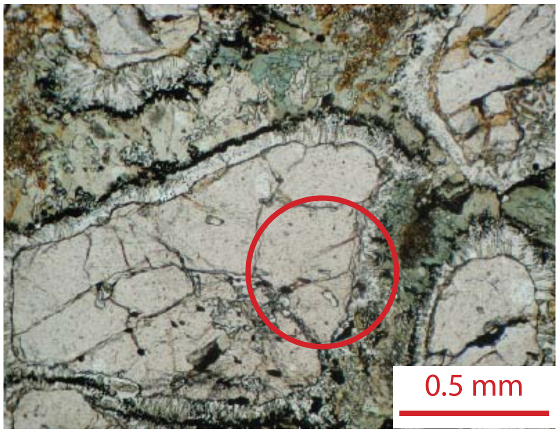

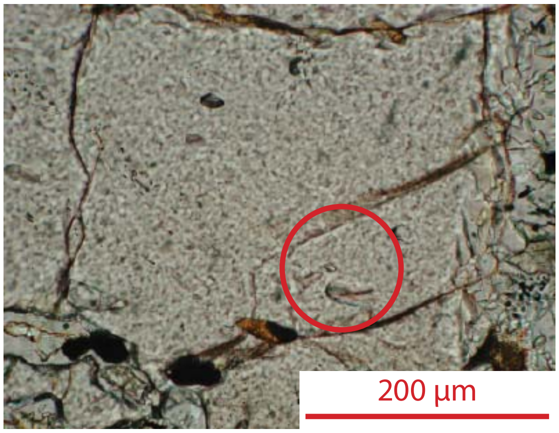

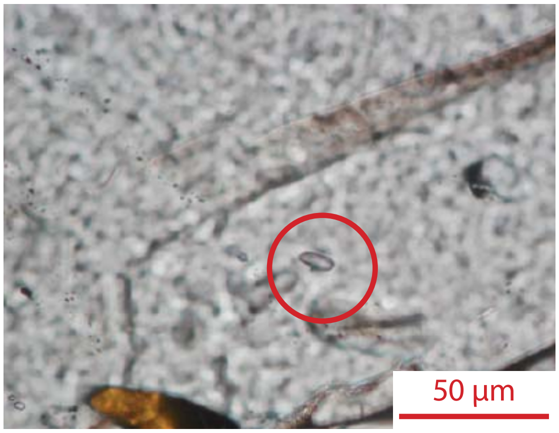

Inclusion Information

Maximum length (X-Y) (µm)	12.6
Minimum length (X-Y) (µm)	6.32
Inclusion thickness (Z) (µm)	11
Location (X-Y coordinates)	-(101.3, 5.9)
Description of shape	Elongate
Garnet composition	$Alm_{54.0}$, $Prp_{27.6}$, $Grs_{18.1}$, $Sps_{0.3}$

Data and Pressure Calculation Results

Depth of spectrum (µm)	-4
$\Delta\omega_1$ (cm^{-1})	-0.96
$\Delta\omega_2$ (cm^{-1})	-0.45
$P_{resid\ [\Delta\omega1]}$ (GPa)	-0.061
$P_{resid\ [\Delta\omega2]}$ (GPa)	-0.022
$P_{entrap\ [\Delta\omega1]}$ (GPa)	0.16
$P_{entrap\ [\Delta\omega2]}$ (GPa)	0.25

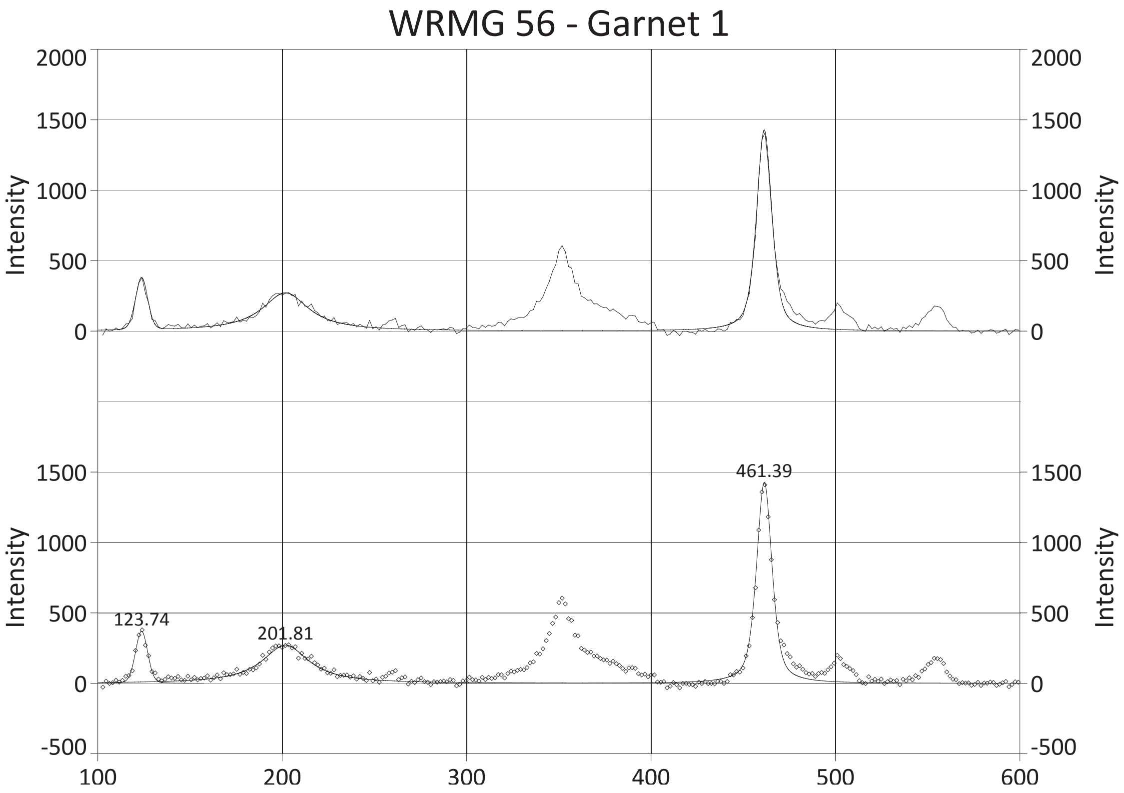
WRMG 56 - Garnet 1
Intensity
2000
1500
1000
500
0
-500
123.74
201.81
461.39
100
200
300
400
500
600

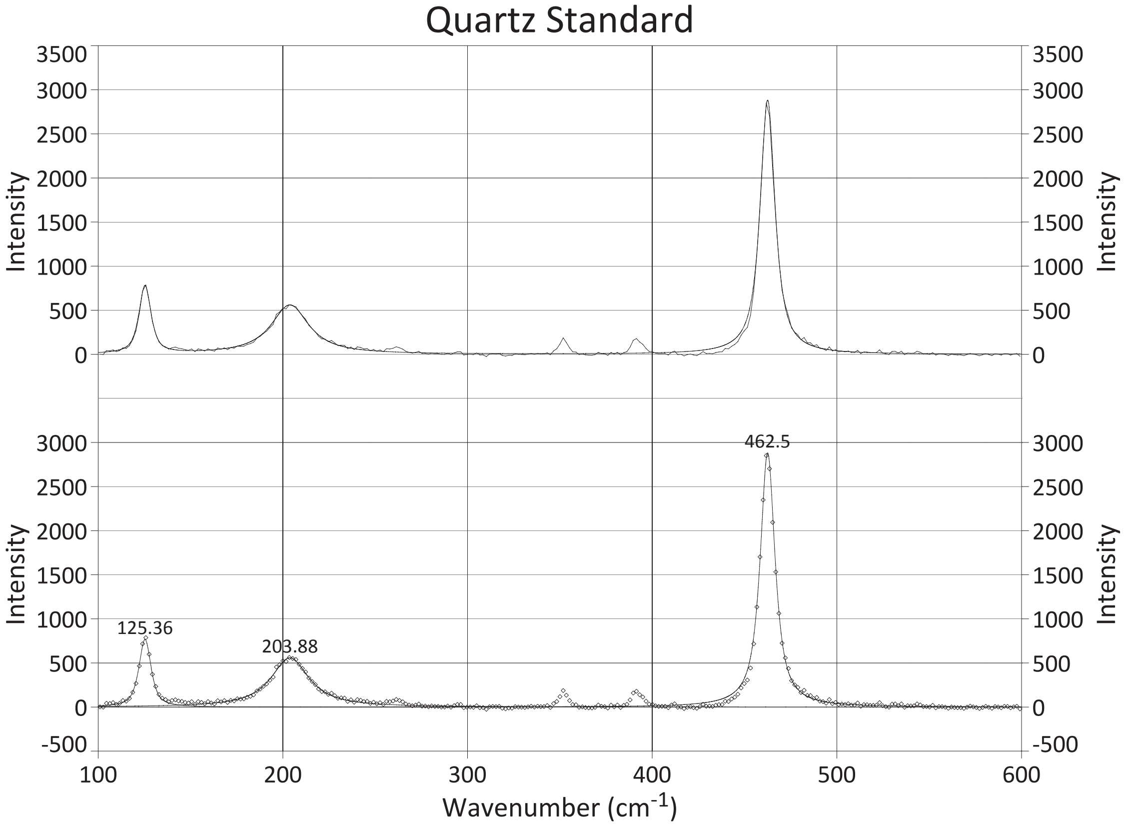
Quartz Standard
Intensity
3500
3000
2500
2000
1500
1000
500
0
-500
125.36
203.88
462.5
100
200
300
400
500
600
Wavenumber (cm-1)

WRMG 56

Garnet 2

Locality: Whitt Ranch
Collected by Susan Harris

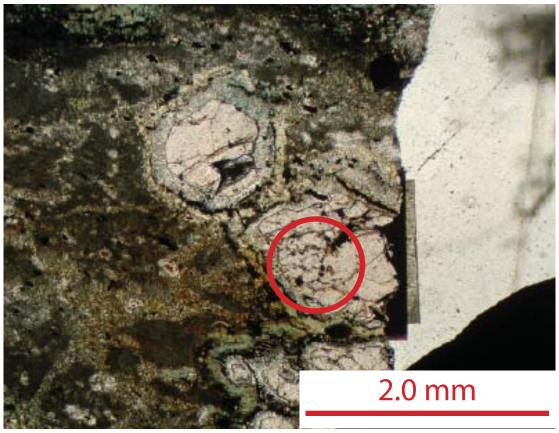

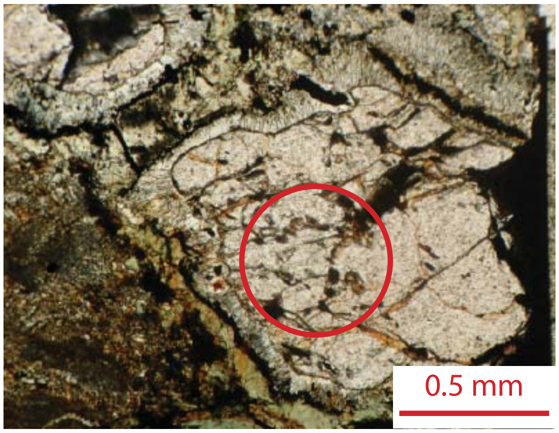

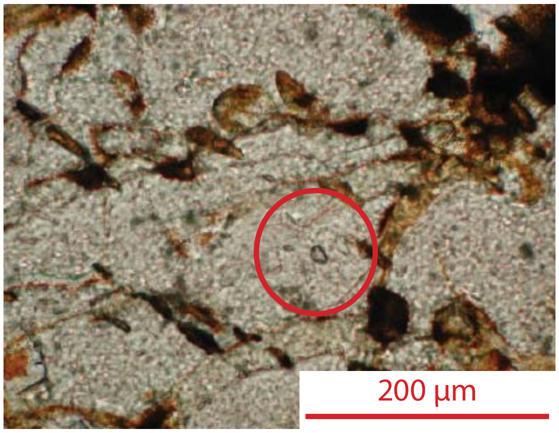

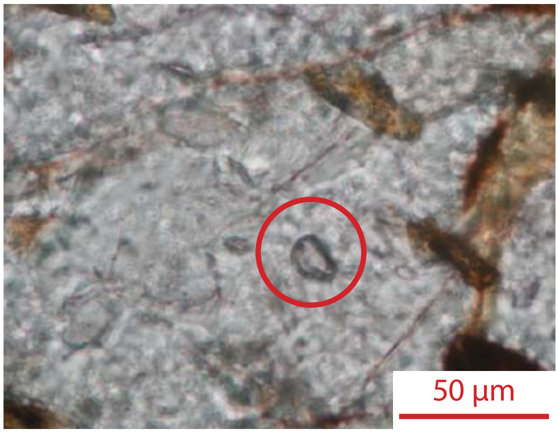

Inclusion Information

Maximum length (X-Y) (µm)	18.9
Minimum length (X-Y) (µm)	12.6
Inclusion thickness (Z) (µm)	10
Location (X-Y coordinates)	(130.5, 18.0)
Description of shape	Ovoid
Garnet composition	$Alm_{54.0}$, $Prp_{27.6}$, $Grs_{18.1}$, $Sps_{0.3}$

Data and Pressure Calculation Results

Depth of spectrum (µm)	-8
$\Delta\omega_1$ (cm^{-1})	6.28
$\Delta\omega_2$ (cm^{-1})	7.83
$P_{resid\ [\Delta\omega1]}$ (GPa)	0.369
$P_{resid\ [\Delta\omega2]}$ (GPa)	0.406
$P_{entrap\ [\Delta\omega1]}$ (GPa)	1.22
$P_{entrap\ [\Delta\omega2]}$ (GPa)	1.31

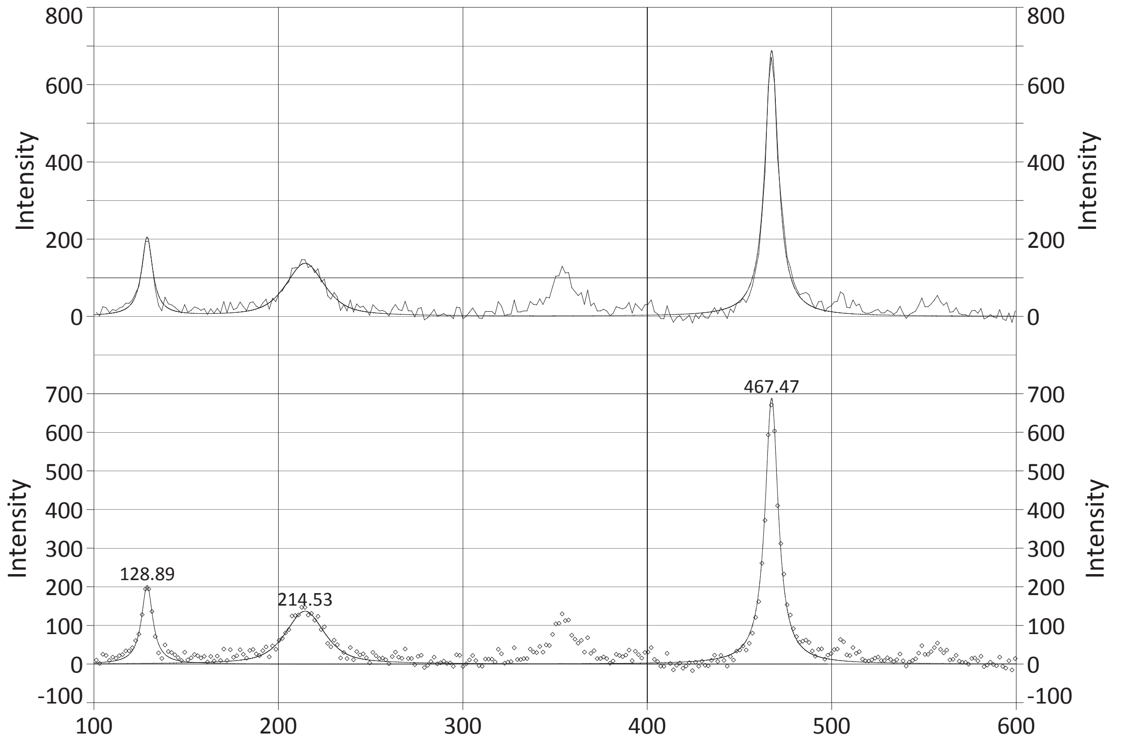

WRMG 56 - Garnet 2

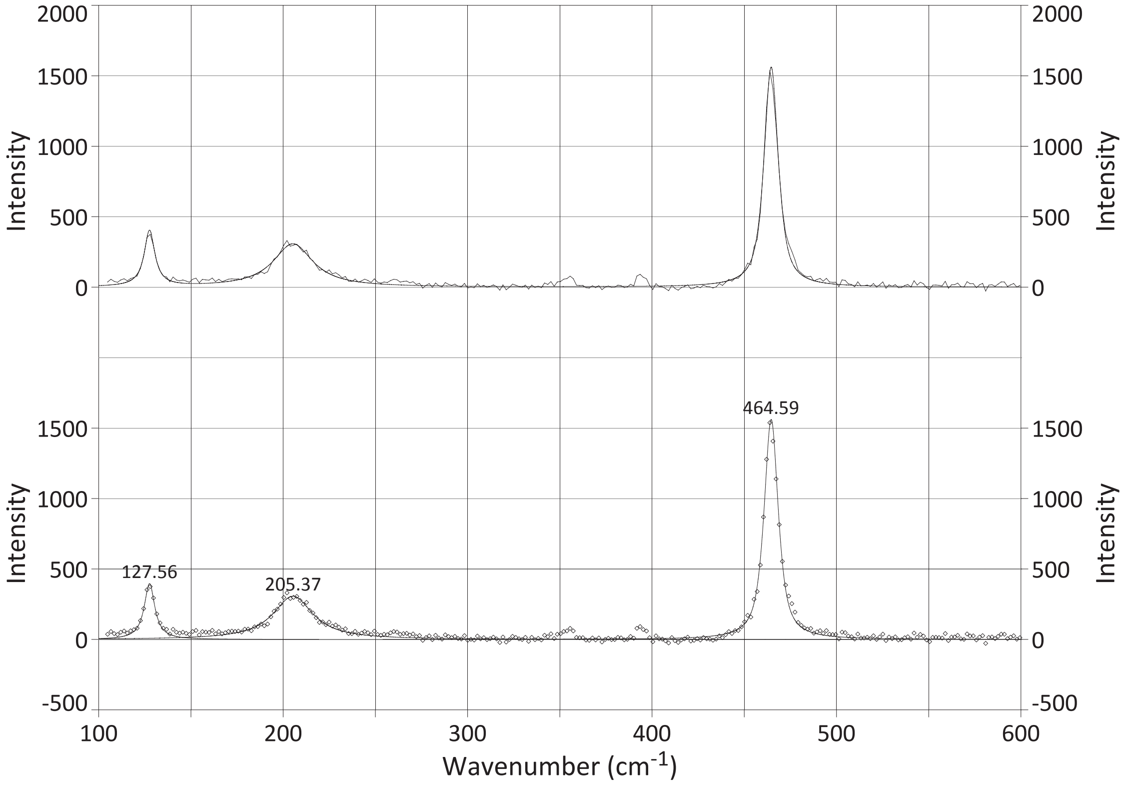

Quartz Standard

WRMG 56

Garnet 3

Locality: Whitt Ranch
Collected by Susan Harris

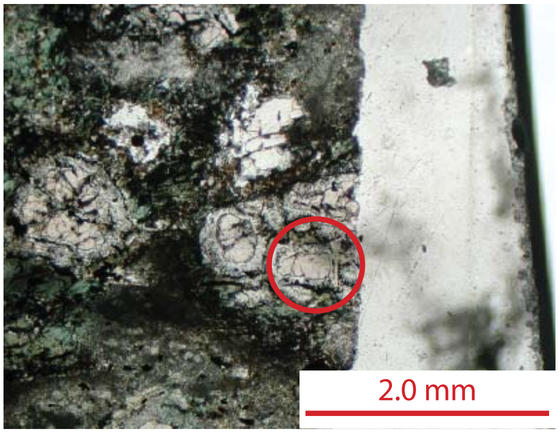

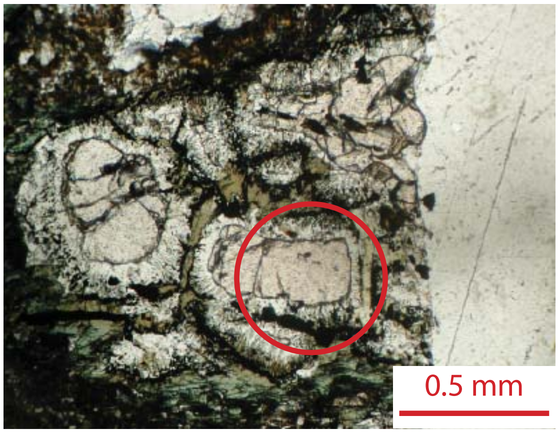

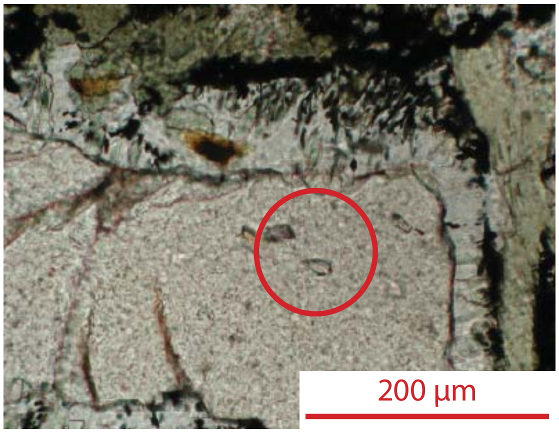

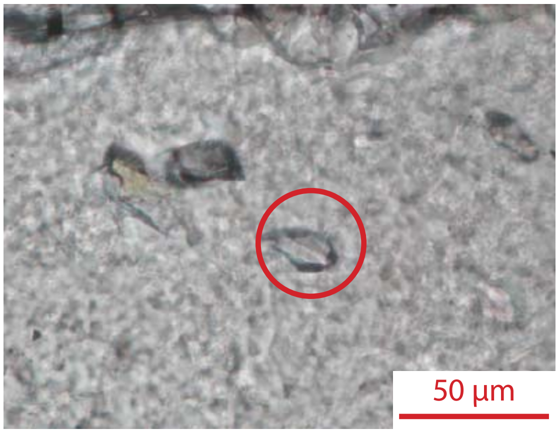

Inclusion Information

Maximum length (X-Y) (µm)	25.3
Minimum length (X-Y) (µm)	15.8
Inclusion thickness (Z) (µm)	19
Location (X-Y coordinates)	(130.5, 15.5)
Description of shape	Ellipsoid
Garnet composition	$Alm_{54.0}$, $Prp_{27.6}$, $Grs_{18.1}$, $Sps_{0.3}$

Data and Pressure Calculation Results

Depth of spectrum (µm)	-10
$\Delta\omega_1$ (cm^{-1})	2.82
$\Delta\omega_2$ (cm^{-1})	3.60
$P_{resid\ [\Delta\omega 1]}$ (GPa)	0.168
$P_{resid\ [\Delta\omega 2]}$ (GPa)	0.180
$P_{entrap\ [\Delta\omega 1]}$ (GPa)	0.73
$P_{entrap\ [\Delta\omega 2]}$ (GPa)	0.76

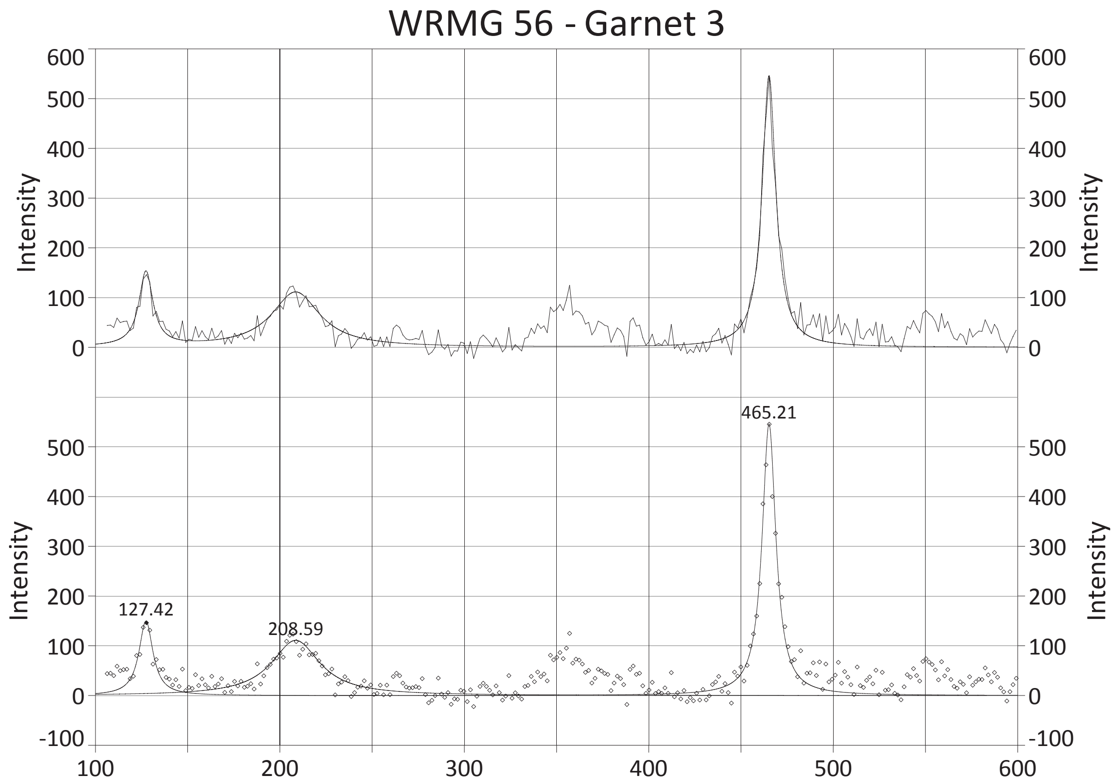
WRMG 56 - Garnet 3
Intensity
Intensity
600
500
400
300
200
100
0
-100
127.42
208.59
465.21
100
200
300
400
500
600

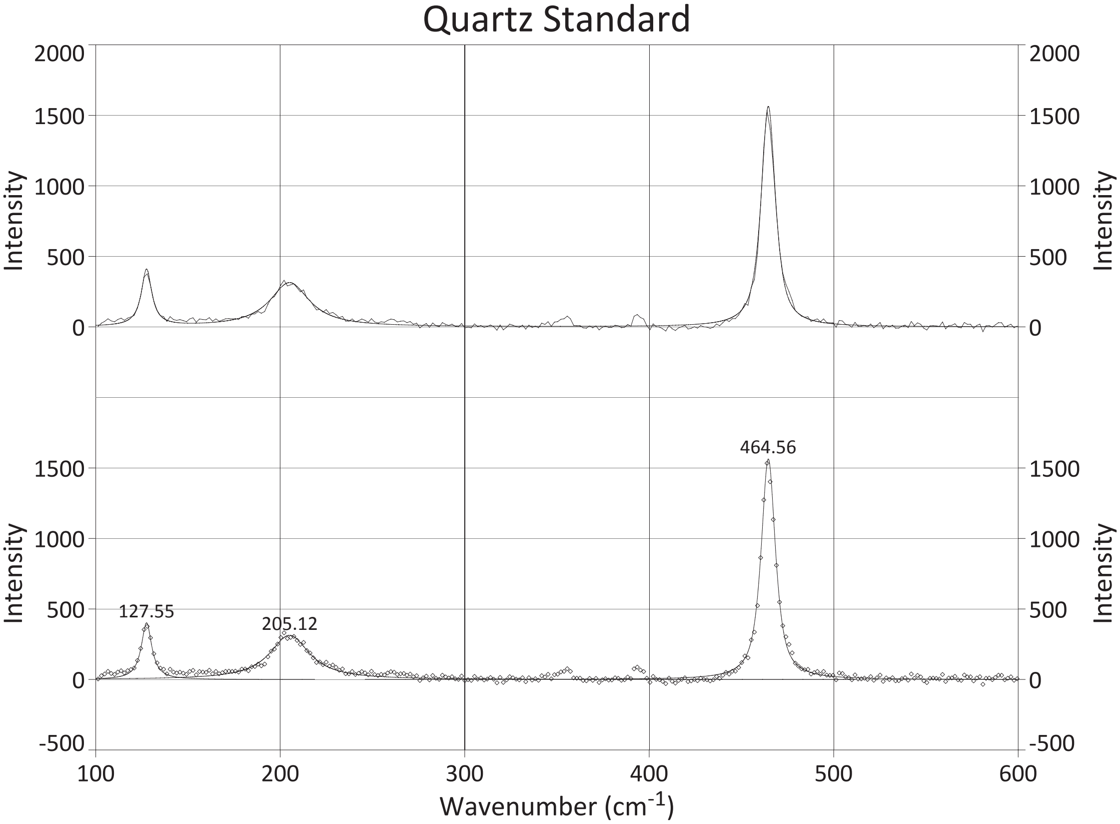
Quartz Standard
Intensity
Intensity
2000
1500
1000
500
0
-500
127.55
205.12
464.56
100
200
300
400
500
600
Wavenumber (cm-1)

WRMG 56

Garnet 4

Locality: Whitt Ranch
Collected by Susan Harris

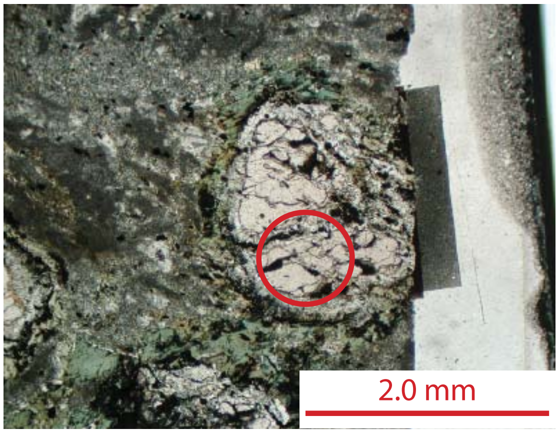

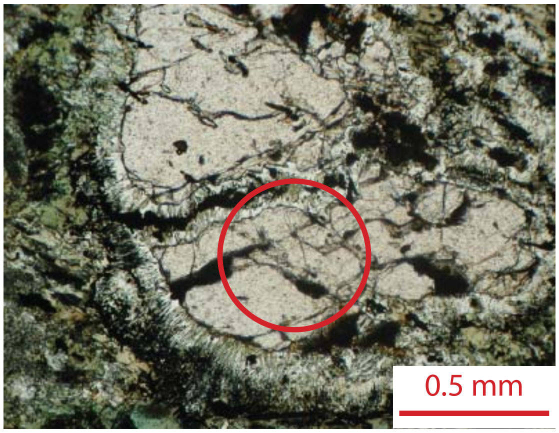

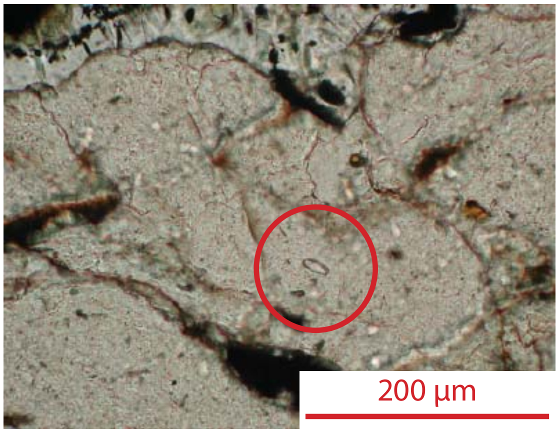

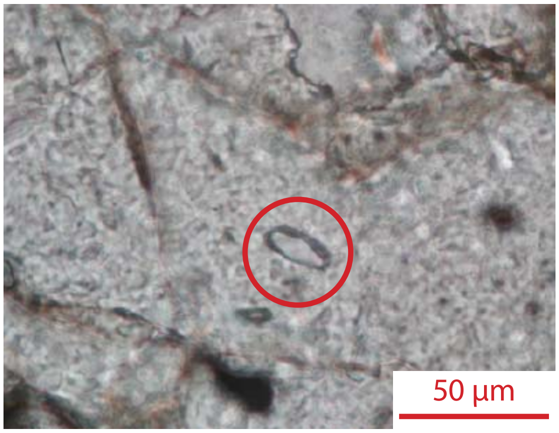

Inclusion Information

Maximum length (X-Y) (µm)	22.1
Minimum length (X-Y) (µm)	11.1
Inclusion thickness (Z) (µm)	14
Location (X-Y coordinates)	(130.3, 12.2)
Description of shape	Elongate
Garnet composition	$Alm_{54.0}$, $Prp_{27.6}$, $Grs_{18.1}$, $Sps_{0.3}$

Data and Pressure Calculation Results

Depth of spectrum (µm)	-10
$\Delta\omega_1$ (cm^{-1})	4.33
$\Delta\omega_2$ (cm^{-1})	5.64
$P_{resid\ [\Delta\omega1]}$ (GPa)	0.255
$P_{resid\ [\Delta\omega2]}$ (GPa)	0.287
$P_{entrap\ [\Delta\omega1]}$ (GPa)	0.94
$P_{entrap\ [\Delta\omega2]}$ (GPa)	1.02

WRMG 56 - Garnet 4

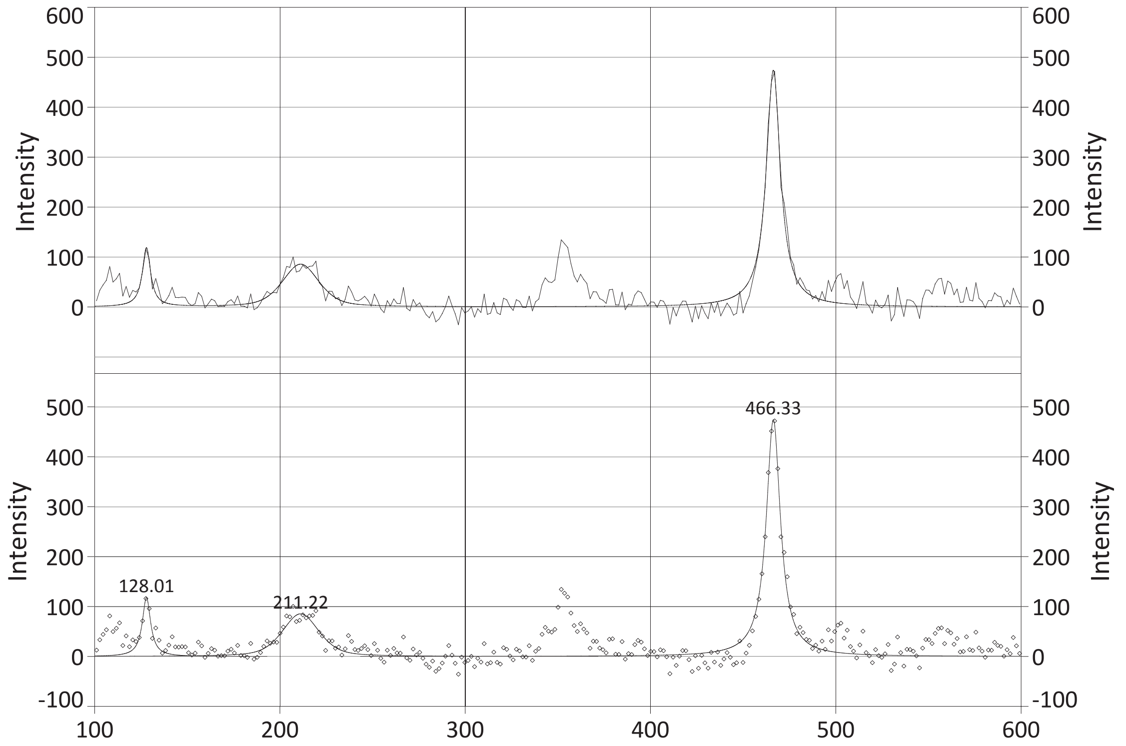

Quartz Standard

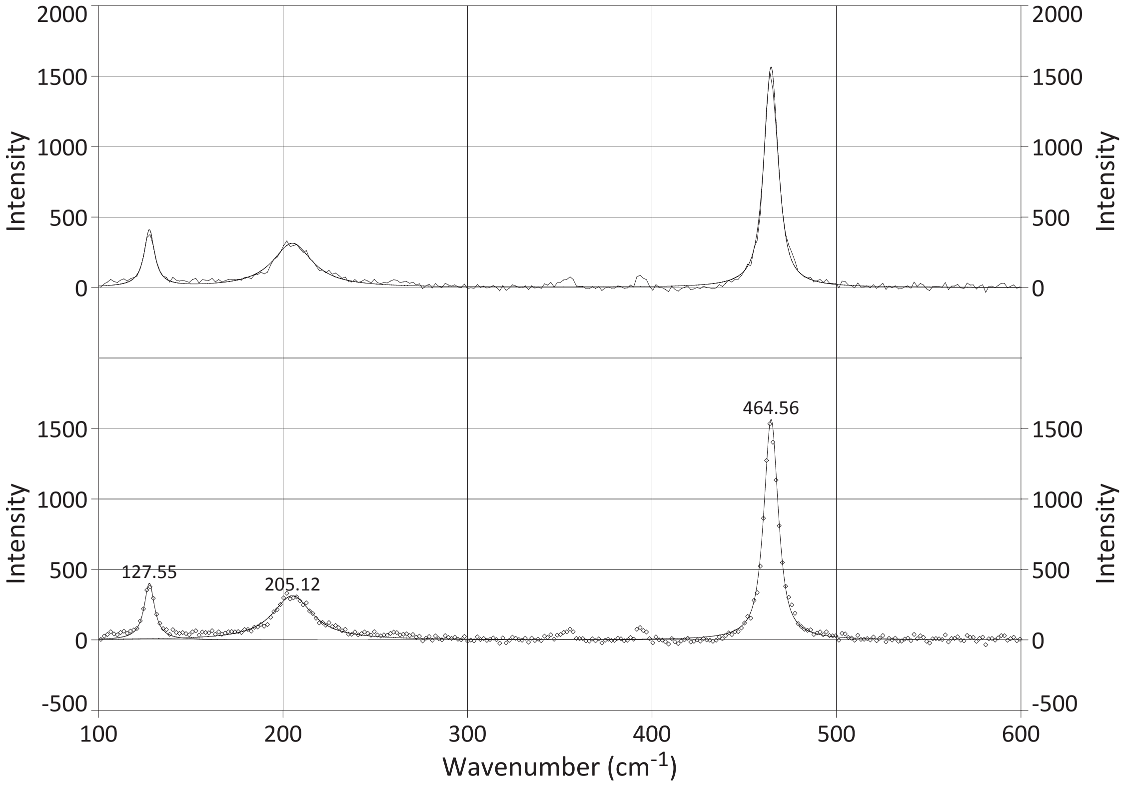

WRMG 56

Garnet 6

Locality: Whitt Ranch
Collected by Susan Harris

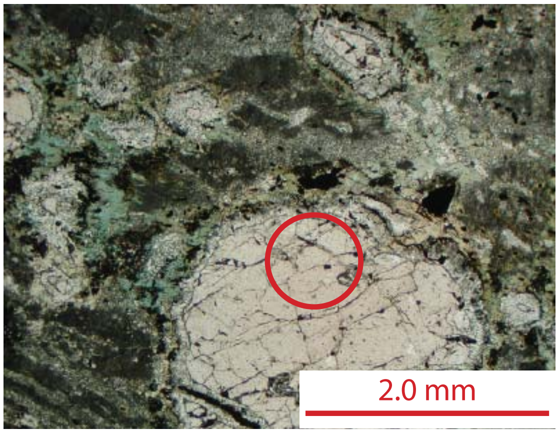

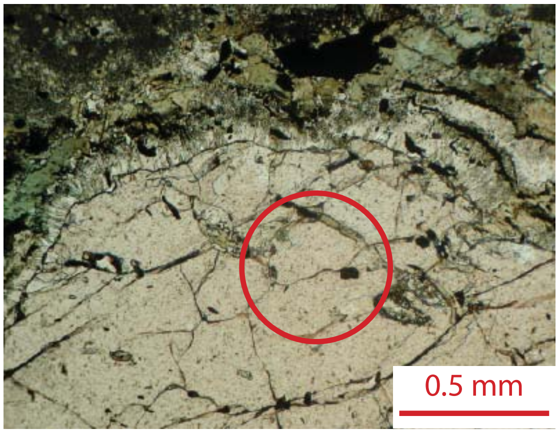

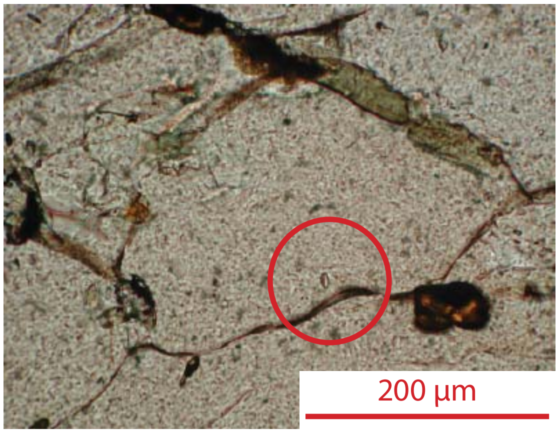

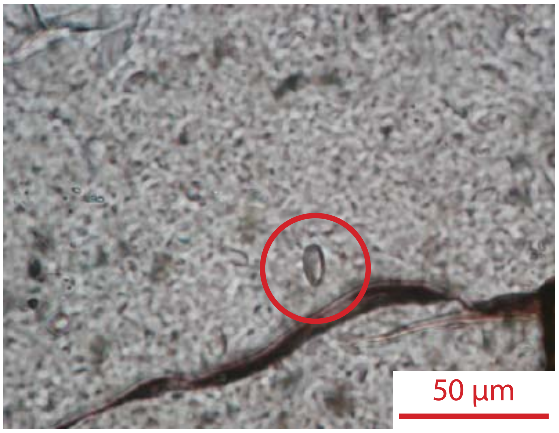

Inclusion Information

Maximum length (X-Y) (µm)	15.0
Minimum length (X-Y) (µm)	7.1
Inclusion thickness (Z) (µm)	10
Location (X-Y coordinates)	(111.0, 12.2)
Description of shape	Ellipsoid
Garnet composition	$Alm_{54.0}$, $Prp_{27.6}$, $Grs_{18.1}$, $Sps_{0.3}$

Data and Pressure Calculation Results

Depth of spectrum (µm)	-6
$\Delta\omega_1$ (cm^{-1})	2.69
$\Delta\omega_2$ (cm^{-1})	1.47
$P_{resid\ [\Delta\omega1]}$ (GPa)	0.160
$P_{resid\ [\Delta\omega2]}$ (GPa)	0.073
$P_{entrap\ [\Delta\omega1]}$ (GPa)	0.71
$P_{entrap\ [\Delta\omega2]}$ (GPa)	0.49

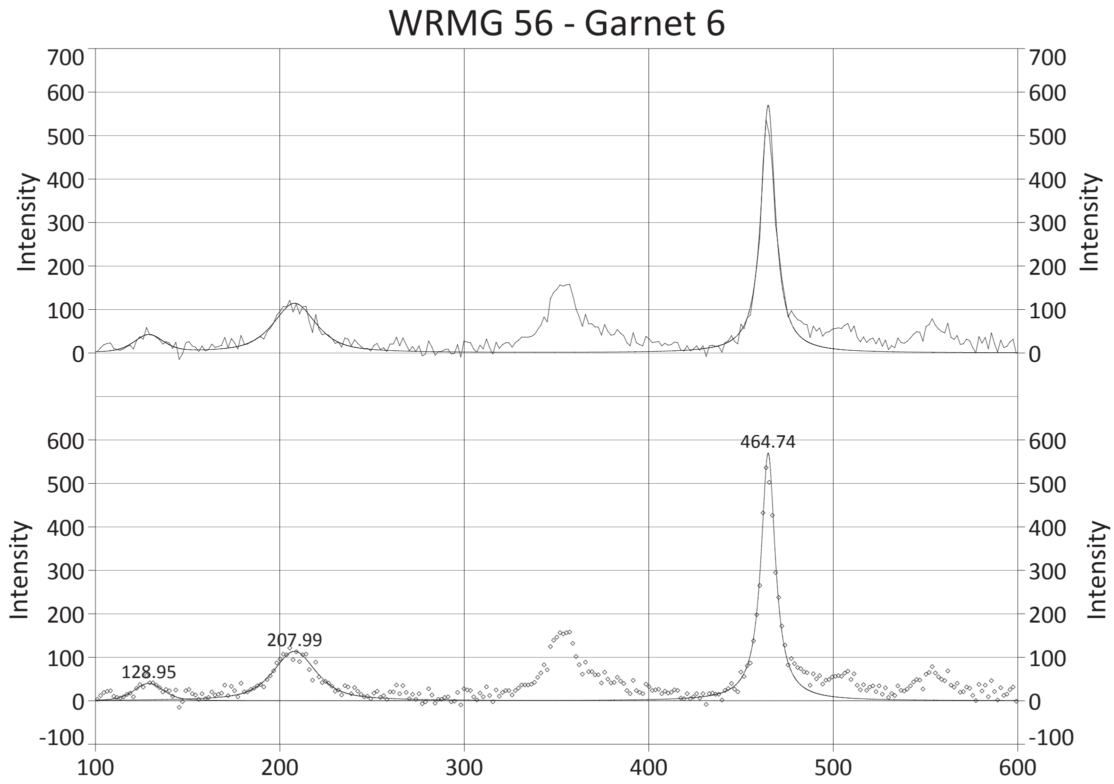
WRMG 56 - Garnet 6
Intensity
0
100
200
300
400
500
600
700
464.74
207.99
128.95
-100
100
200
300
400
500
600

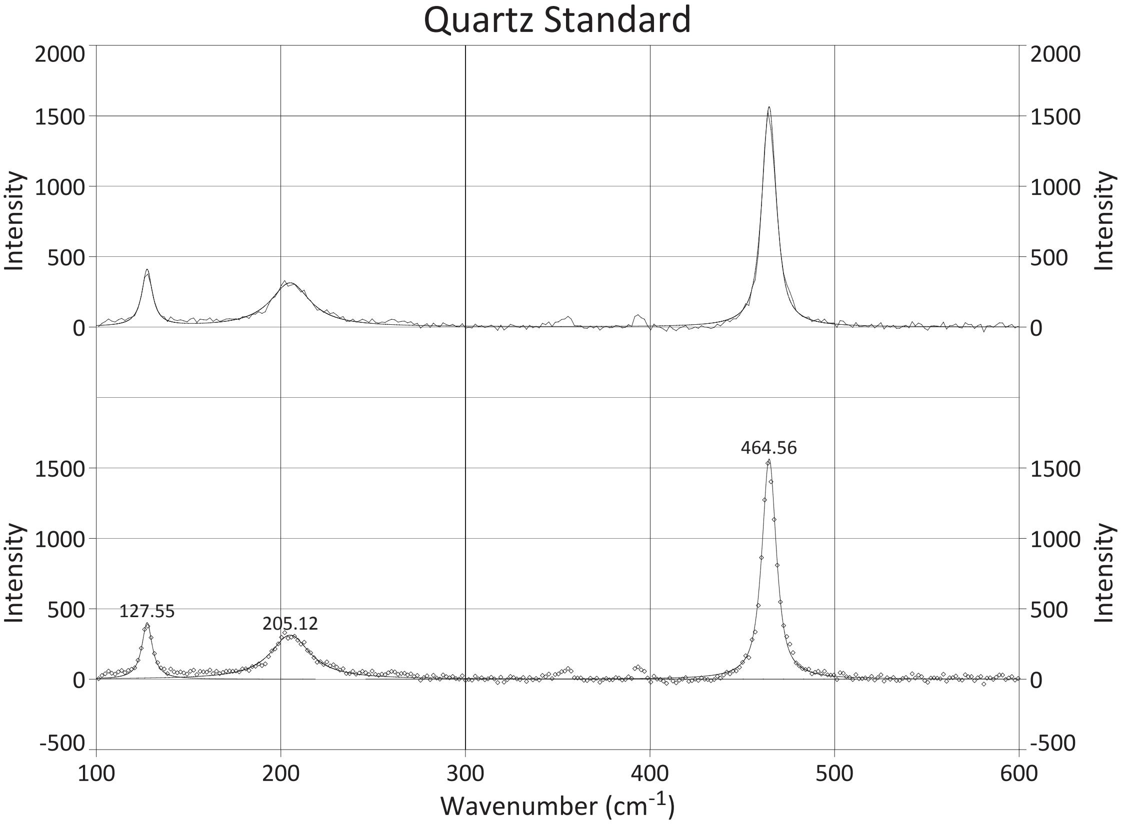
Quartz Standard
Intensity
0
500
1000
1500
2000
464.56
205.12
127.55
-500
100
200
300
400
500
600
Wavenumber (cm-1)

WRMG 56

Garnet 7

Locality: Whitt Ranch
Collected by Susan Harris

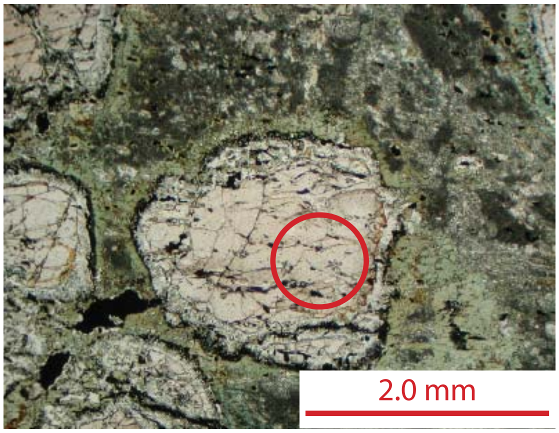

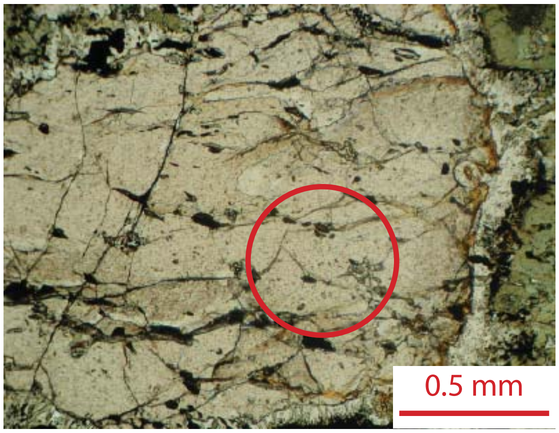

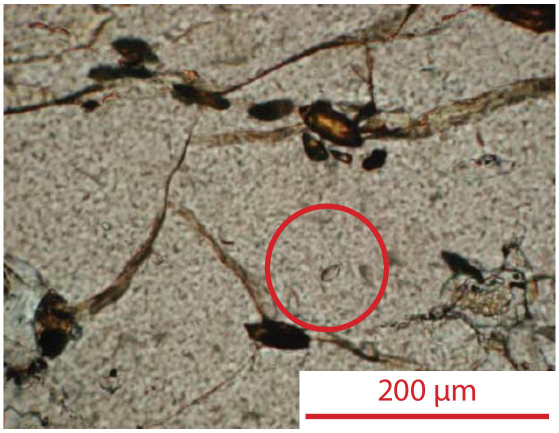

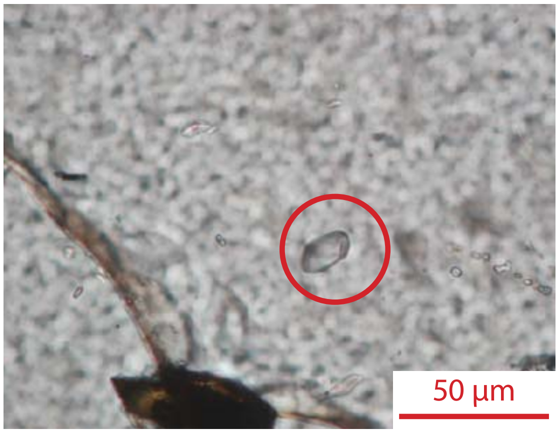

Inclusion Information

Maximum length (X-Y) (μm)	19.8
Minimum length (X-Y) (μm)	10.3
Inclusion thickness (Z) (μm)	16
Location (X-Y coordinates)	(112.7, 4.2)
Description of shape	Ellipsoid
Garnet composition	$Alm_{54.0}$, $Prp_{27.6}$, $Grs_{18.1}$, $Sps_{0.3}$

Data and Pressure Calculation Results

Depth of spectrum (μm)	-2
$\Delta\omega_1$ (cm^{-1})	1.78
$\Delta\omega_2$ (cm^{-1})	1.75
$P_{resid\ [\Delta\omega1]}$ (GPa)	0.107
$P_{resid\ [\Delta\omega2]}$ (GPa)	0.087
$P_{entrap\ [\Delta\omega1]}$ (GPa)	0.57
$P_{entrap\ [\Delta\omega2]}$ (GPa)	0.52

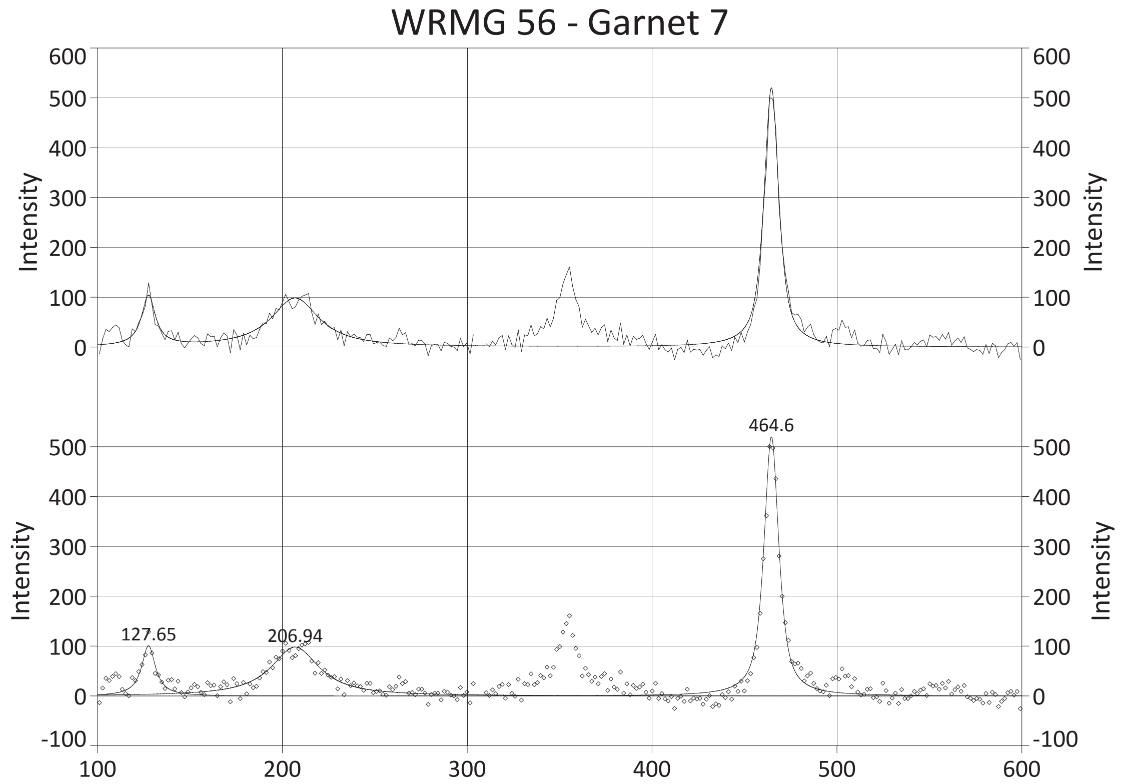

WRMG 56 - Garnet 7

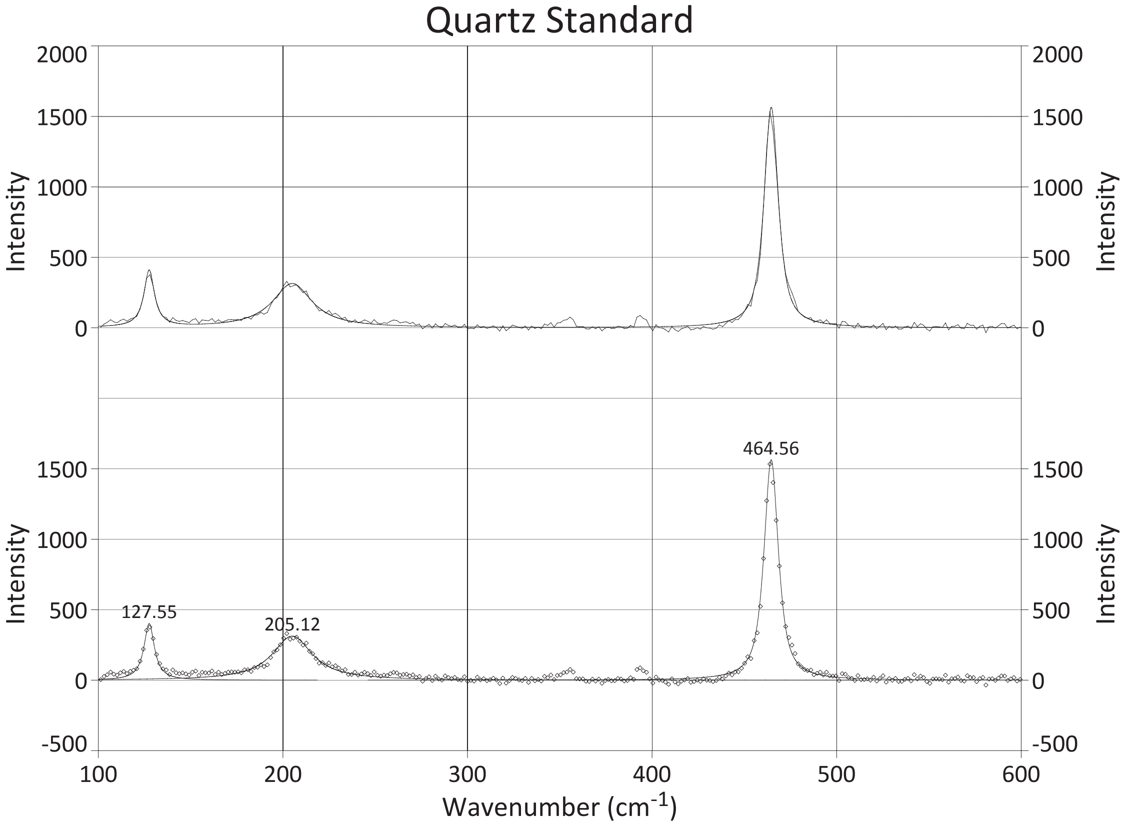

Quartz Standard

WRMG 60

Garnet 1

Locality: Whitt Ranch
Collected by Susan Harris

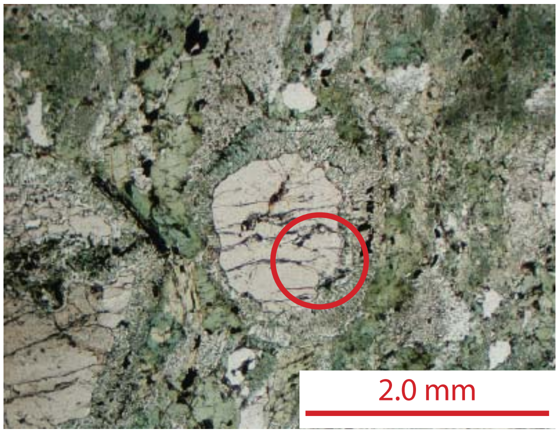

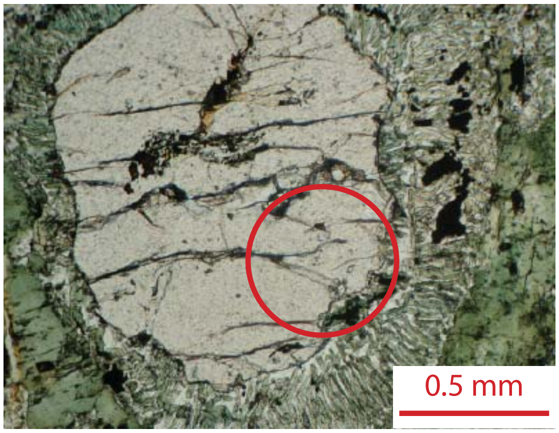

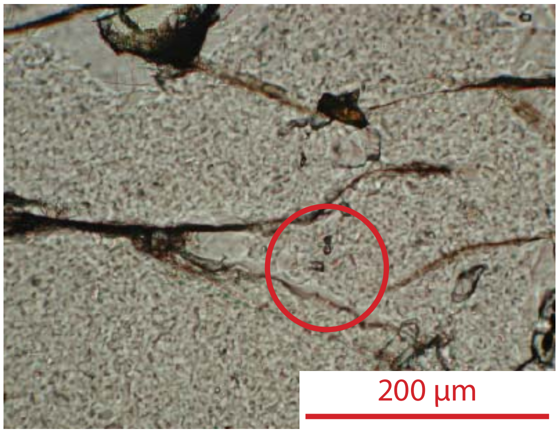

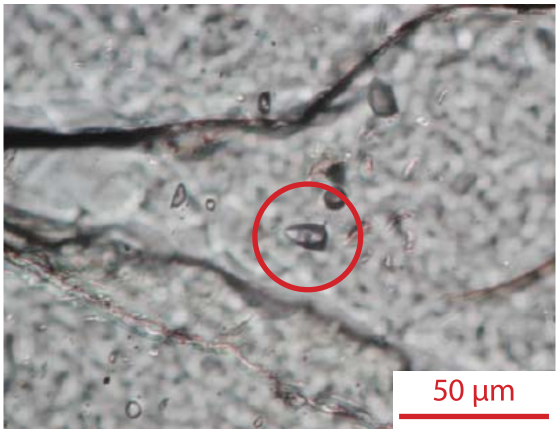

Inclusion Information

Maximum length (X-Y) (µm)	15.8
Minimum length (X-Y) (µm)	9.5
Inclusion thickness (Z) (µm)	18
Location (X-Y coordinates)	(125.7, 14.4)
Description of shape	Teardrop
Garnet composition	$Alm_{54.0}$, $Prp_{27.6}$, $Grs_{18.1}$, $Sps_{0.3}$

Data and Pressure Calculation Results

Depth of spectrum (µm)	-6
$\Delta\omega_1$ (cm^{-1})	-0.14
$\Delta\omega_2$ (cm^{-1})	-0.06
$P_{resid\ [\Delta\omega1]}$ (GPa)	-0.009
$P_{resid\ [\Delta\omega2]}$ (GPa)	-0.003
$P_{entrap\ [\Delta\omega1]}$ (GPa)	0.29
$P_{entrap\ [\Delta\omega2]}$ (GPa)	0.30

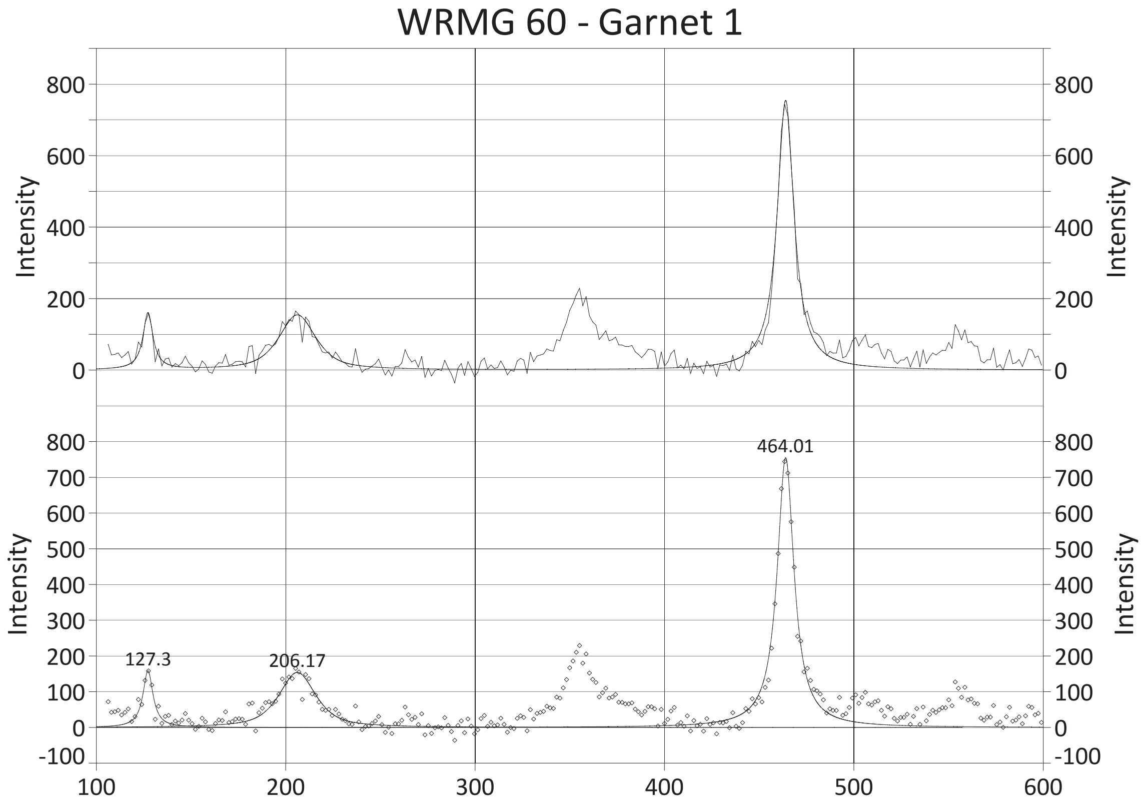

WRMG 60 - Garnet 1

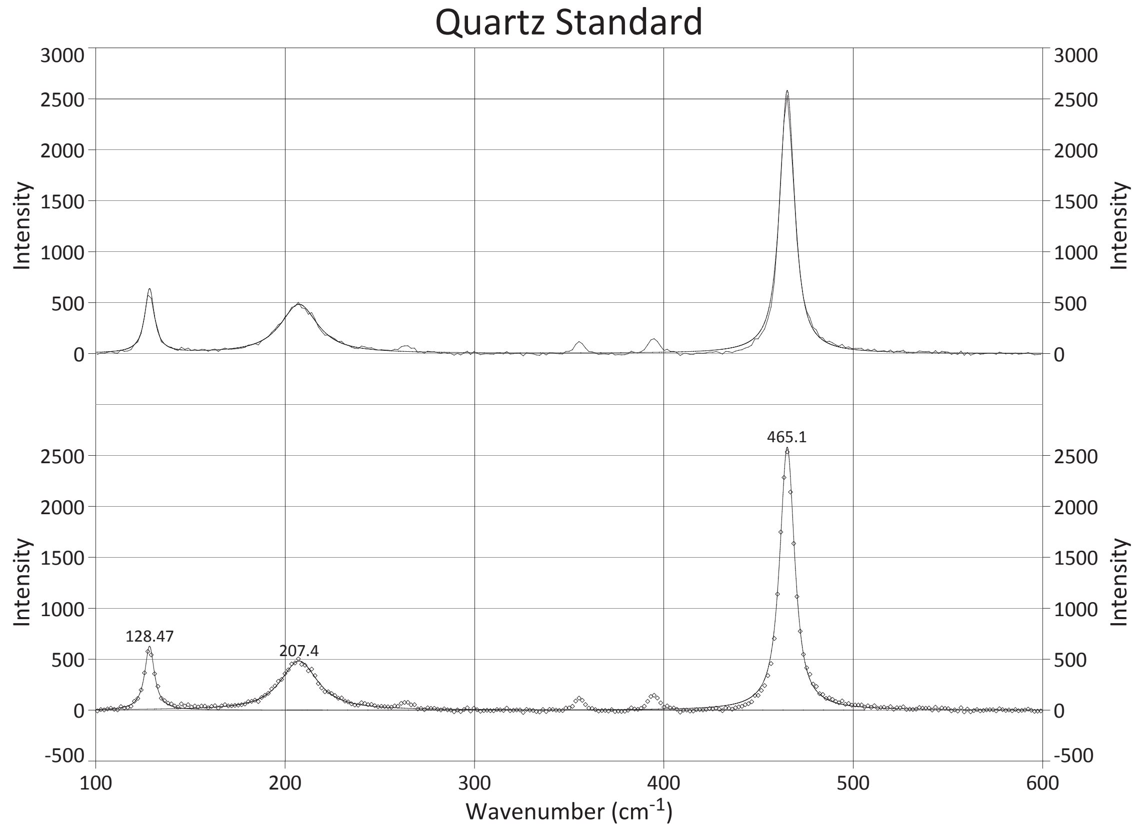

Quartz Standard

WRMG 60

Garnet 4

Locality: Whitt Ranch
Collected by Susan Harris

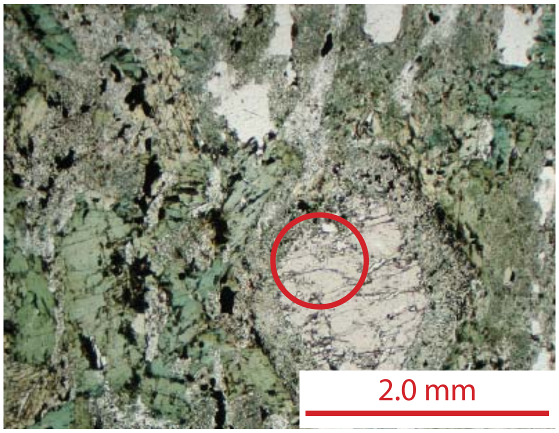

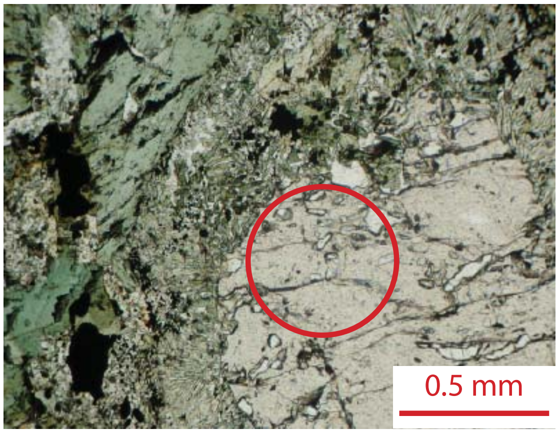

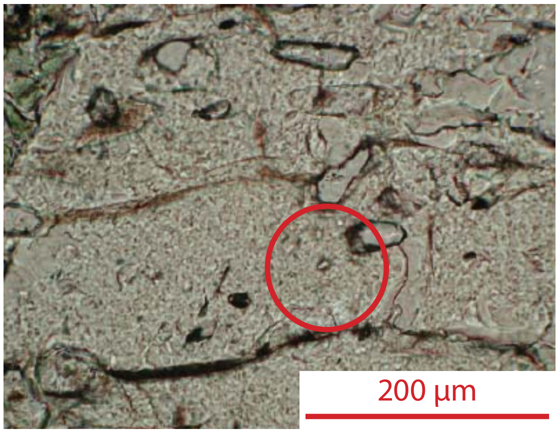

Inclusion Information

Maximum length (X-Y) (μm)	14.2
Minimum length (X-Y) (μm)	11.1
Inclusion thickness (Z) (μm)	12
Location (X-Y coordinates)	(125.4, 5.1)
Description of shape	Teardrop
Garnet composition	$Alm_{54.0}$, $Prp_{27.6}$, $Grs_{18.1}$, $Sps_{0.3}$

Data and Pressure Calculation Results

Depth of spectrum (μm)	-2
$\Delta\omega_1$ (cm^{-1})	0.13
$\Delta\omega_2$ (cm^{-1})	0.26
$P_{resid\ [\Delta\omega1]}$ (GPa)	0.008
$P_{resid\ [\Delta\omega2]}$ (GPa)	0.013
$P_{entrap\ [\Delta\omega1]}$ (GPa)	0.33
$P_{entrap\ [\Delta\omega2]}$ (GPa)	0.34

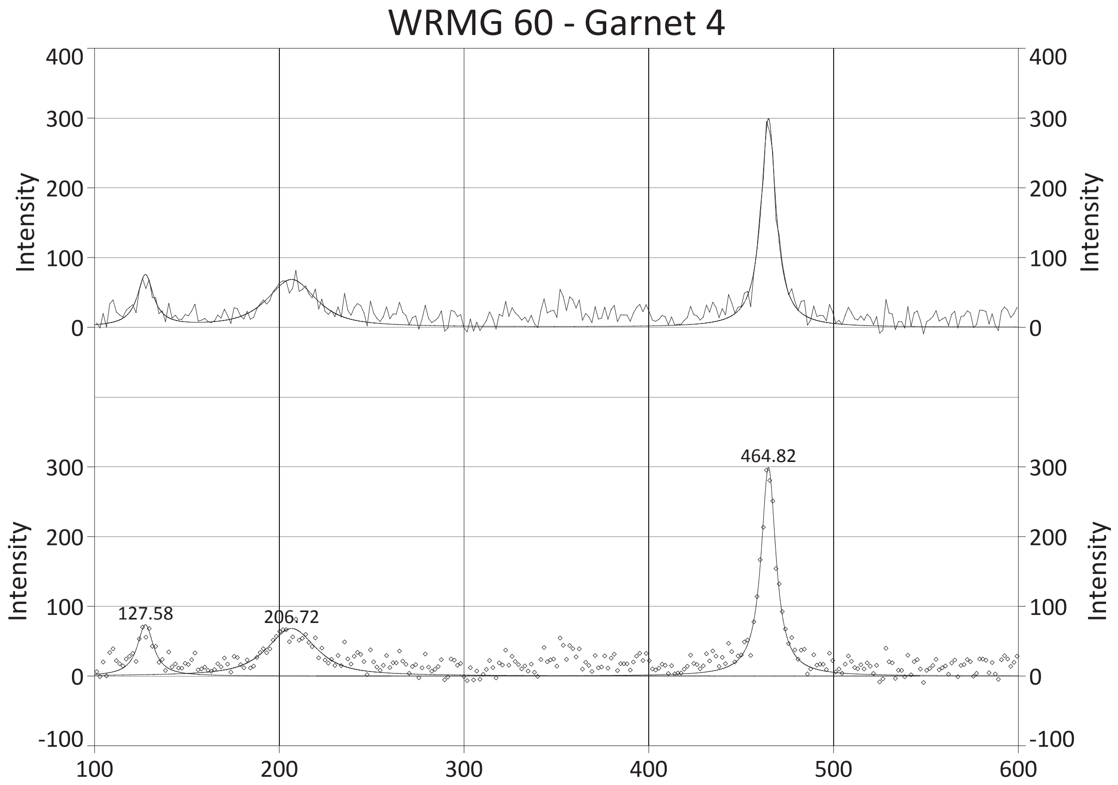

WRMG 60 - Garnet 4

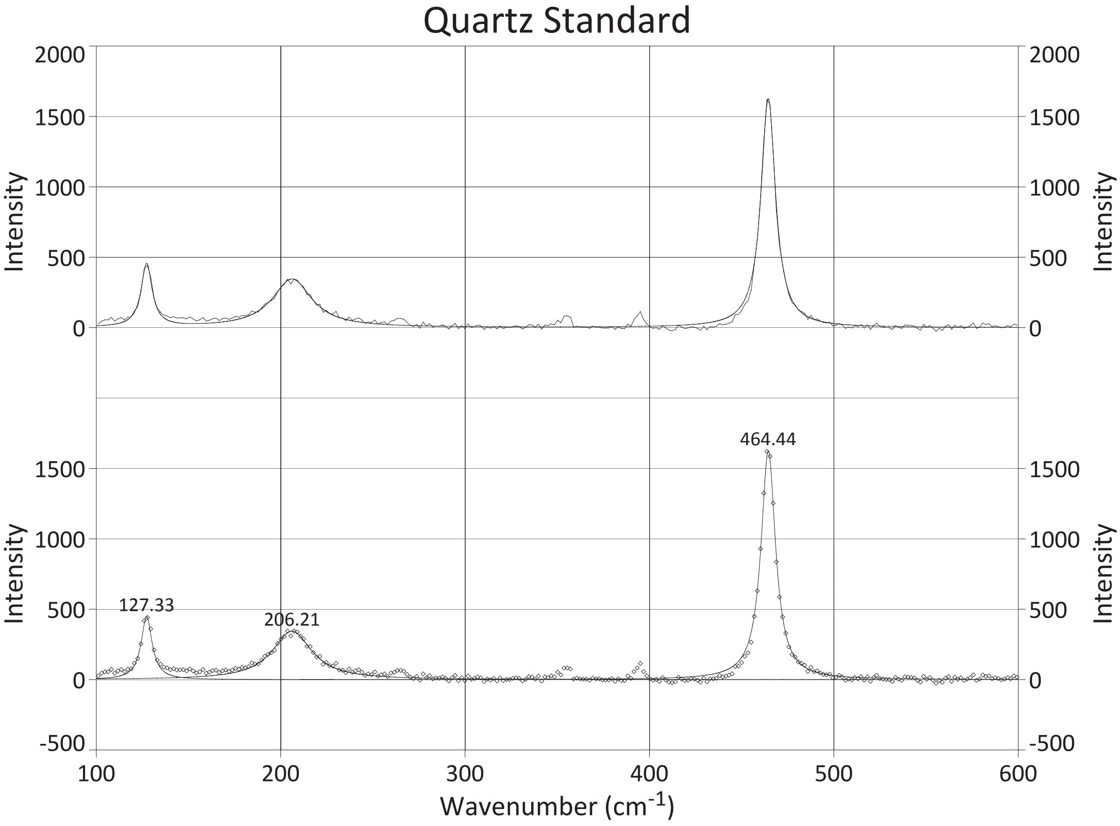

Quartz Standard

WRMG 60

Garnet 5

Locality: Whitt Ranch
Collected by Susan Harris

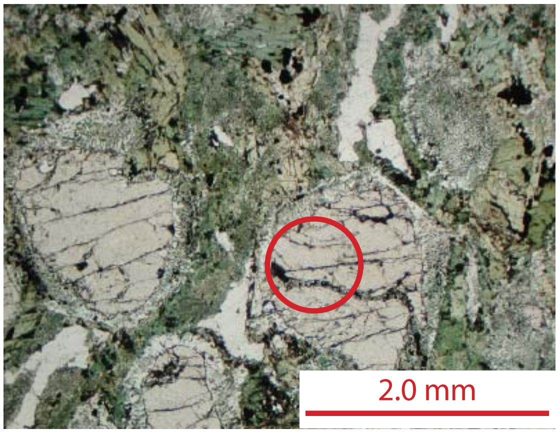

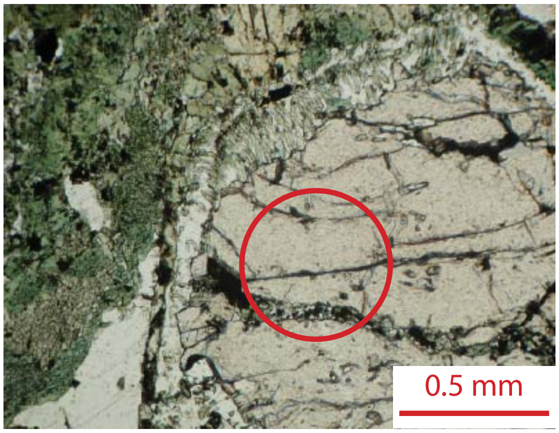

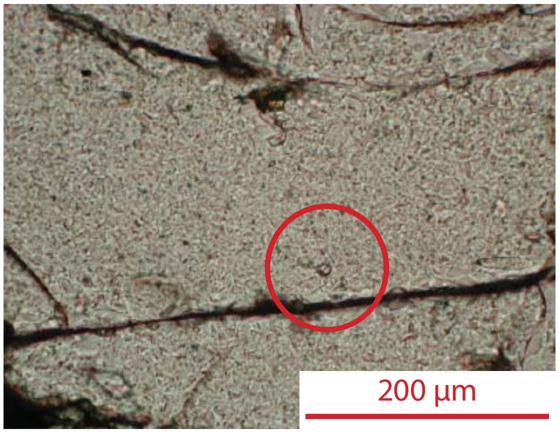

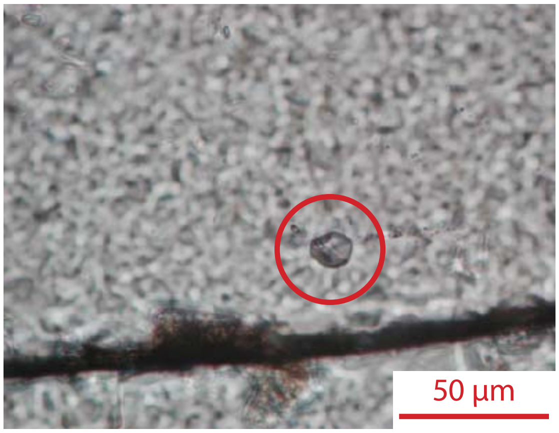

Inclusion Information

Maximum length (X-Y) (µm)	15.0
Minimum length (X-Y) (µm)	12.6
Inclusion thickness (Z) (µm)	15
Location (X-Y coordinates)	(120.5, 0.8)
Description of shape	Subspherical
Garnet composition	$Alm_{54.0}$, $Prp_{27.6}$, $Grs_{18.1}$, $Sps_{0.3}$

Data and Pressure Calculation Results

Depth of spectrum (µm)	-5
$\Delta\omega_1$ (cm^{-1})	5.00
$\Delta\omega_2$ (cm^{-1})	4.27
$P_{resid\ [\Delta\omega1]}$ (GPa)	0.294
$P_{resid\ [\Delta\omega2]}$ (GPa)	0.215
$P_{entrap\ [\Delta\omega1]}$ (GPa)	1.04
$P_{entrap\ [\Delta\omega2]}$ (GPa)	0.84

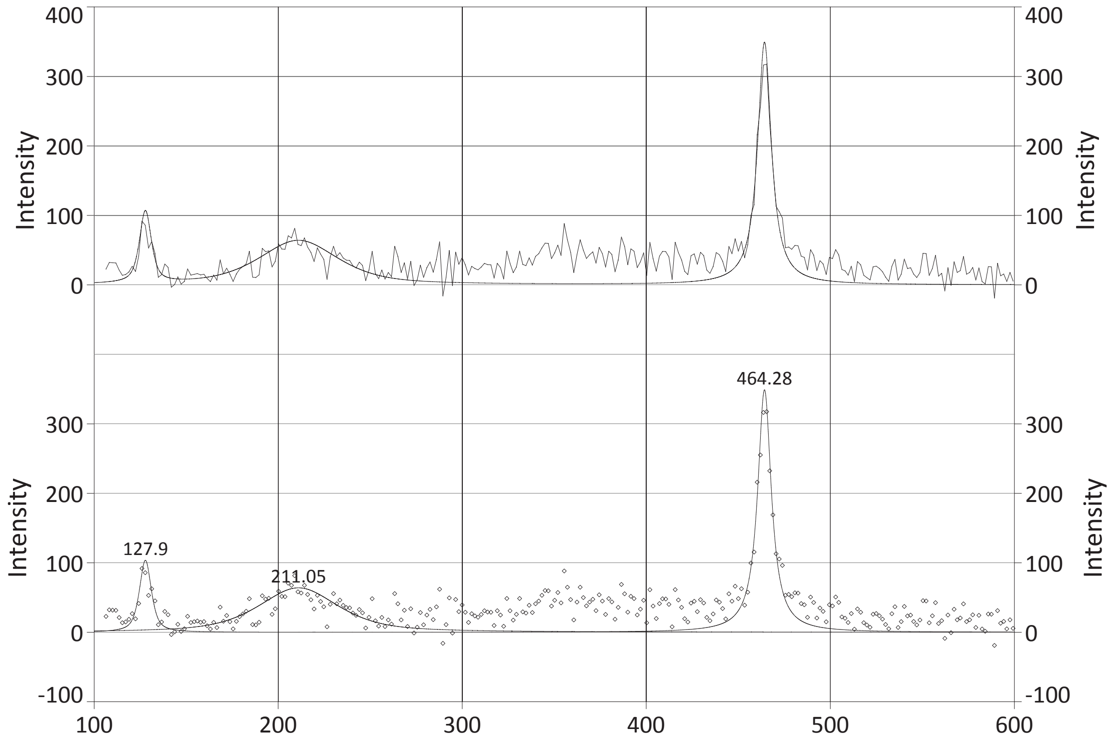

WRMG 60 - Garnet 5

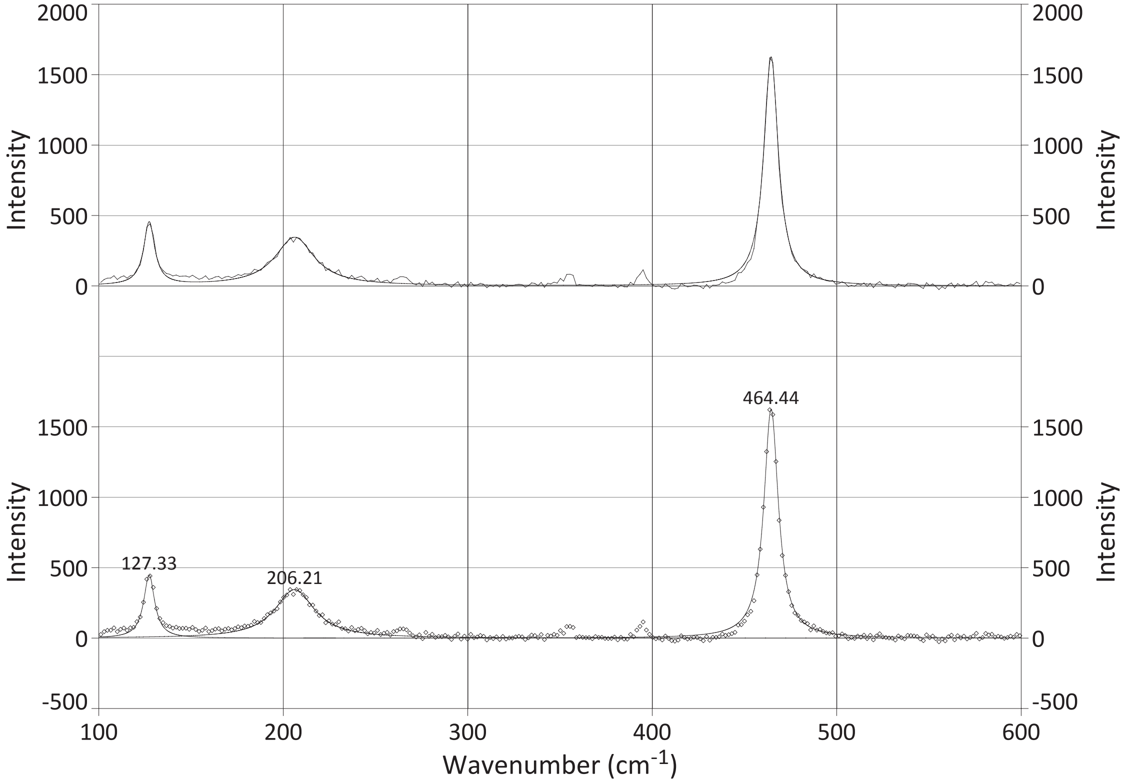

Quartz Standard

WRMG 60

Garnet 7

Locality: Whitt Ranch
Collected by Susan Harris

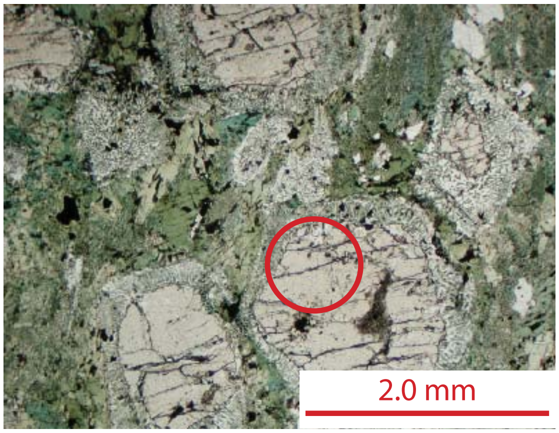

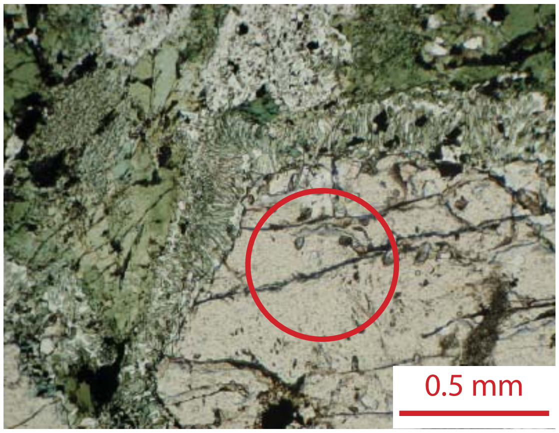

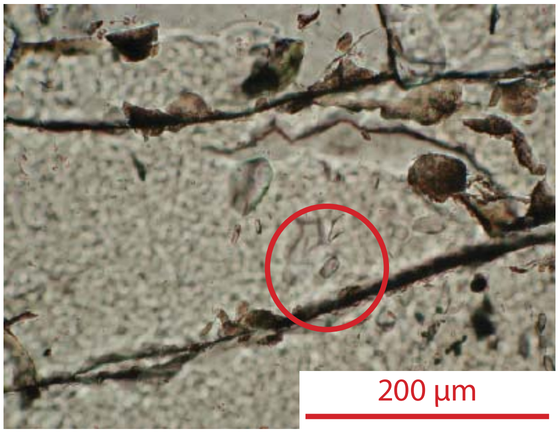

Inclusion Information

Maximum length (X-Y) (μm)	20.5
Minimum length (X-Y) (μm)	11.9
Inclusion thickness (Z) (μm)	15
Location (X-Y coordinates)	(105.5, 0.6)
Description of shape	Tabular
Garnet composition	$Alm_{54.0}$, $Prp_{27.6}$, $Grs_{18.1}$, $Sps_{0.3}$

Data and Pressure Calculation Results

Depth of spectrum (μm)	-2
$\Delta\omega_1$ (cm^{-1})	0.83
$\Delta\omega_2$ (cm^{-1})	-1.14
$P_{resid\ [\Delta\omega1]}$ (GPa)	0.051
$P_{resid\ [\Delta\omega2]}$ (GPa)	-0.056
$P_{entrap\ [\Delta\omega1]}$ (GPa)	0.43
$P_{entrap\ [\Delta\omega2]}$ (GPa)	0.17

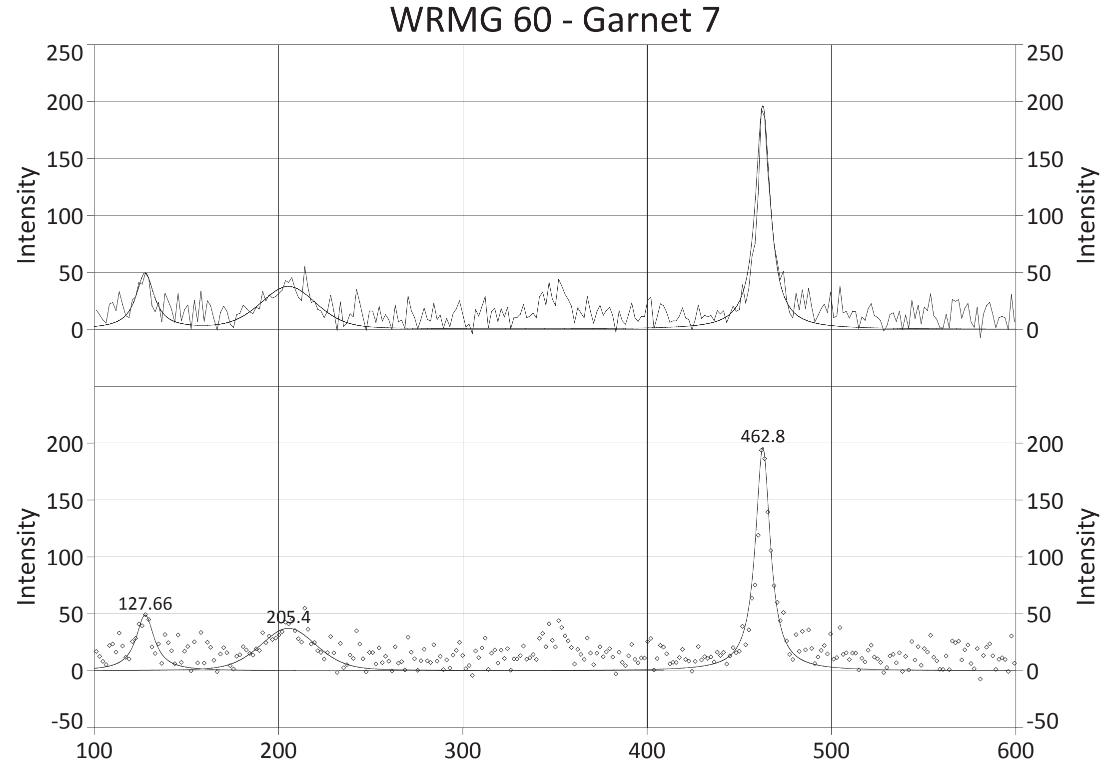

WRMG 60 - Garnet 7

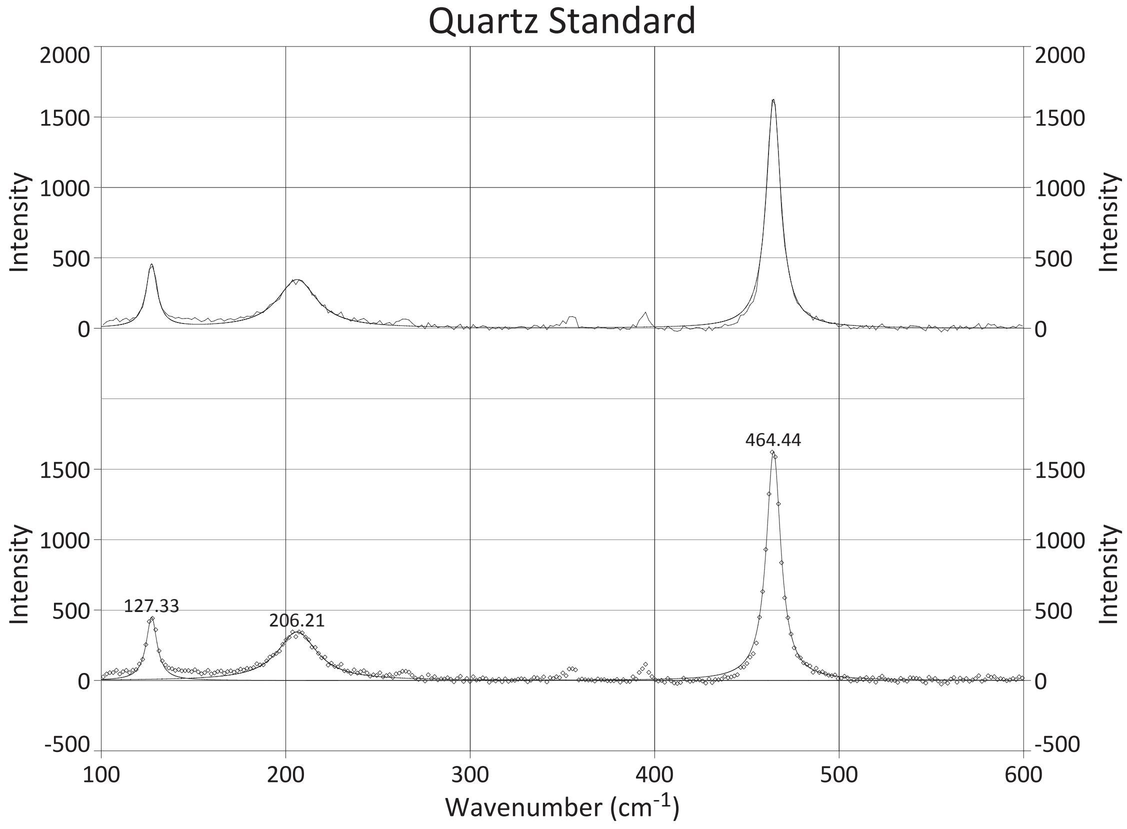

Quartz Standard

WRMG 60

Garnet 9

Locality: Whitt Ranch
Collected by Susan Harris

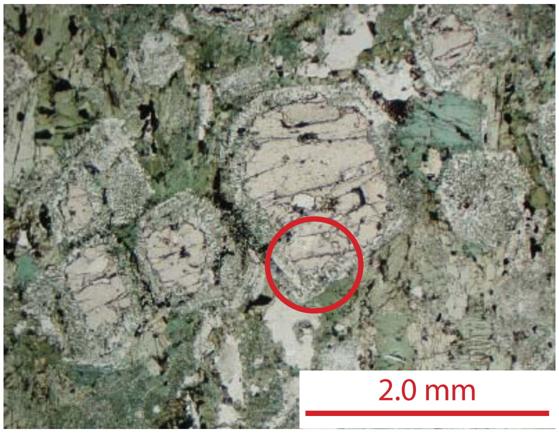

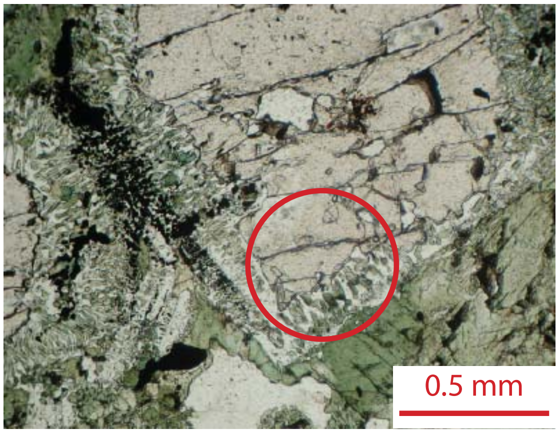

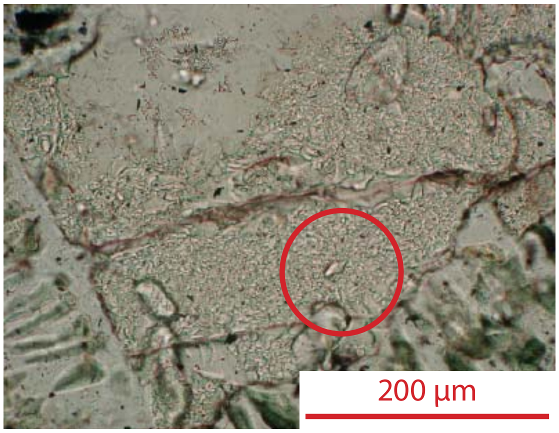

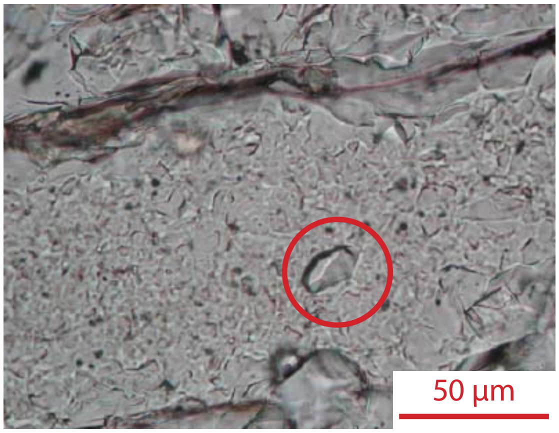

Inclusion Information

Maximum length (X-Y) (μm)	23.7
Minimum length (X-Y) (μm)	13.4
Inclusion thickness (Z) (μm)	11
Location (X-Y coordinates)	(109.3, 10.1)
Description of shape	Ellipsoid
Garnet composition	$Alm_{54.0}$, $Prp_{27.6}$, $Grs_{18.1}$, $Sps_{0.3}$

Data and Pressure Calculation Results

Depth of spectrum (μm)	-7
$\Delta\omega_1$ (cm^{-1})	9.67
$\Delta\omega_2$ (cm^{-1})	10.02
$P_{resid\ [\Delta\omega1]}$ (GPa)	0.582
$P_{resid\ [\Delta\omega2]}$ (GPa)	0.531
$P_{entrap\ [\Delta\omega1]}$ (GPa)	1.76
$P_{entrap\ [\Delta\omega2]}$ (GPa)	1.63

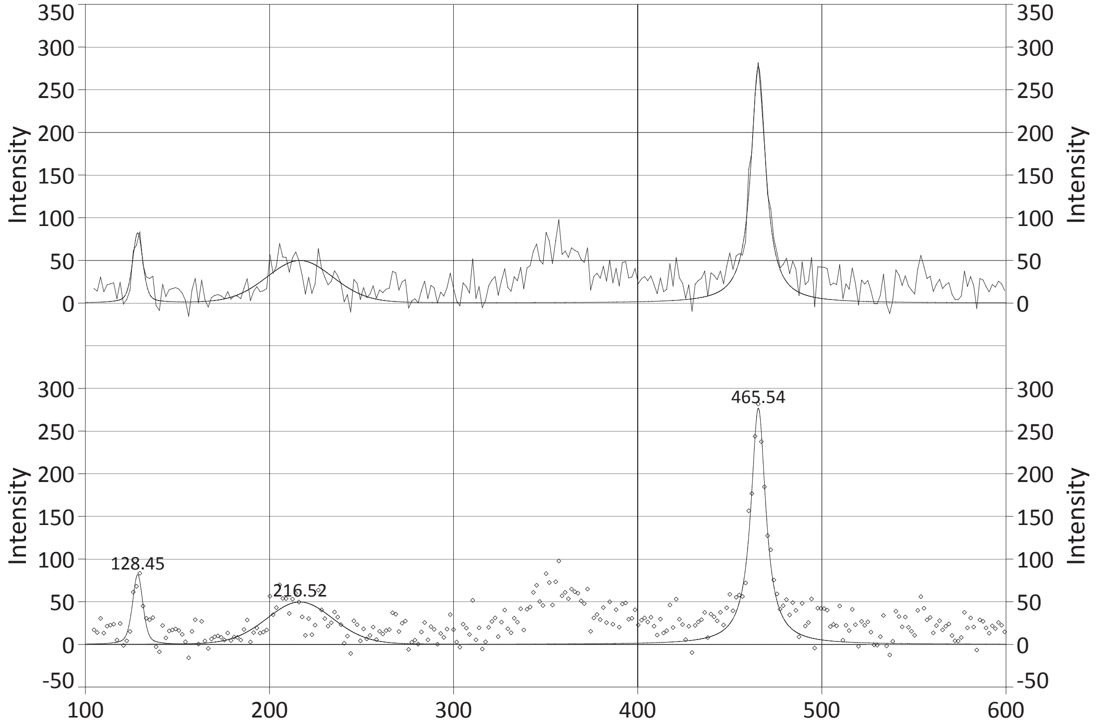

WRMG 60 - Garnet 9

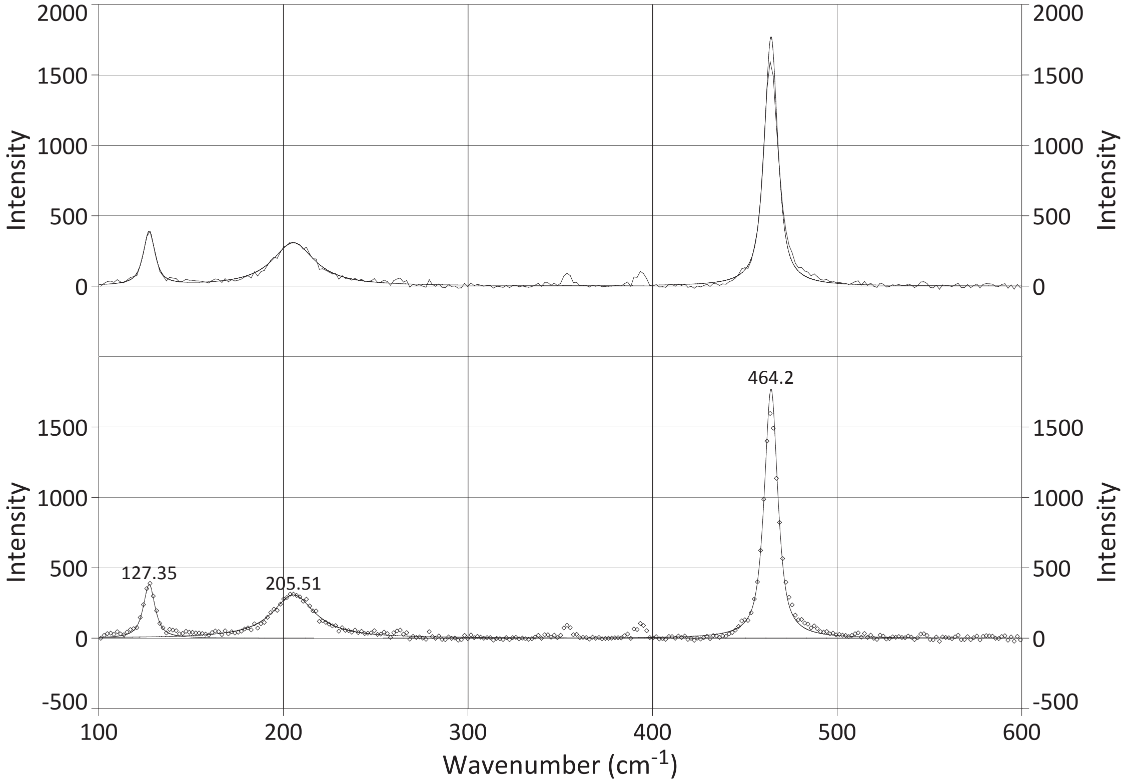

Quartz Standard

WRMG 61

Garnet 1

Locality: Whitt Ranch
Collected by Susan Harris

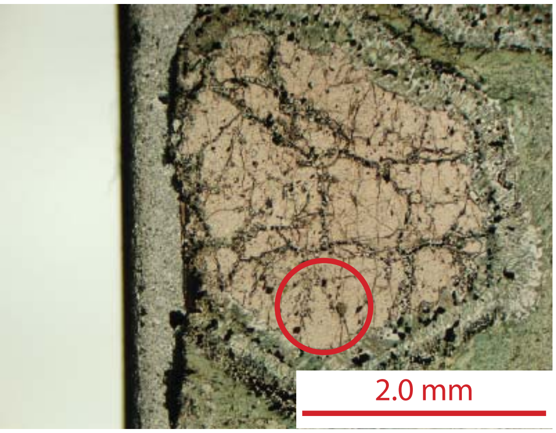

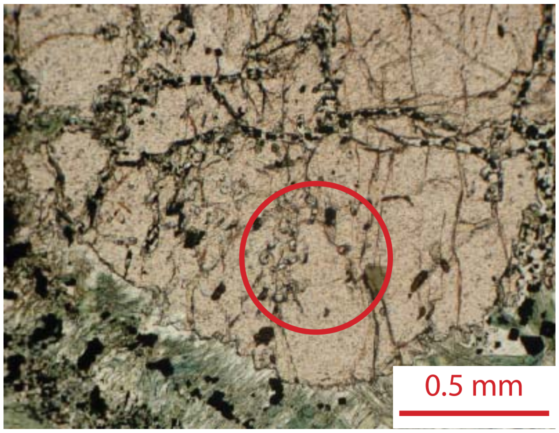

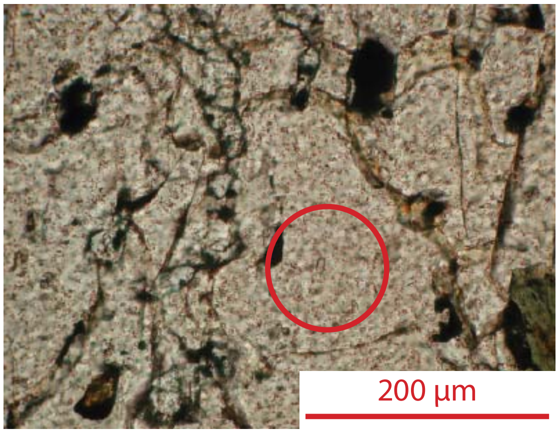

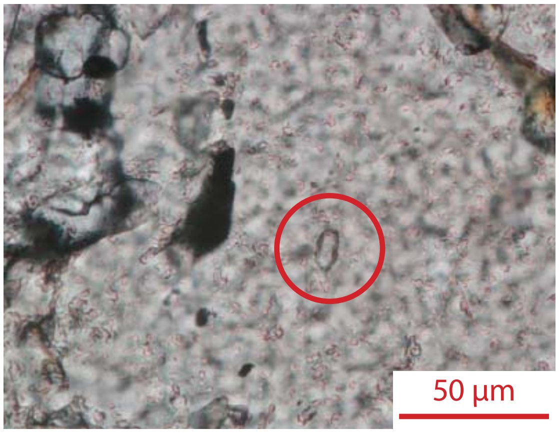

Inclusion Information

Maximum length (X-Y) (µm)	14.2
Minimum length (X-Y) (µm)	7.9
Inclusion thickness (Z) (µm)	11
Location (X-Y coordinates)	-(105.6, 13.5)
Description of shape	Spherical
Garnet composition	$Alm_{54.0}$, $Prp_{27.6}$, $Grs_{18.1}$, $Sps_{0.3}$

Data and Pressure Calculation Results

Depth of spectrum (µm)	-6
$\Delta\omega_1$ (cm^{-1})	2.27
$\Delta\omega_2$ (cm^{-1})	-3.10
$P_{\text{resid }[\Delta\omega1]}$ (GPa)	0.136
$P_{\text{resid }[\Delta\omega2]}$ (GPa)	0.142
$P_{\text{entrap }[\Delta\omega1]}$ (GPa)	0.65
$P_{\text{entrap }[\Delta\omega2]}$ (GPa)	0.66

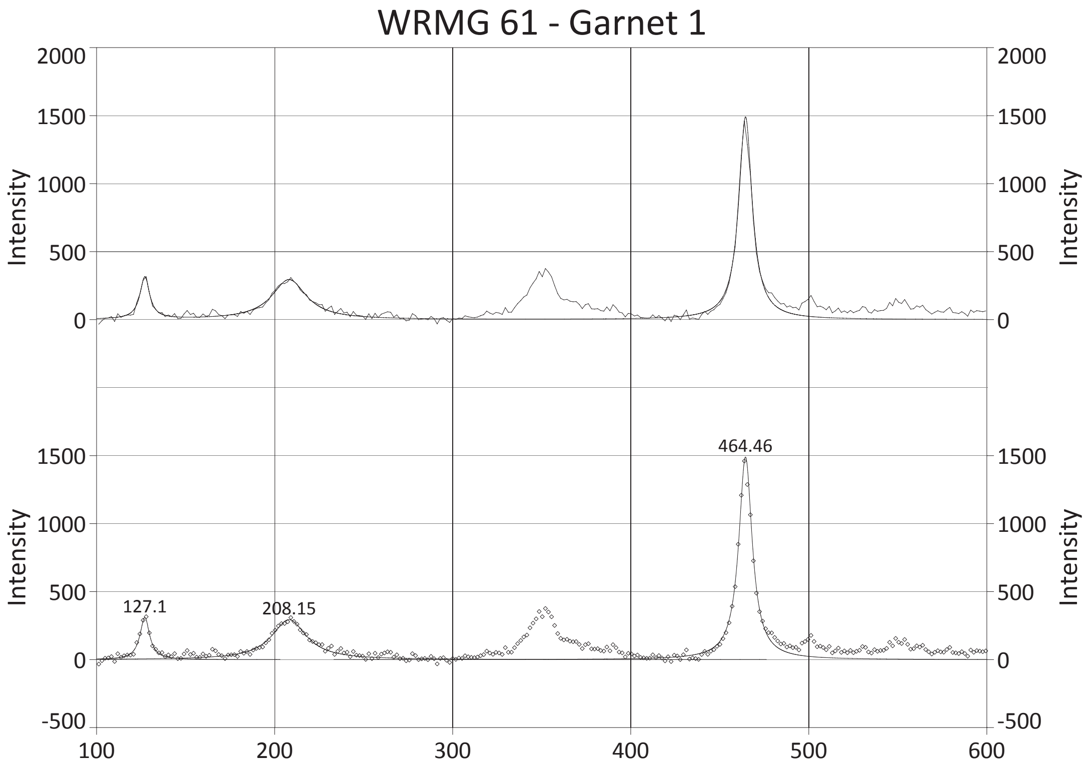
WRMG 61 - Garnet 1
Intensity
2000
1500
1000
500
0
-500
464.46
127.1
208.15
100
200
300
400
500
600

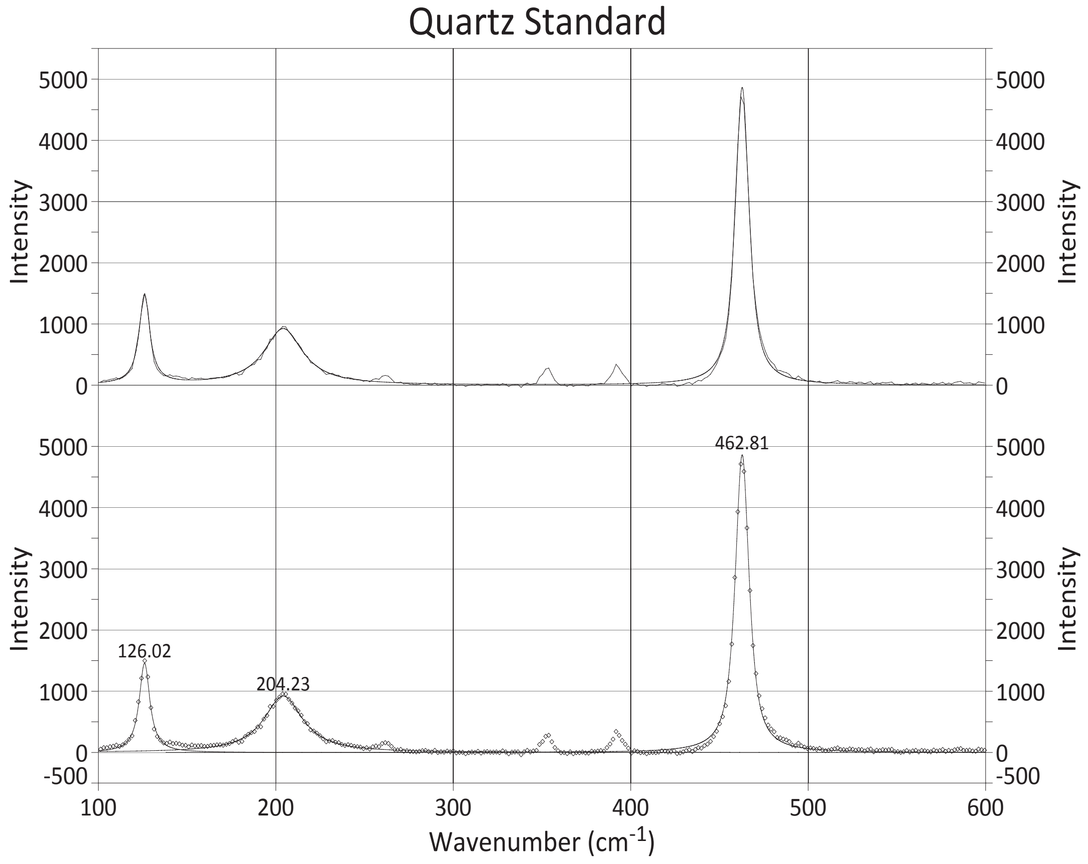
Quartz Standard
Intensity
5000
4000
3000
2000
1000
0
-500
462.81
126.02
204.23
100
200
300
400
500
600
Wavenumber (cm-1)

WRMG 61

Garnet 4

Locality: Whitt Ranch
Collected by Susan Harris

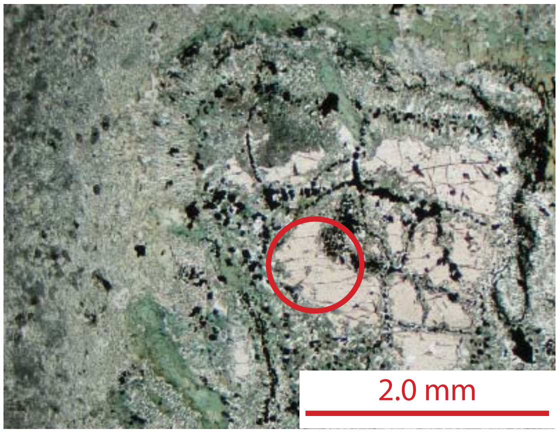

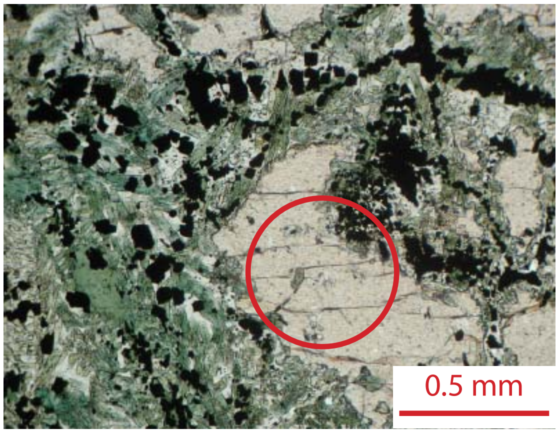

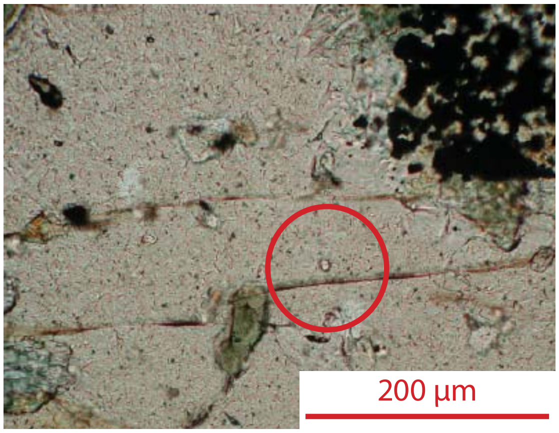

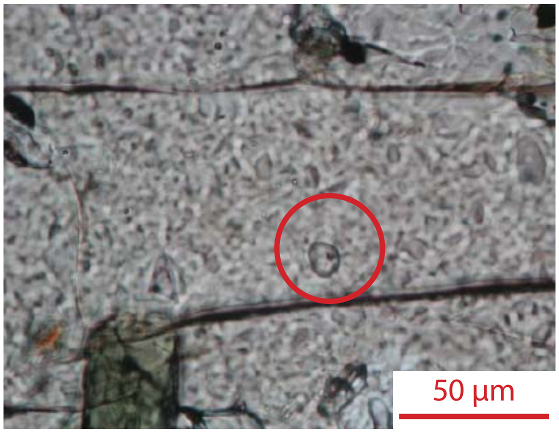

Inclusion Information

Maximum length (X-Y) (µm)	14.2
Minimum length (X-Y) (µm)	10.3
Inclusion thickness (Z) (µm)	10
Location (X-Y coordinates)	(124.3, 2.2)
Description of shape	Spherical
Garnet composition	$Alm_{54.0}$, $Prp_{27.6}$, $Grs_{18.1}$, $Sps_{0.3}$

Data and Pressure Calculation Results

Depth of spectrum (µm)	-8
$\Delta\omega_1$ (cm^{-1})	2.26
$\Delta\omega_2$ (cm^{-1})	1.88
$P_{resid\ [\Delta\omega1]}$ (GPa)	0.135
$P_{resid\ [\Delta\omega2]}$ (GPa)	0.093
$P_{entrap\ [\Delta\omega1]}$ (GPa)	0.64
$P_{entrap\ [\Delta\omega2]}$ (GPa)	0.54

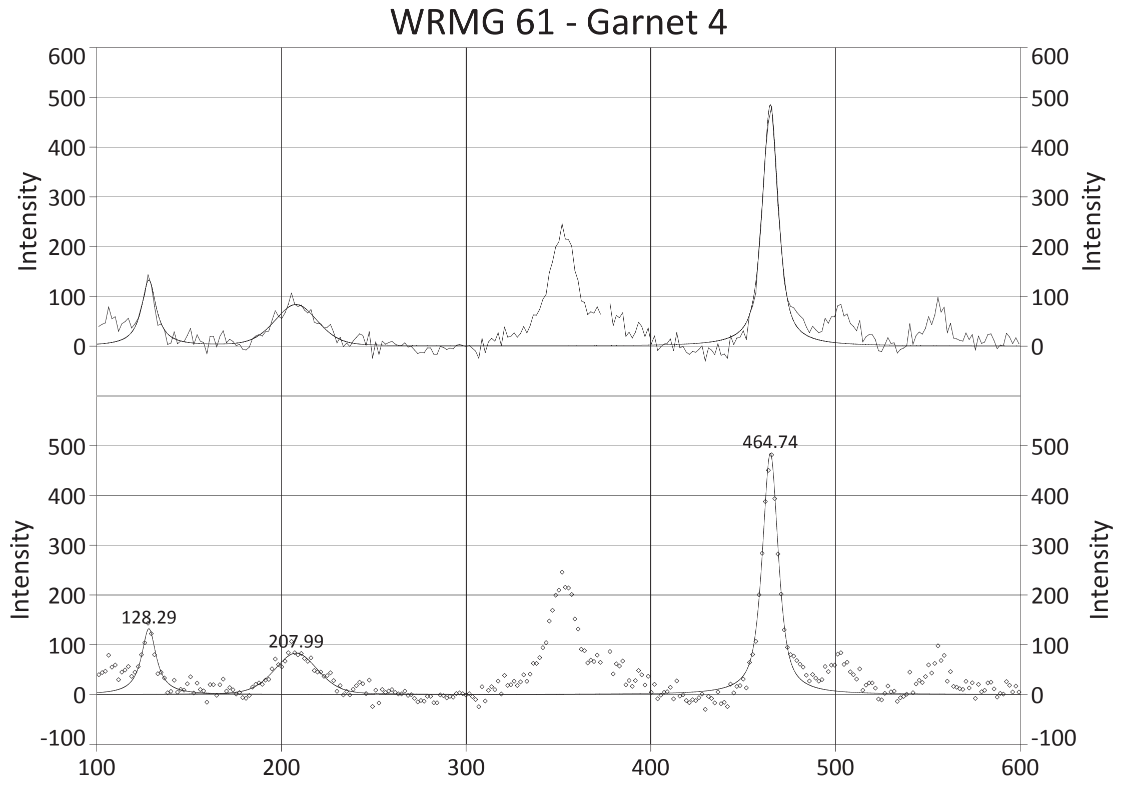
WRMG 61 - Garnet 4
Intensity
600
500
400
300
200
100
0
-100
464.74
128.29
207.99
100
200
300
400
500
600

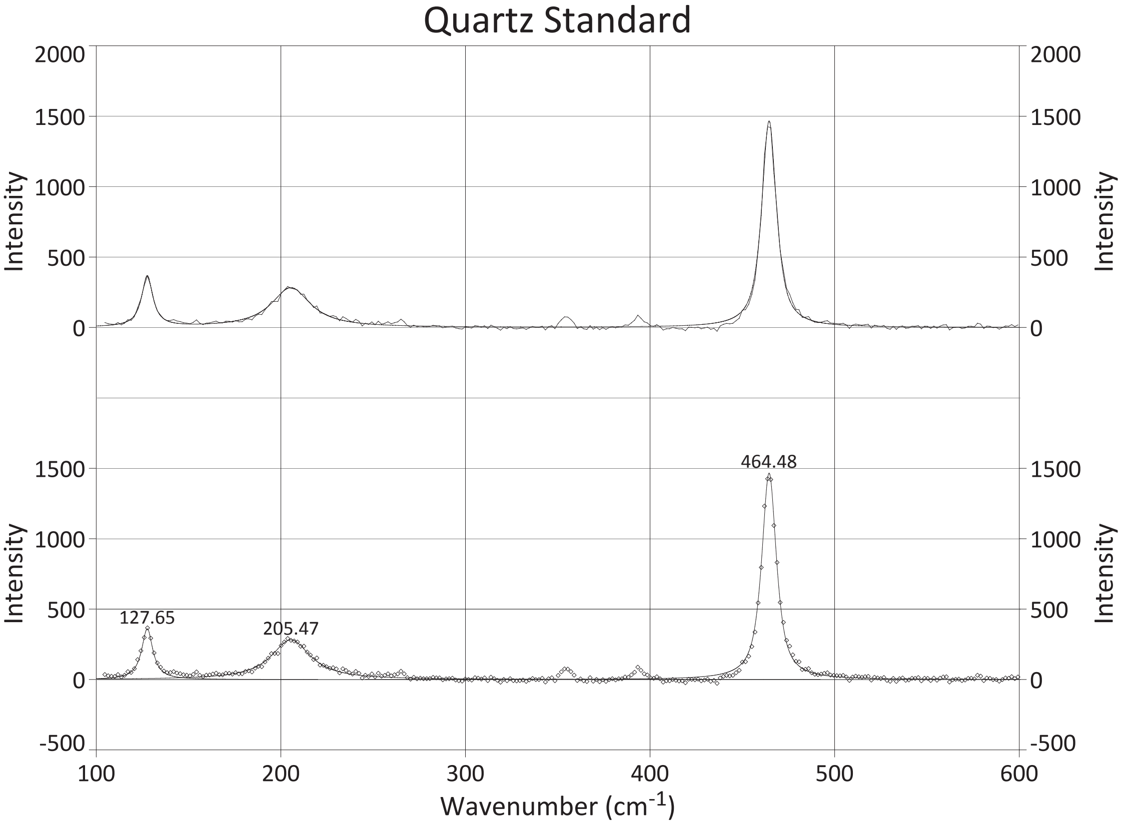
Quartz Standard
Intensity
2000
1500
1000
500
0
-500
464.48
127.65
205.47
100
200
300
400
500
600
Wavenumber (cm-1)

WRMG 61

Garnet 5

Locality: Whitt Ranch
Collected by Susan Harris

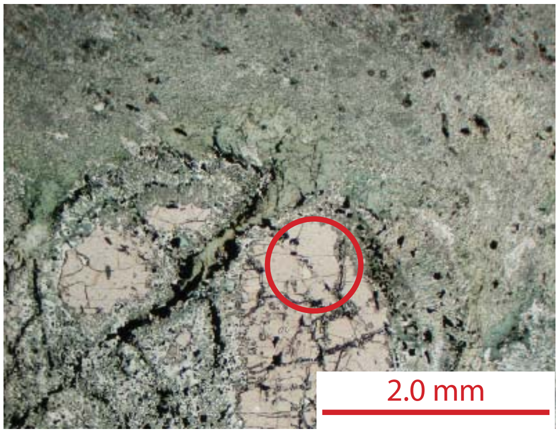

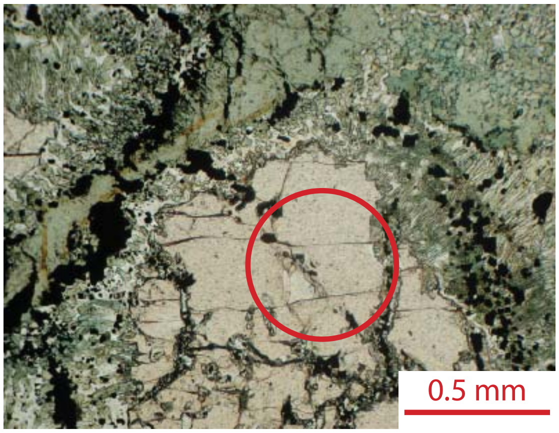

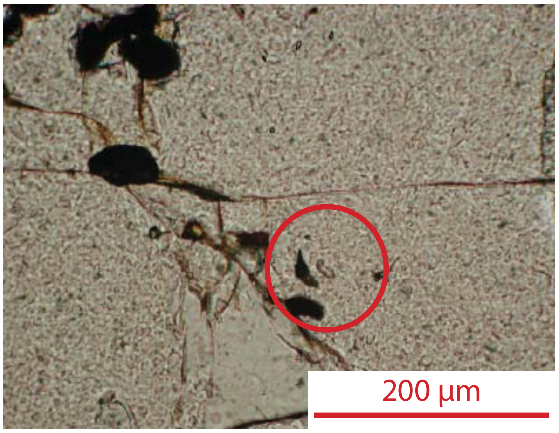

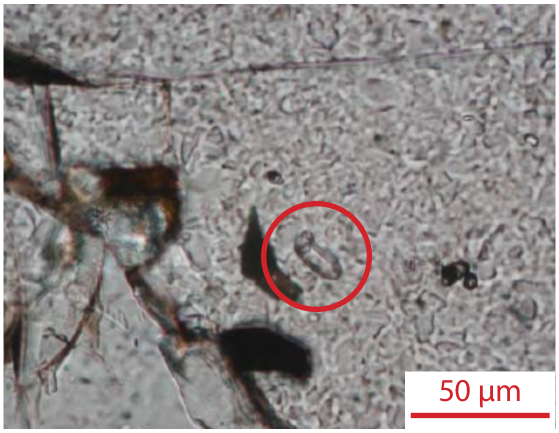

Inclusion Information

Maximum length (X-Y) (µm)	20.5
Minimum length (X-Y) (µm)	9.5
Inclusion thickness (Z) (µm)	15
Location (X-Y coordinates)	(120.2, 6.3)
Description of shape	Elongate
Garnet composition	$Alm_{54.0}$, $Prp_{27.6}$, $Grs_{18.1}$, $Sps_{0.3}$

Data and Pressure Calculation Results

Depth of spectrum (µm)	-8
$\Delta\omega_1$ (cm^{-1})	1.26
$\Delta\omega_2$ (cm^{-1})	1.80
$P_{resid\ [\Delta\omega 1]}$ (GPa)	0.077
$P_{resid\ [\Delta\omega 2]}$ (GPa)	0.089
$P_{entrap\ [\Delta\omega 1]}$ (GPa)	0.50
$P_{entrap\ [\Delta\omega 2]}$ (GPa)	0.53

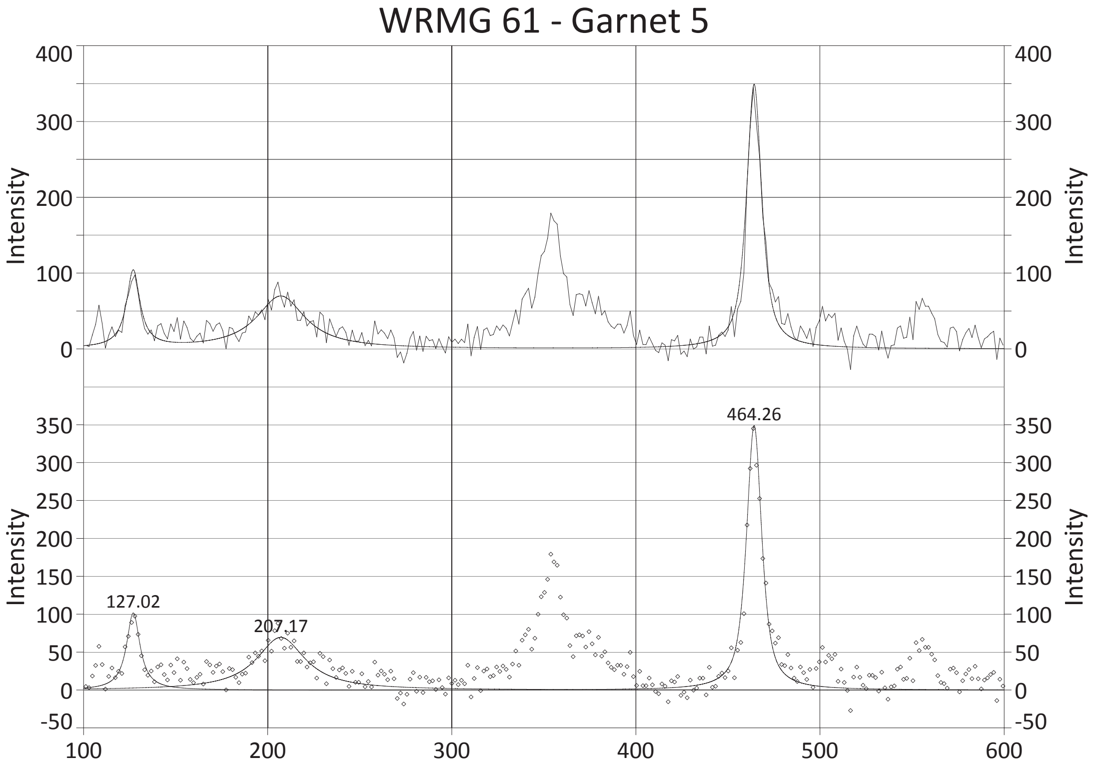
WRMG 61 - Garnet 5
Intensity
400
300
200
100
0
350
250
150
50
-50
127.02
207.17
464.26
100
200
300
400
500
600

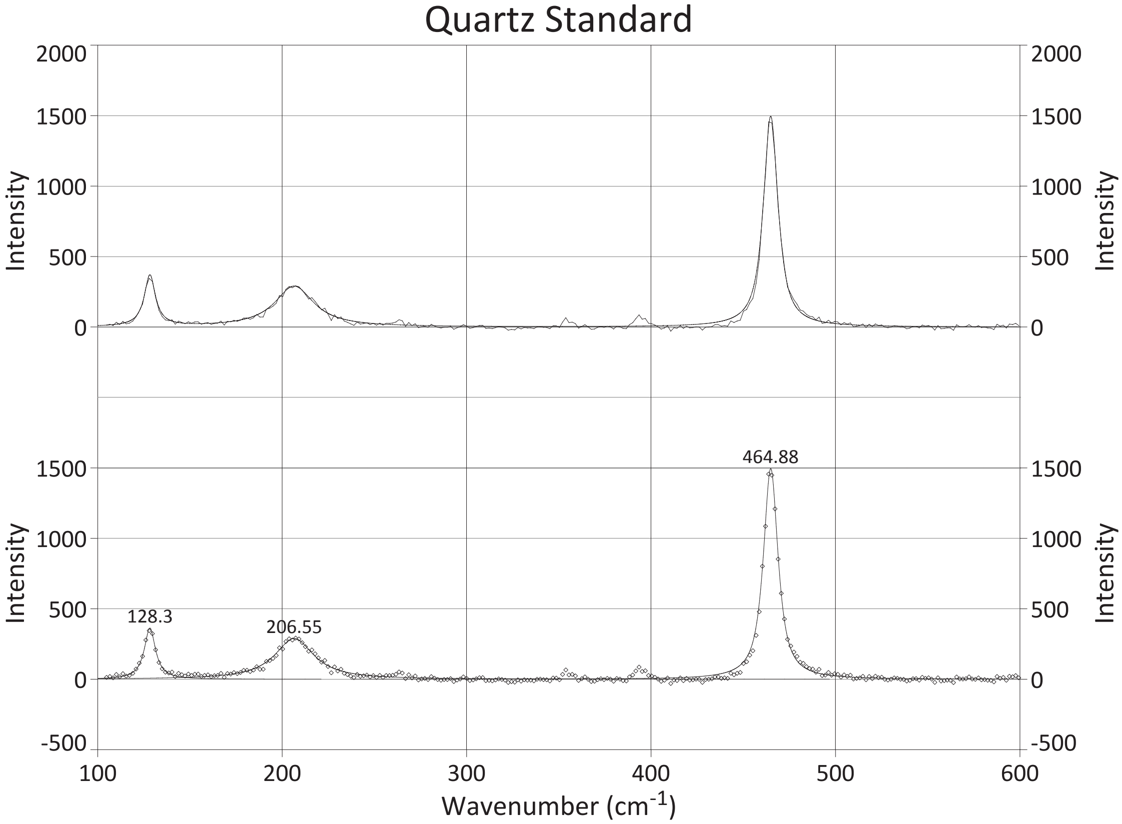
Quartz Standard
Intensity
2000
1500
1000
500
0
-500
128.3
206.55
464.88
100
200
300
400
500
600
Wavenumber (cm-1)

WRMG 61

Garnet 6

Locality: Whitt Ranch
Collected by Susan Harris

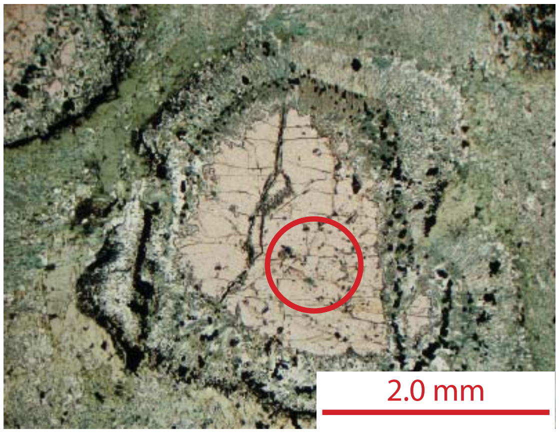

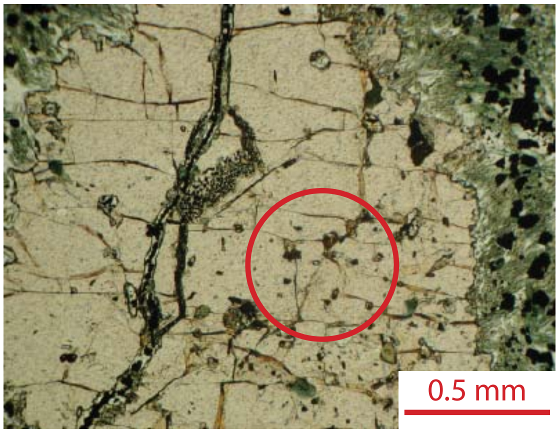

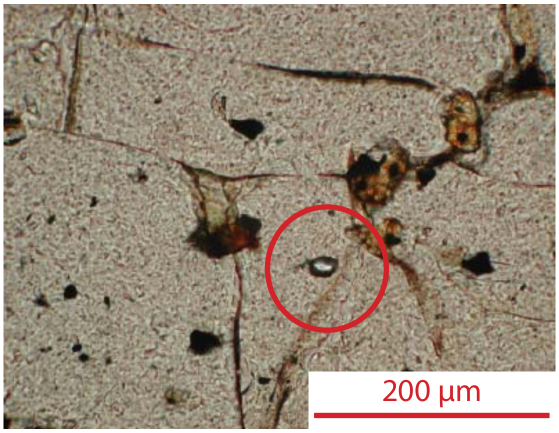

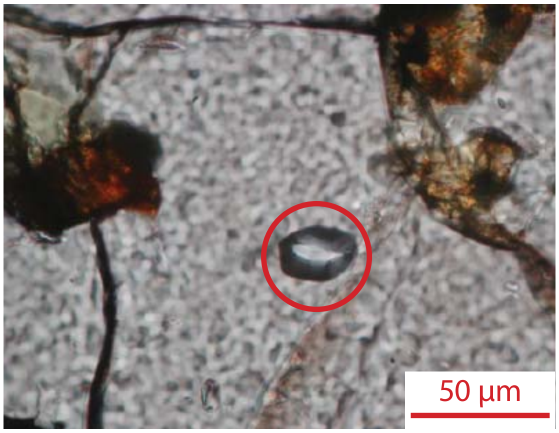

Inclusion Information

Maximum length (X-Y) (µm)	27.7
Minimum length (X-Y) (µm)	19.0
Inclusion thickness (Z) (µm)	22
Location (X-Y coordinates)	(120.1, 15.1)
Description of shape	Ellipsoid
Garnet composition	Alm$_{54.0}$, Prp$_{27.6}$, Grs$_{18.1}$, Sps$_{0.3}$

Data and Pressure Calculation Results

Depth of spectrum (µm)	-4
$\Delta\omega_1$ (cm^{-1})	-0.33
$\Delta\omega_2$ (cm^{-1})	-0.31
$P_{resid\ [\Delta\omega1]}$ (GPa)	-0.021
$P_{resid\ [\Delta\omega2]}$ (GPa)	-0.031
$P_{entrap\ [\Delta\omega1]}$ (GPa)	0.26
$P_{entrap\ [\Delta\omega2]}$ (GPa)	0.27

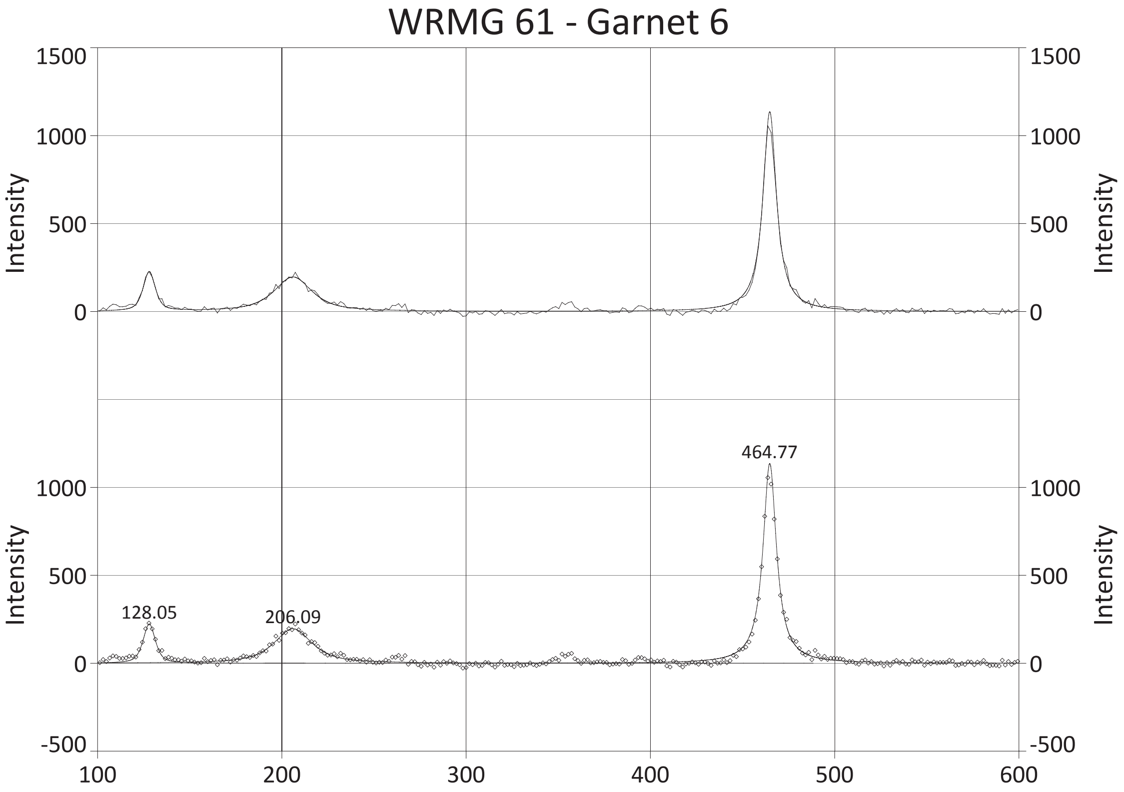
WRMG 61 - Garnet 6
Intensity
1500
1000
500
0
-500
464.77
128.05
206.09
100
200
300
400
500
600

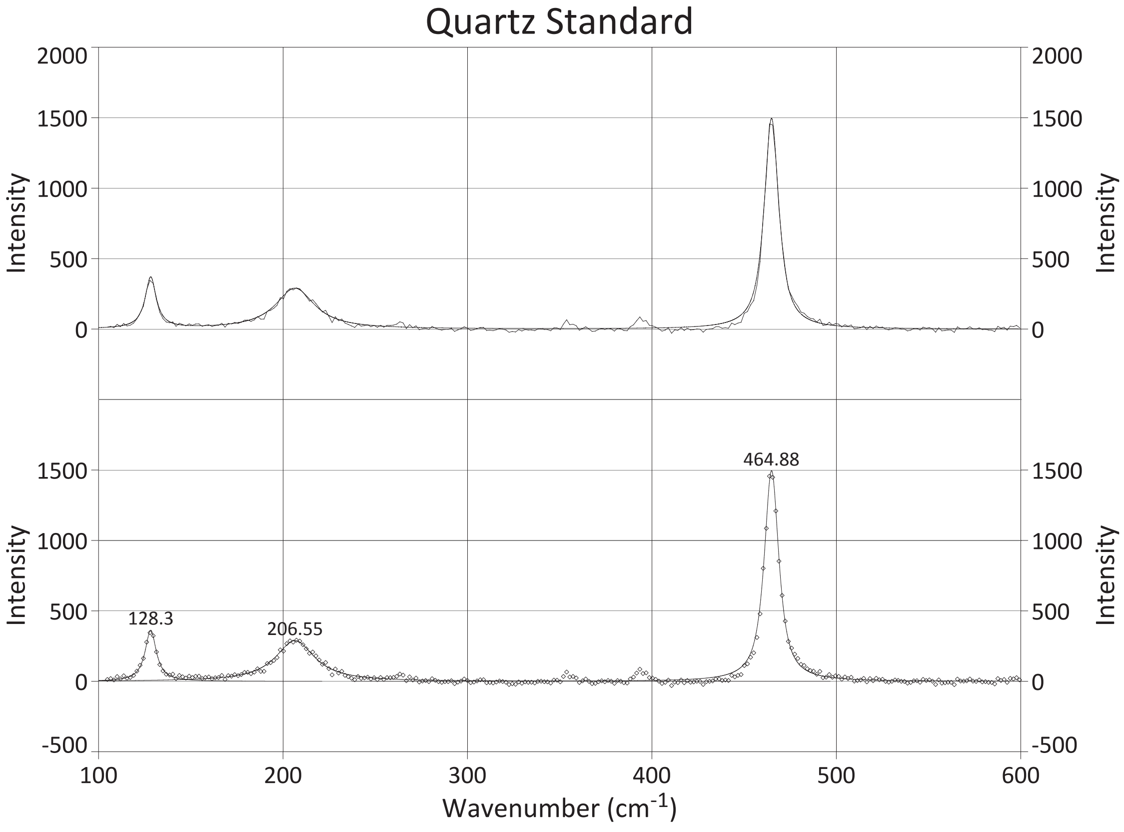
Quartz Standard
Intensity
2000
1500
1000
500
0
-500
464.88
128.3
206.55
100
200
300
400
500
600
Wavenumber (cm-1)

WRMG 61

Garnet 7

Locality: Whitt Ranch
Collected by Susan Harris

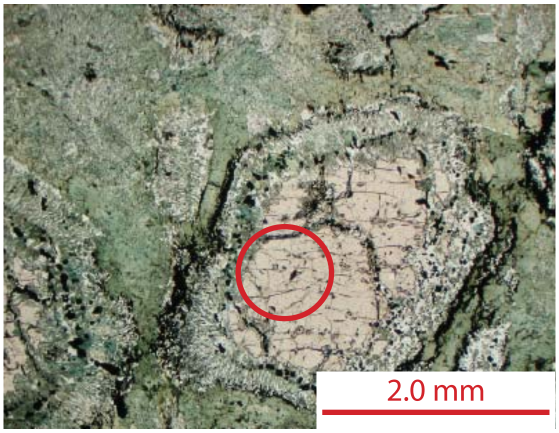

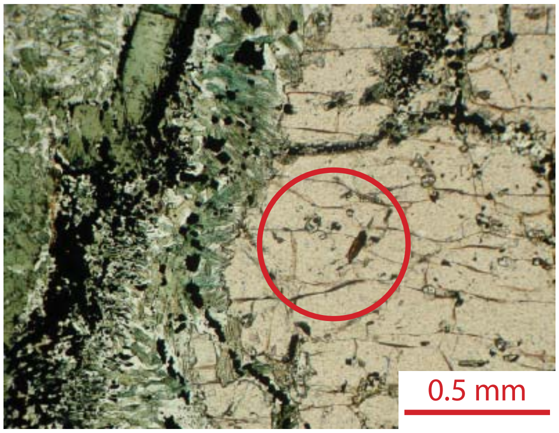

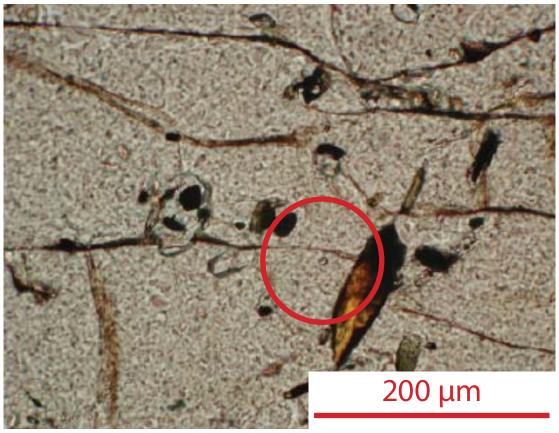

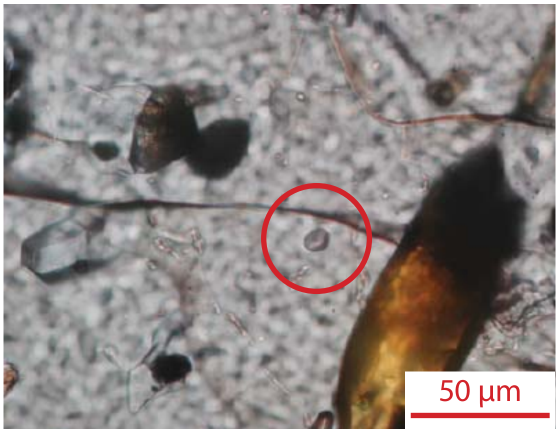

Inclusion Information

Maximum length (X-Y) (µm)	7.9
Minimum length (X-Y) (µm)	7.9
Inclusion thickness (Z) (µm)	10
Location (X-Y coordinates)	(113.4, 14.1)
Description of shape	Spherical
Garnet composition	$Alm_{54.0}$, $Prp_{27.6}$, $Grs_{18.1}$, $Sps_{0.3}$

Data and Pressure Calculation Results

Depth of spectrum (µm)	-2
$\Delta\omega_1$ (cm^{-1})	-0.95
$\Delta\omega_2$ (cm^{-1})	-0.63
$P_{resid\ [\Delta\omega1]}$ (GPa)	-0.060
$P_{resid\ [\Delta\omega2]}$ (GPa)	-0.031
$P_{entrap\ [\Delta\omega1]}$ (GPa)	0.16
$P_{entrap\ [\Delta\omega2]}$ (GPa)	0.23

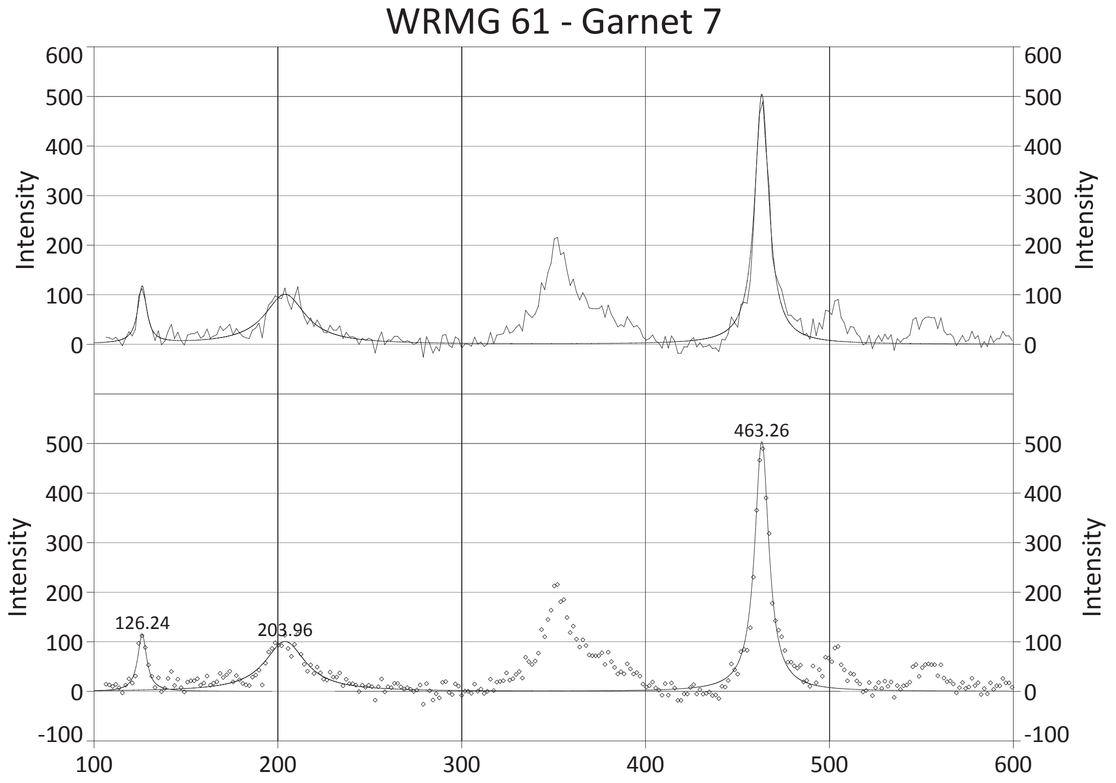
WRMG 61 - Garnet 7

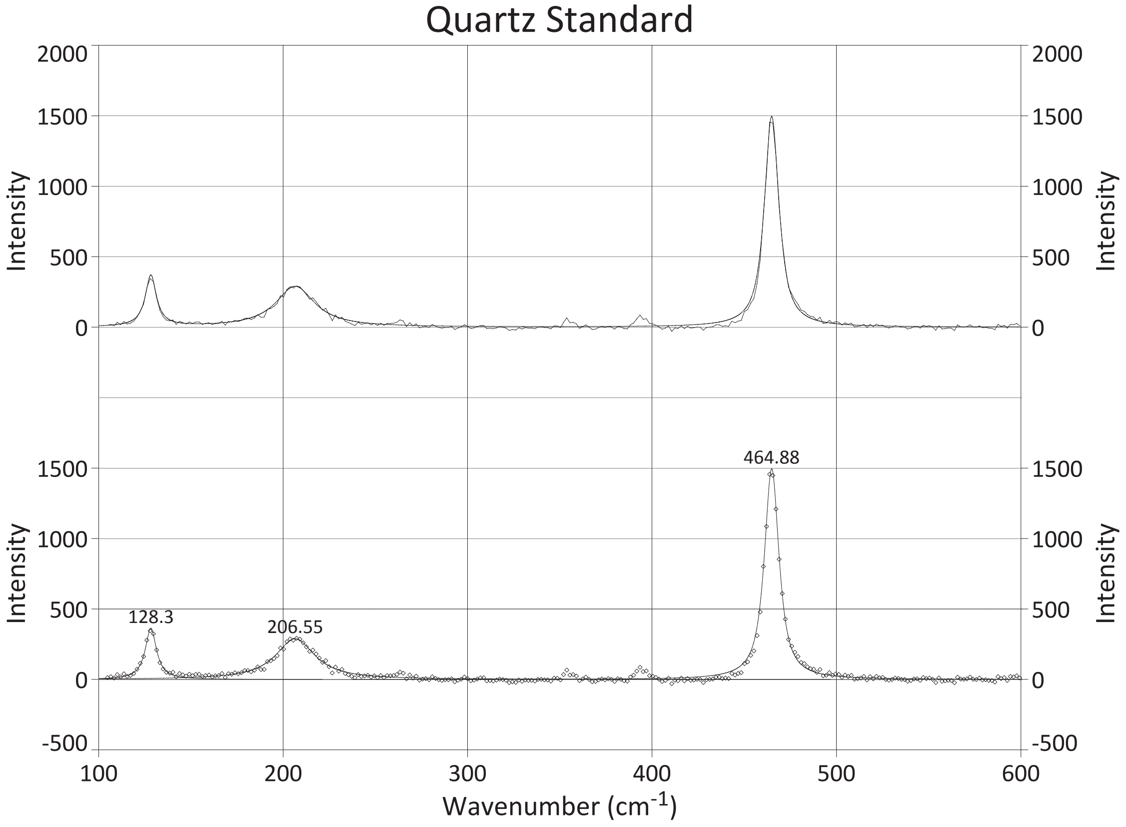
Quartz Standard

WRMG 90

Garnet 1

Locality: Whitt Ranch
Collected by Susan Harris

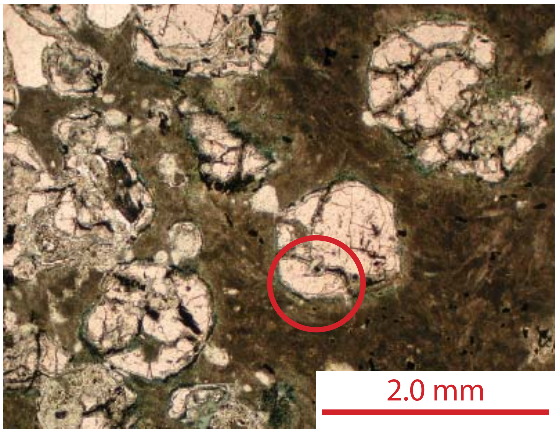

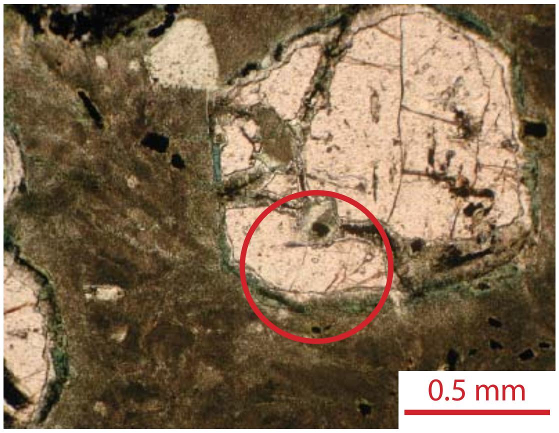

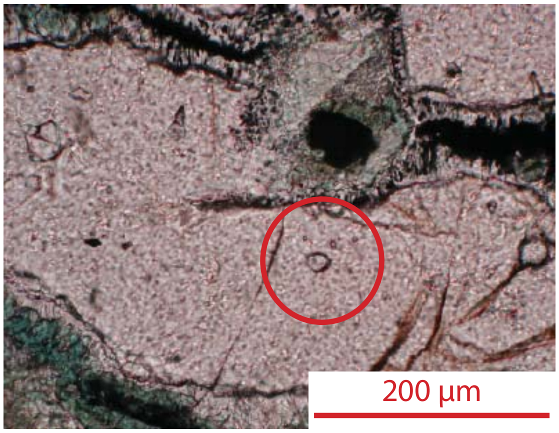

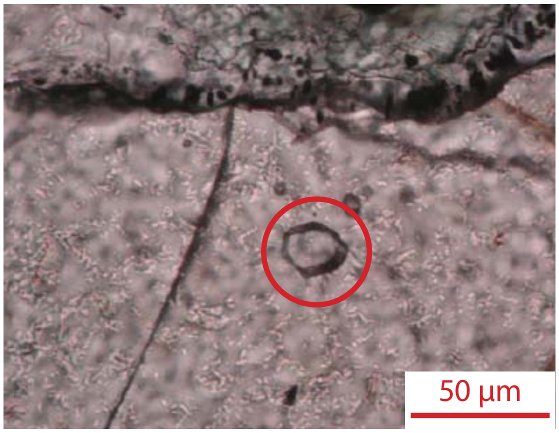

Inclusion Information

Maximum length (X-Y) (µm)	22.9
Minimum length (X-Y) (µm)	20.5
Inclusion thickness (Z) (µm)	18
Location (X-Y coordinates)	(128.4, 10.9)
Description of shape	Hexagonal
Garnet composition	$Alm_{54.0}$, $Prp_{27.6}$, $Grs_{18.1}$, $Sps_{0.3}$

Data and Pressure Calculation Results

Depth of spectrum (µm)	-6
$\Delta\omega_1$ (cm^{-1})	-1.43
$\Delta\omega_2$ (cm^{-1})	-0.46
$P_{resid\ [\Delta\omega 1]}$ (GPa)	-0.092
$P_{resid\ [\Delta\omega 2]}$ (GPa)	-0.023
$P_{entrap\ [\Delta\omega 1]}$ (GPa)	0.08
$P_{entrap\ [\Delta\omega 2]}$ (GPa)	0.25

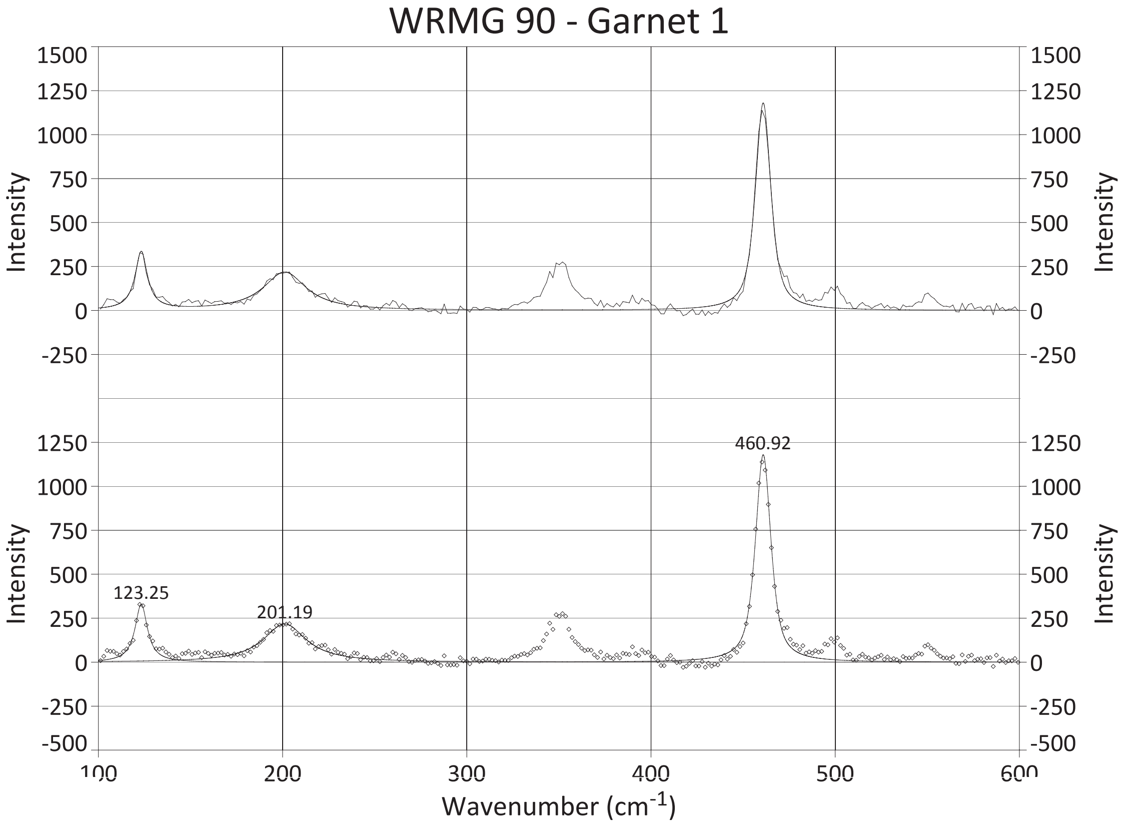
WRMG 90 - Garnet 1
Intensity
1500
1250
1000
750
500
250
0
-250
-500
460.92
123.25
201.19
100
200
300
400
500
600
Wavenumber (cm^{-1})

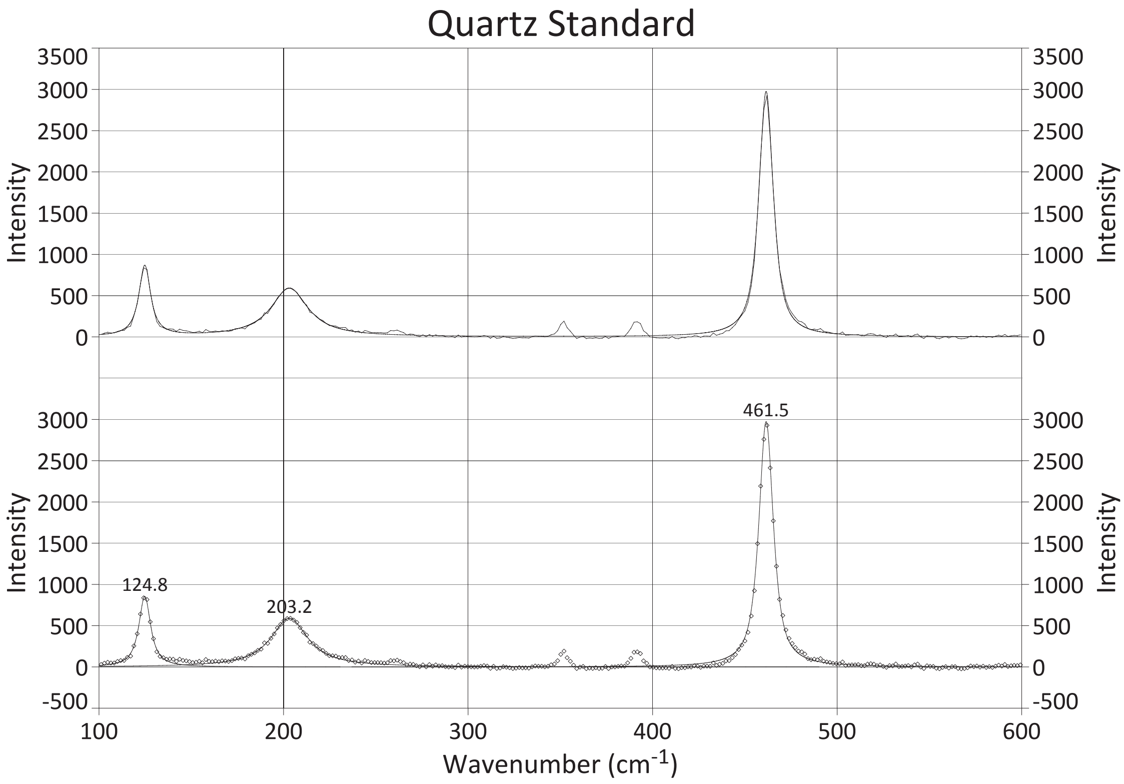
Quartz Standard
Intensity
3500
3000
2500
2000
1500
1000
500
0
-500
461.5
124.8
203.2
100
200
300
400
500
600
Wavenumber (cm^{-1})

WRMG 1036

Garnet 2

Locality: Whitt Ranch
Collected by Michael Jordan

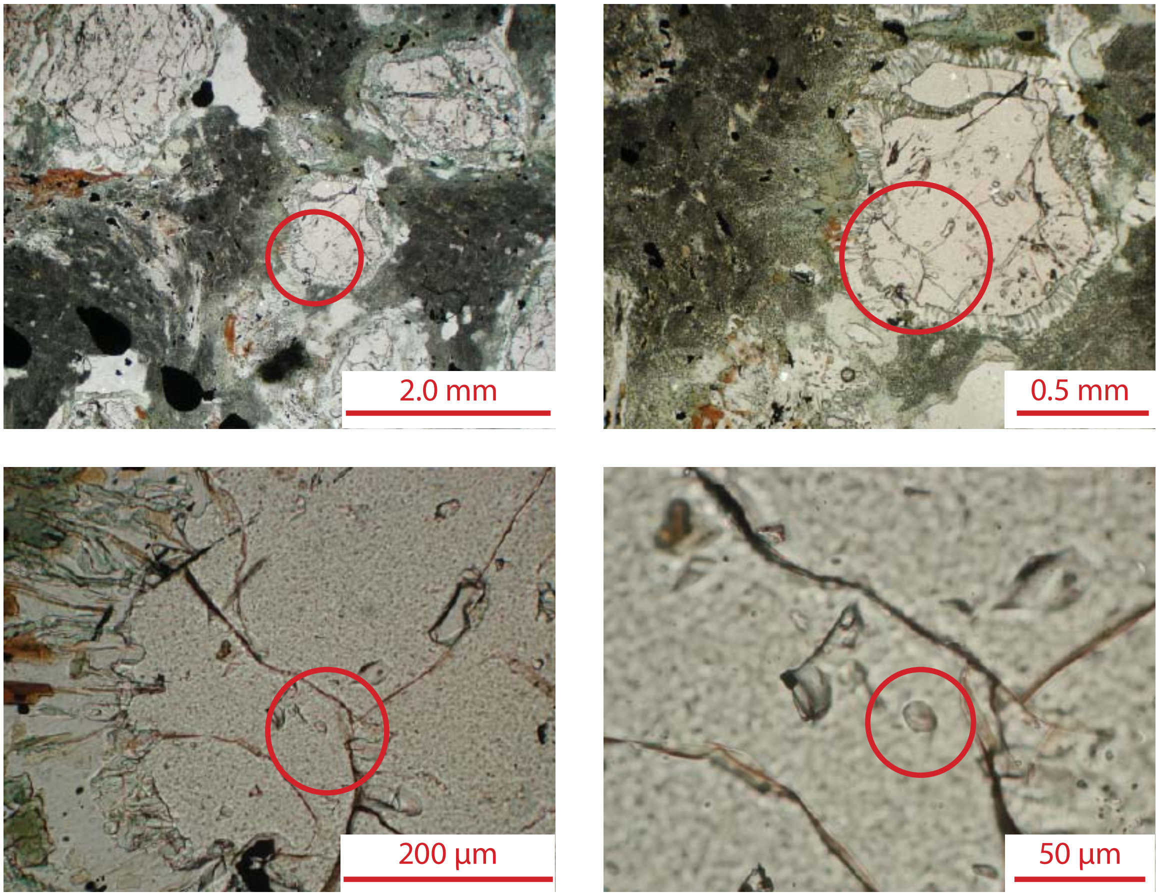

Inclusion Information

Maximum length (X-Y) (µm)	14.2
Minimum length (X-Y) (µm)	13.4
Inclusion thickness (Z) (µm)	16
Location (X-Y coordinates)	-(100.6, 8.1)
Description of shape	Spherical
Garnet composition	$Alm_{54.0}$, $Prp_{27.6}$, $Grs_{18.1}$, $Sps_{0.3}$

Data and Pressure Calculation Results

Depth of spectrum (µm)	-4
$\Delta\omega_1$ (cm^{-1})	-2.49
$\Delta\omega_2$ (cm^{-1})	-3.10
$P_{resid\ [\Delta\omega1]}$ (GPa)	-0.164
$P_{resid\ [\Delta\omega2]}$ (GPa)	-0.150
$P_{entrap\ [\Delta\omega1]}$ (GPa)	-0.10
$P_{entrap\ [\Delta\omega2]}$ (GPa)	-0.06

WRMG 1036

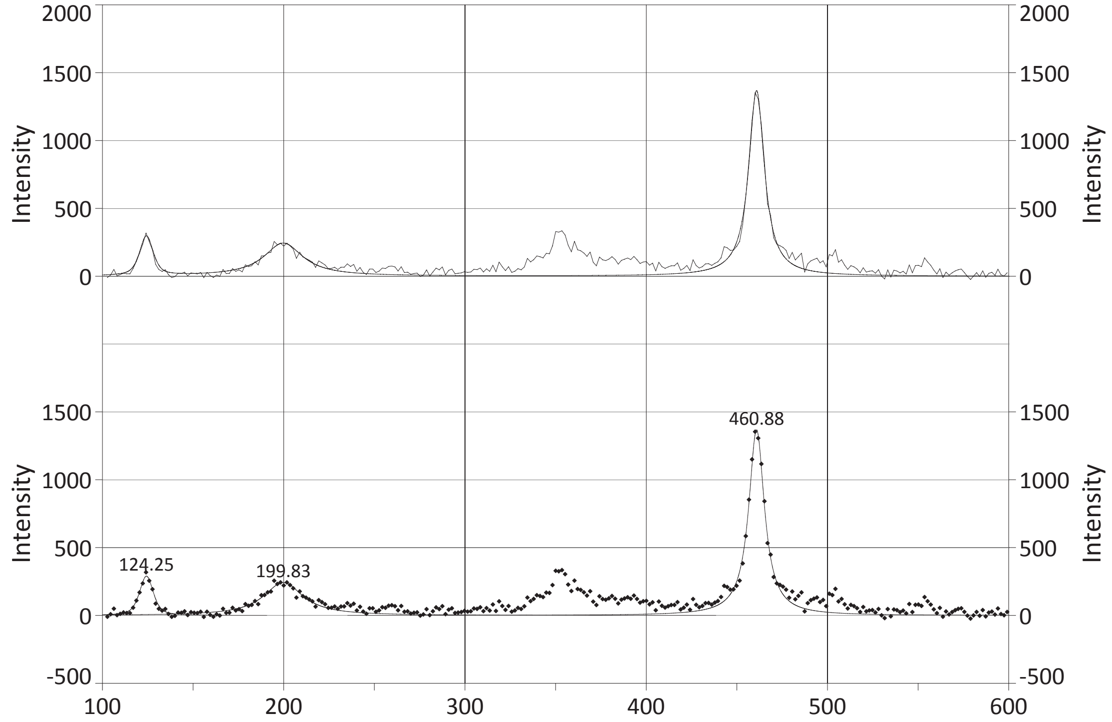

Quartz Standard

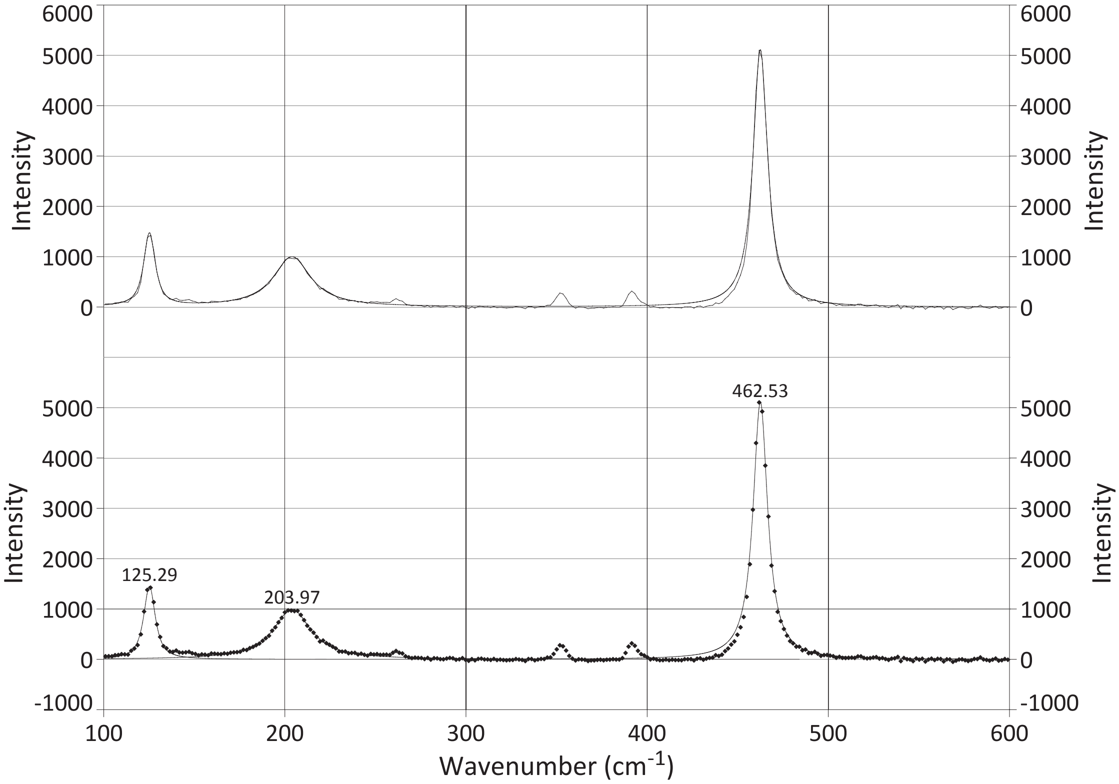

WRMG SR-3

Garnet 1

Locality: Whitt Ranch
Collected by Stephen Robertson

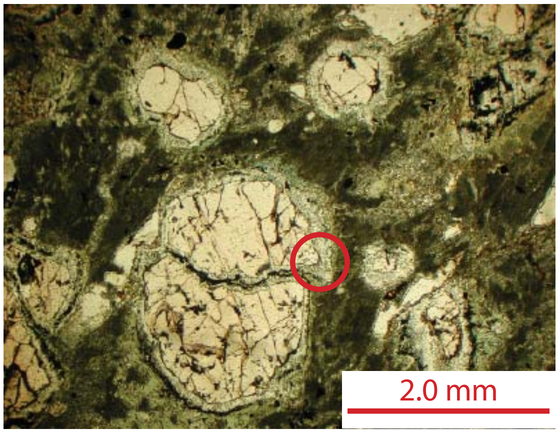

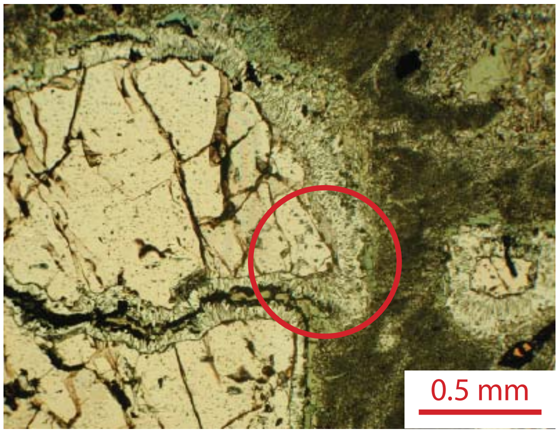

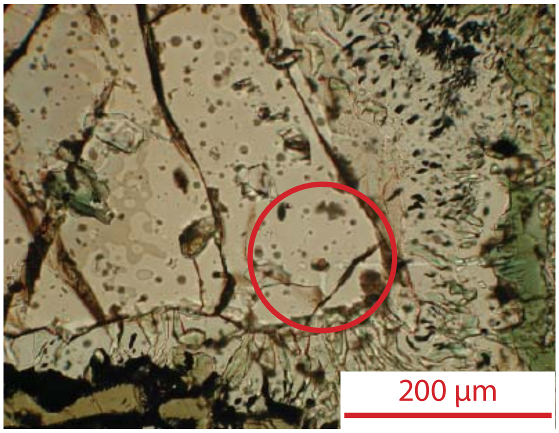

Inclusion Information

Maximum length (X-Y) (µm)	13.4
Minimum length (X-Y) (µm)	11.1
Inclusion thickness (Z) (µm)	16
Location (X-Y coordinates)	-(120.5, 9.5)
Description of shape	Teardrop
Garnet composition	Alm$_{54.0}$, Prp$_{27.6}$, Grs$_{18.1}$, Sps$_{0.3}$

Data and Pressure Calculation Results

Depth of spectrum (µm)	-1
$\Delta\omega_1$ (cm^{-1})	2.69
$\Delta\omega_2$ (cm^{-1})	4.05
$P_{\text{resid } [\Delta\omega1]}$ (GPa)	0.160
$P_{\text{resid } [\Delta\omega2]}$ (GPa)	0.204
$P_{\text{entrap } [\Delta\omega1]}$ (GPa)	0.71
$P_{\text{entrap } [\Delta\omega2]}$ (GPa)	0.81

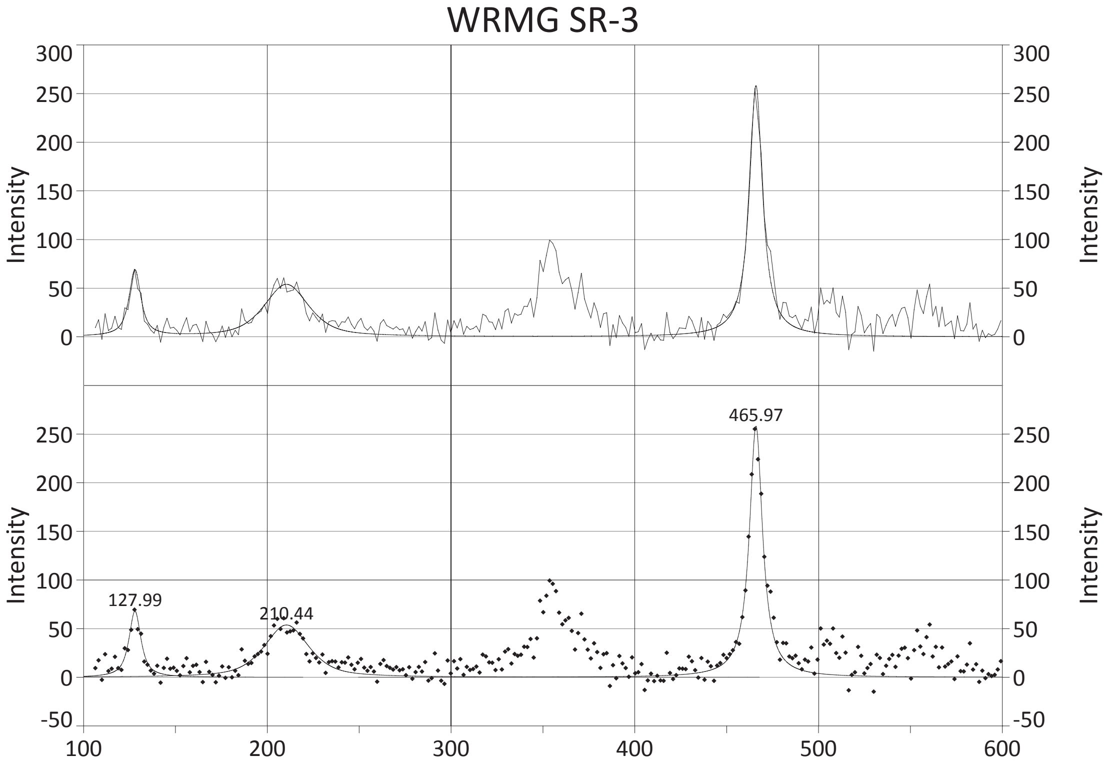

WRMG SR-3

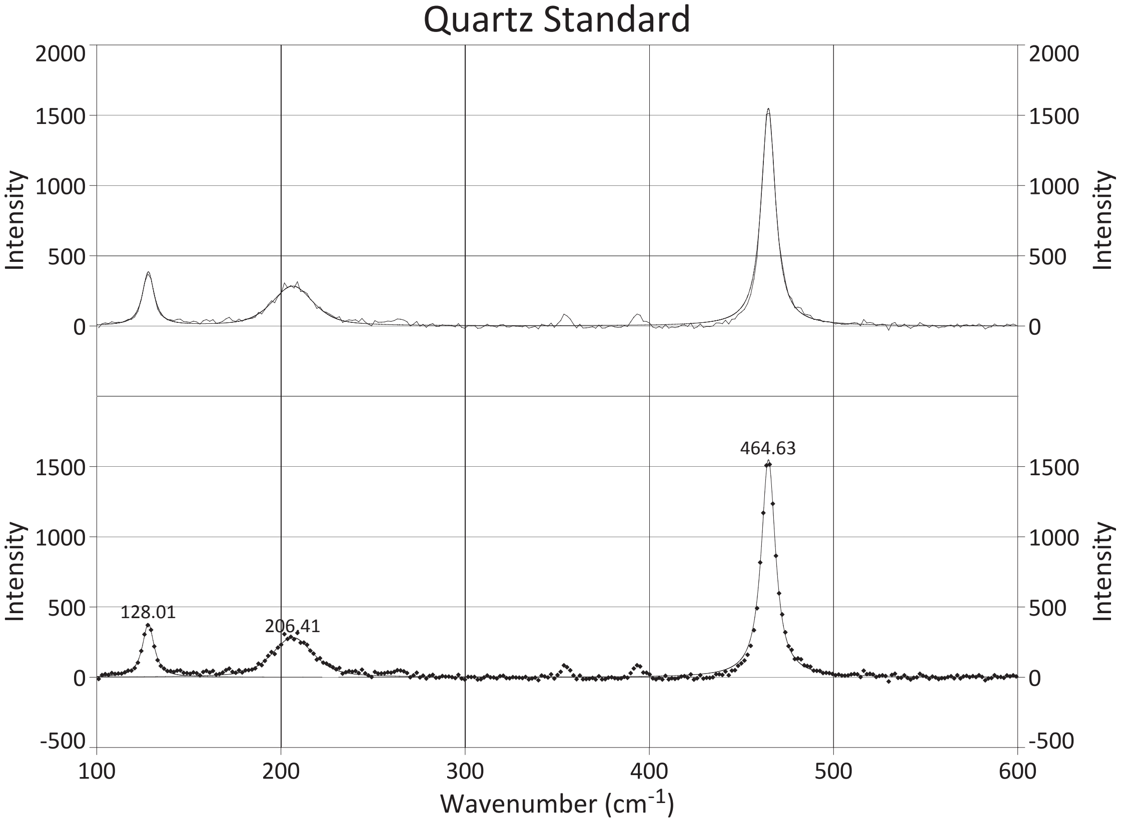

Quartz Standard

PH 97-29

Garnet 1

Locality: Purdy Hill
Collected by Susan Anderson

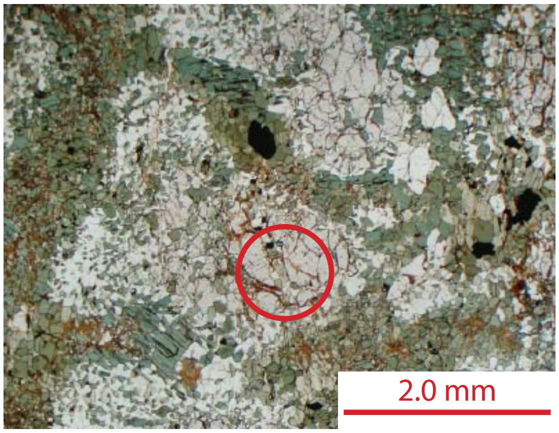

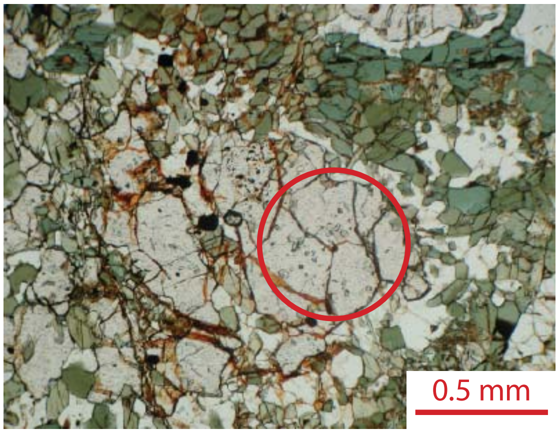

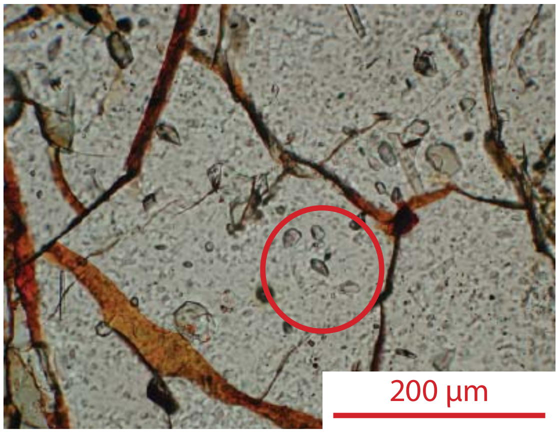

Inclusion Information

Maximum length (X-Y) (µm)	22.1
Minimum length (X-Y) (µm)	12.6
Inclusion thickness (Z) (µm)	14
Location (X-Y coordinates)	(122.7, 8.6)
Description of shape	Teardrop
Garnet composition	Alm$_{54.9}$, Prp$_{22.8}$, Grs$_{20.2}$, Sps$_{2.1}$

Data and Pressure Calculation Results

Depth of spectrum (µm)	-2
$\Delta\omega_1$ (cm^{-1})	-2.28
$\Delta\omega_2$ (cm^{-1})	-1.65
$P_{resid\ [\Delta\omega1]}$ (GPa)	-0.149
$P_{resid\ [\Delta\omega2]}$ (GPa)	-0.080
$P_{entrap\ [\Delta\omega1]}$ (GPa)	0.01
$P_{entrap\ [\Delta\omega2]}$ (GPa)	0.18

PH 97-29 - Garnet 1

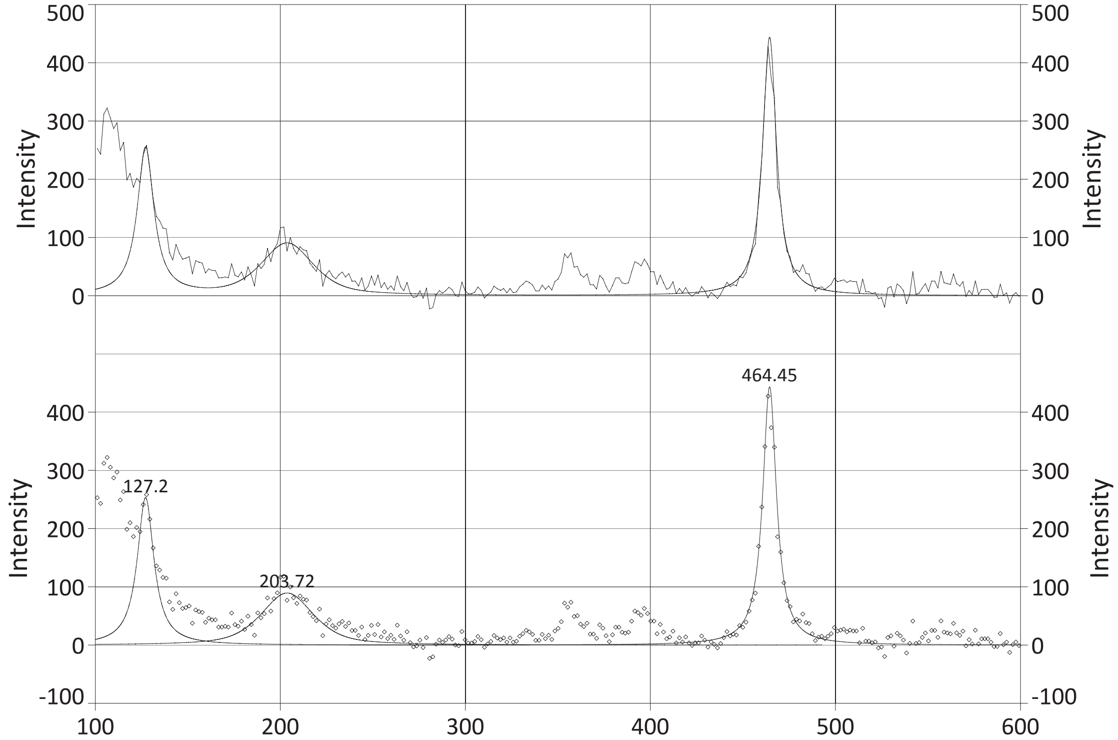

Quartz Standard

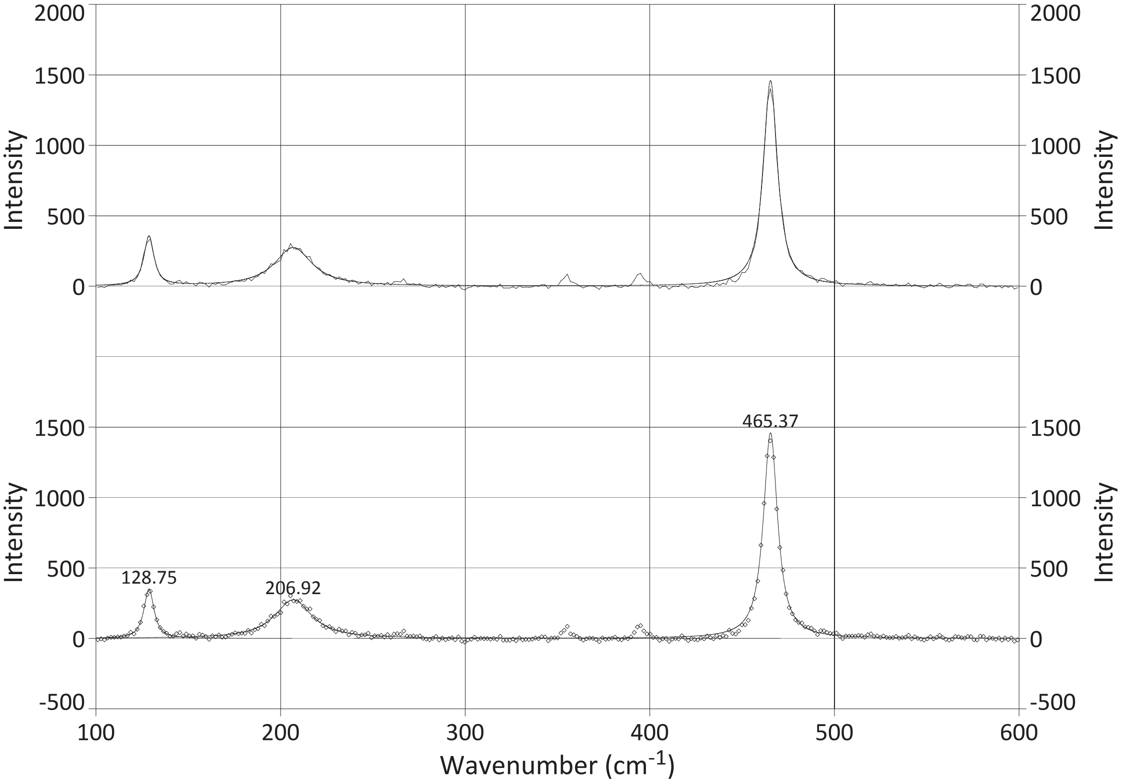

PH 97-29

Garnet 2

Locality: Purdy Hill
Collected by Susan Anderson

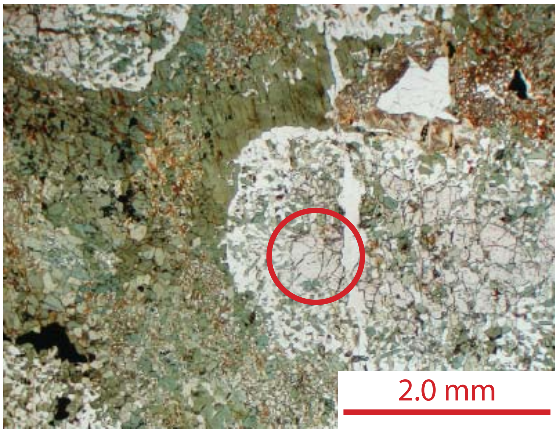

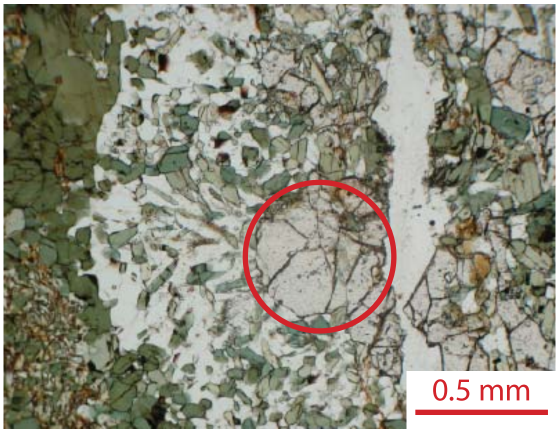

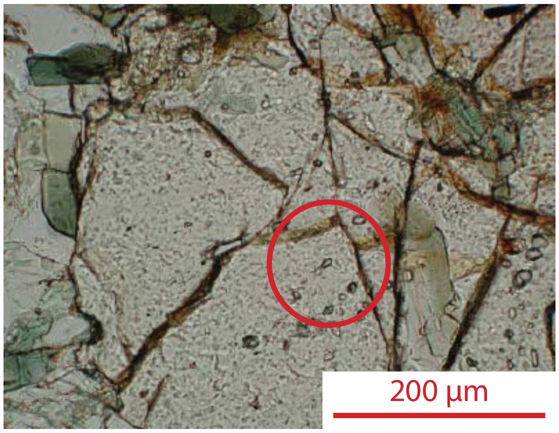

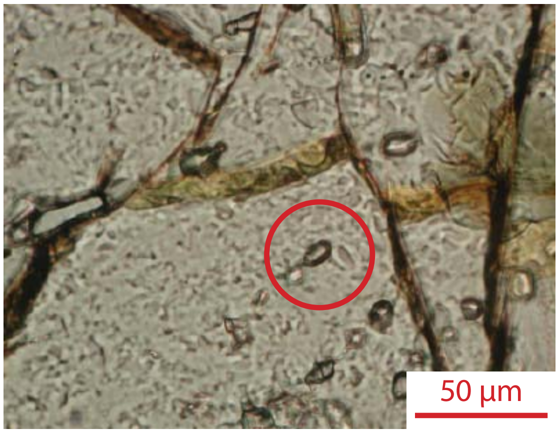

Inclusion Information

Maximum length (X-Y) (µm)	12.6
Minimum length (X-Y) (µm)	9.5
Inclusion thickness (Z) (µm)	11
Location (X-Y coordinates)	(122.7, 8.6)
Description of shape	Teardrop
Garnet composition	$Alm_{54.9}$, $Prp_{22.8}$, $Grs_{20.2}$, $Sps_{2.1}$

Data and Pressure Calculation Results

Depth of spectrum (µm)	-4
$\Delta\omega_1$ (cm^{-1})	-2.26
$\Delta\omega_2$ (cm^{-1})	-1.85
$P_{\text{resid }[\Delta\omega1]}$ (GPa)	-0.148
$P_{\text{resid }[\Delta\omega2]}$ (GPa)	-0.090
$P_{\text{entrap }[\Delta\omega1]}$ (GPa)	0.01
$P_{\text{entrap }[\Delta\omega2]}$ (GPa)	0.16

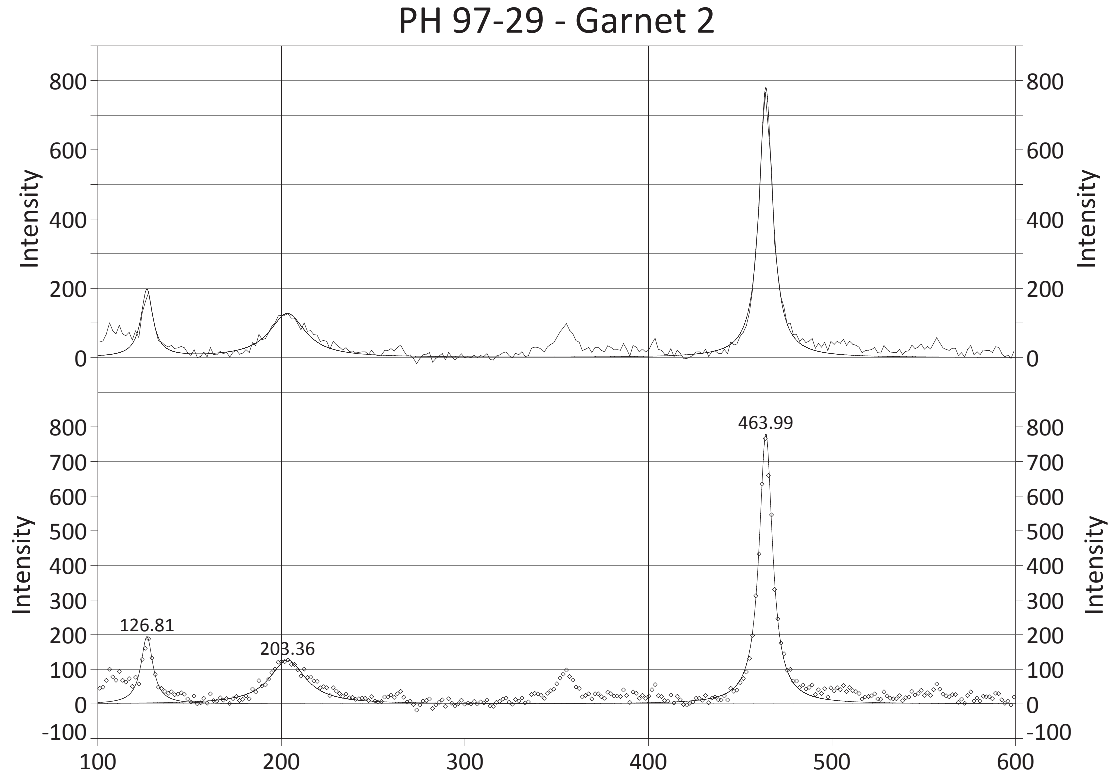
PH 97-29 - Garnet 2
Intensity
800
600
400
200
0
800
700
600
500
400
300
200
100
0
-100
463.99
126.81
203.36
100
200
300
400
500
600

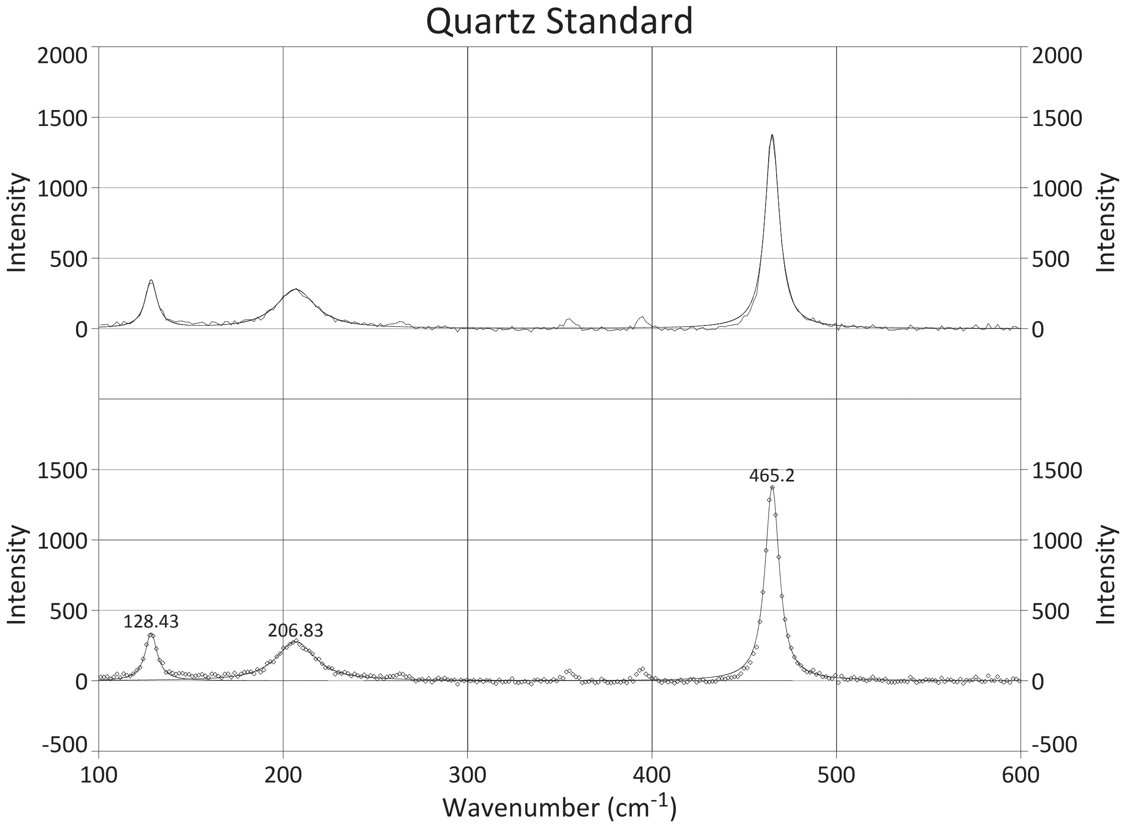
Quartz Standard
Intensity
2000
1500
1000
500
0
-500
465.2
128.43
206.83
100
200
300
400
500
600
Wavenumber (cm-1)

PH 97-29

Garnet 3

Locality: Purdy Hill
Collected by Susan Anderson

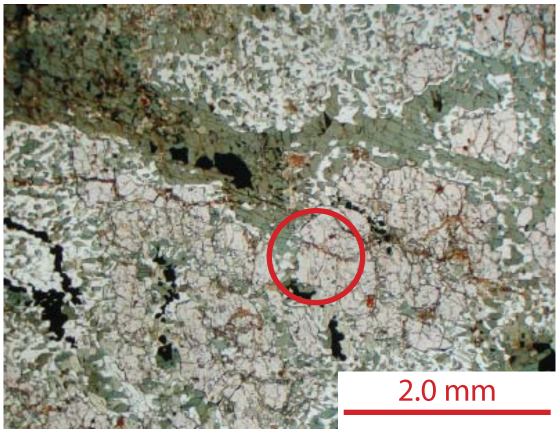

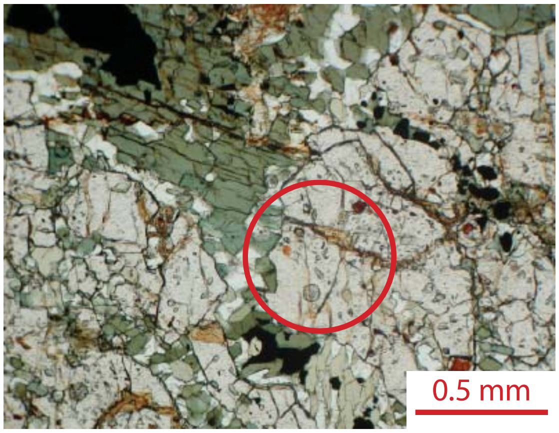

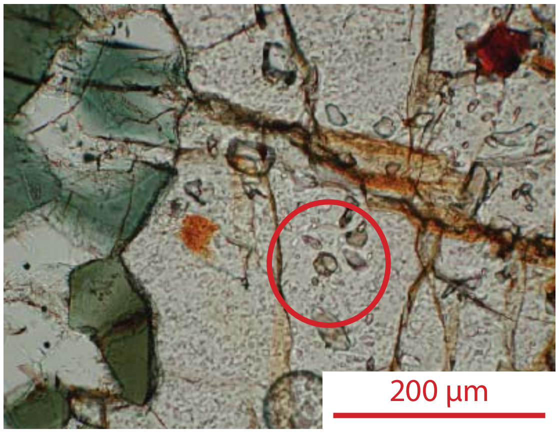

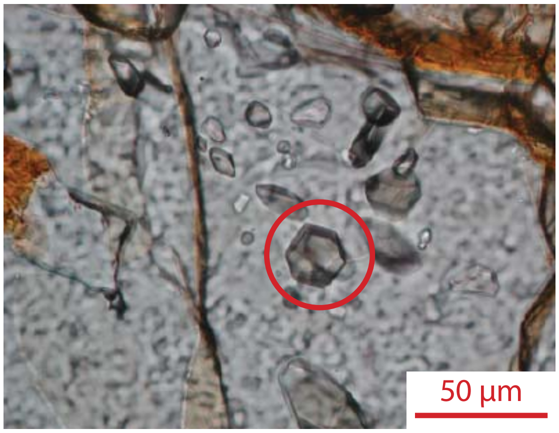

Inclusion Information

Maximum length (X-Y) (μm)	26.9
Minimum length (X-Y) (μm)	22.1
Inclusion thickness (Z) (μm)	10
Location (X-Y coordinates)	(103.5, 9.1)
Description of shape	Hexagonal
Garnet composition	Alm$_{54.9}$, Prp$_{22.8}$, Grs$_{20.2}$, Sps$_{2.1}$

Data and Pressure Calculation Results

Depth of spectrum (μm)	-2
$\Delta\omega_1$ (cm^{-1})	0.29
$\Delta\omega_2$ (cm^{-1})	1.72
$P_{\text{resid }[\Delta\omega1]}$ (GPa)	0.018
$P_{\text{resid }[\Delta\omega2]}$ (GPa)	0.085
$P_{\text{entrap }[\Delta\omega1]}$ (GPa)	0.42
$P_{\text{entrap }[\Delta\omega2]}$ (GPa)	0.59

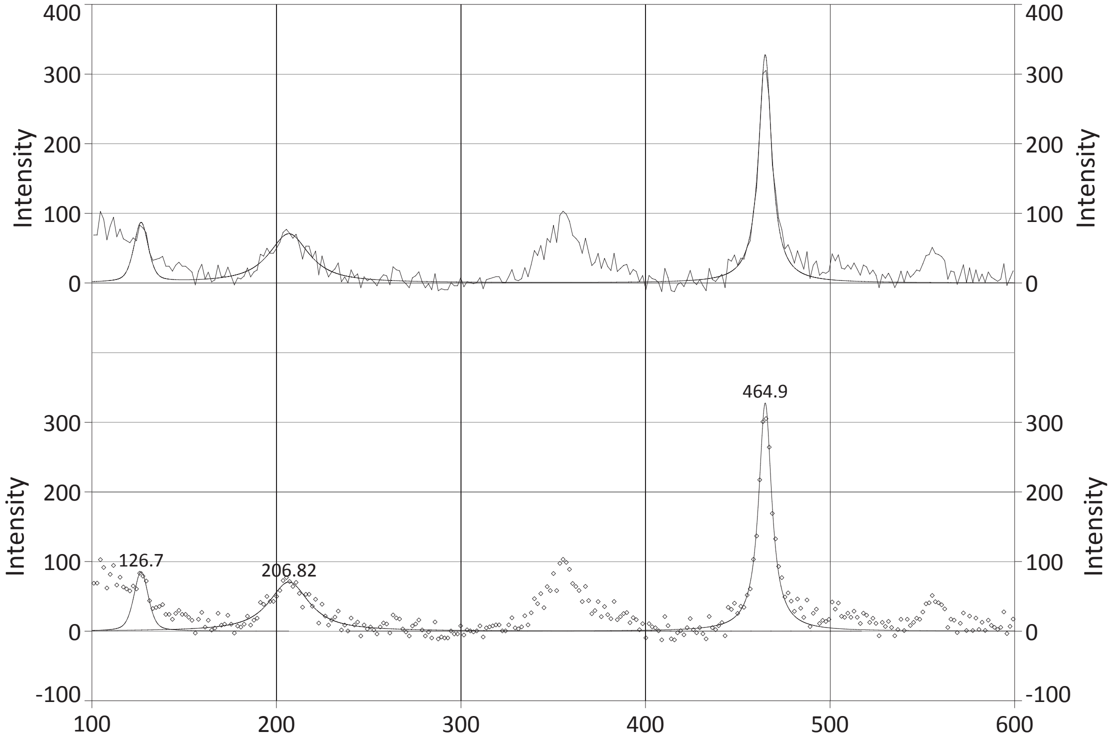

PH 97-29 - Garnet 3

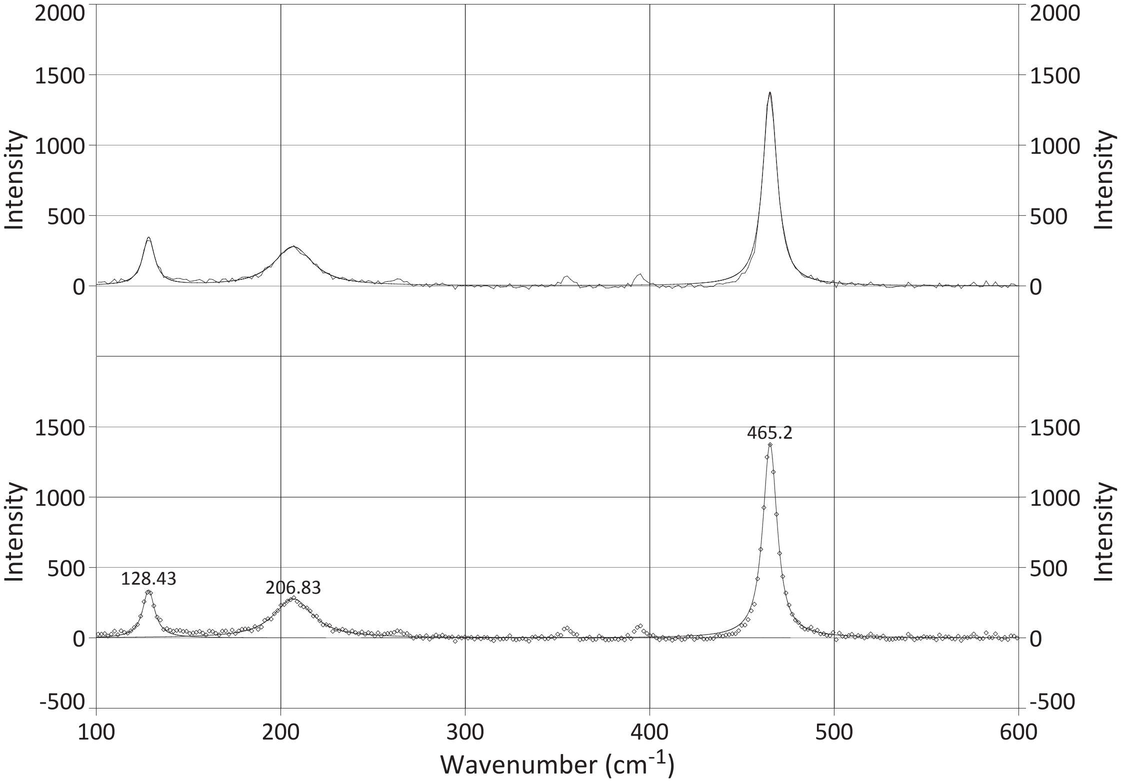

Quartz Standard

PH 97-29

Garnet 4

Locality: Purdy Hill
Collected by Susan Anderson

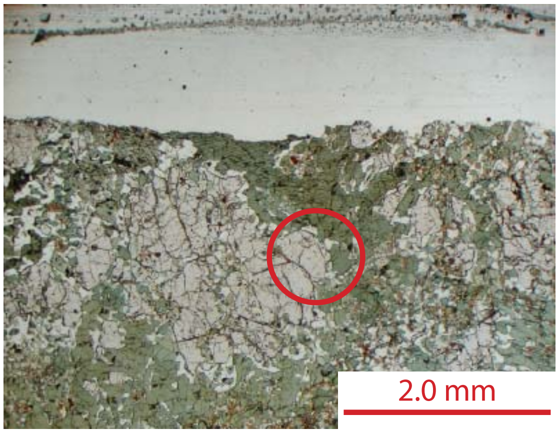

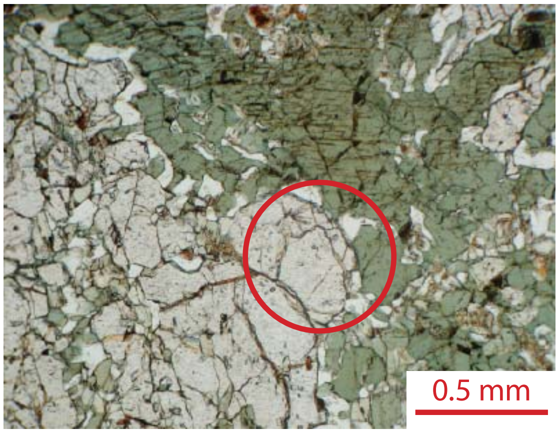

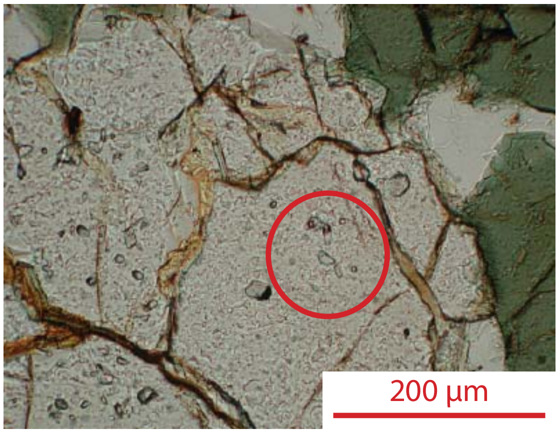

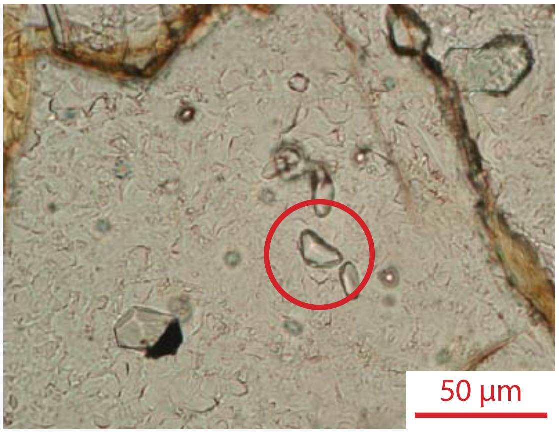

Inclusion Information

Maximum length (X-Y) (µm)	18.9
Minimum length (X-Y) (µm)	11.1
Inclusion thickness (Z) (µm)	9
Location (X-Y coordinates)	(111.5, 0.8)
Description of shape	Triangular
Garnet composition	$Alm_{54.9}$, $Prp_{22.8}$, $Grs_{20.2}$, $Sps_{2.1}$

Data and Pressure Calculation Results

Depth of spectrum (µm)	-4
$\Delta\omega_1$ (cm^{-1})	1.12
$\Delta\omega_2$ (cm^{-1})	2.00
$P_{resid\ [\Delta\omega1]}$ (GPa)	0.068
$P_{resid\ [\Delta\omega2]}$ (GPa)	0.099
$P_{entrap\ [\Delta\omega1]}$ (GPa)	0.55
$P_{entrap\ [\Delta\omega2]}$ (GPa)	0.63

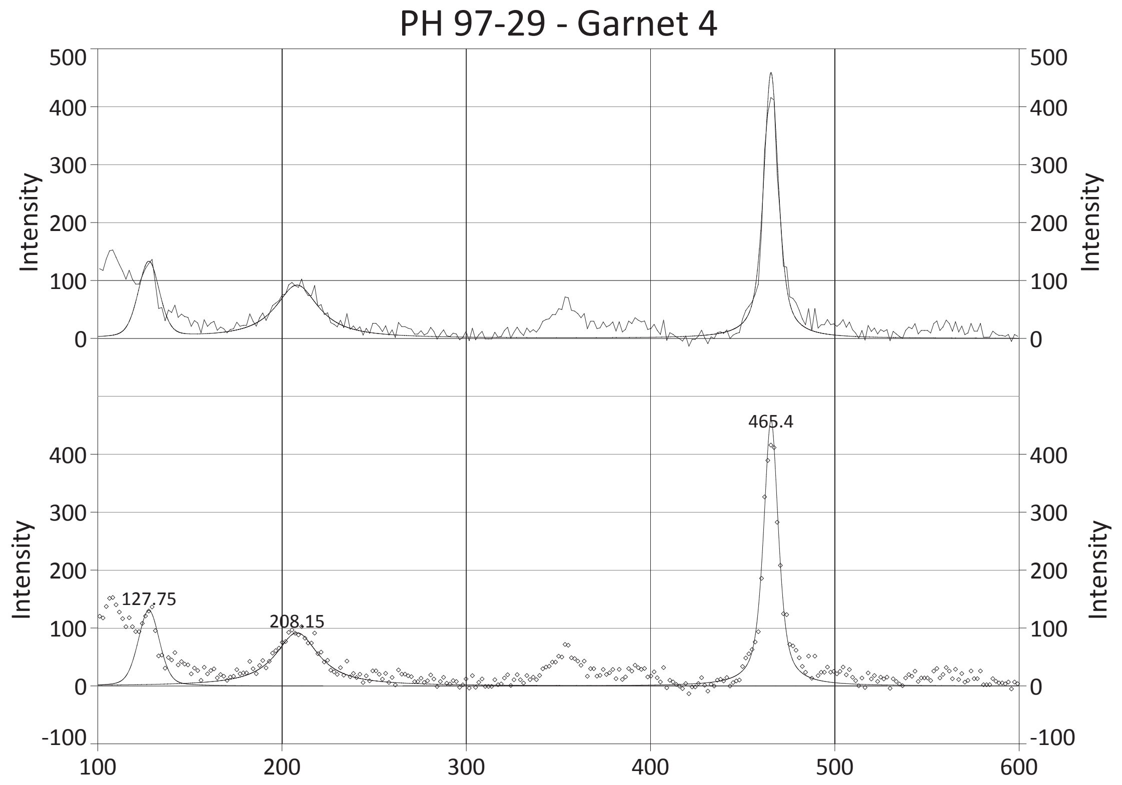

PH 97-29 - Garnet 4

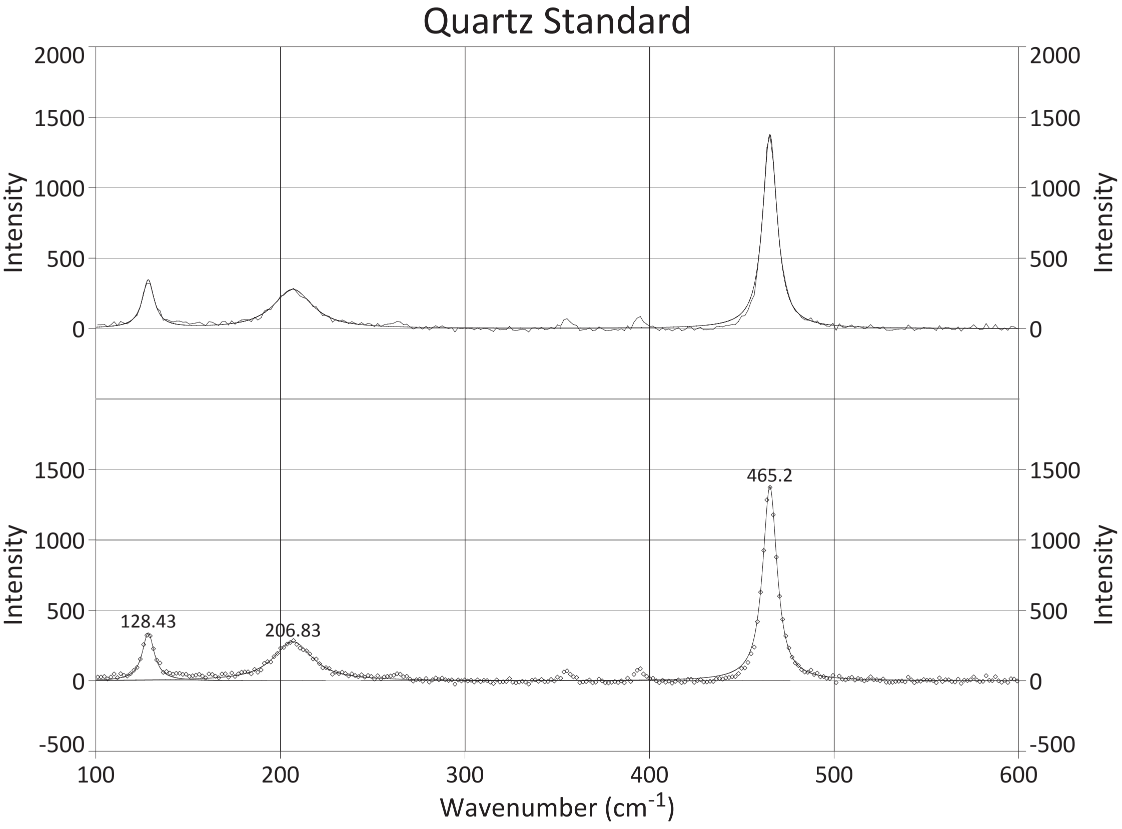

Quartz Standard

PH 97-29

Garnet 5

Locality: Purdy Hill
Collected by Susan Anderson

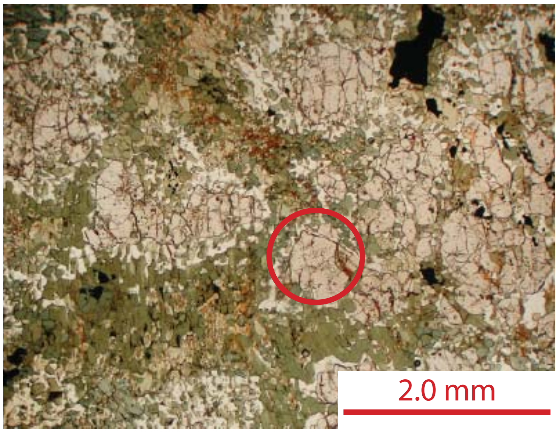

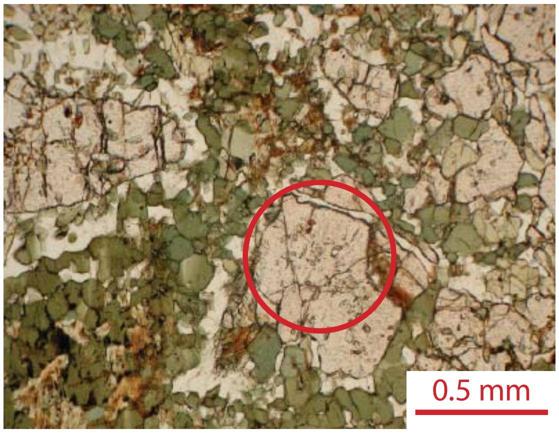

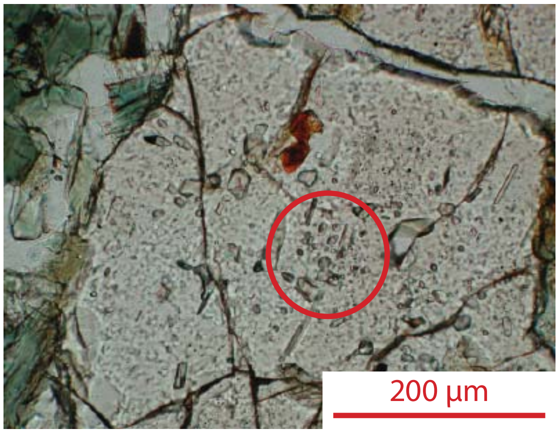

Inclusion Information

Maximum length (X-Y) (µm)	12.6
Minimum length (X-Y) (µm)	11.1
Inclusion thickness (Z) (µm)	10
Location (X-Y coordinates)	(115.2, 13.2)
Description of shape	Spherical
Garnet composition	$Alm_{54.9}$, $Prp_{22.8}$, $Grs_{20.2}$, $Sps_{2.1}$

Data and Pressure Calculation Results

Depth of spectrum (µm)	-2
$\Delta\omega_1$ (cm^{-1})	-1.17
$\Delta\omega_2$ (cm^{-1})	-0.26
$P_{\text{resid }[\Delta\omega 1]}$ (GPa)	-0.074
$P_{\text{resid }[\Delta\omega 2]}$ (GPa)	-0.013
$P_{\text{entrap }[\Delta\omega 1]}$ (GPa)	0.19
$P_{\text{entrap }[\Delta\omega 2]}$ (GPa)	0.35

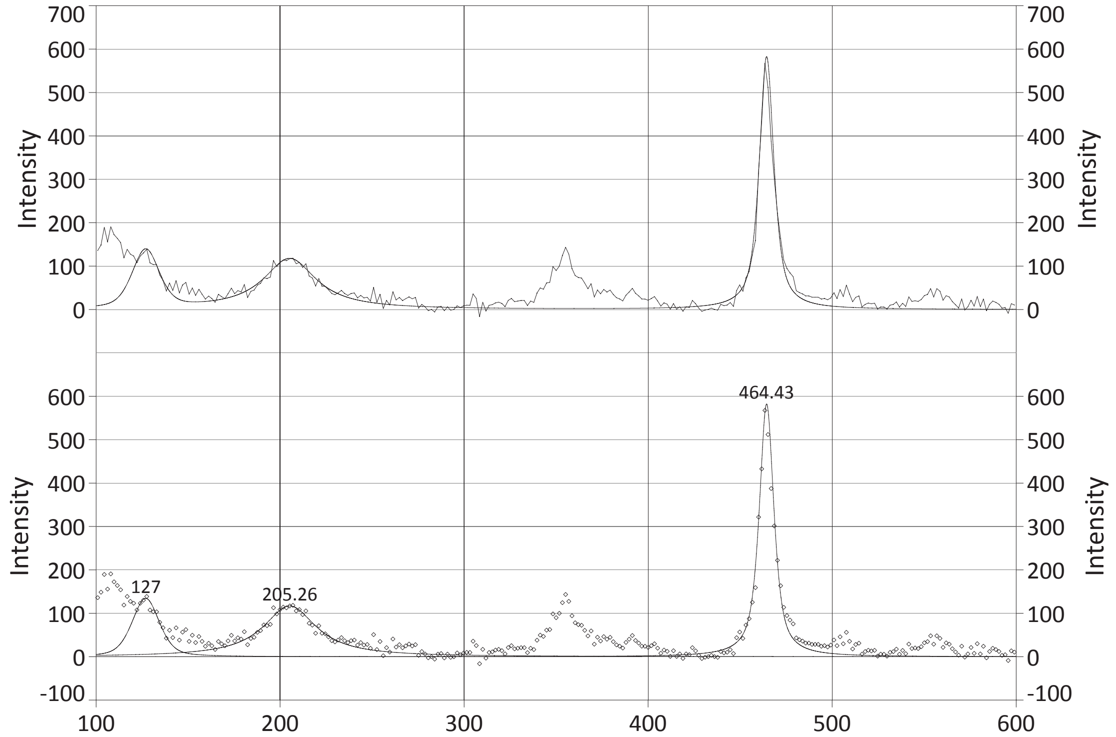

PH 97-29 - Garnet 5

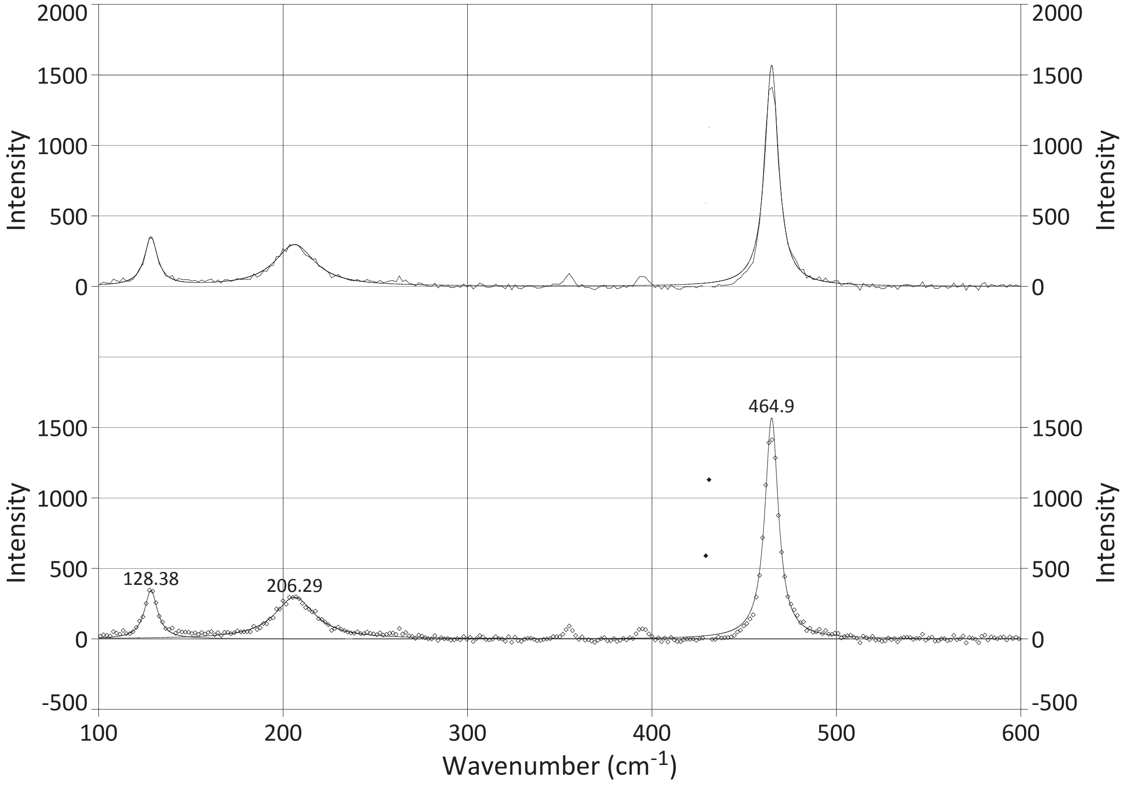

Quartz Standard

PH 97-33

Garnet 1

Locality: Purdy Hill
Collected by Susan Anderson

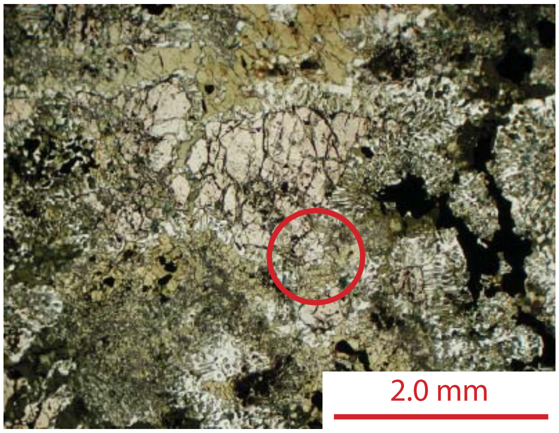

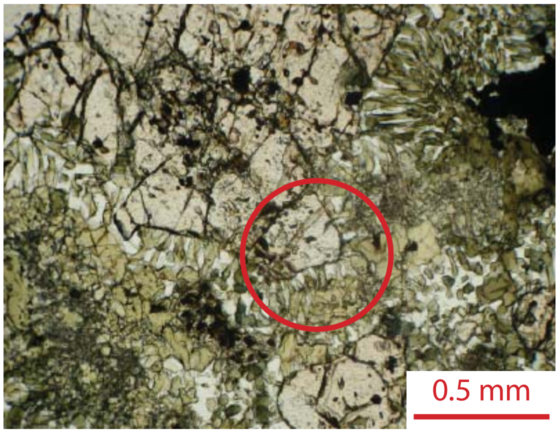

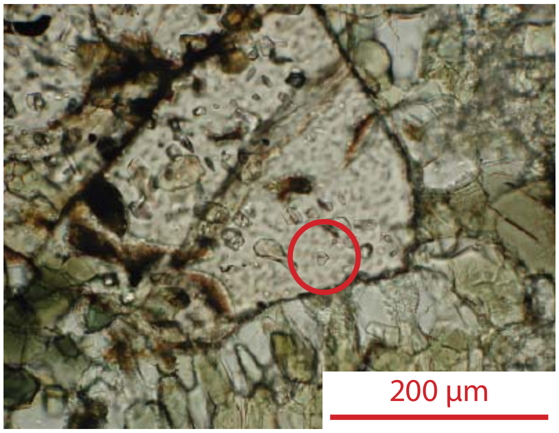

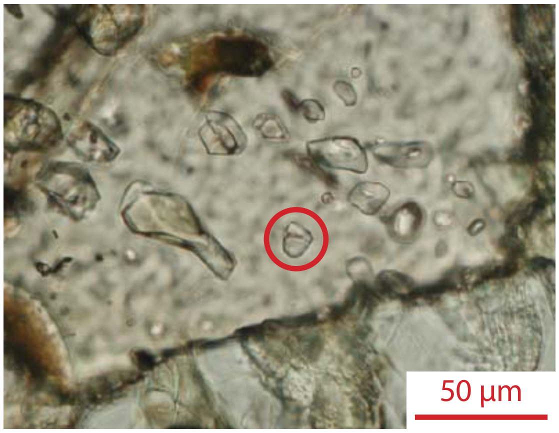

Inclusion Information

Maximum length (X-Y) (μm)	12.6
Minimum length (X-Y) (μm)	9.5
Inclusion thickness (Z) (μm)	20
Location (X-Y coordinates)	(117.4, 2.6)
Description of shape	Heart
Garnet composition	$Alm_{54.9}$, $Prp_{22.8}$, $Grs_{20.2}$, $Sps_{2.1}$

Data and Pressure Calculation Results

Depth of spectrum (μm)	0
$\Delta\omega_1$ (cm^{-1})	1.06
$\Delta\omega_2$ (cm^{-1})	1.13
$P_{resid\ [\Delta\omega1]}$ (GPa)	0.065
$P_{resid\ [\Delta\omega2]}$ (GPa)	0.056
$P_{entrap\ [\Delta\omega1]}$ (GPa)	0.54
$P_{entrap\ [\Delta\omega2]}$ (GPa)	1.03

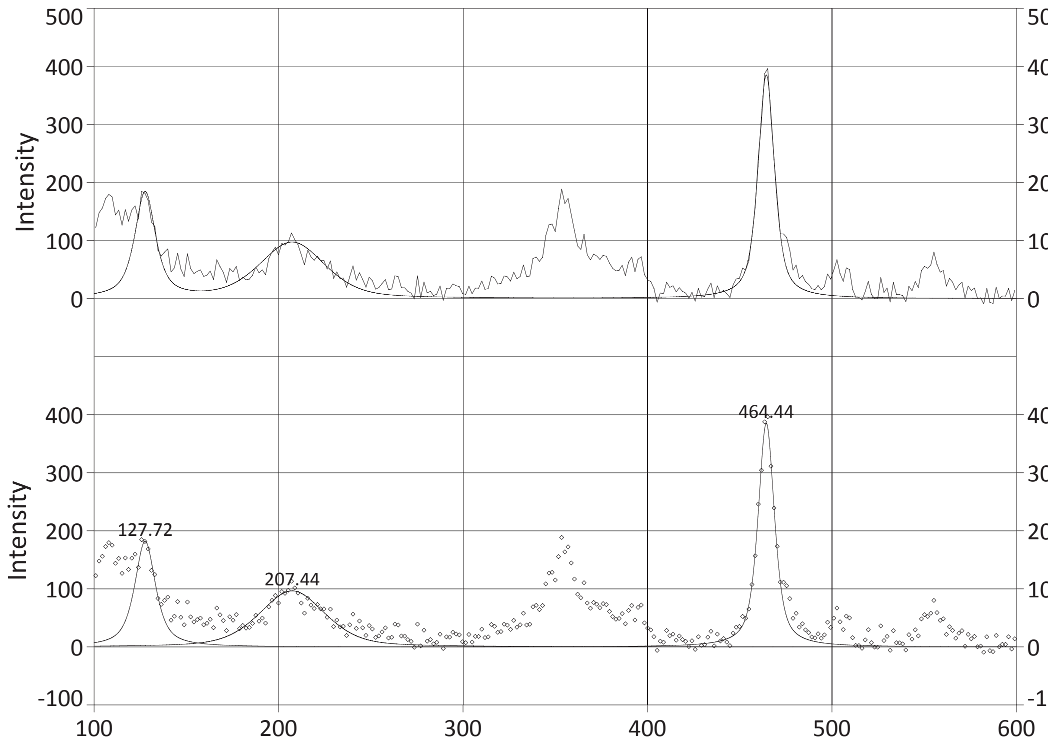

PH 97-33 - Garnet 1

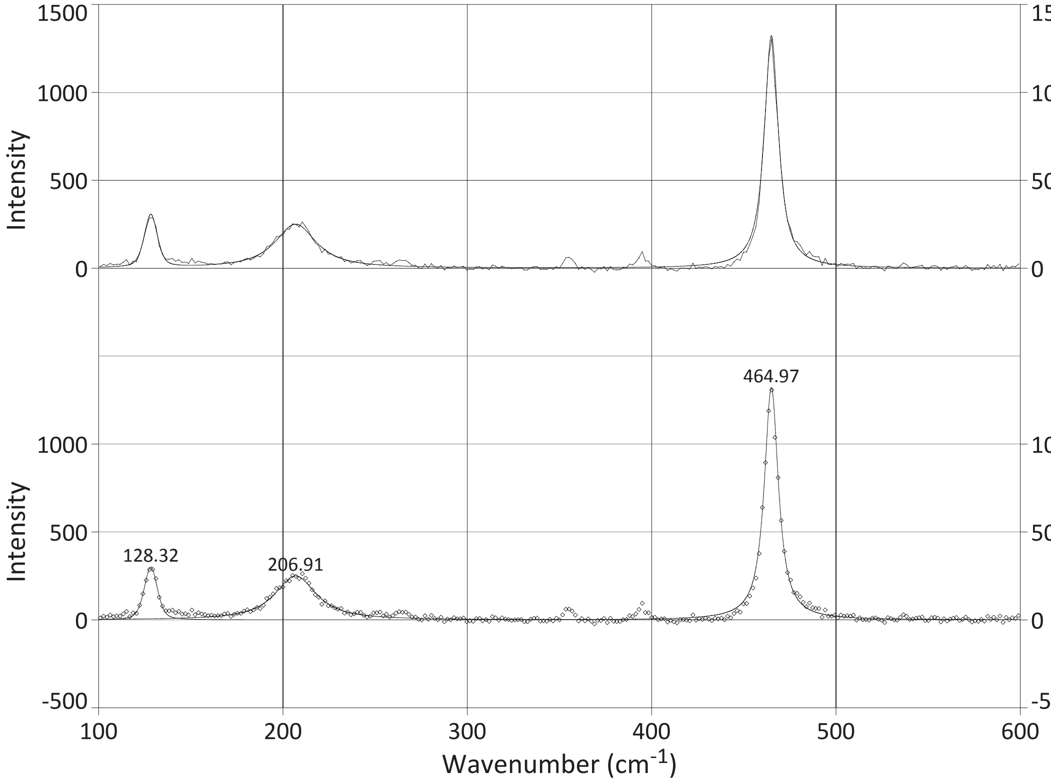

Quartz Standard

PH 97-33

Garnet 2

Locality: Purdy Hill
Collected by Susan Anderson

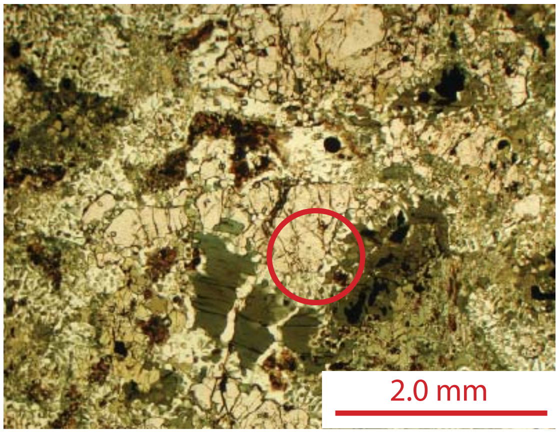

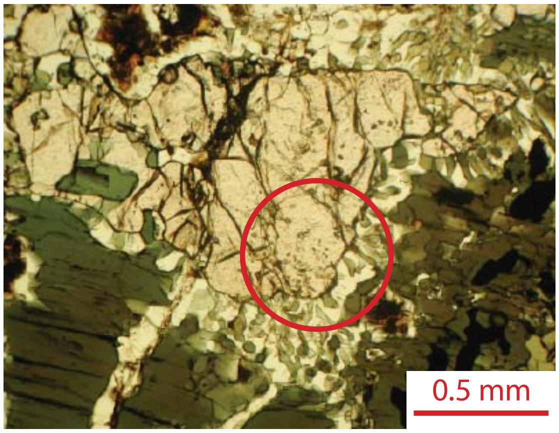

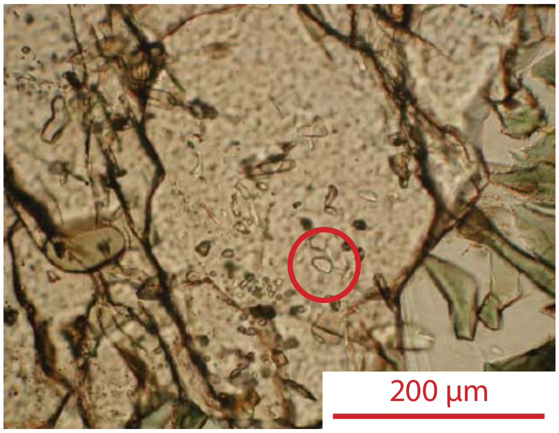

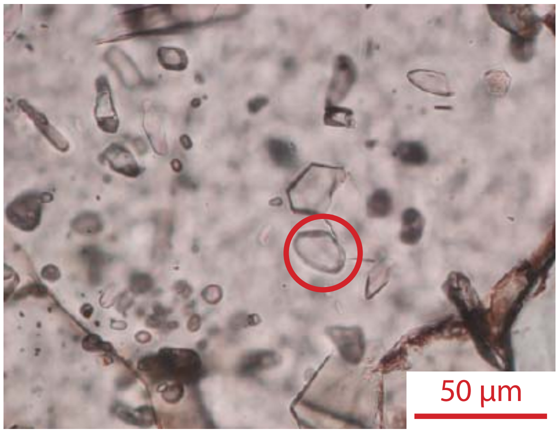

Inclusion Information

Maximum length (X-Y) (µm)	20.5
Minimum length (X-Y) (µm)	14.2
Inclusion thickness (Z) (µm)	18
Location (X-Y coordinates)	(107.3, 10.1)
Description of shape	Ellipsoid
Garnet composition	$Alm_{54.9}$, $Prp_{22.8}$, $Grs_{20.2}$, $Sps_{2.1}$

Data and Pressure Calculation Results

Depth of spectrum (µm)	-8
$\Delta\omega_1$ (cm^{-1})	1.32
$\Delta\omega_2$ (cm^{-1})	0.12
$P_{resid\ [\Delta\omega1]}$ (GPa)	0.080
$P_{resid\ [\Delta\omega2]}$ (GPa)	0.006
$P_{entrap\ [\Delta\omega1]}$ (GPa)	0.58
$P_{entrap\ [\Delta\omega2]}$ (GPa)	0.91

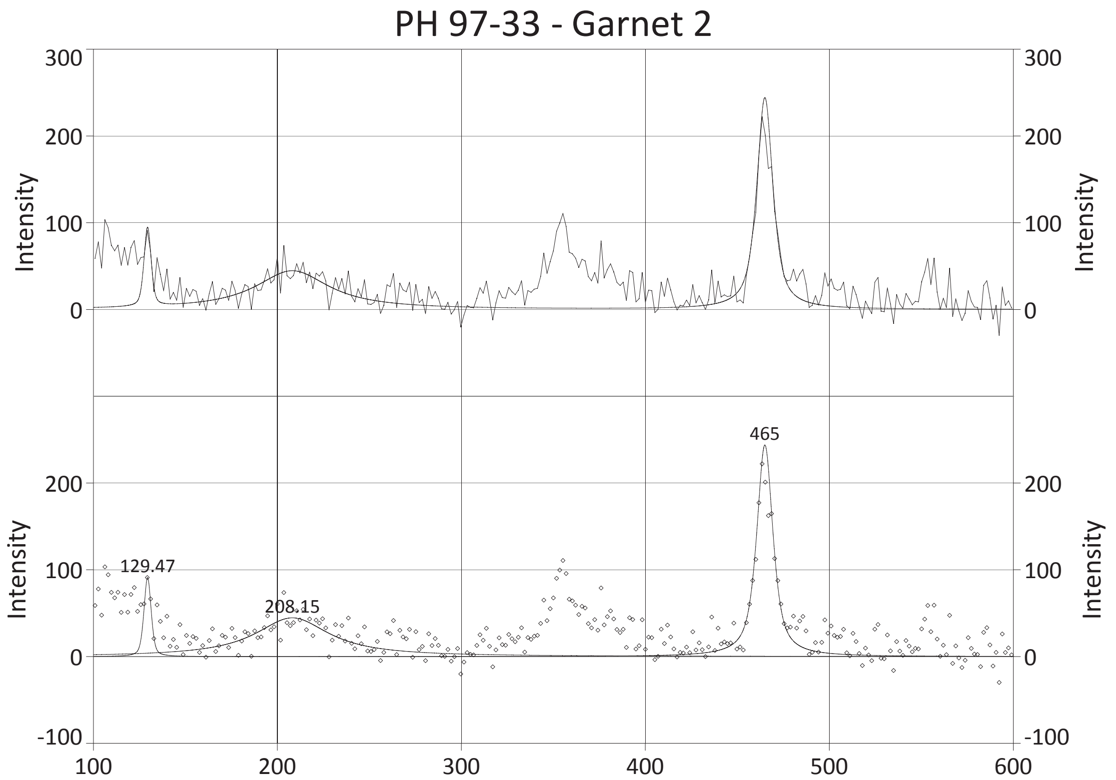

PH 97-33 - Garnet 2

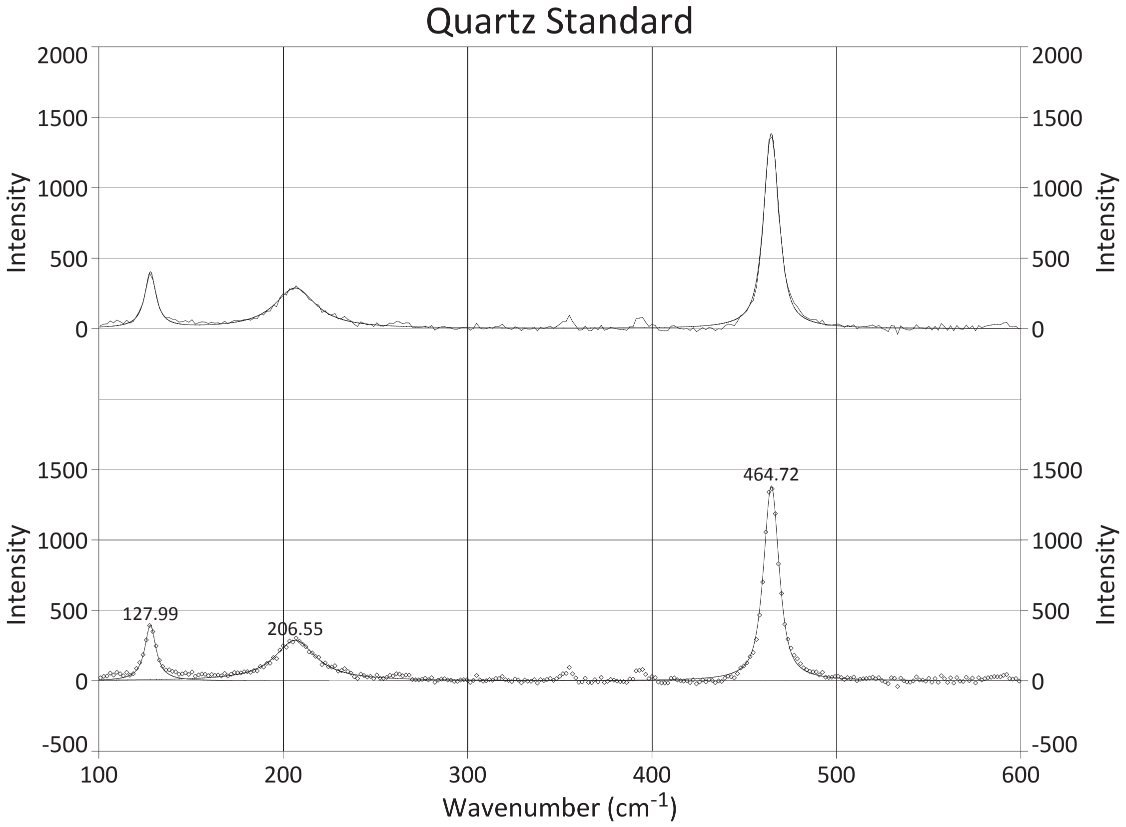

Quartz Standard

PH 97-33

Garnet 3

Locality: Purdy Hill
Collected by Susan Anderson

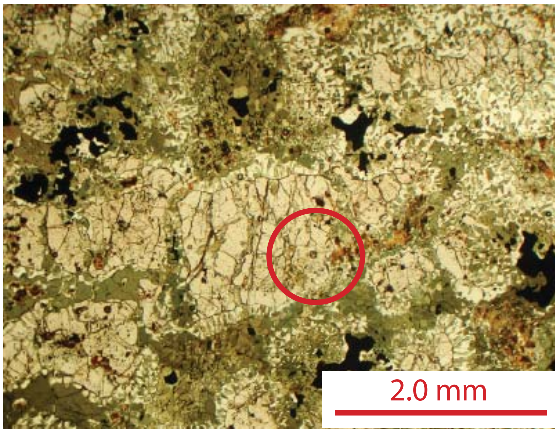

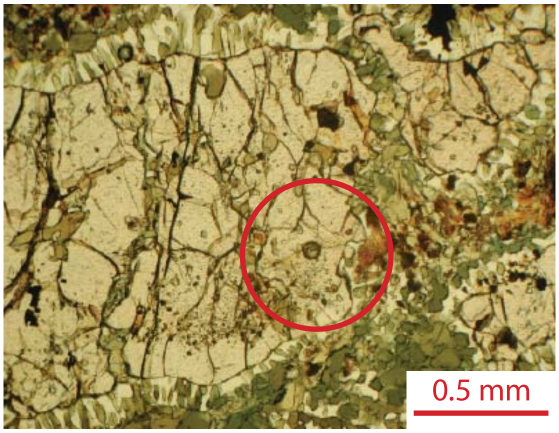

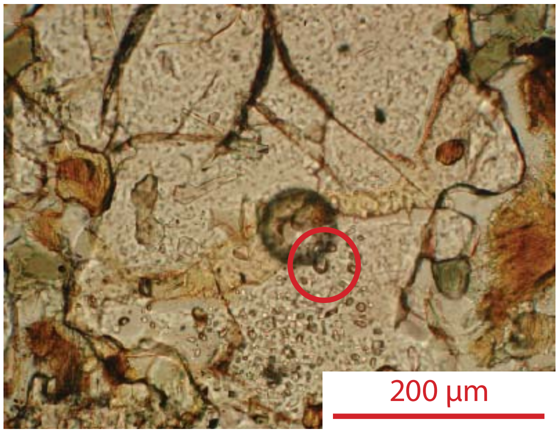

Inclusion Information

Maximum length (X-Y) (µm)	18.9
Minimum length (X-Y) (µm)	15.8
Inclusion thickness (Z) (µm)	12
Location (X-Y coordinates)	-(120.7, 6.9)
Description of shape	Spherical
Garnet composition	$Alm_{54.9}$, $Prp_{22.8}$, $Grs_{20.2}$, $Sps_{2.1}$

Data and Pressure Calculation Results

Depth of spectrum (µm)	-2
$\Delta\omega_1$ (cm^{-1})	-0.92
$\Delta\omega_2$ (cm^{-1})	0.02
$P_{resid\ [\Delta\omega1]}$ (GPa)	-0.058
$P_{resid\ [\Delta\omega2]}$ (GPa)	0.001
$P_{entrap\ [\Delta\omega1]}$ (GPa)	0.23
$P_{entrap\ [\Delta\omega2]}$ (GPa)	0.38

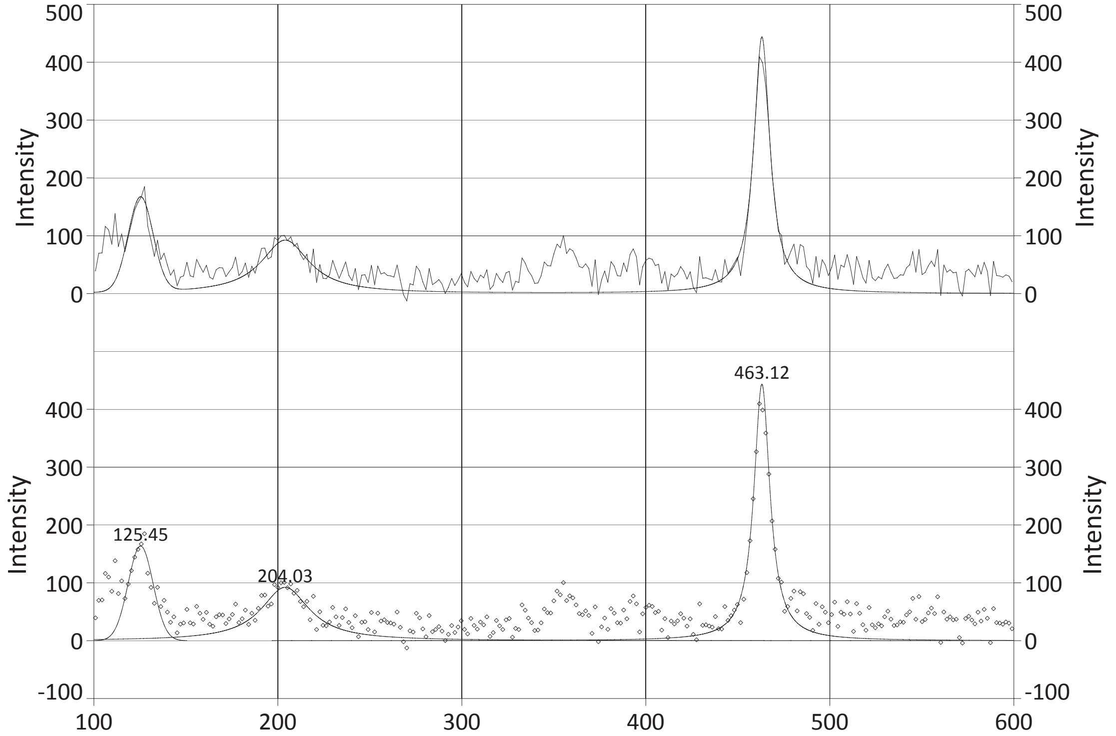

PH 97-33 - Garnet 3

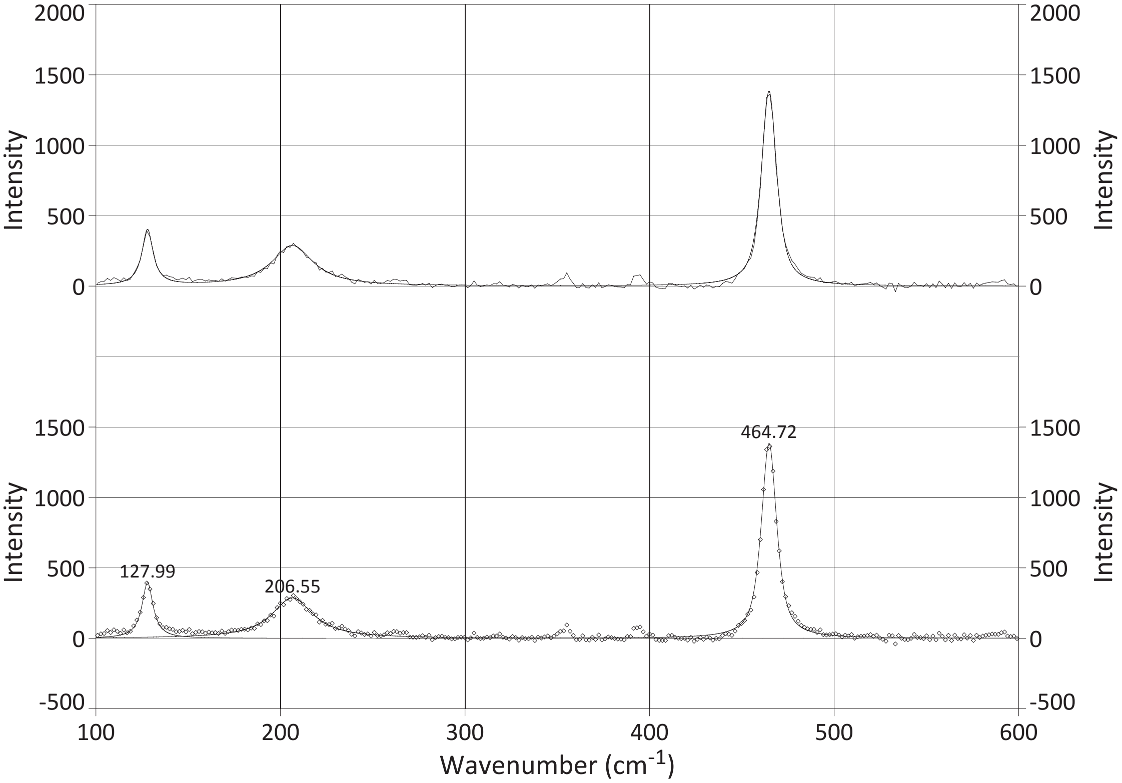

Quartz Standard

PH 97-33

Garnet 4

Locality: Purdy Hill
Collected by Susan Anderson

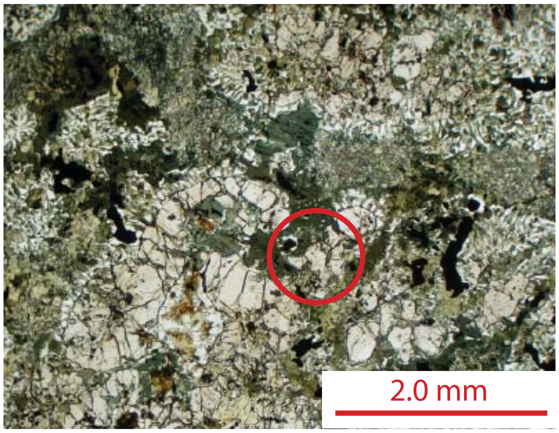

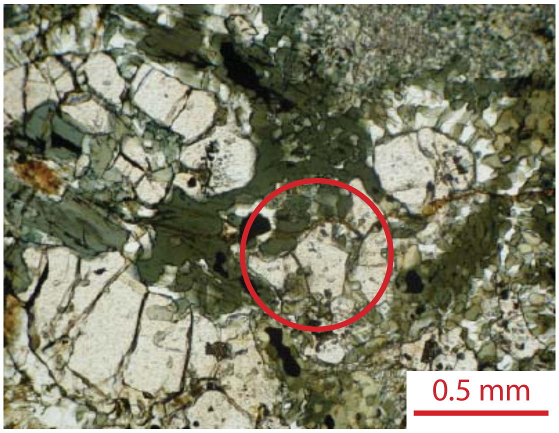

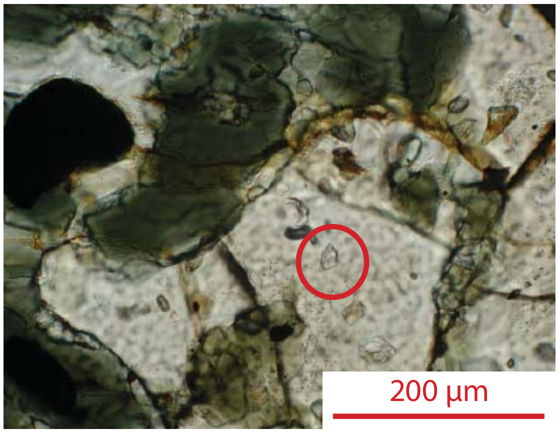

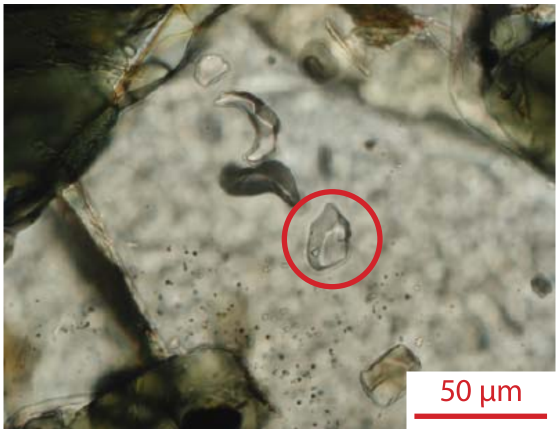

Inclusion Information

Maximum length (X-Y) (µm)	25.3
Minimum length (X-Y) (µm)	15.8
Inclusion thickness (Z) (µm)	18
Location (X-Y coordinates)	(109.1, 5.7)
Description of shape	Angular
Garnet composition	$Alm_{54.9}$, $Prp_{22.8}$, $Grs_{20.2}$, $Sps_{2.1}$

Data and Pressure Calculation Results

Depth of spectrum (µm)	-10
$\Delta\omega_1$ (cm^{-1})	-1.78
$\Delta\omega_2$ (cm^{-1})	2.15
$P_{resid\ [\Delta\omega1]}$ (GPa)	-0.115
$P_{resid\ [\Delta\omega2]}$ (GPa)	0.107
$P_{entrap\ [\Delta\omega1]}$ (GPa)	0.09
$P_{entrap\ [\Delta\omega2]}$ (GPa)	0.64

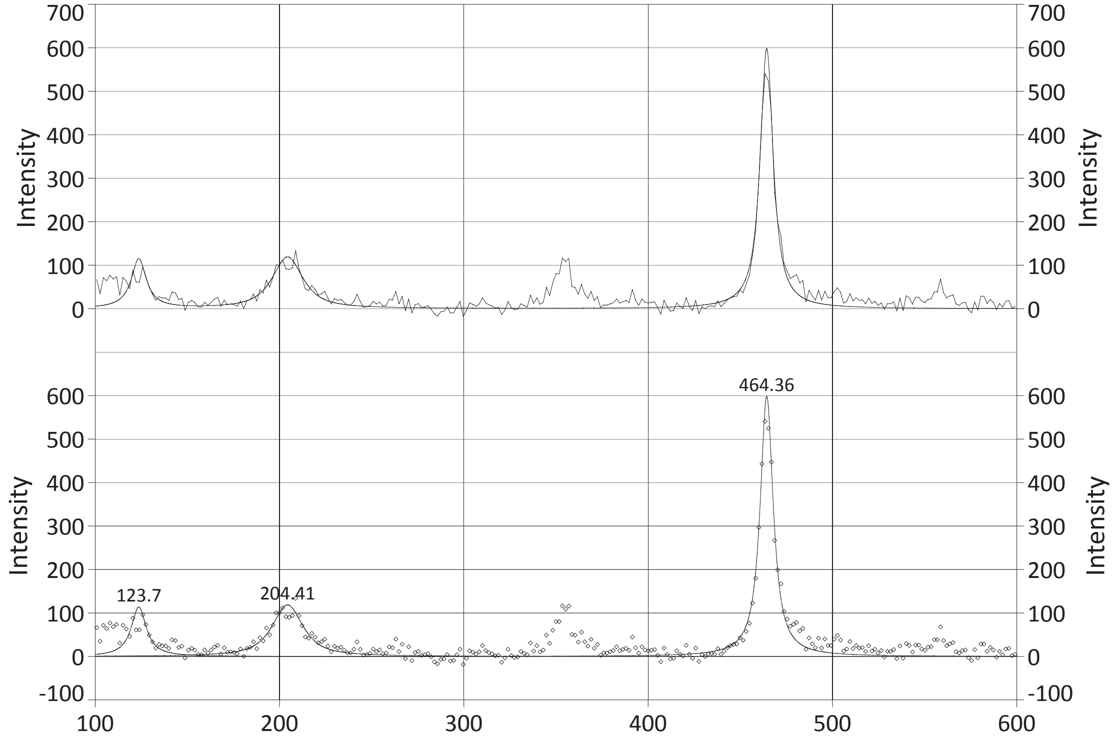

PH 97-33 - Garnet 4

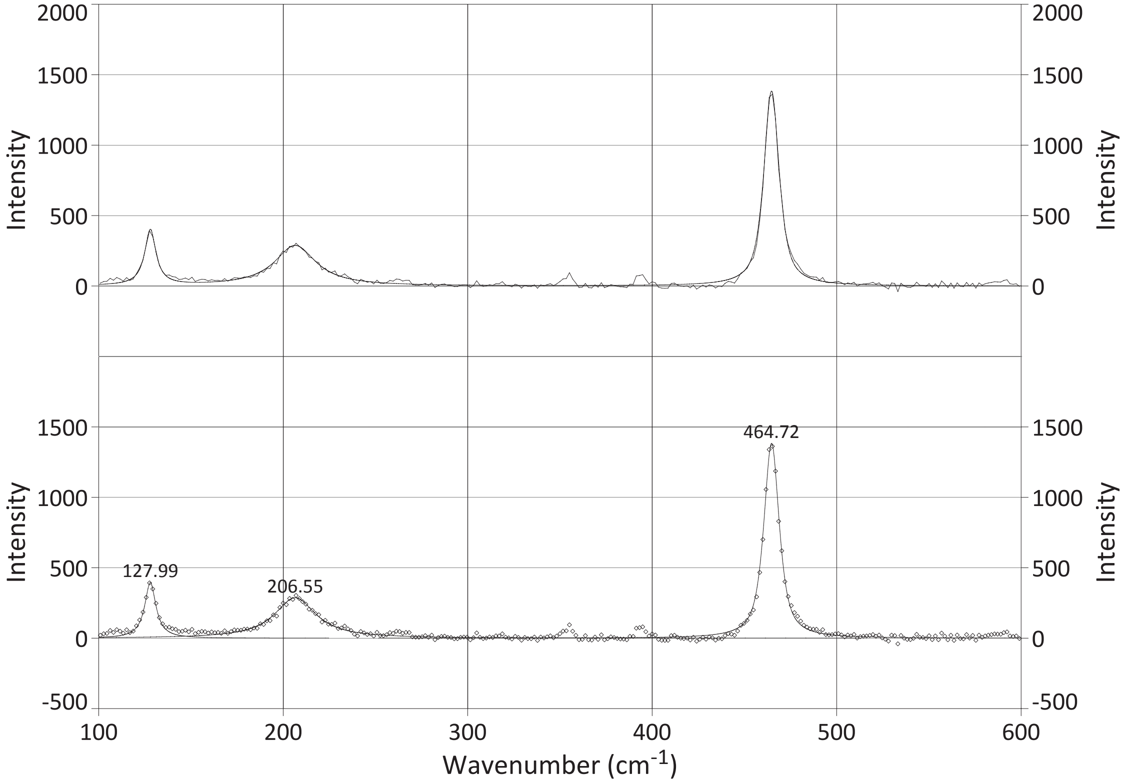

Quartz Standard

PH 97-33

Garnet 5

Locality: Purdy Hill
Collected by Susan Anderson

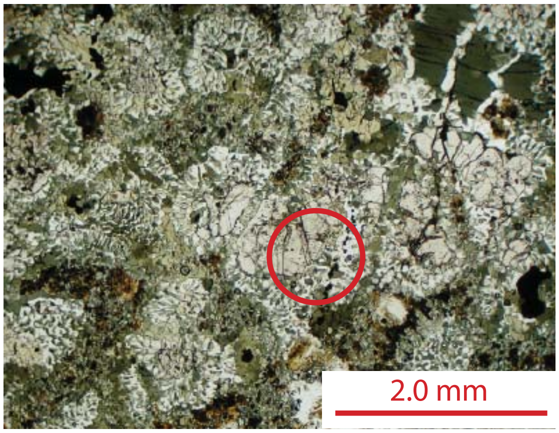

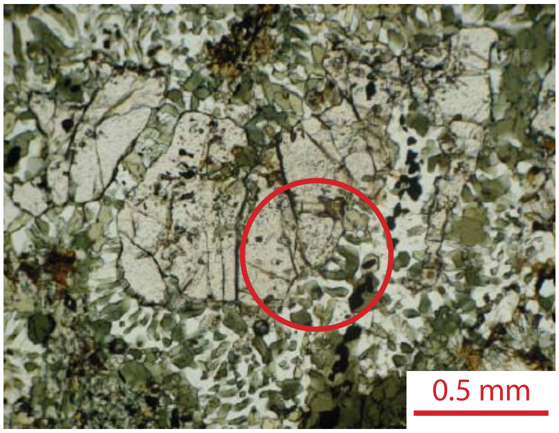

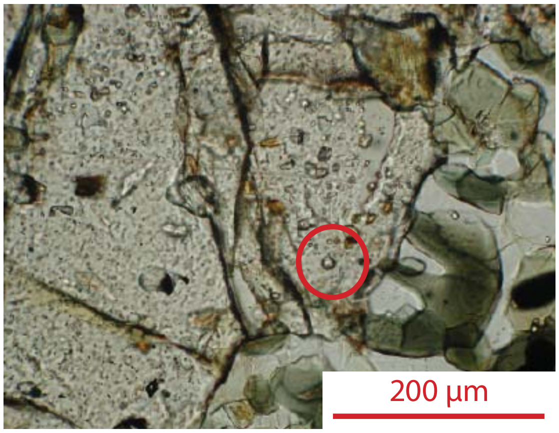

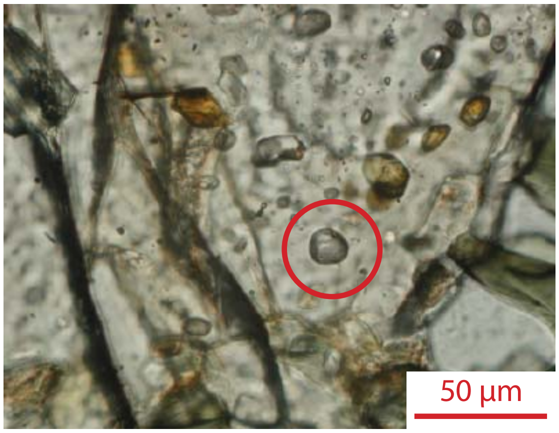

Inclusion Information

Maximum length (X-Y) (μm)	12.6
Minimum length (X-Y) (μm)	12.6
Inclusion thickness (Z) (μm)	12
Location (X-Y coordinates)	(105.2, 21.1)
Description of shape	Spherical
Garnet composition	$Alm_{54.9}$, $Prp_{22.8}$, $Grs_{20.2}$, $Sps_{2.1}$

Data and Pressure Calculation Results

Depth of spectrum (μm)	-4
$\Delta\omega_1$ (cm^{-1})	-1.71
$\Delta\omega_2$ (cm^{-1})	-1.37
$P_{resid\ [\Delta\omega1]}$ (GPa)	-0.110
$P_{resid\ [\Delta\omega2]}$ (GPa)	-0.067
$P_{entrap\ [\Delta\omega1]}$ (GPa)	0.10
$P_{entrap\ [\Delta\omega2]}$ (GPa)	0.21

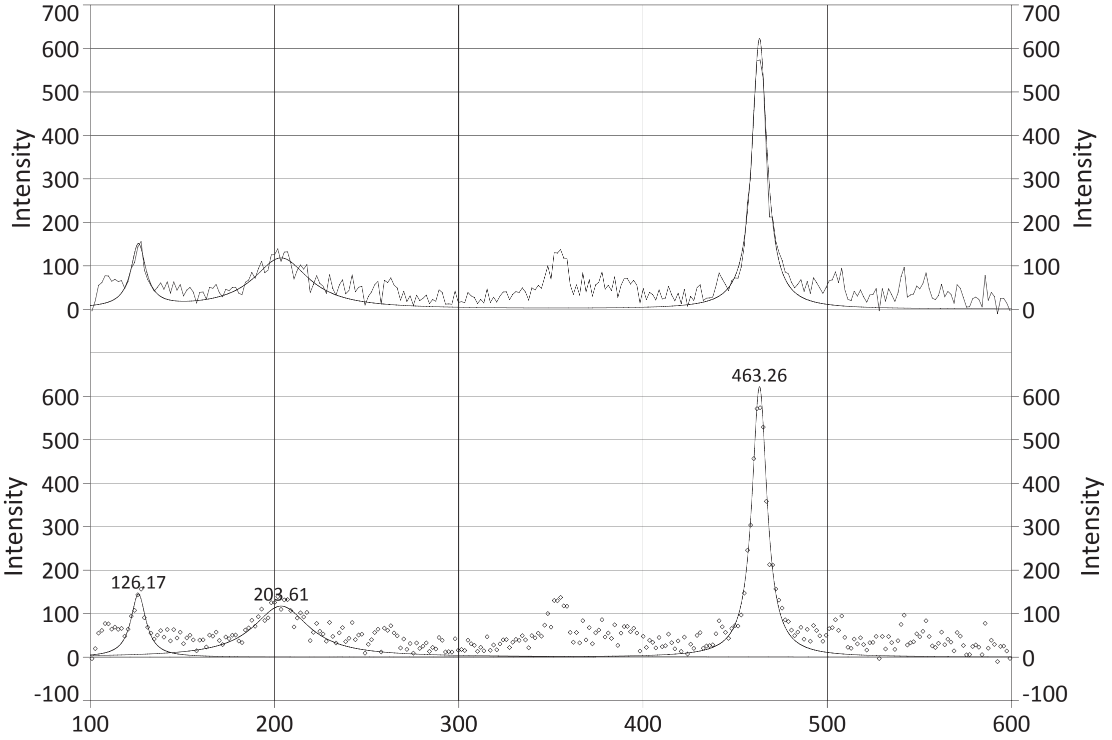

PH 97-33 - Garnet 5

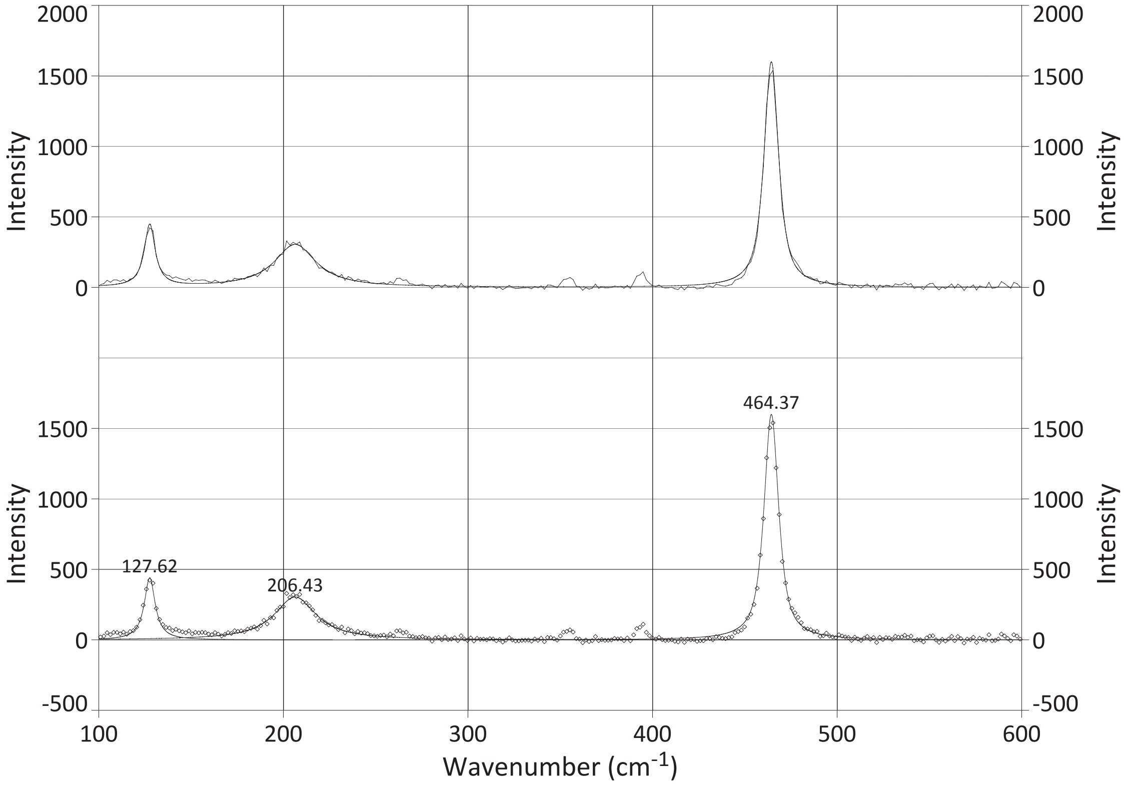

Quartz Standard

PH 97-62

Garnet 2

Locality: Purdy Hill
Collected by Susan Anderson

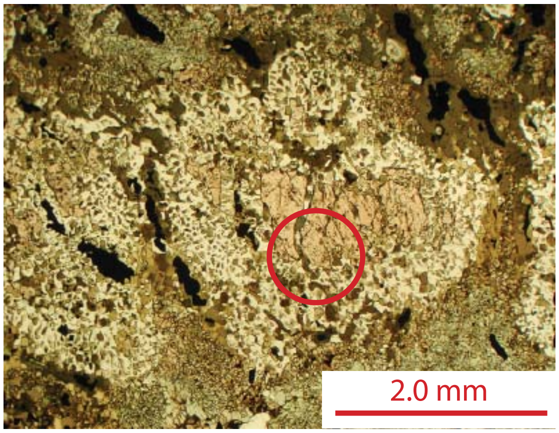

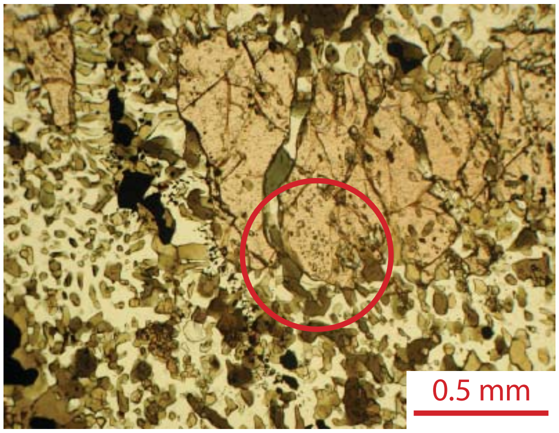

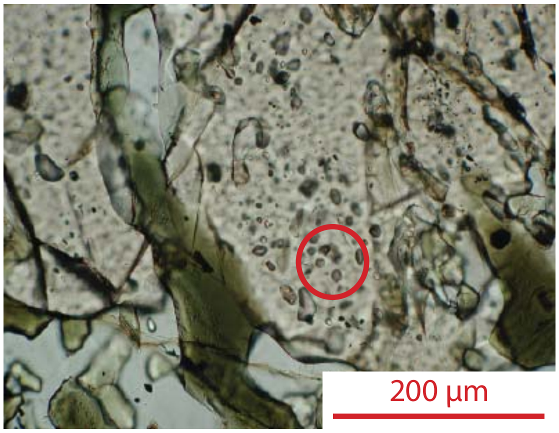

Inclusion Information

Maximum length (X-Y) (µm)	9.5
Minimum length (X-Y) (µm)	7.9
Inclusion thickness (Z) (µm)	16
Location (X-Y coordinates)	(100.5, 8.4)
Description of shape	Spherical
Garnet composition	$Alm_{62.3}$, $Prp_{15.8}$, $Grs_{21.2}$, $Sps_{0.6}$

Data and Pressure Calculation Results

Depth of spectrum (µm)	-6
$\Delta\omega_1$ (cm^{-1})	-5.77
$\Delta\omega_2$ (cm^{-1})	-7.91
$P_{resid\ [\Delta\omega1]}$ (GPa)	-0.418
$P_{resid\ [\Delta\omega2]}$ (GPa)	-0.380
$P_{entrap\ [\Delta\omega1]}$ (GPa)	-0.64
$P_{entrap\ [\Delta\omega2]}$ (GPa)	-0.55

PH 97-62 - Garnet 2

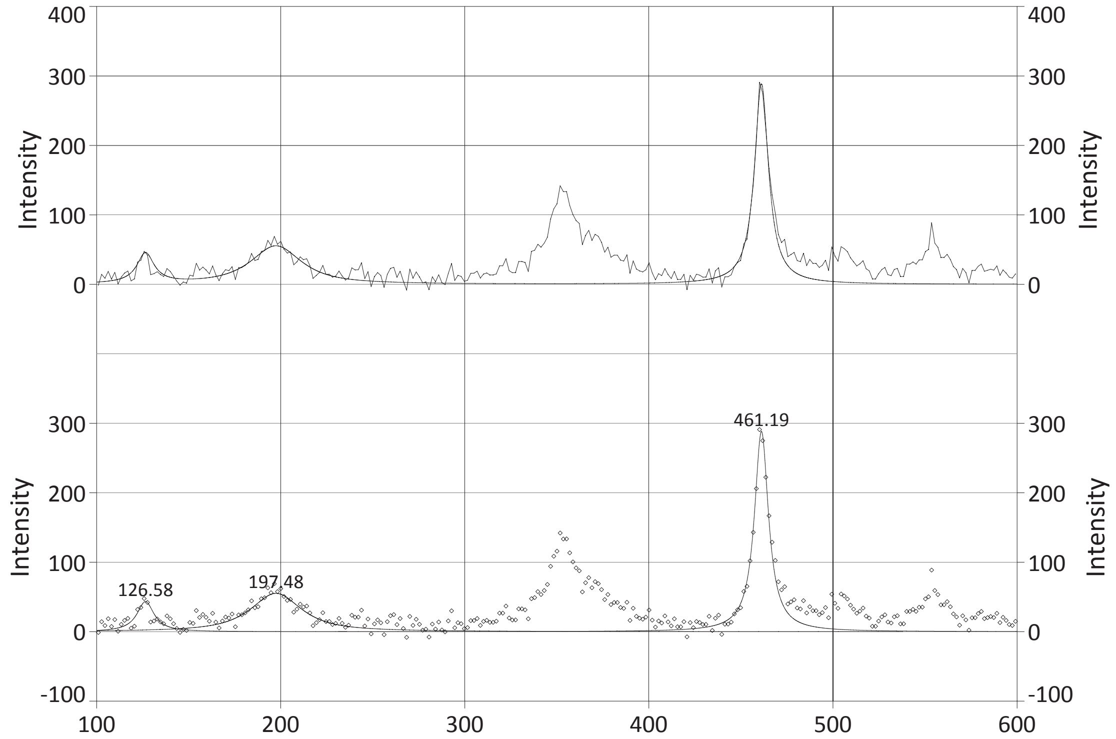

Quartz Standard

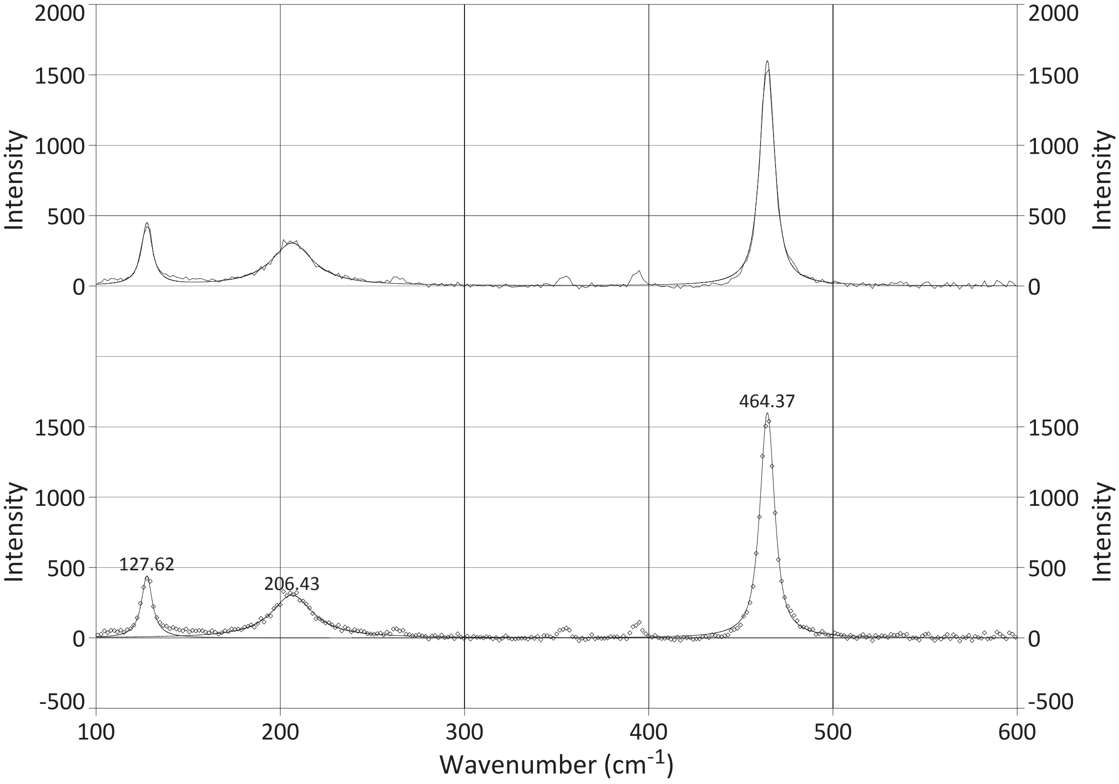

PH 97-62

Garnet 3

Locality: Purdy Hill
Collected by Susan Anderson

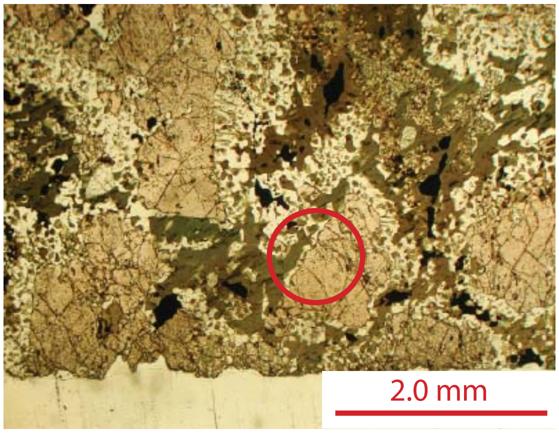

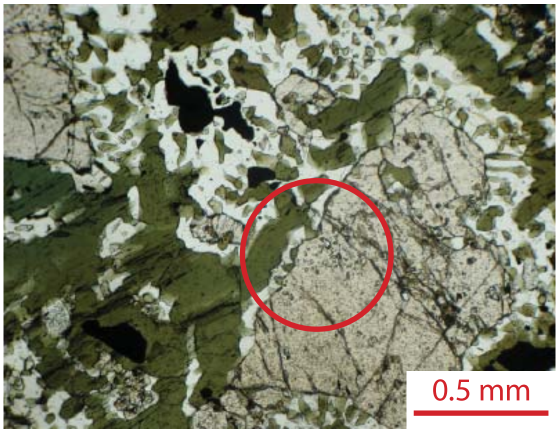

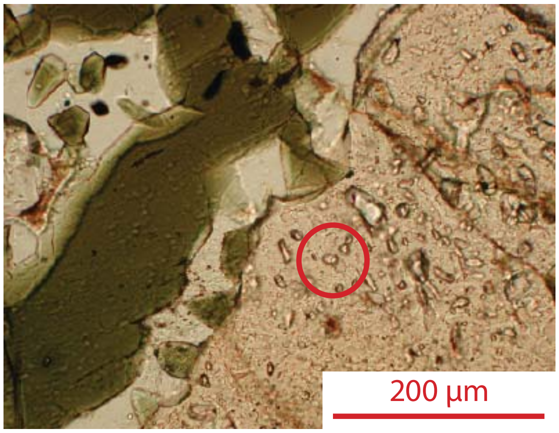

Inclusion Information

Maximum length (X-Y) (µm)	17.4
Minimum length (X-Y) (µm)	12.6
Inclusion thickness (Z) (µm)	13
Location (X-Y coordinates)	-(117.2, 18.1)
Description of shape	Ellipsoid
Garnet composition	$Alm_{62.3}$, $Prp_{15.8}$, $Grs_{21.2}$, $Sps_{0.6}$

Data and Pressure Calculation Results

Depth of spectrum (µm)	-4
$\Delta\omega_1$ (cm^{-1})	-8.87
$\Delta\omega_2$ (cm^{-1})	-8.87
$P_{resid\ [\Delta\omega 1]}$ (GPa)	-0.716
$P_{resid\ [\Delta\omega 2]}$ (GPa)	-0.427
$P_{entrap\ [\Delta\omega 1]}$ (GPa)	-1.39
$P_{entrap\ [\Delta\omega 2]}$ (GPa)	-0.67

PH 97-62 - Garnet 3

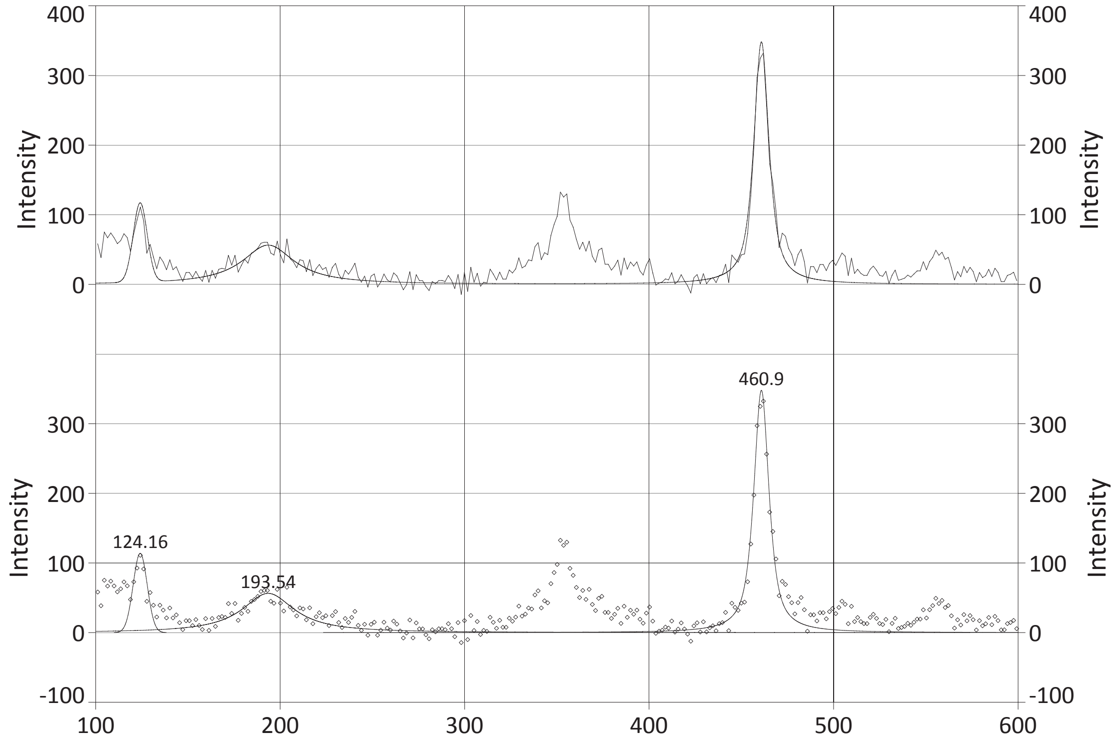

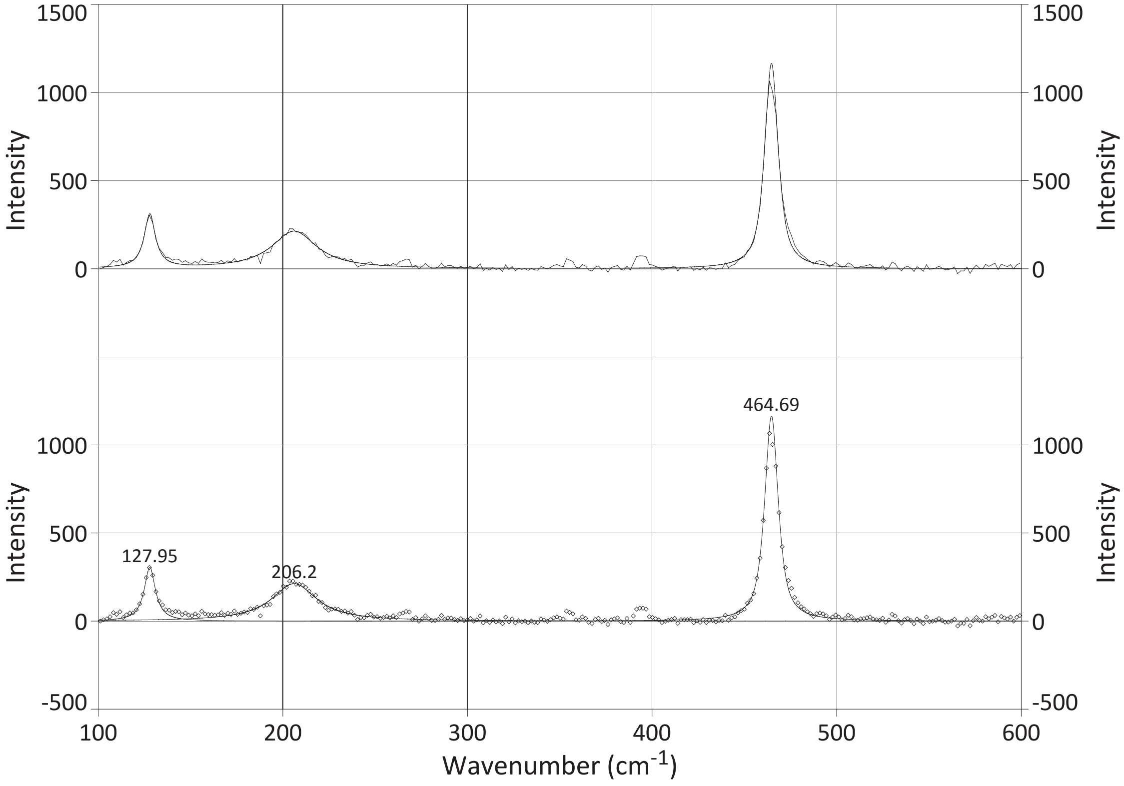

PH 97-62

Garnet 4

Locality: Purdy Hill
Collected by Susan Anderson

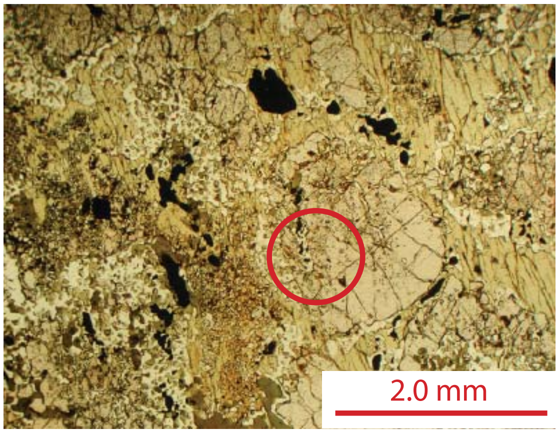

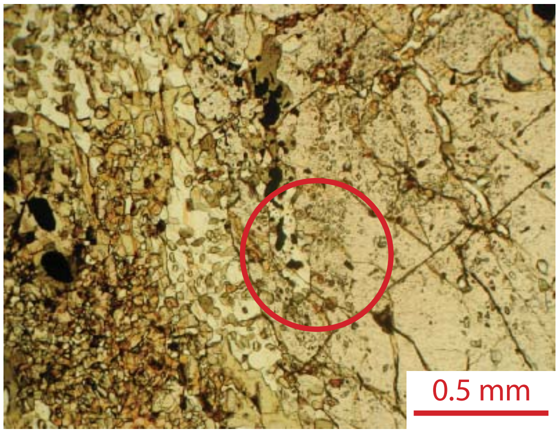

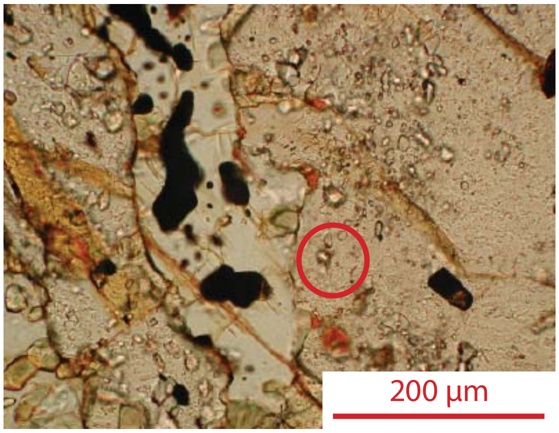

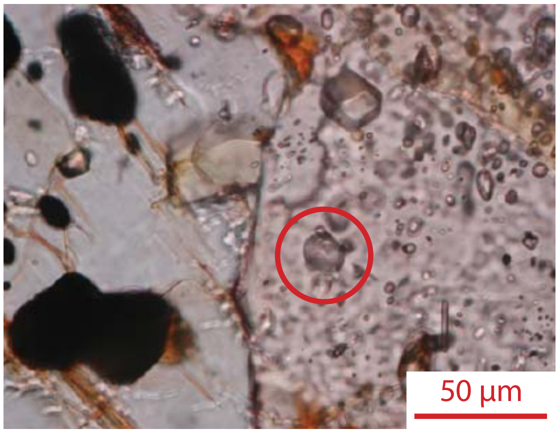

Inclusion Information

Maximum length (X-Y) (µm)	17.4
Minimum length (X-Y) (µm)	12.6
Inclusion thickness (Z) (µm)	13
Location (X-Y coordinates)	(119.3, 2.5)
Description of shape	Ellipsoid
Garnet composition	$Alm_{62.3}$, $Prp_{15.8}$, $Grs_{21.2}$, $Sps_{0.6}$

Data and Pressure Calculation Results

Depth of spectrum (µm)	-8
$\Delta\omega_1$ (cm^{-1})	-2.08
$\Delta\omega_2$ (cm^{-1})	-1.79
$P_{resid\ [\Delta\omega1]}$ (GPa)	-0.135
$P_{resid\ [\Delta\omega2]}$ (GPa)	-0.087
$P_{entrap\ [\Delta\omega1]}$ (GPa)	0.06
$P_{entrap\ [\Delta\omega2]}$ (GPa)	0.18

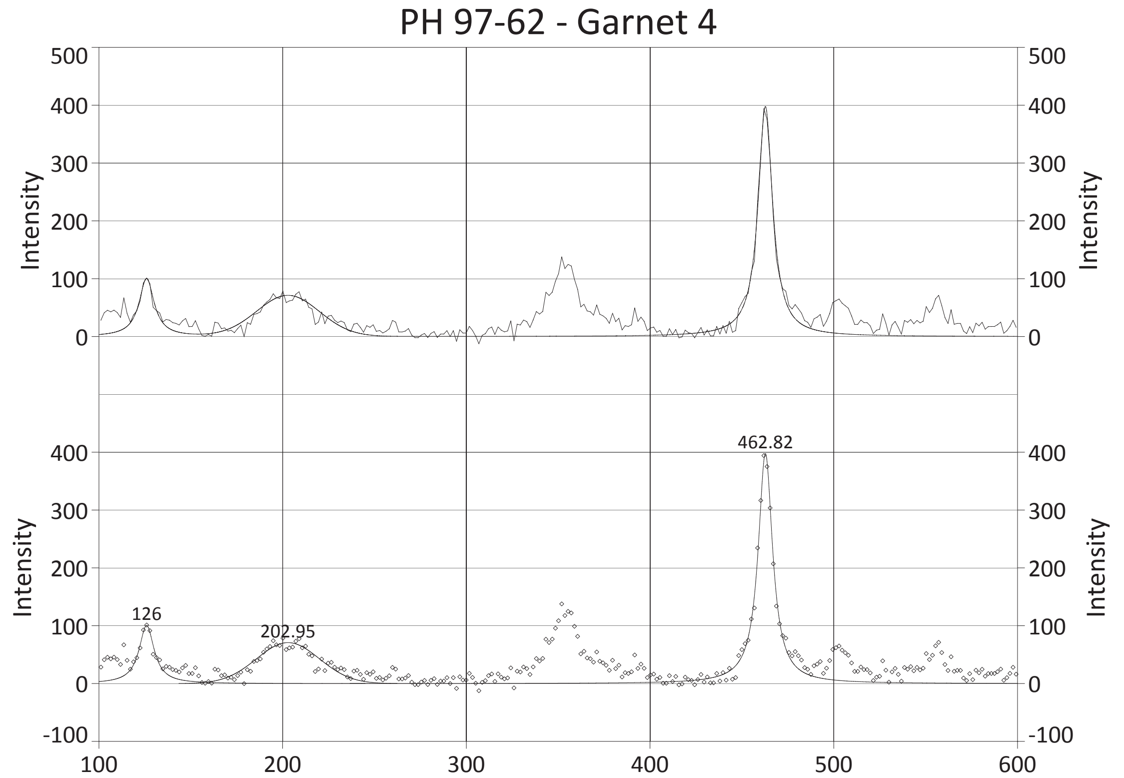

PH 97-62 - Garnet 4

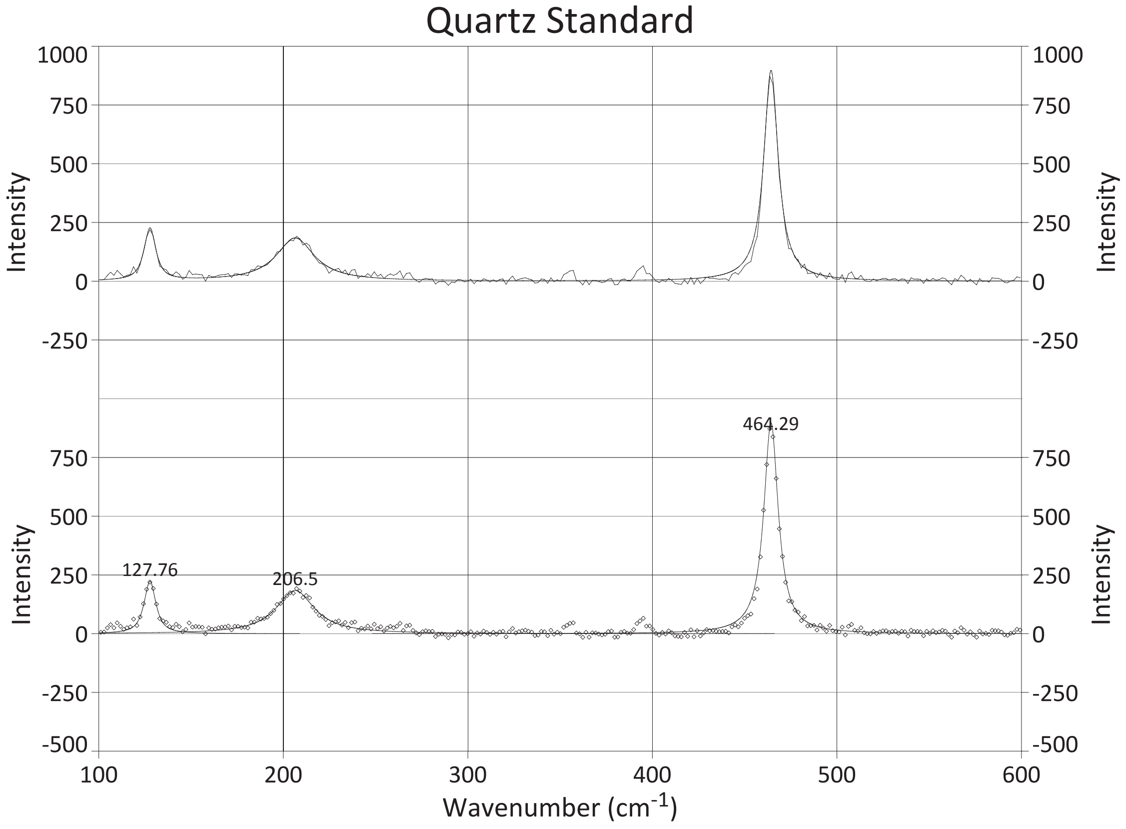

Quartz Standard

PH 97-62

Garnet 5

Locality: Purdy Hill
Collected by Susan Anderson

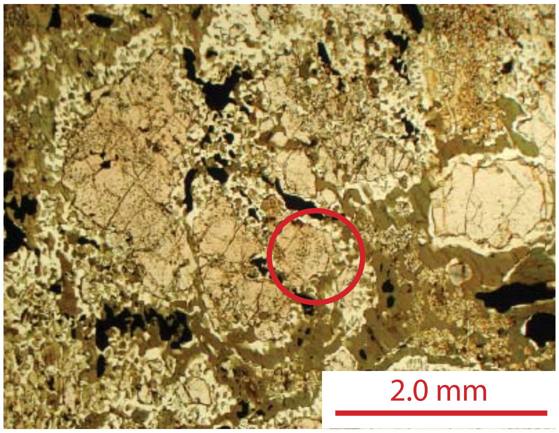

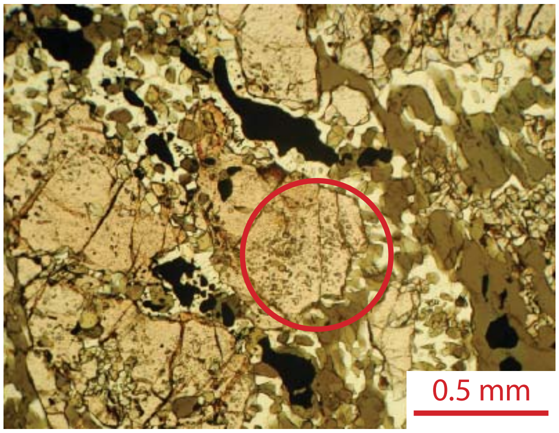

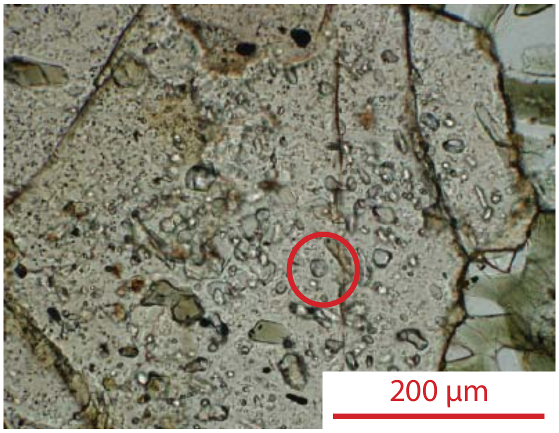

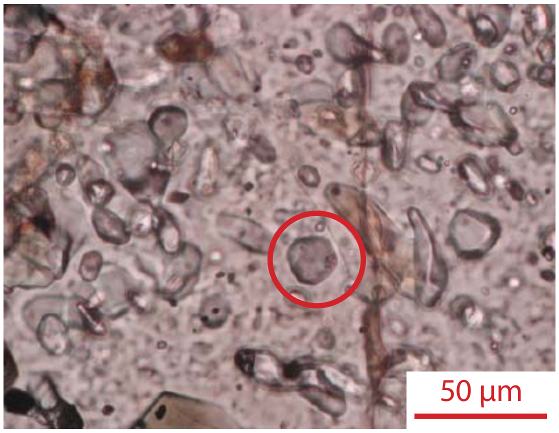

Inclusion Information

Maximum length (X-Y) (µm)	20.5
Minimum length (X-Y) (µm)	17.4
Inclusion thickness (Z) (µm)	12
Location (X-Y coordinates)	(117.0, 5.0)
Description of shape	Rounded
Garnet composition	$\text{Alm}_{62.3}$, $\text{Prp}_{15.8}$, $\text{Grs}_{21.2}$, $\text{Sps}_{0.6}$

Data and Pressure Calculation Results

Depth of spectrum (µm)	-5
$\Delta\omega_1$ (cm^{-1})	-6.74
$\Delta\omega_2$ (cm^{-1})	-6.52
$P_{\text{resid }[\Delta\omega1]}$ (GPa)	-0.504
$P_{\text{resid }[\Delta\omega2]}$ (GPa)	-0.314
$P_{\text{entrap }[\Delta\omega1]}$ (GPa)	-0.86
$P_{\text{entrap }[\Delta\omega2]}$ (GPa)	0.39

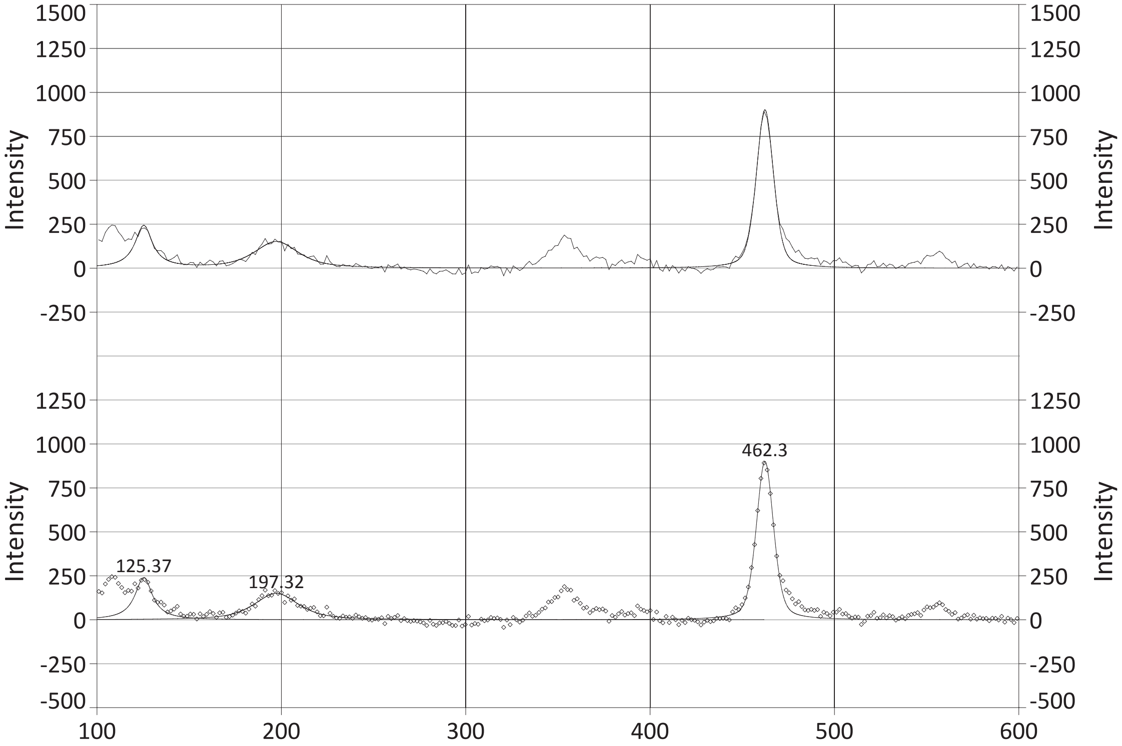

PH 97-62 - Garnet 5

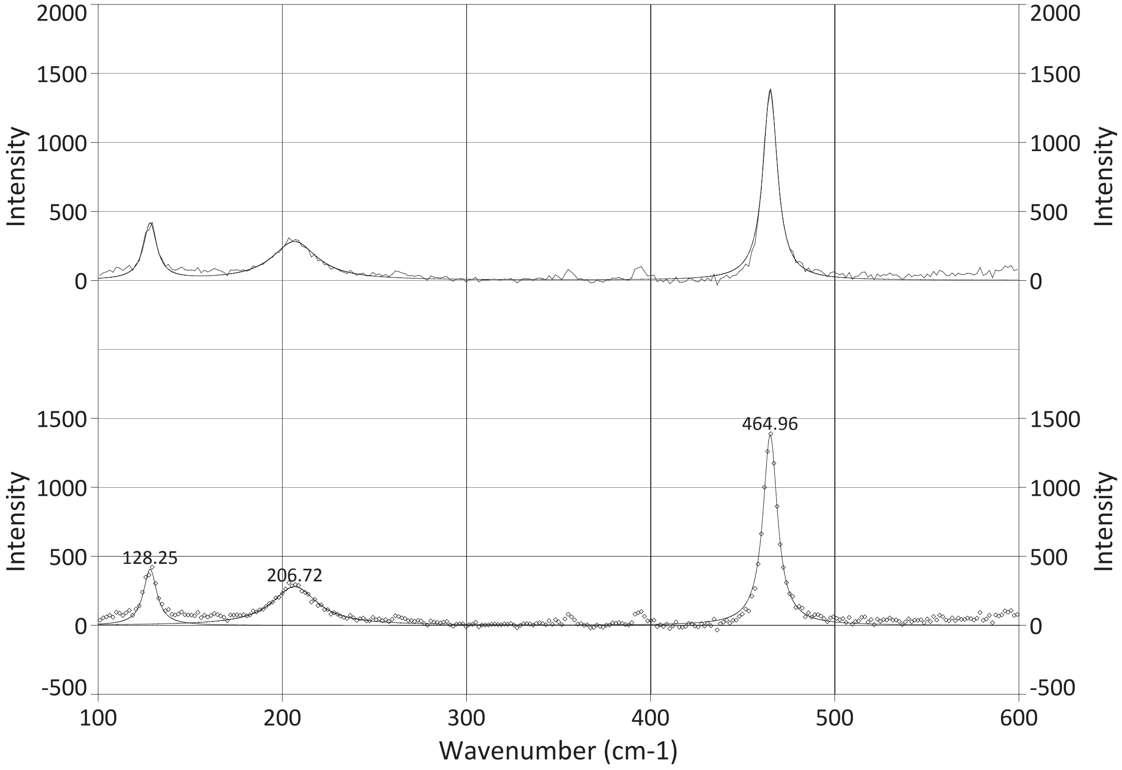

Quartz Standard

PH 97-62

Garnet 6

Locality: Purdy Hill
Collected by Susan Anderson

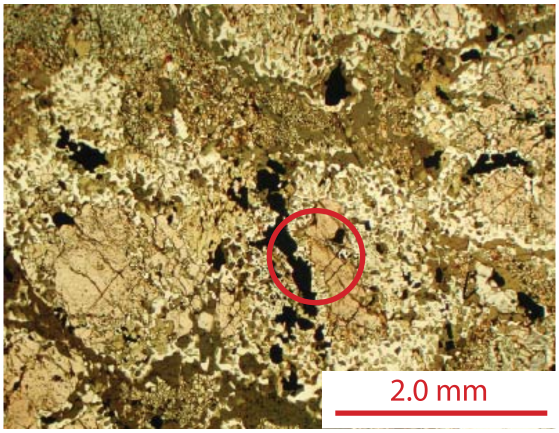

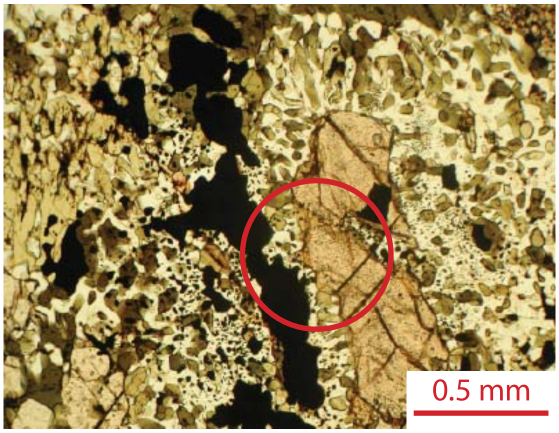

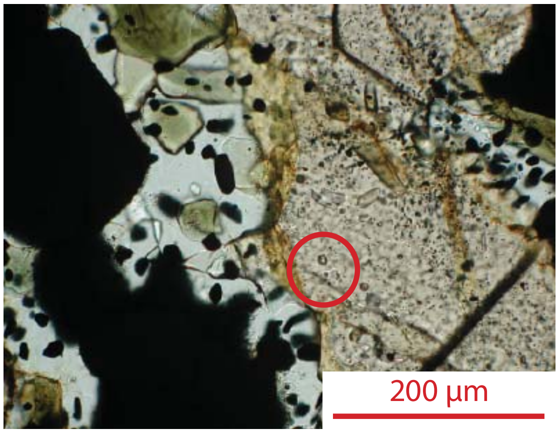

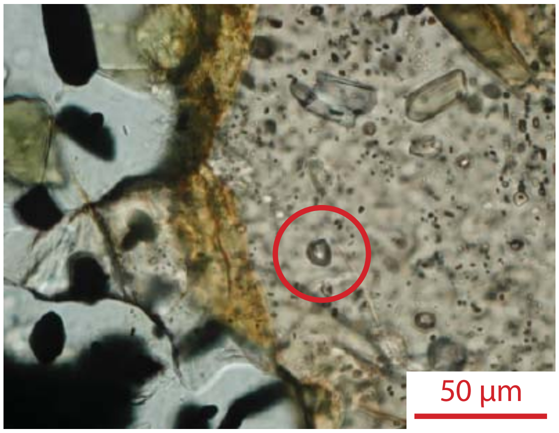

Inclusion Information

Maximum length (X-Y) (µm)	11.1
Minimum length (X-Y) (µm)	9.5
Inclusion thickness (Z) (µm)	12
Location (X-Y coordinates)	(114.4, 8.3)
Description of shape	Spherical
Garnet composition	$Alm_{62.3}$, $Prp_{15.8}$, $Grs_{21.2}$, $Sps_{0.6}$

Data and Pressure Calculation Results

Depth of spectrum (µm)	-4
$\Delta\omega_1$ (cm^{-1})	-3.70
$\Delta\omega_2$ (cm^{-1})	-4.15
$P_{resid\ [\Delta\omega 1]}$ (GPa)	-0.251
$P_{resid\ [\Delta\omega 2]}$ (GPa)	-0.200
$P_{entrap\ [\Delta\omega 1]}$ (GPa)	-0.23
$P_{entrap\ [\Delta\omega 2]}$ (GPa)	-0.10

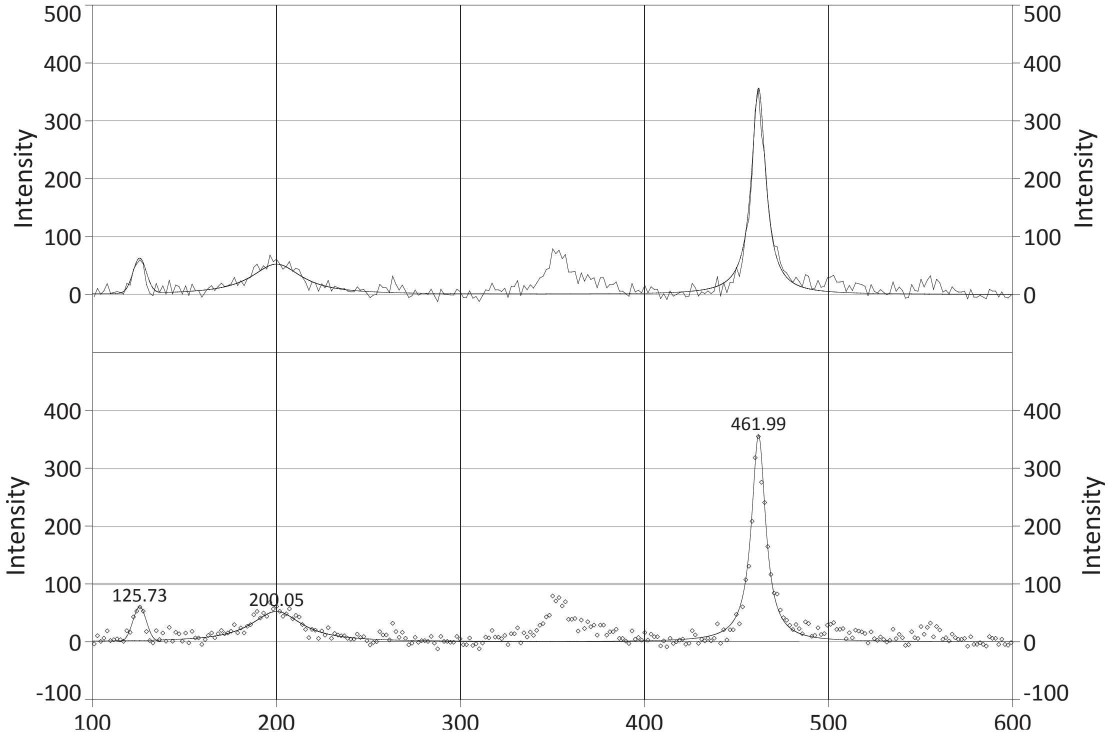
PH 97-62 - Garnet 6

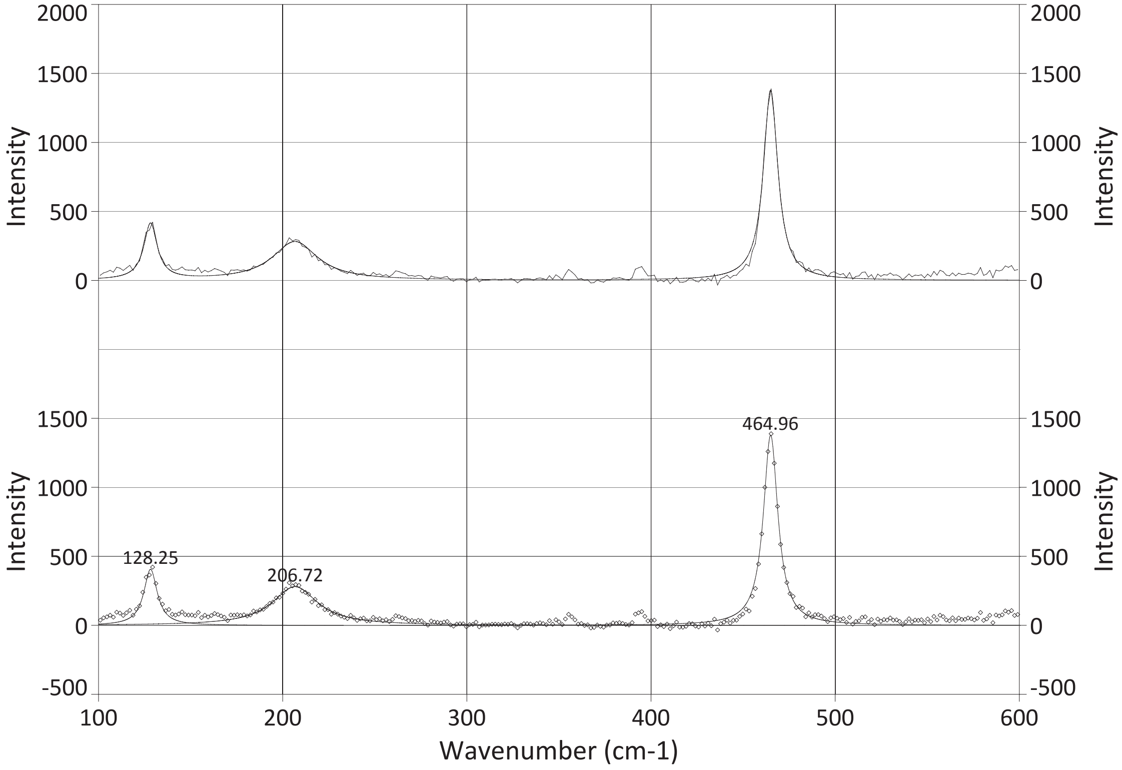
Quartz Standard

PH 97-62

Garnet 7

Locality: Purdy Hill
Collected by Susan Anderson

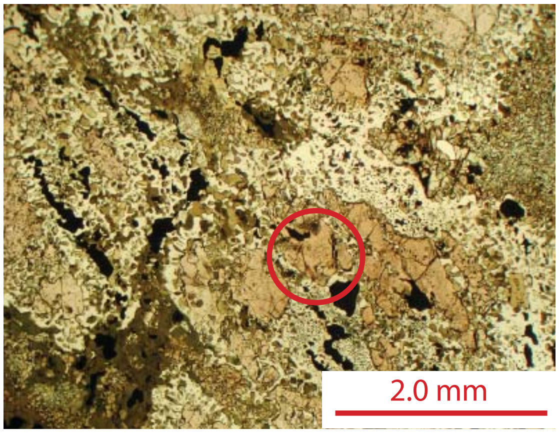

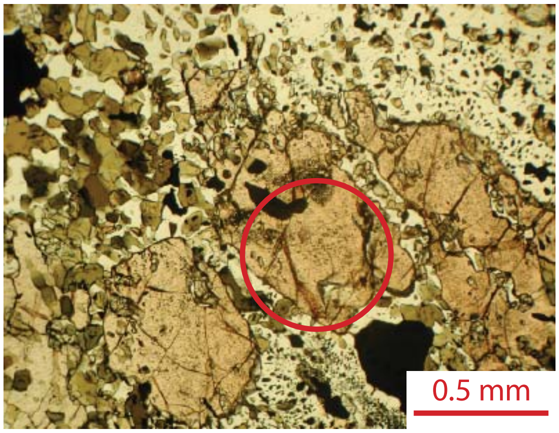

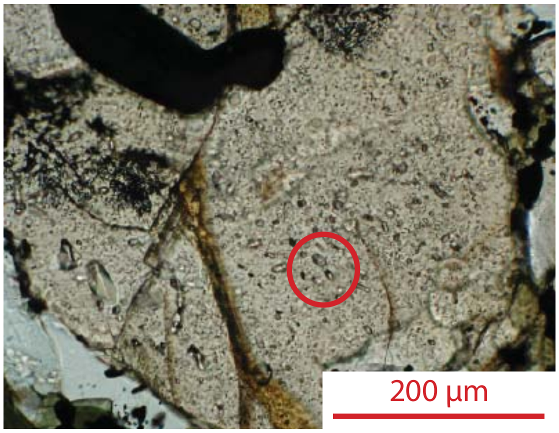

Inclusion Information

Maximum length (X-Y) (µm)	15.8
Minimum length (X-Y) (µm)	11.1
Inclusion thickness (Z) (µm)	12
Location (X-Y coordinates)	(104.6, 5.8)
Description of shape	Ellipsoid
Garnet composition	$Alm_{62.3}$, $Prp_{15.8}$, $Grs_{21.2}$, $Sps_{0.6}$

Data and Pressure Calculation Results

Depth of spectrum (µm)	-10
$\Delta\omega_1$ (cm^{-1})	-6.91
$\Delta\omega_2$ (cm^{-1})	-7.40
$P_{resid\ [\Delta\omega 1]}$ (GPa)	-0.520
$P_{resid\ [\Delta\omega 2]}$ (GPa)	-0.356
$P_{entrap\ [\Delta\omega 1]}$ (GPa)	-0.90
$P_{entrap\ [\Delta\omega 2]}$ (GPa)	-0.49

PH 97-62 - Garnet 7

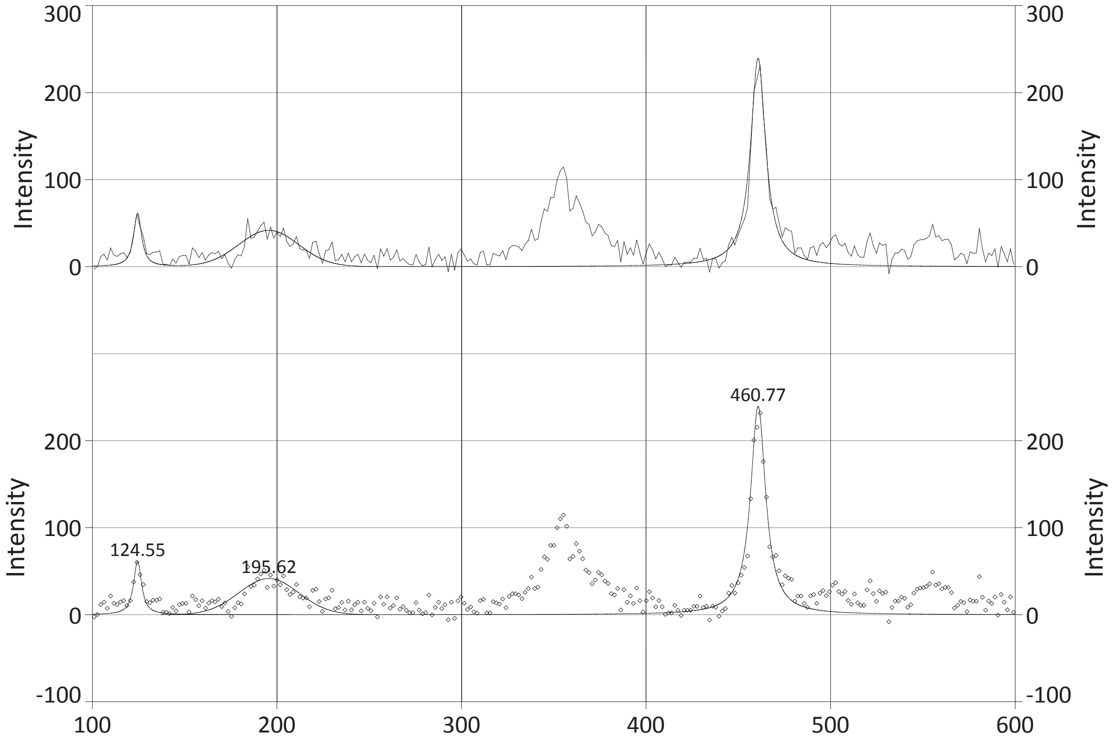

Quartz Standard

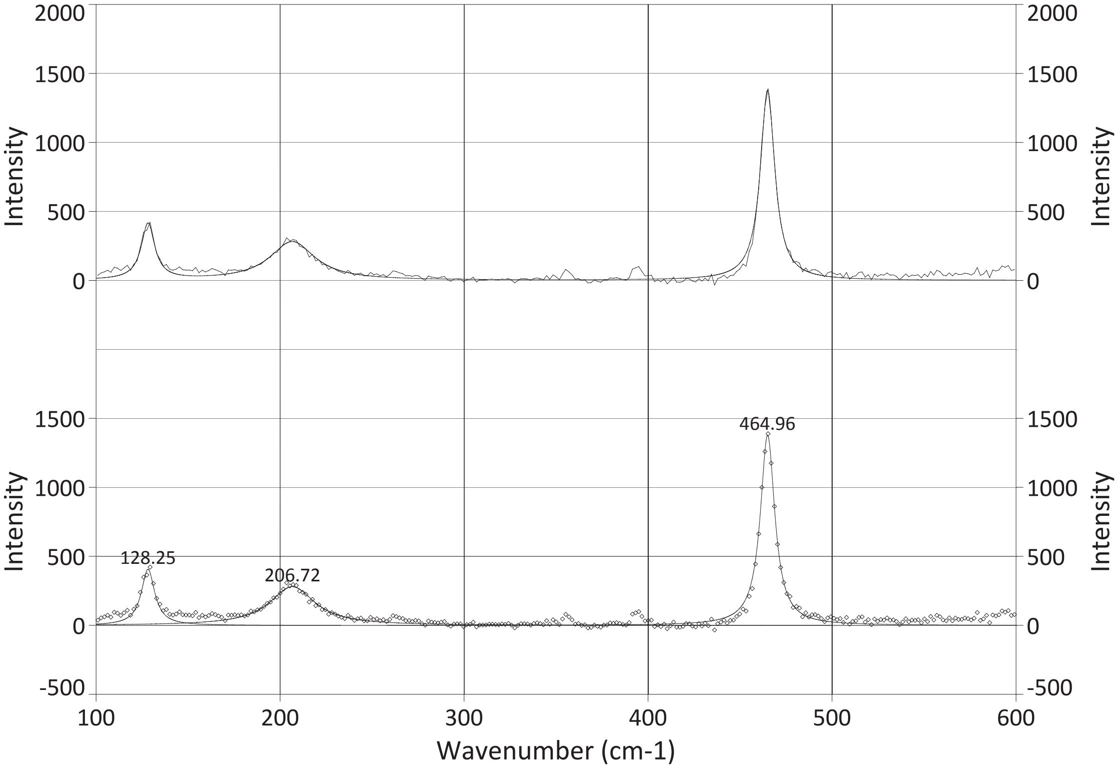

PH 97-63b

Garnet 1

Locality: Purdy Hill
Collected by Susan Anderson

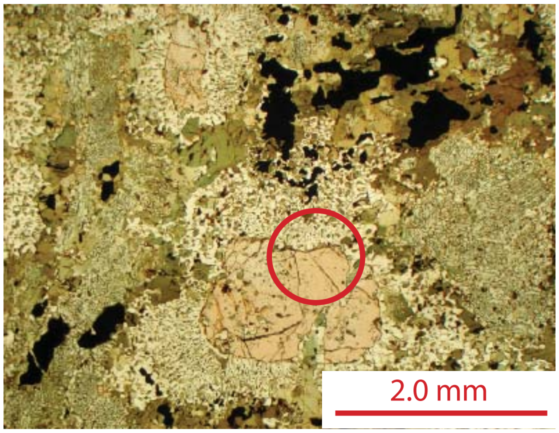

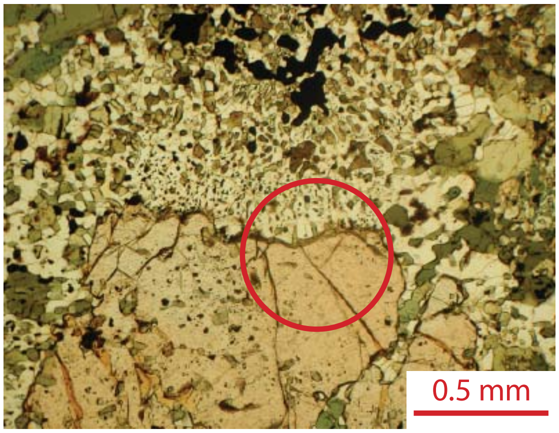

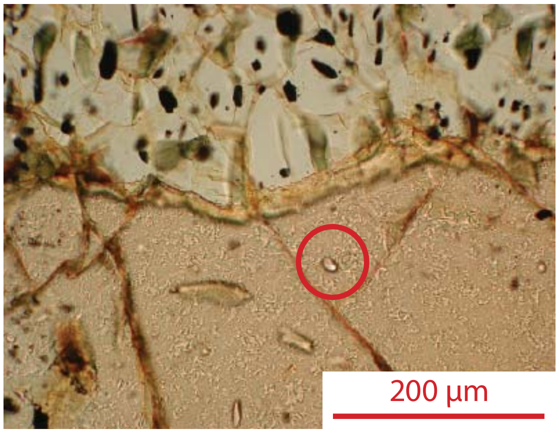

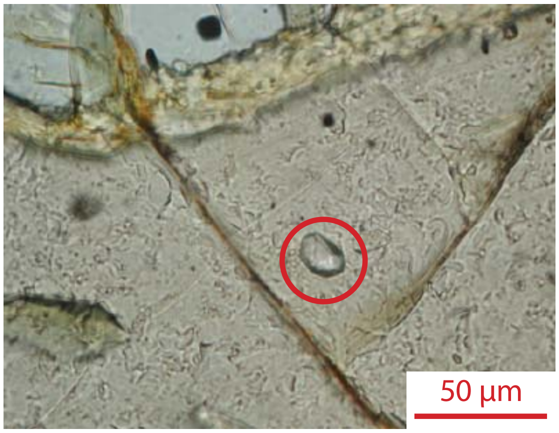

Inclusion Information

Maximum length (X-Y) (μm)	20.5
Minimum length (X-Y) (μm)	12.6
Inclusion thickness (Z) (μm)	11
Location (X-Y coordinates)	(101.0, 1.0)
Description of shape	Ellipsoid
Garnet composition	$\text{Alm}_{62.3}$, $\text{Prp}_{15.8}$, $\text{Grs}_{21.2}$, $\text{Sps}_{0.6}$

Data and Pressure Calculation Results

Depth of spectrum (μm)	-8
$\Delta\omega_1$ (cm^{-1})	0.42
$\Delta\omega_2$ (cm^{-1})	1.39
$P_{\text{resid }[\Delta\omega1]}$ (GPa)	0.026
$P_{\text{resid }[\Delta\omega2]}$ (GPa)	0.069
$P_{\text{entrap }[\Delta\omega1]}$ (GPa)	0.46
$P_{\text{entrap }[\Delta\omega2]}$ (GPa)	0.57

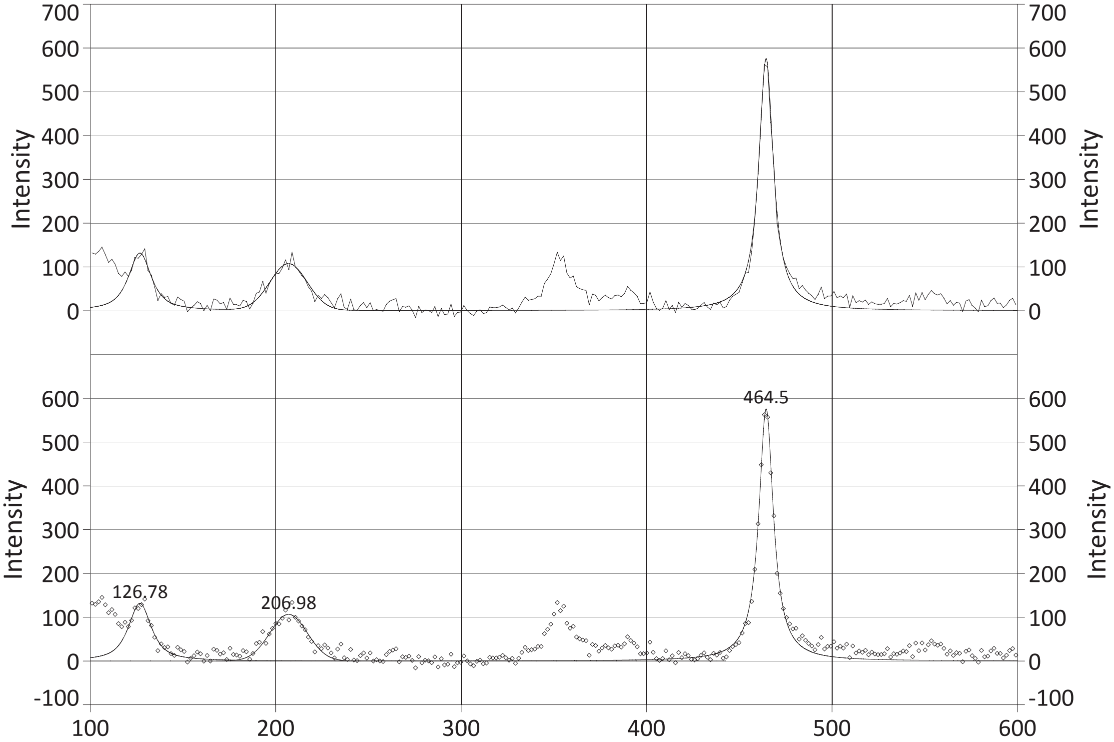

PH 97-63b - Garnet 1

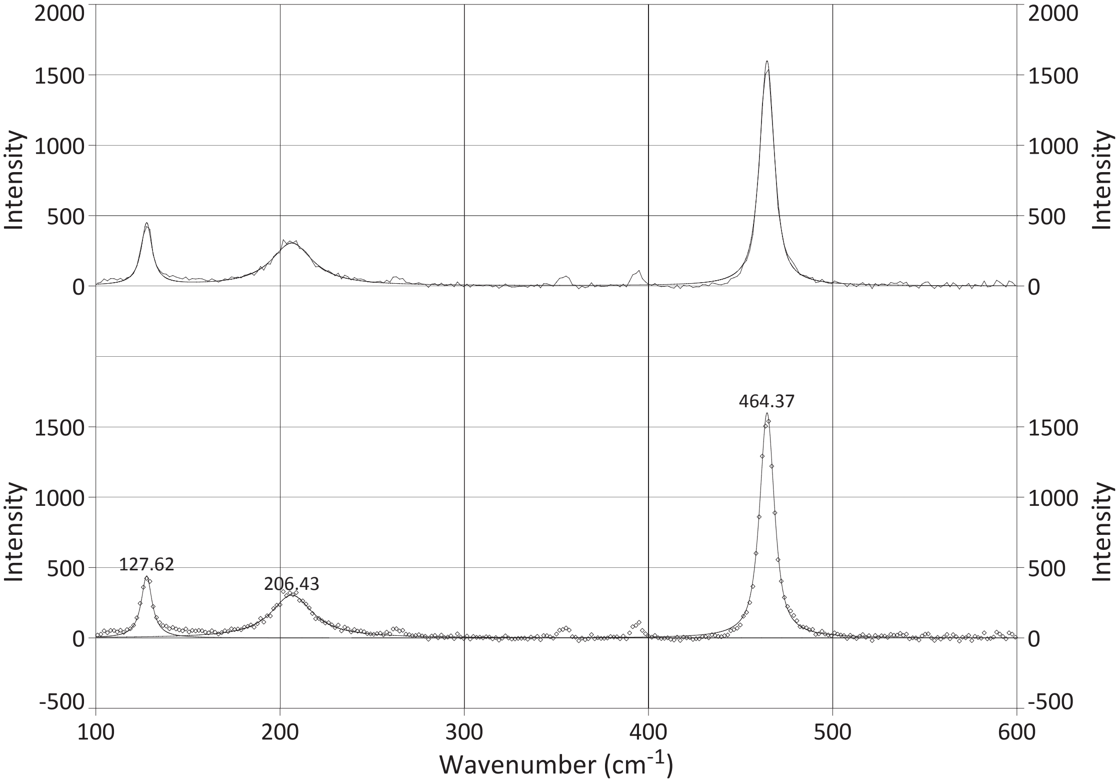

Quartz Standard

PH 97-63b

Garnet 2

Locality: Purdy Hill
Collected by Susan Anderson

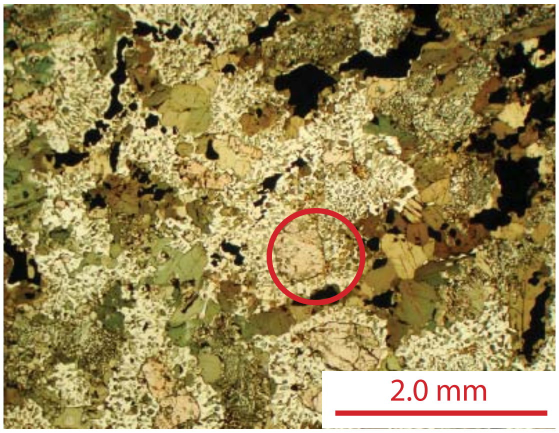

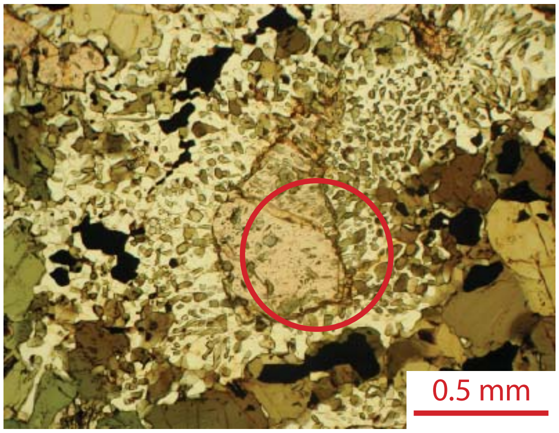

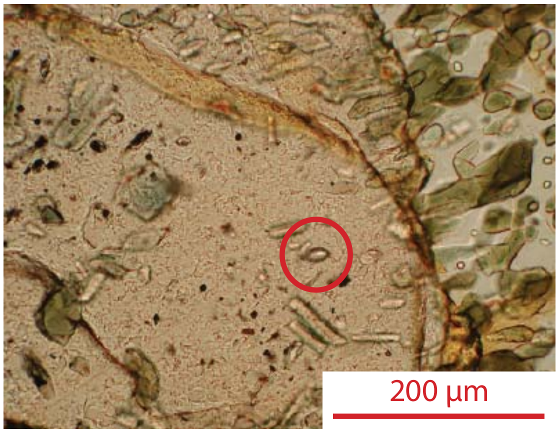

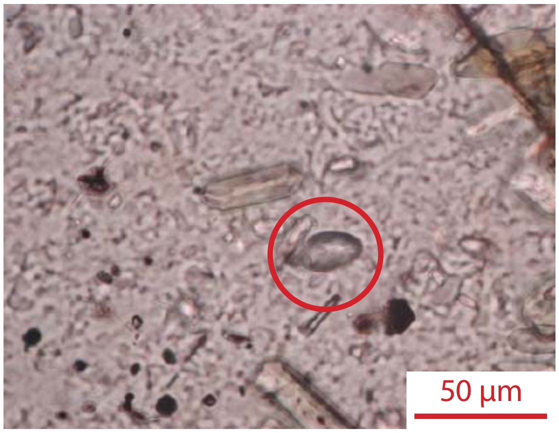

Inclusion Information

Maximum length (X-Y) (µm)	23.7
Minimum length (X-Y) (µm)	14.2
Inclusion thickness (Z) (µm)	13
Location (X-Y coordinates)	(106.5, 8.8)
Description of shape	Ellipsoid
Garnet composition	$Alm_{62.3}$, $Prp_{15.8}$, $Grs_{21.2}$, $Sps_{0.6}$

Data and Pressure Calculation Results

Depth of spectrum (µm)	-6
$\Delta\omega_1$ (cm^{-1})	-3.59
$\Delta\omega_2$ (cm^{-1})	-3.04
$P_{resid\ [\Delta\omega1]}$ (GPa)	-0.243
$P_{resid\ [\Delta\omega2]}$ (GPa)	-0.147
$P_{entrap\ [\Delta\omega1]}$ (GPa)	-0.21
$P_{entrap\ [\Delta\omega2]}$ (GPa)	0.03

PH 97-63b - Garnet 2

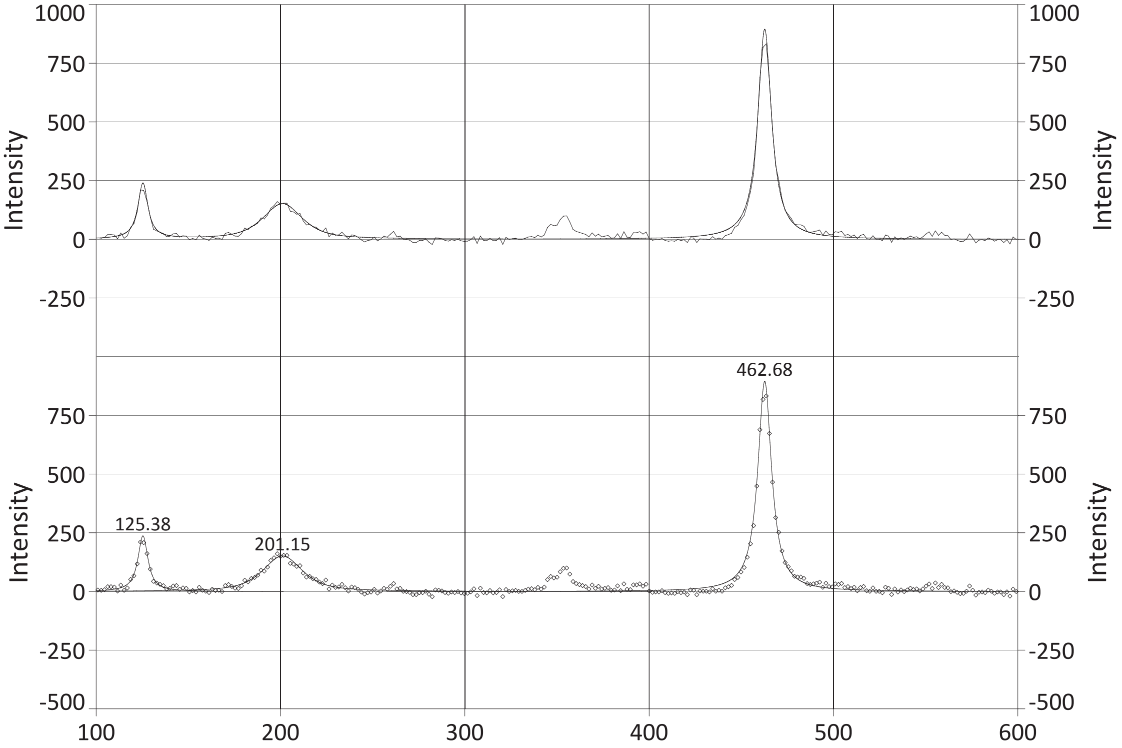

Quartz Standard

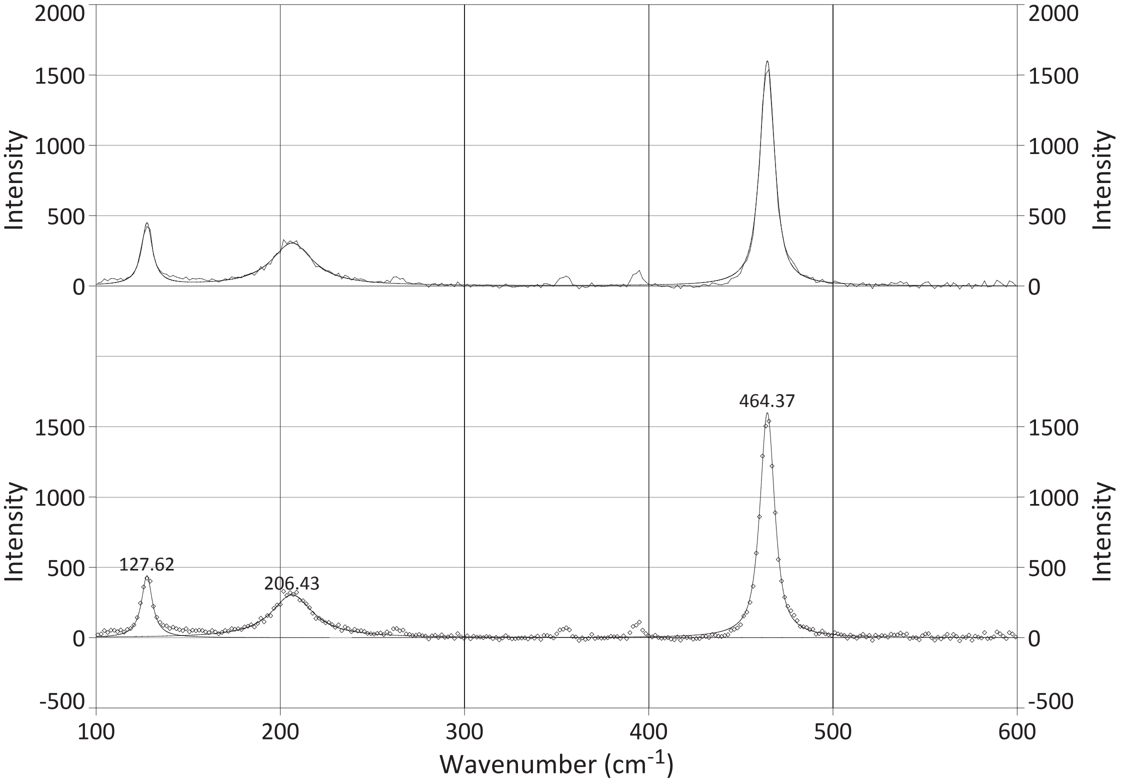

LU 02-6

Garnet E

Locality: Purdy Hill
Collected by William Carlson

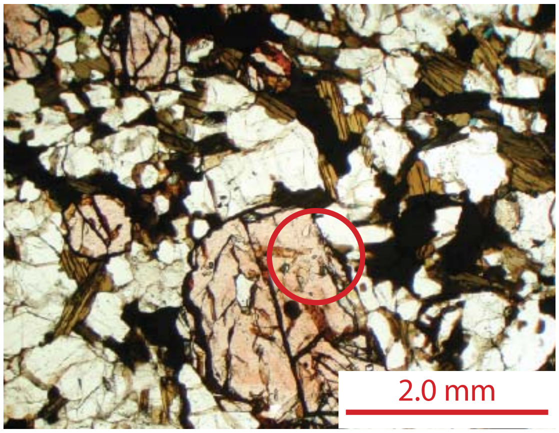

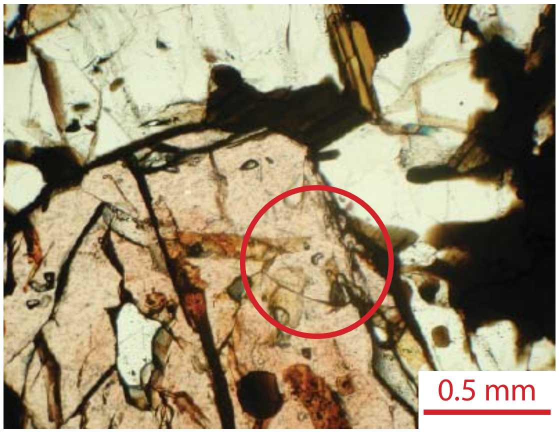

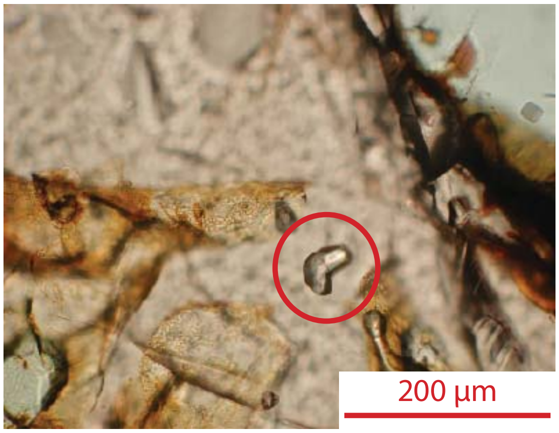

Inclusion Information

Maximum length (X-Y) (µm)	56.9
Minimum length (X-Y) (µm)	30.0
Inclusion thickness (Z) (µm)	33
Location (X-Y coordinates)	-(121.6, 13.2)
Description of shape	Bent, elongate
Garnet composition	$Alm_{79.6}$, $Prp_{12.8}$, $Grs_{4.0}$, $Sps_{3.6}$

Data and Pressure Calculation Results

Depth of spectrum (µm)	-8
$\Delta\omega_1$ (cm^{-1})	-2.72
$\Delta\omega_2$ (cm^{-1})	-2.86
$P_{resid\ [\Delta\omega1]}$ (GPa)	-0.180
$P_{resid\ [\Delta\omega2]}$ (GPa)	-0.139
$P_{entrap\ [\Delta\omega1]}$ (GPa)	-0.04
$P_{entrap\ [\Delta\omega2]}$ (GPa)	0.06

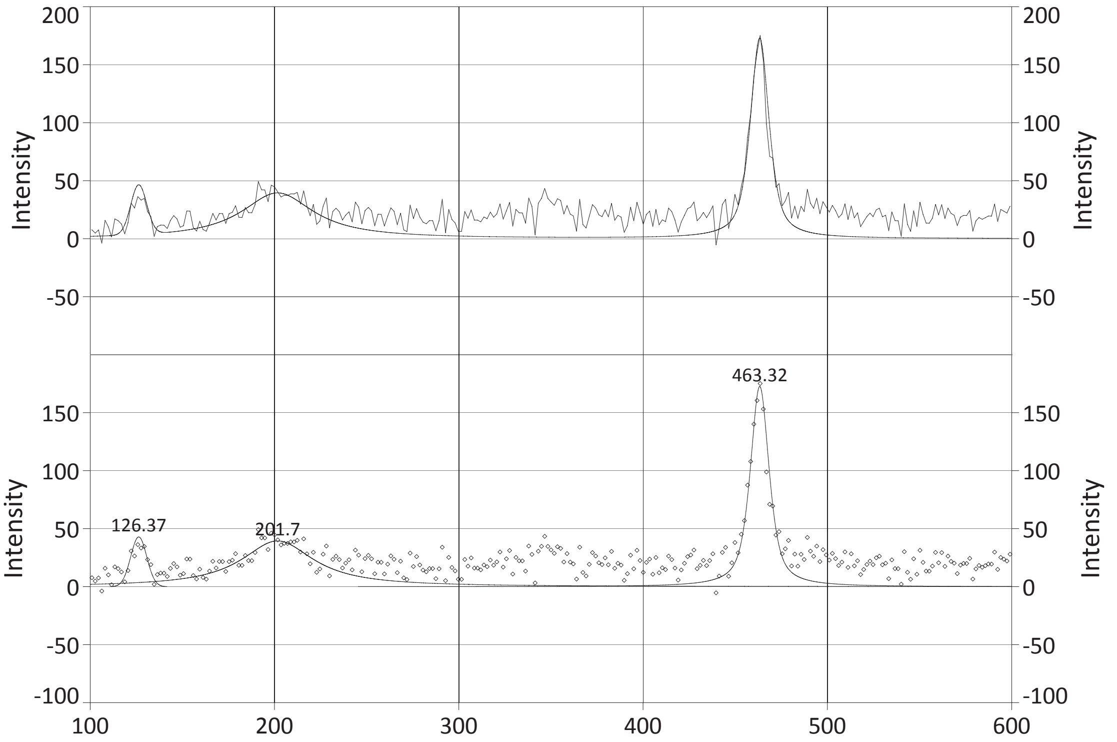
LU 02-6 - Garnet E

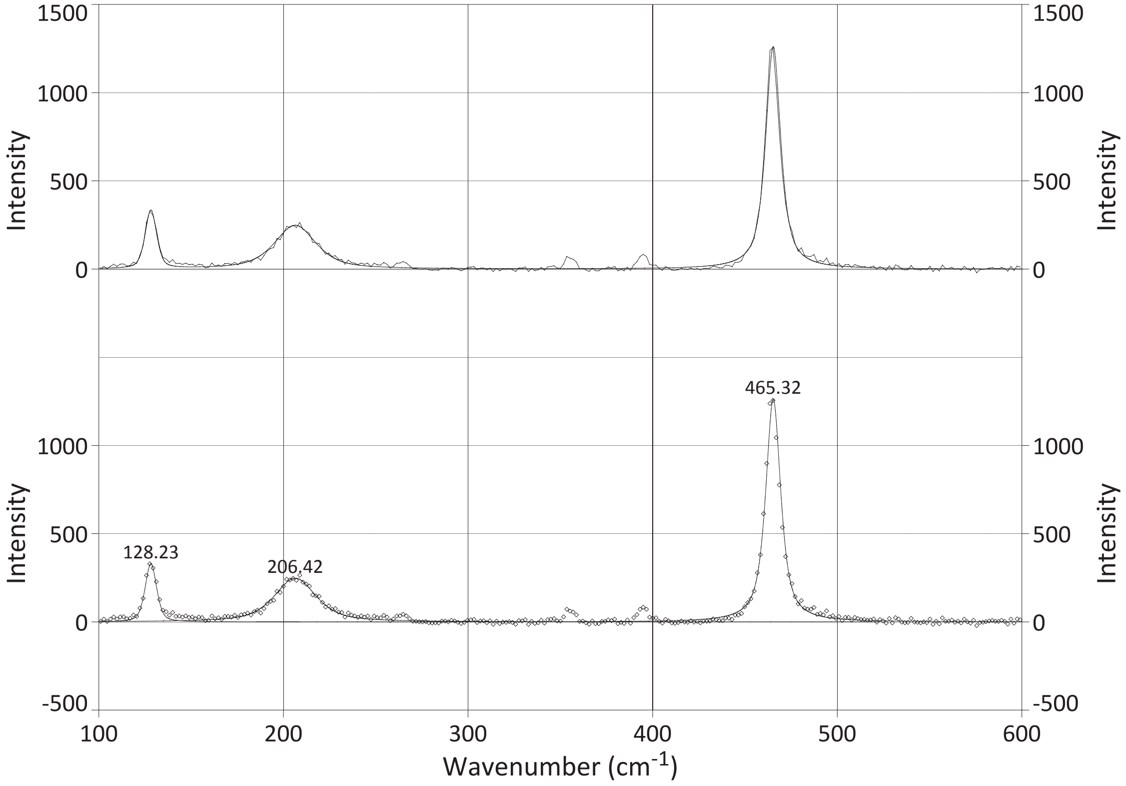
Quartz Standard

LU 02-6

Garnet G

Locality: Purdy Hill
Collected by William Carlson

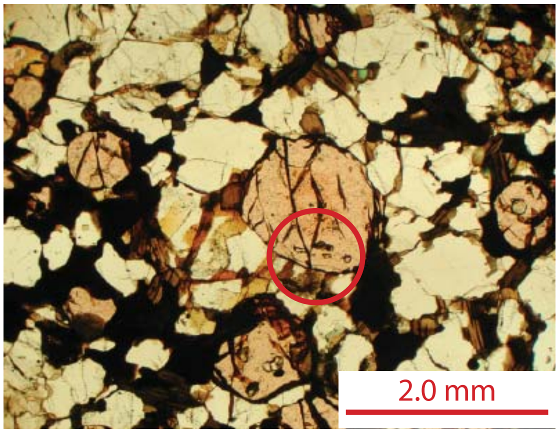

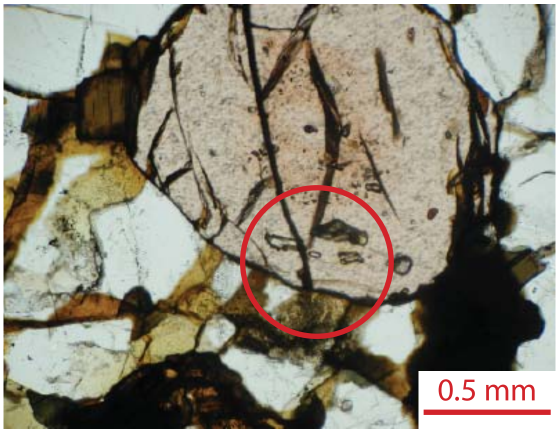

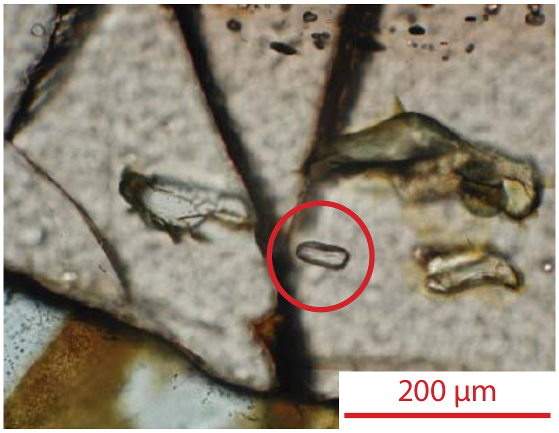

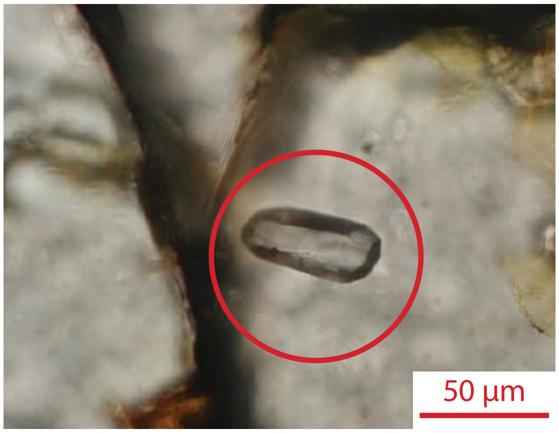

Inclusion Information

Maximum length (X-Y) (μm)	53.72
Minimum length (X-Y) (μm)	25.3
Inclusion thickness (Z) (μm)	22
Location (X-Y coordinates)	-(119.6, 3.9)
Description of shape	Elongate
Garnet composition	$Alm_{79.6}$, $Prp_{12.8}$, $Grs_{4.0}$, $Sps_{3.6}$

Data and Pressure Calculation Results

Depth of spectrum (μm)	-10
$\Delta\omega_1$ (cm^{-1})	1.52
$\Delta\omega_2$ (cm^{-1})	0.99
$P_{resid\ [\Delta\omega1]}$ (GPa)	0.092
$P_{resid\ [\Delta\omega2]}$ (GPa)	0.049
$P_{entrap\ [\Delta\omega1]}$ (GPa)	0.63
$P_{entrap\ [\Delta\omega2]}$ (GPa)	0.53

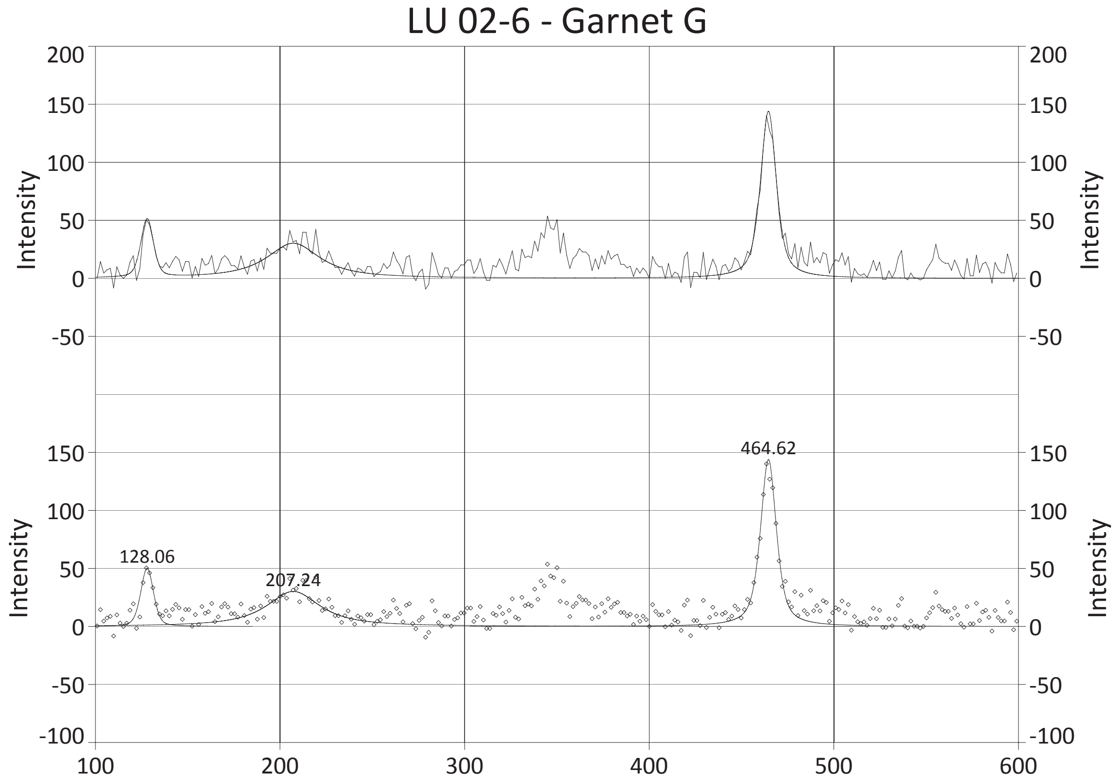
LU 02-6 - Garnet G
Intensity
200
150
100
50
0
-50
-100
128.06
207.24
464.62
100
200
300
400
500
600

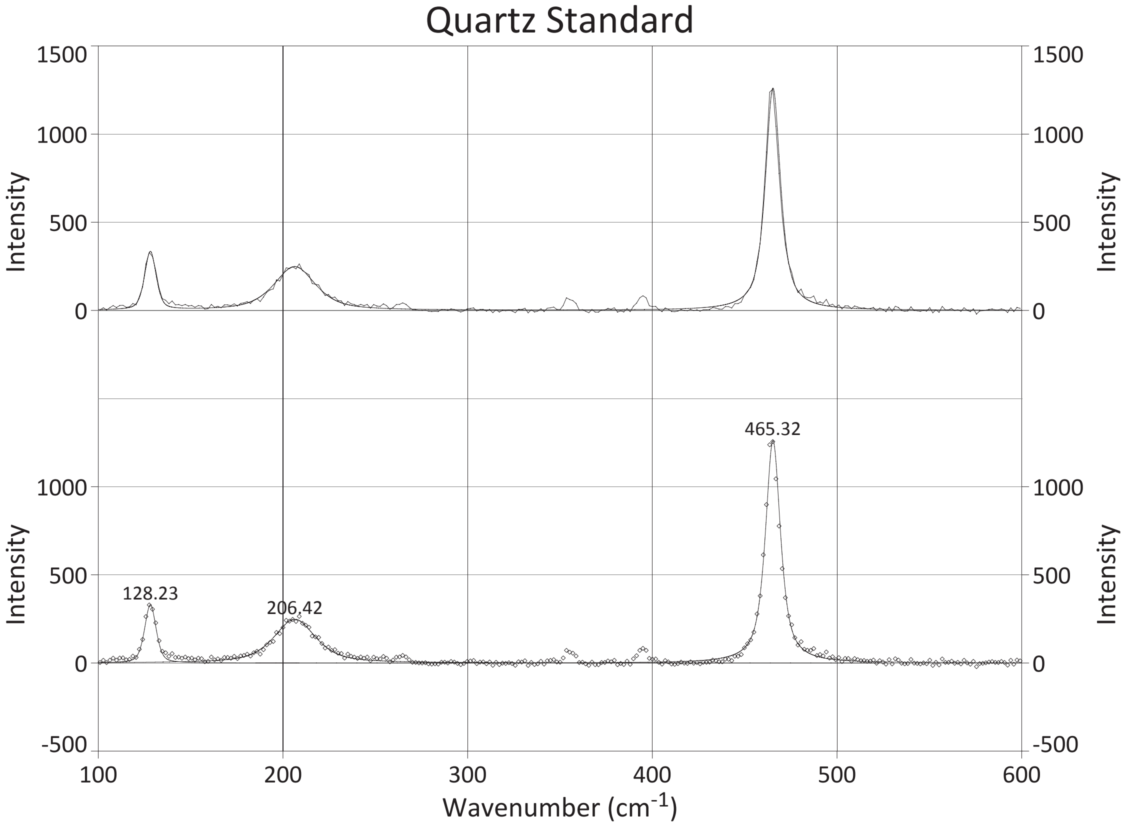
Quartz Standard
Intensity
1500
1000
500
0
-500
128.23
206.42
465.32
100
200
300
400
500
600
Wavenumber (cm-1)

LU 02-6

Garnet J

Locality: Purdy Hill
Collected by William Carlson

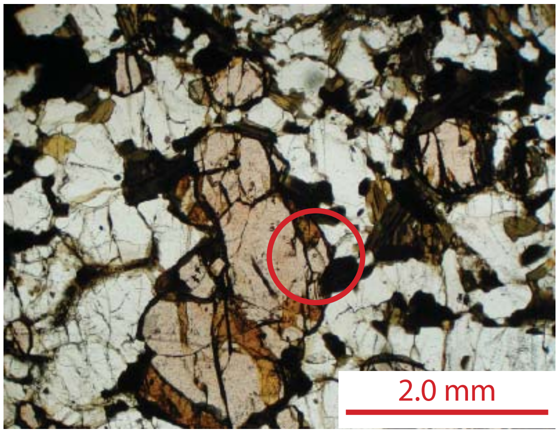

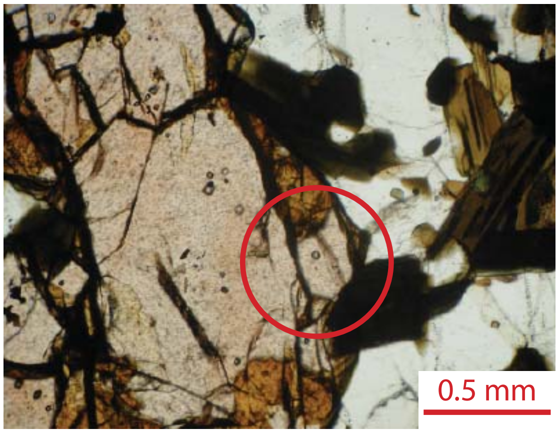

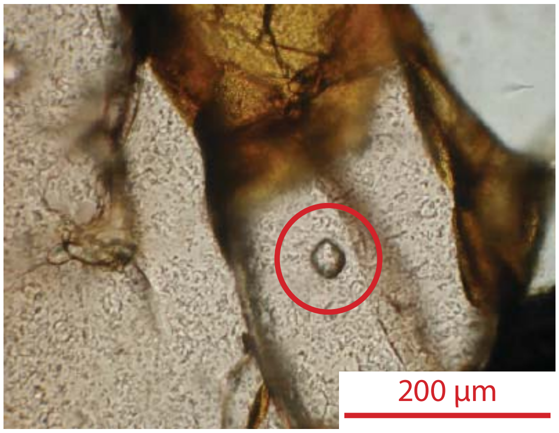

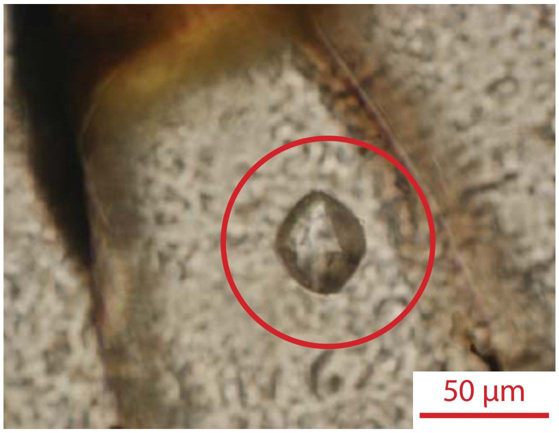

Inclusion Information

Maximum length (X-Y) (µm)	41.1
Minimum length (X-Y) (µm)	36.3
Inclusion thickness (Z) (µm)	29
Location (X-Y coordinates)	(108.7, 17.1)
Description of shape	Rounded
Garnet composition	$\mathrm{Alm}_{79.6}$, $\mathrm{Prp}_{12.8}$, $\mathrm{Grs}_{4.0}$, $\mathrm{Sps}_{3.6}$

Data and Pressure Calculation Results

Depth of spectrum (µm)	-22
$\Delta\omega_1$ (cm^{-1})	-3.42
$\Delta\omega_2$ (cm^{-1})	-6.54
$P_{\mathrm{resid}\ [\Delta\omega1]}$ (GPa)	-0.230
$P_{\mathrm{resid}\ [\Delta\omega2]}$ (GPa)	-0.315
$P_{\mathrm{entrap}\ [\Delta\omega1]}$ (GPa)	-0.17
$P_{\mathrm{entrap}\ [\Delta\omega2]}$ (GPa)	-0.38

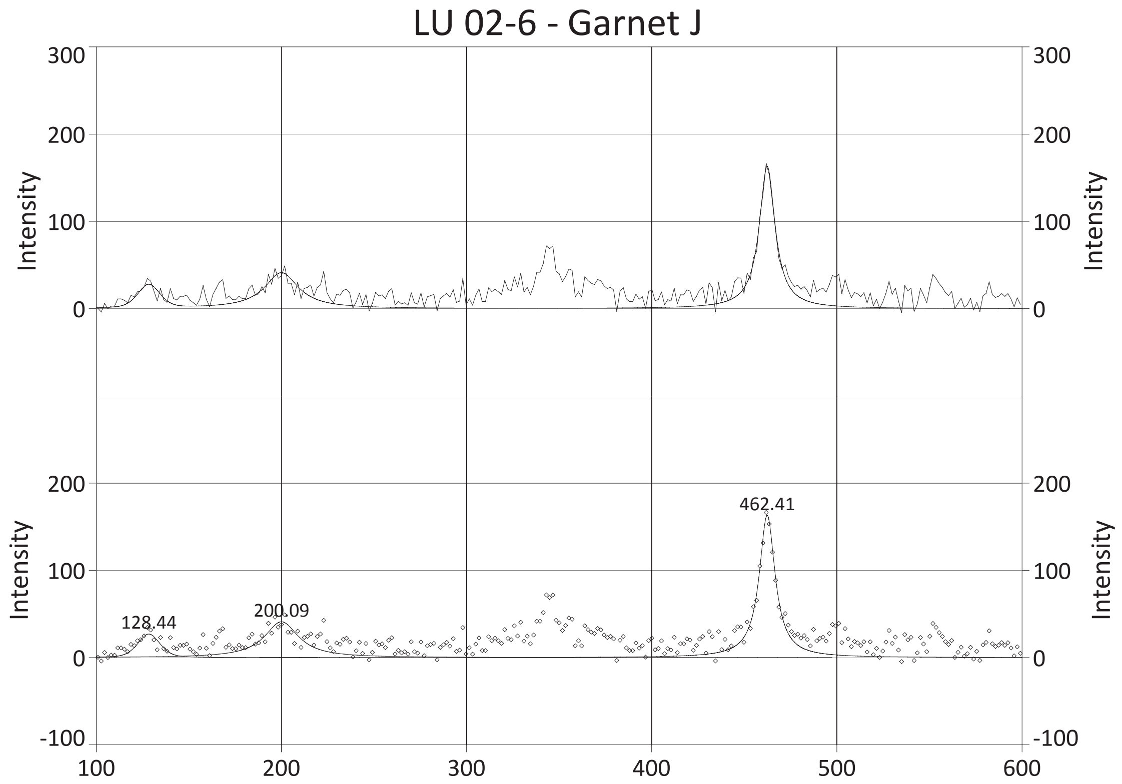
LU 02-6 - Garnet J
Intensity
300
200
100
0
-100
128.44
200.09
462.41
100
200
300
400
500
600

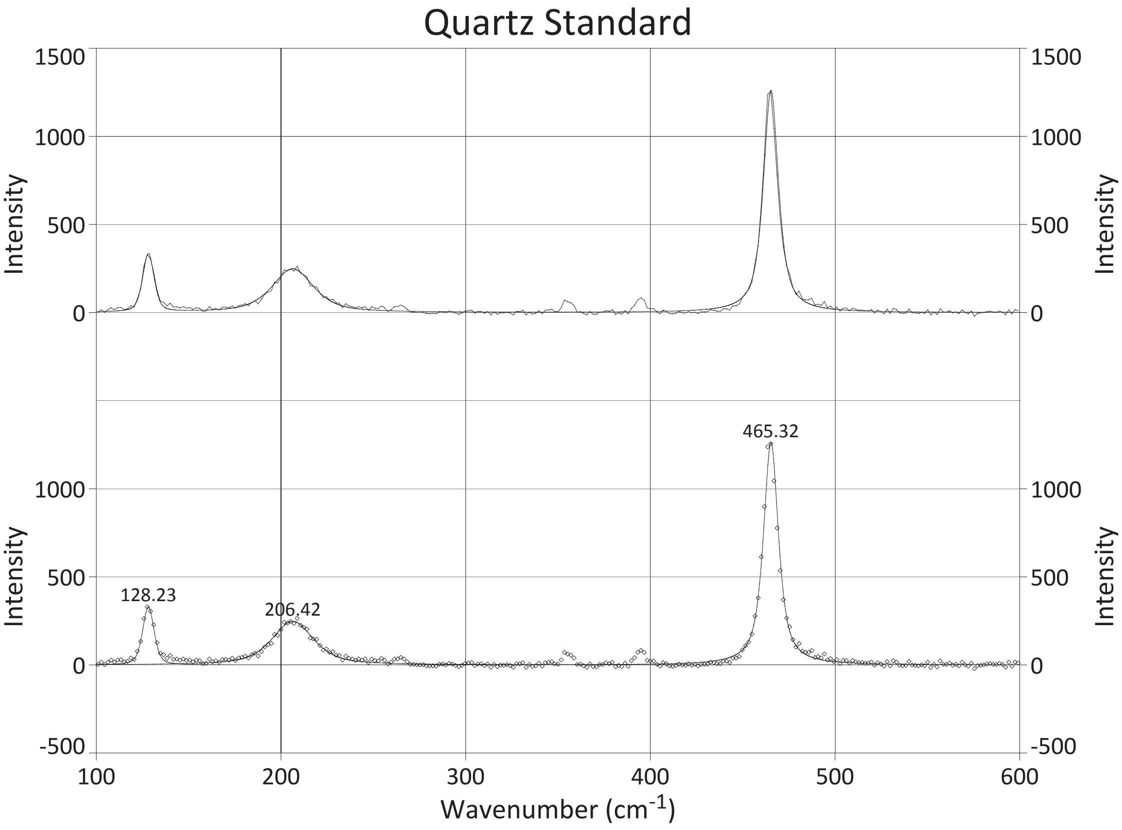
Quartz Standard
Intensity
1500
1000
500
0
-500
128.23
206.42
465.32
100
200
300
400
500
600
Wavenumber (cm-1)

LU 02-6

Garnet K

Locality: Purdy Hill
Collected by William Carlson

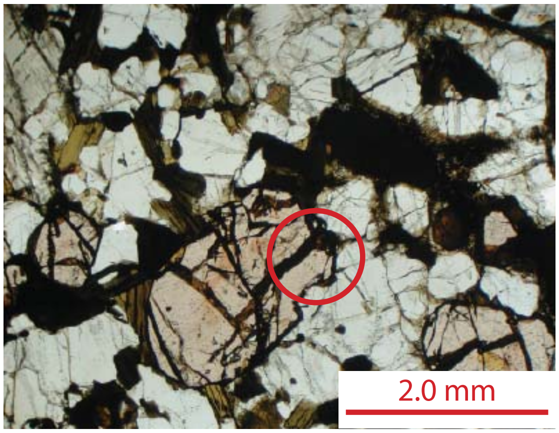

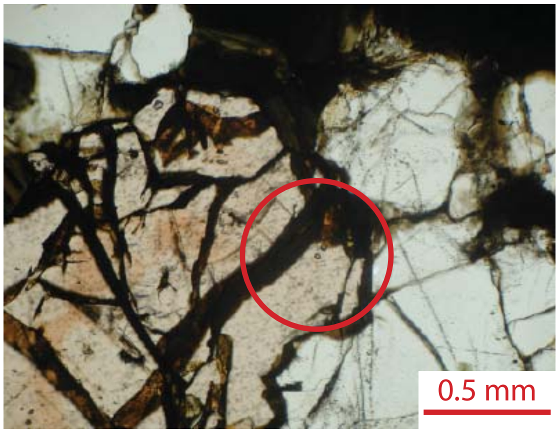

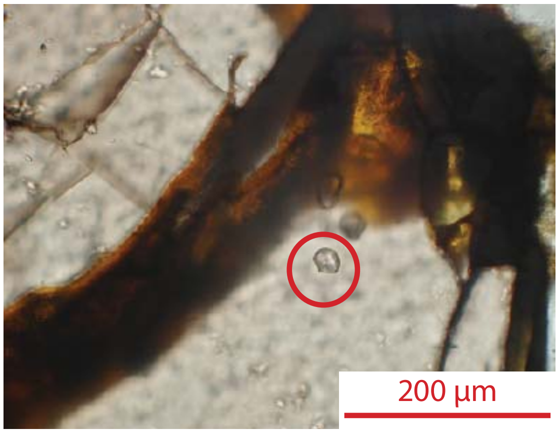

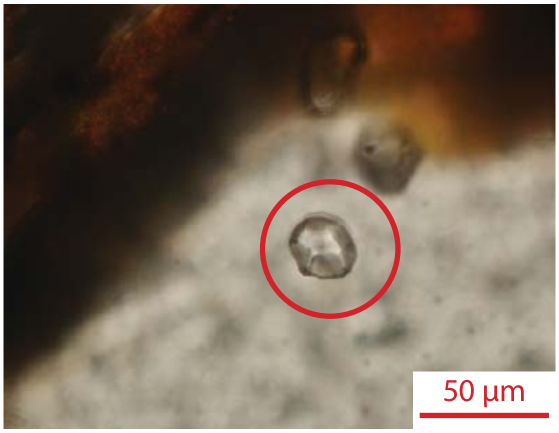

Inclusion Information

Maximum length (X-Y) (µm)	28.4
Minimum length (X-Y) (µm)	23.7
Inclusion thickness (Z) (µm)	25
Location (X-Y coordinates)	(117.1, 16.3)
Description of shape	Spherical
Garnet composition	$Alm_{79.6}$, $Prp_{12.9}$, $Grs_{3.9}$, $Sps_{3.5}$

Data and Pressure Calculation Results

Depth of spectrum (µm)	-8
$\Delta\omega_1$ (cm^{-1})	-0.01
$\Delta\omega_2$ (cm^{-1})	0.08
$P_{resid\ [\Delta\omega1]}$ (GPa)	-0.001
$P_{resid\ [\Delta\omega2]}$ (GPa)	0.004
$P_{entrap\ [\Delta\omega1]}$ (GPa)	0.40
$P_{entrap\ [\Delta\omega2]}$ (GPa)	0.41

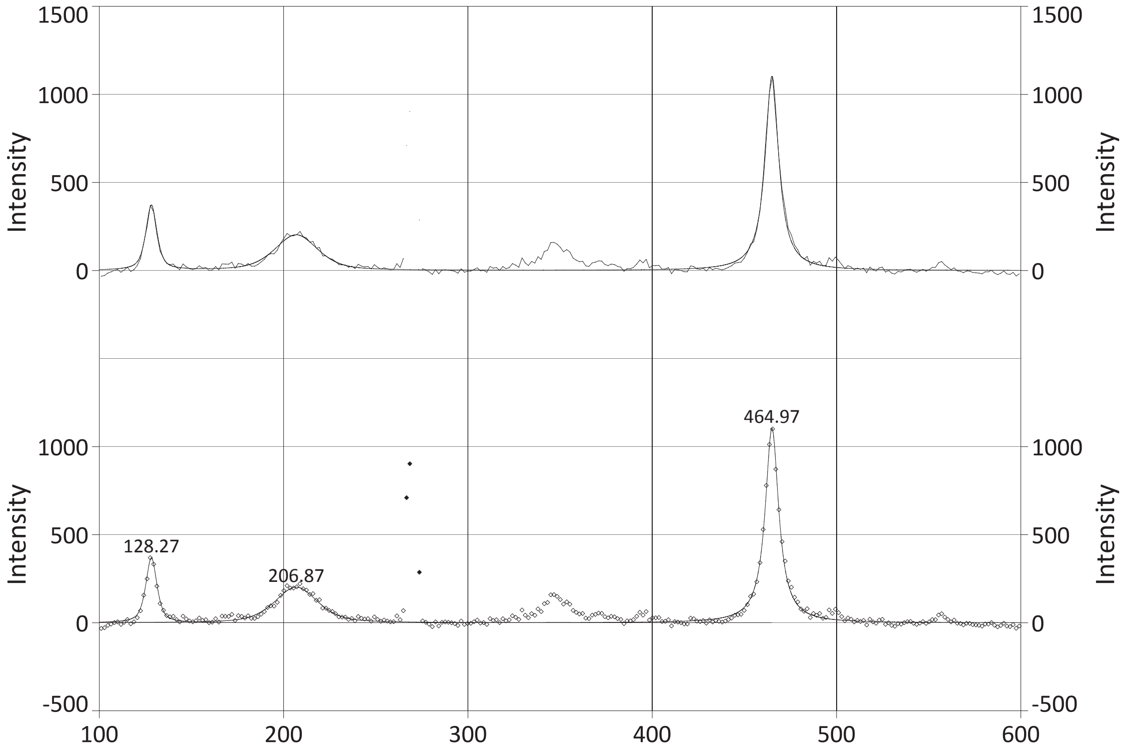

LU 02-6 - Garnet K

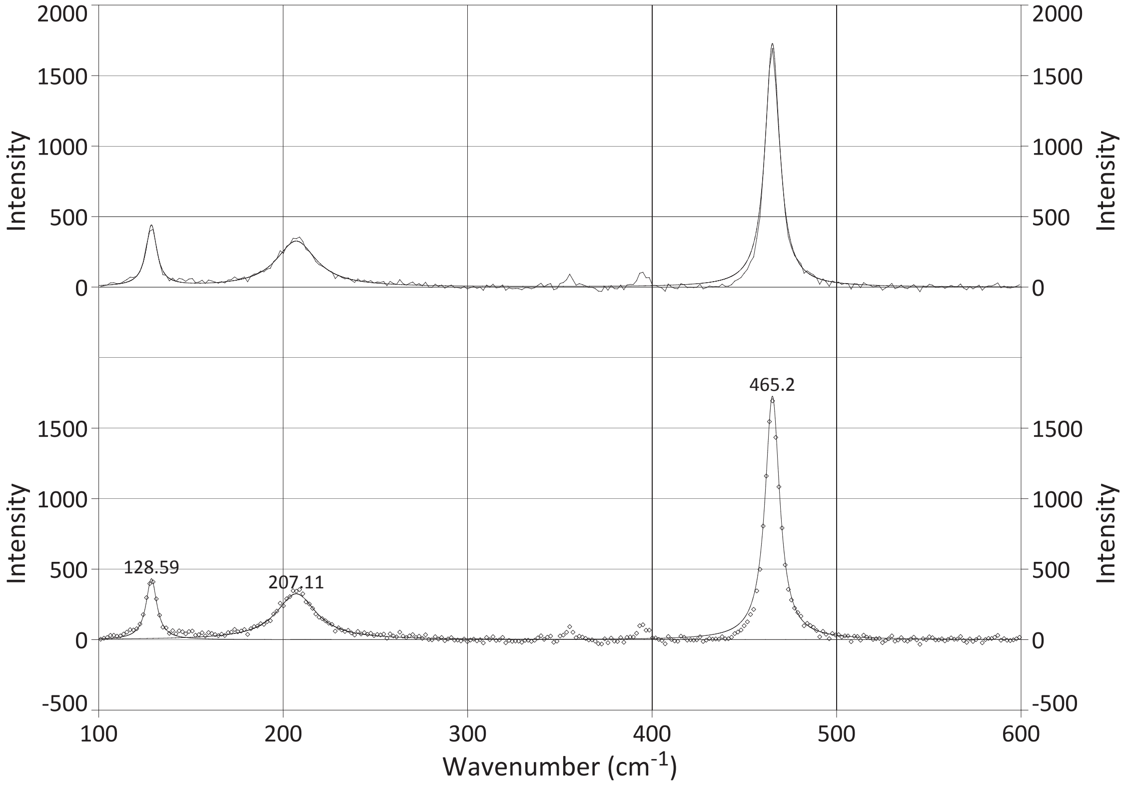

Quartz Standard

LU 02-6

Garnet X

Locality: Purdy Hill
Collected by William Carlson

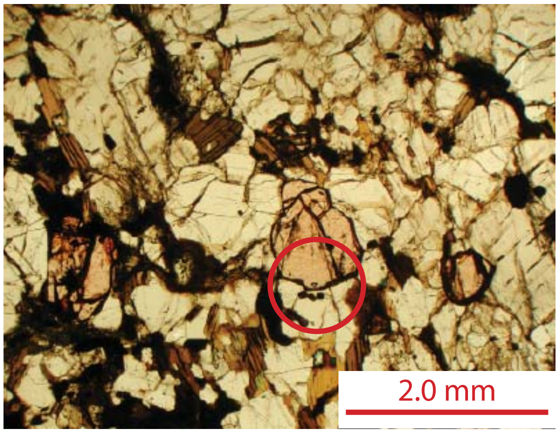

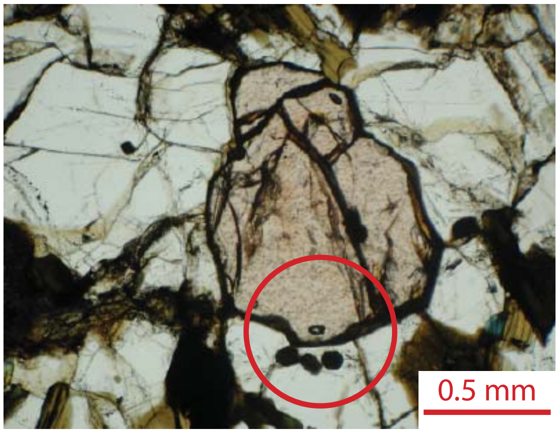

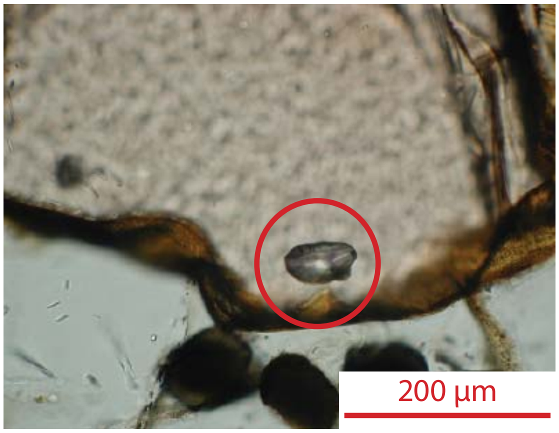

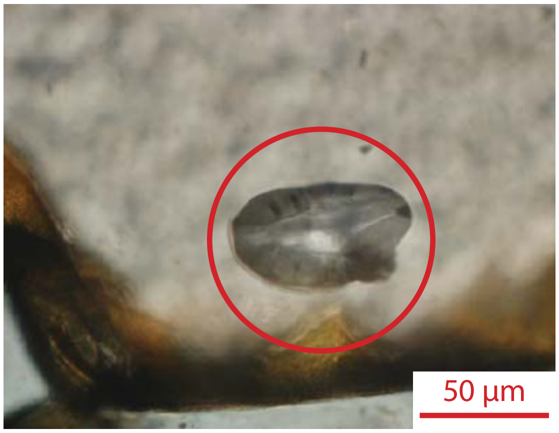

Inclusion Information

Maximum length (X-Y) (µm)	71.1
Minimum length (X-Y) (µm)	39.5
Inclusion thickness (Z) (µm)	39
Location (X-Y coordinates)	(112.4, 14.2)
Description of shape	Ellipsoid
Garnet composition	$Alm_{79.6}$, $Prp_{12.8}$, $Grs_{4.0}$, $Sps_{3.6}$

Data and Pressure Calculation Results

Depth of spectrum (µm)	-15
$\Delta\omega_1$ (cm^{-1})	-3.02
$\Delta\omega_2$ (cm^{-1})	-2.43
$P_{resid\ [\Delta\omega1]}$ (GPa)	-0.201
$P_{resid\ [\Delta\omega2]}$ (GPa)	-0.118
$P_{entrap\ [\Delta\omega1]}$ (GPa)	-0.10
$P_{entrap\ [\Delta\omega2]}$ (GPa)	0.11

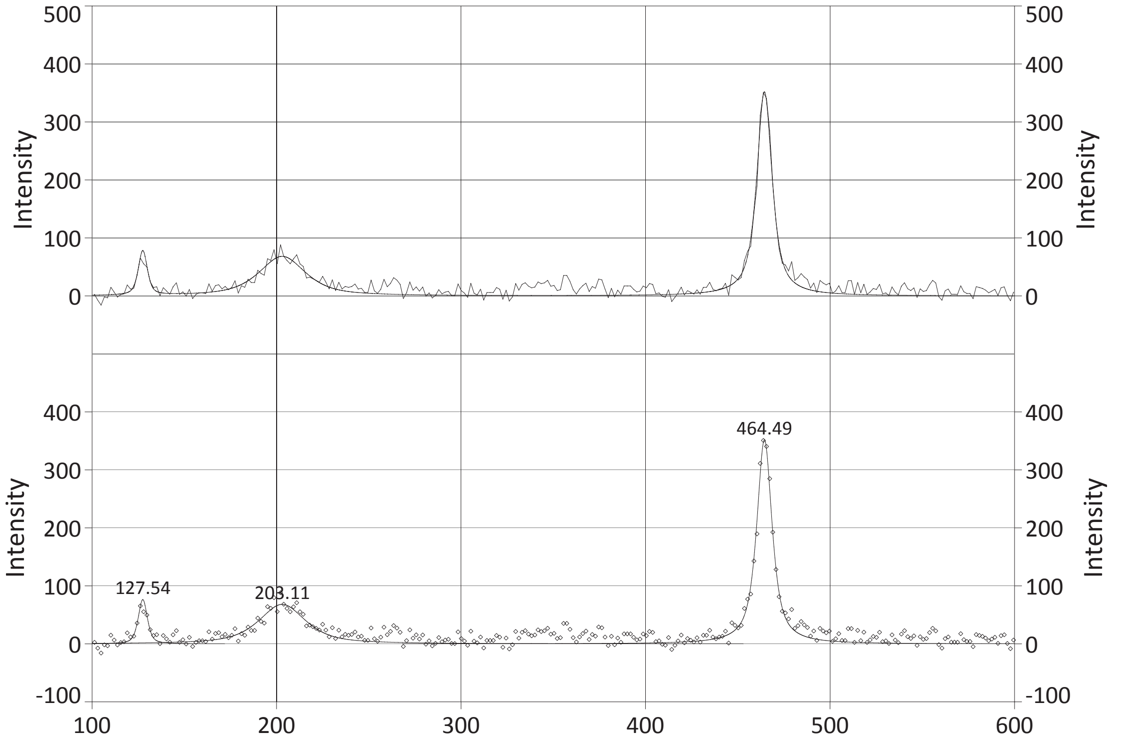

LU 02-6 - Garnet X

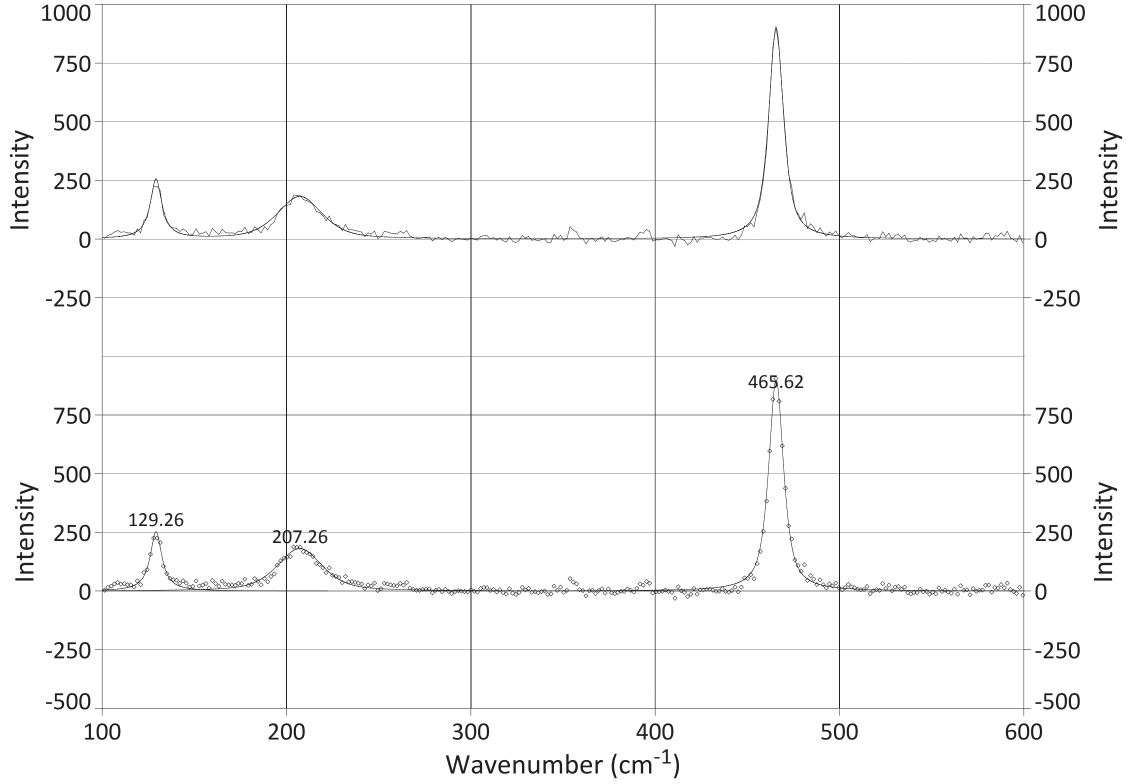

Quartz Standard

LU 02-8

Garnet G

Locality: Purdy Hill
Collected by William Carlson

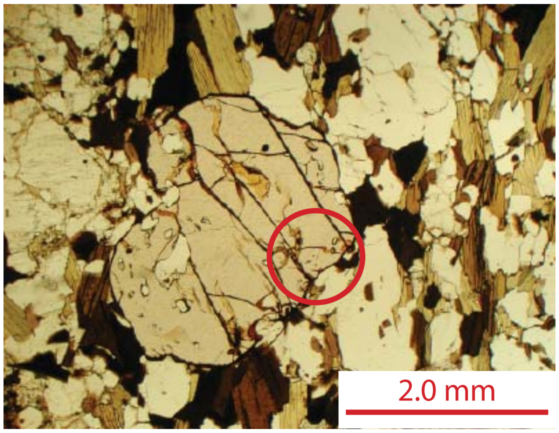

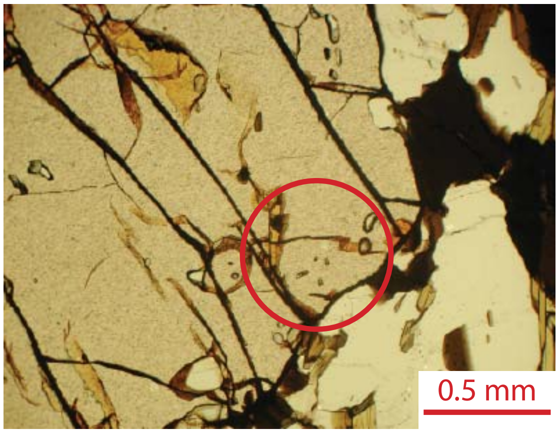

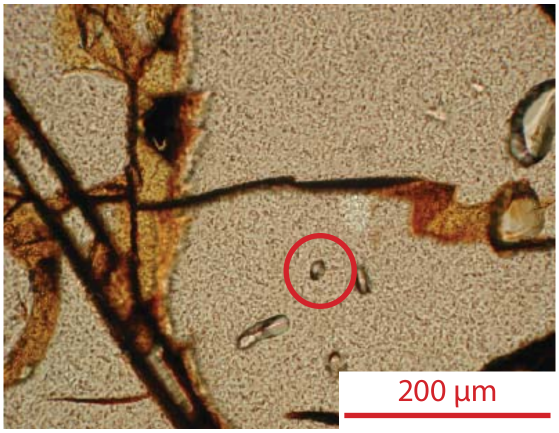

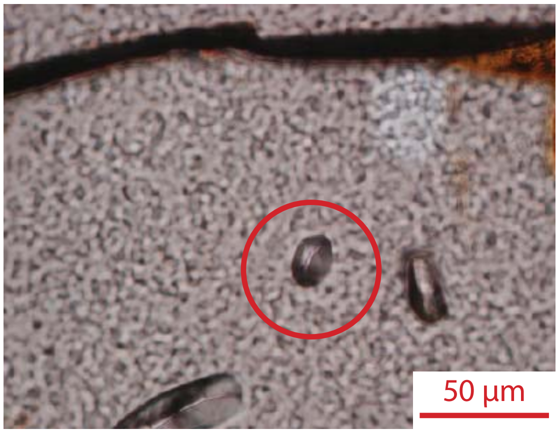

Inclusion Information

Maximum length (X-Y) (µm)	20.5
Minimum length (X-Y) (µm)	15.8
Inclusion thickness (Z) (µm)	13
Location (X-Y coordinates)	(113.3, 9.1)
Description of shape	Ellipsoid
Garnet composition	$Alm_{79.6}$, $Prp_{12.8}$, $Grs_{4.0}$, $Sps_{3.6}$

Data and Pressure Calculation Results

Depth of spectrum (µm)	-12
$\Delta\omega_1$ (cm^{-1})	-8.30
$\Delta\omega_2$ (cm^{-1})	-8.49
$P_{resid\ [\Delta\omega1]}$ (GPa)	-0.656
$P_{resid\ [\Delta\omega2]}$ (GPa)	-0.408
$P_{entrap\ [\Delta\omega1]}$ (GPa)	-1.23
$P_{entrap\ [\Delta\omega2]}$ (GPa)	-0.61

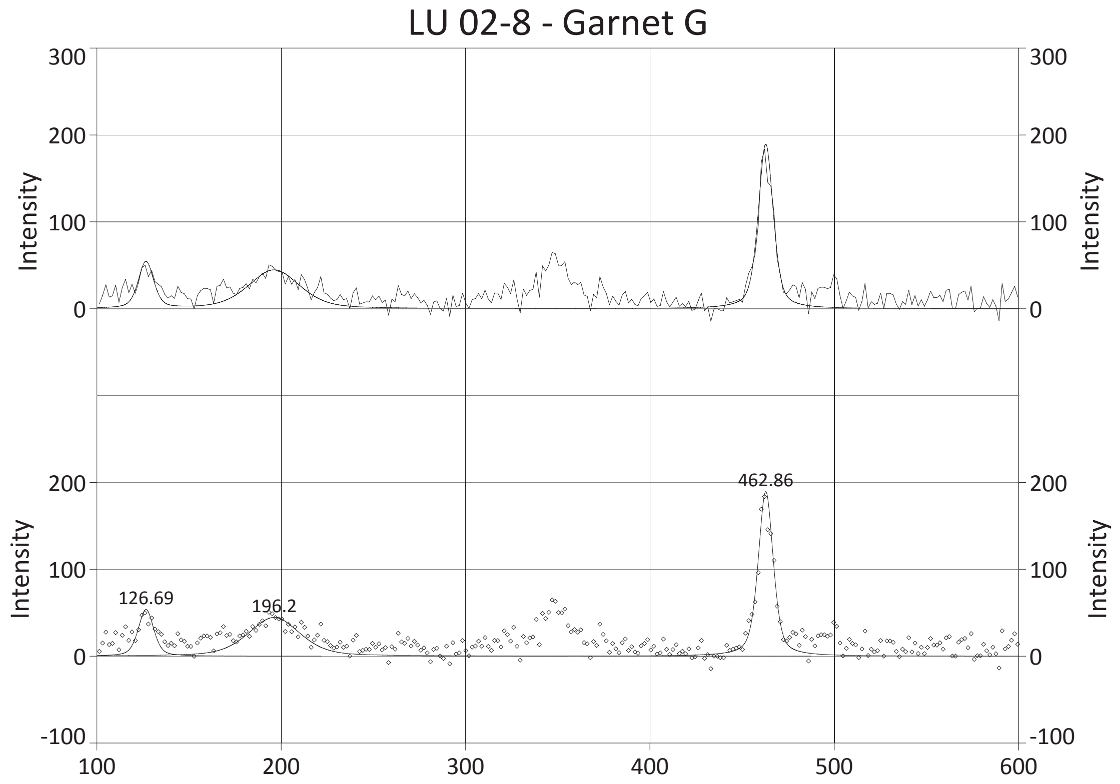

LU 02-8 - Garnet G

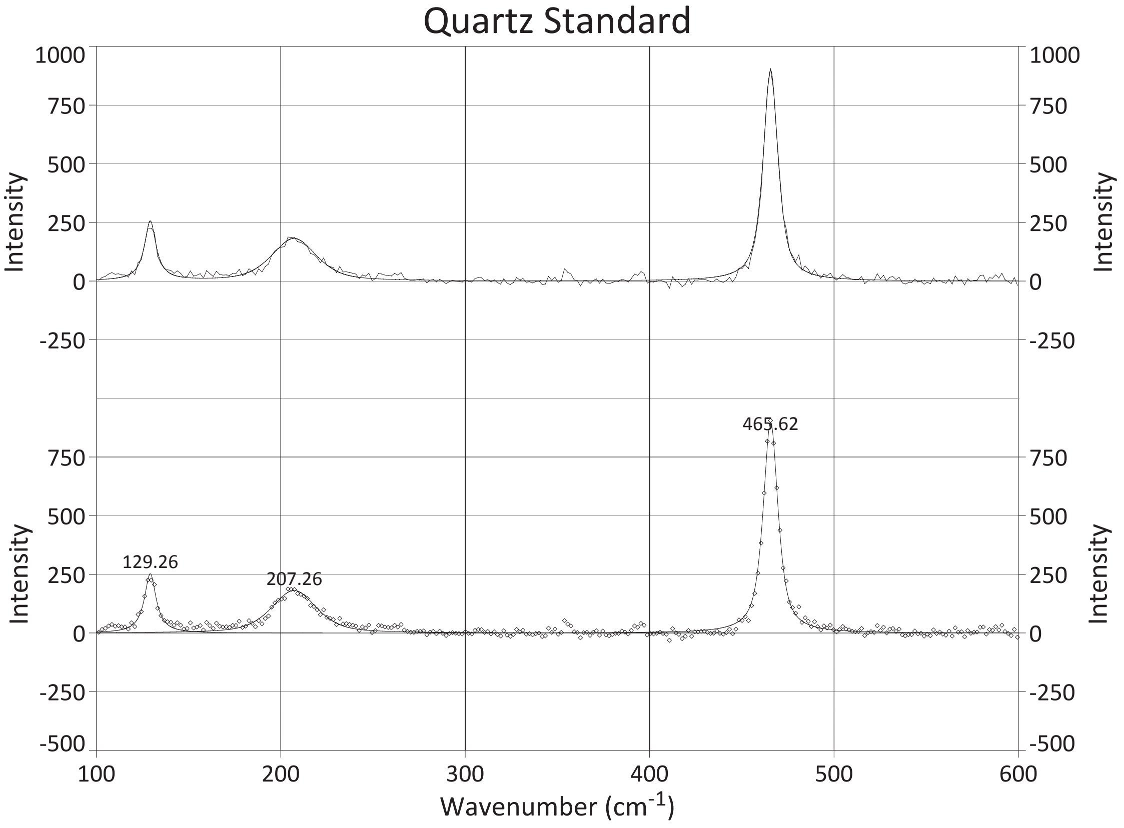

Quartz Standard

LU 02-8

Garnet H

Locality: Purdy Hill
Collected by William Carlson

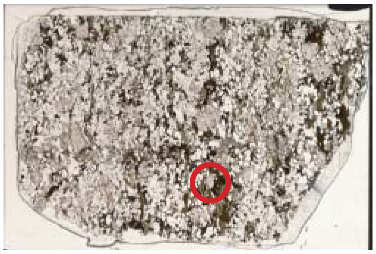

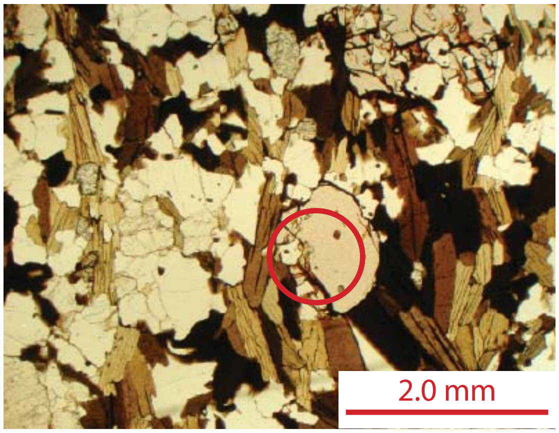

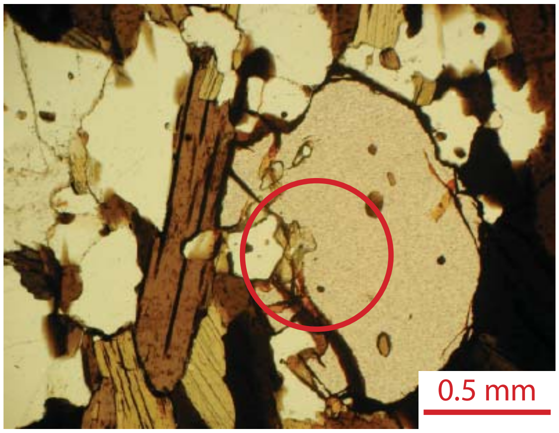

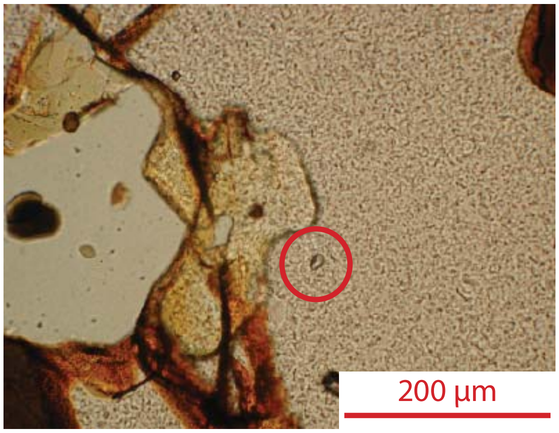

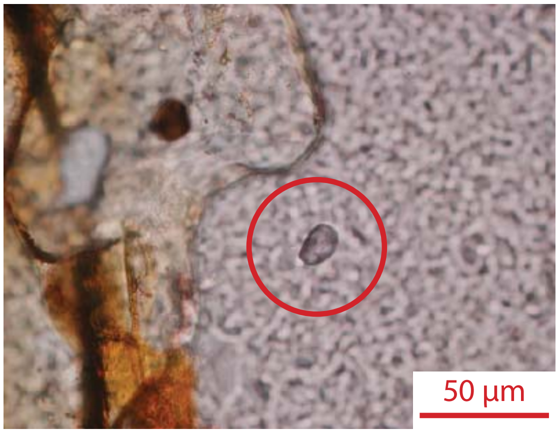

Inclusion Information

Maximum length (X-Y) (µm)	17.4
Minimum length (X-Y) (µm)	12.6
Inclusion thickness (Z) (µm)	10
Location (X-Y coordinates)	(112.5, 15.1)
Description of shape	Ellipsoid
Garnet composition	$Alm_{79.6}$, $Prp_{12.8}$, $Grs_{4.0}$, $Sps_{3.6}$

Data and Pressure Calculation Results

Depth of spectrum (µm)	-6
$\Delta\omega_1$ (cm^{-1})	-4.75
$\Delta\omega_2$ (cm^{-1})	-3.14
$P_{resid\ [\Delta\omega1]}$ (GPa)	-0.333
$P_{resid\ [\Delta\omega2]}$ (GPa)	-0.152
$P_{entrap\ [\Delta\omega1]}$ (GPa)	-0.42
$P_{entrap\ [\Delta\omega2]}$ (GPa)	0.03

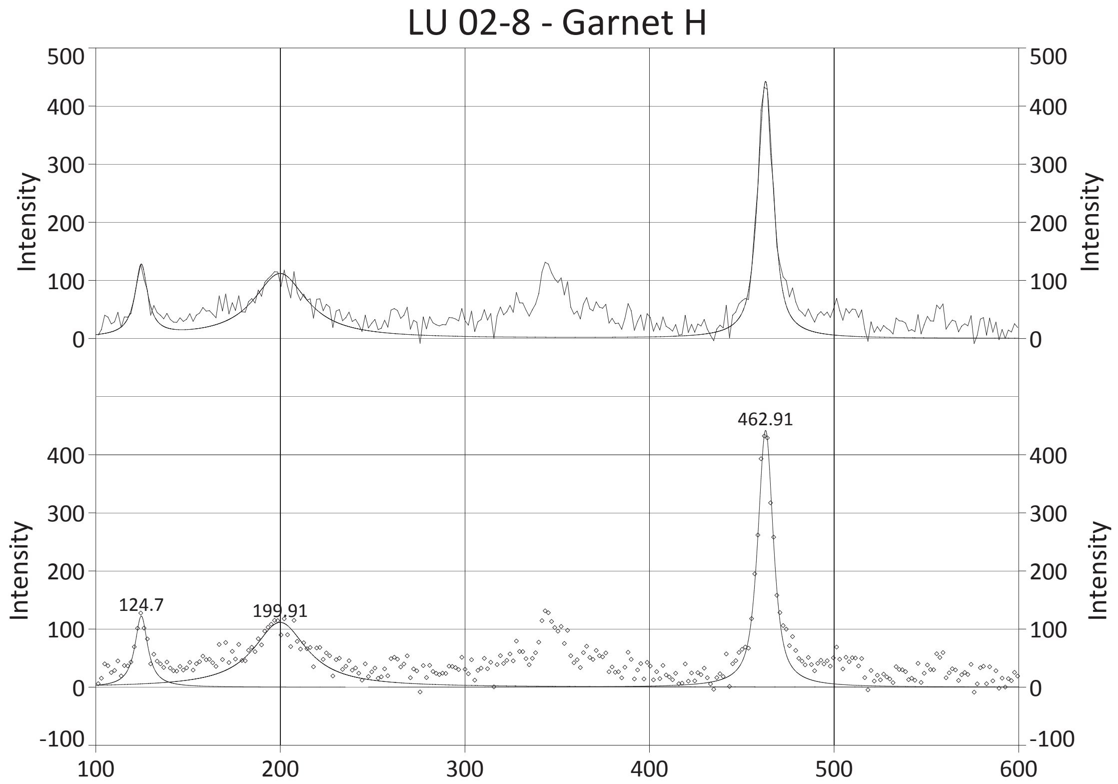

LU 02-8 - Garnet H

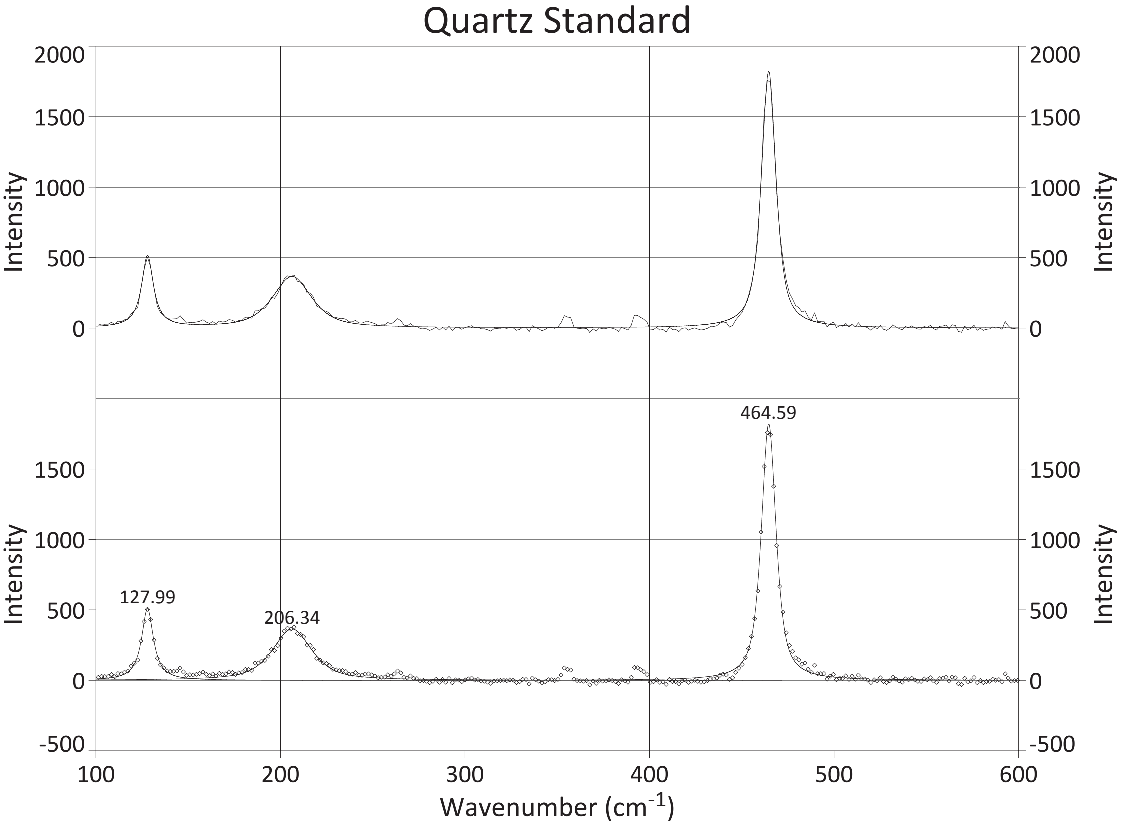

Quartz Standard

LU 02-8

Garnet I

Locality: Purdy Hill
Collected by William Carlson

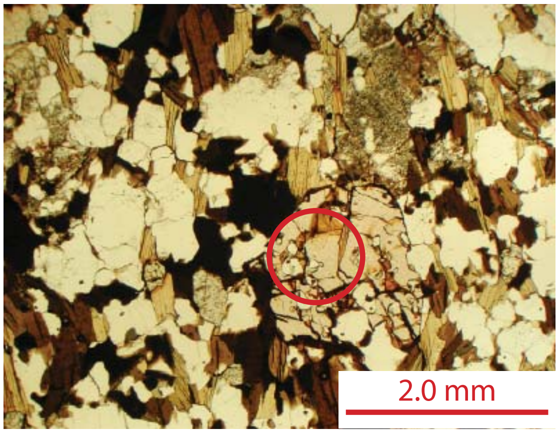

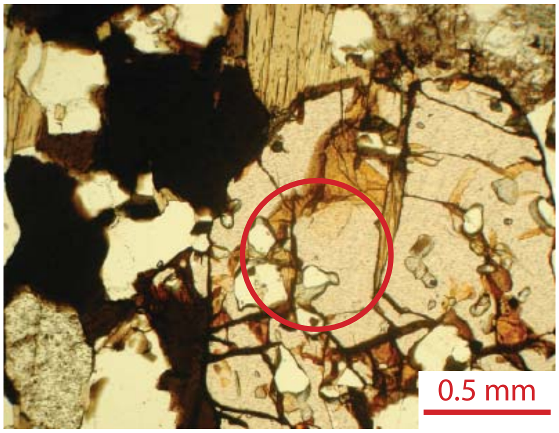

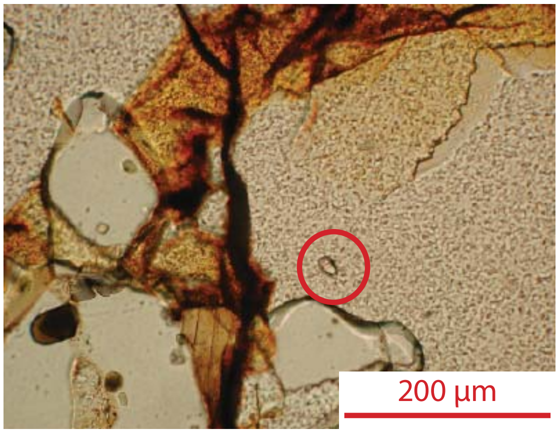

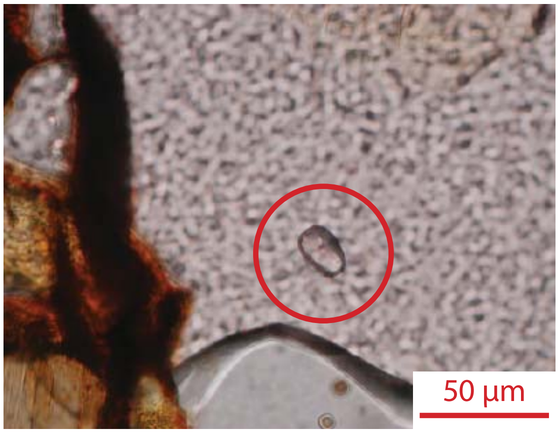

Inclusion Information

Maximum length (X-Y) (µm)	22.1
Minimum length (X-Y) (µm)	14.2
Inclusion thickness (Z) (µm)	12
Location (X-Y coordinates)	(113.5, 12.7)
Description of shape	Ellipsoid
Garnet composition	$Alm_{79.6}$, $Prp_{12.8}$, $Grs_{4.0}$, $Sps_{3.6}$

Data and Pressure Calculation Results

Depth of spectrum (µm)	-8
$\Delta\omega_1$ (cm^{-1})	1.01
$\Delta\omega_2$ (cm^{-1})	1.05
$P_{resid\ [\Delta\omega1]}$ (GPa)	0.062
$P_{resid\ [\Delta\omega2]}$ (GPa)	0.052
$P_{entrap\ [\Delta\omega1]}$ (GPa)	0.56
$P_{entrap\ [\Delta\omega2]}$ (GPa)	0.53

LU 02-8 - Garnet I

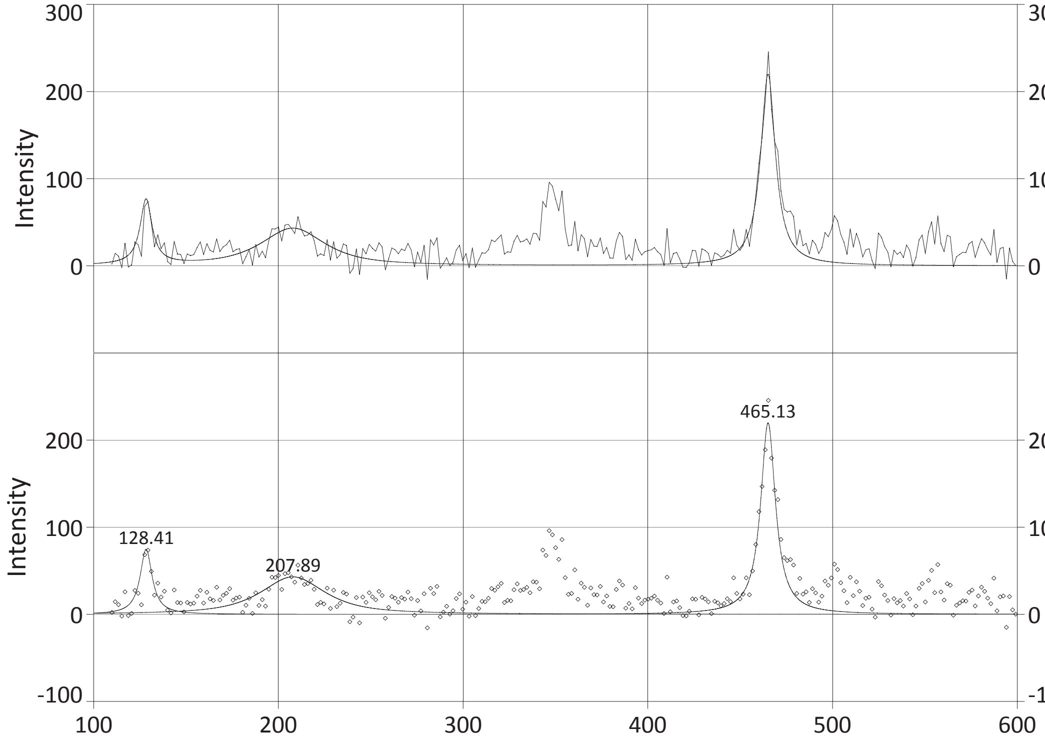

Quartz Standard

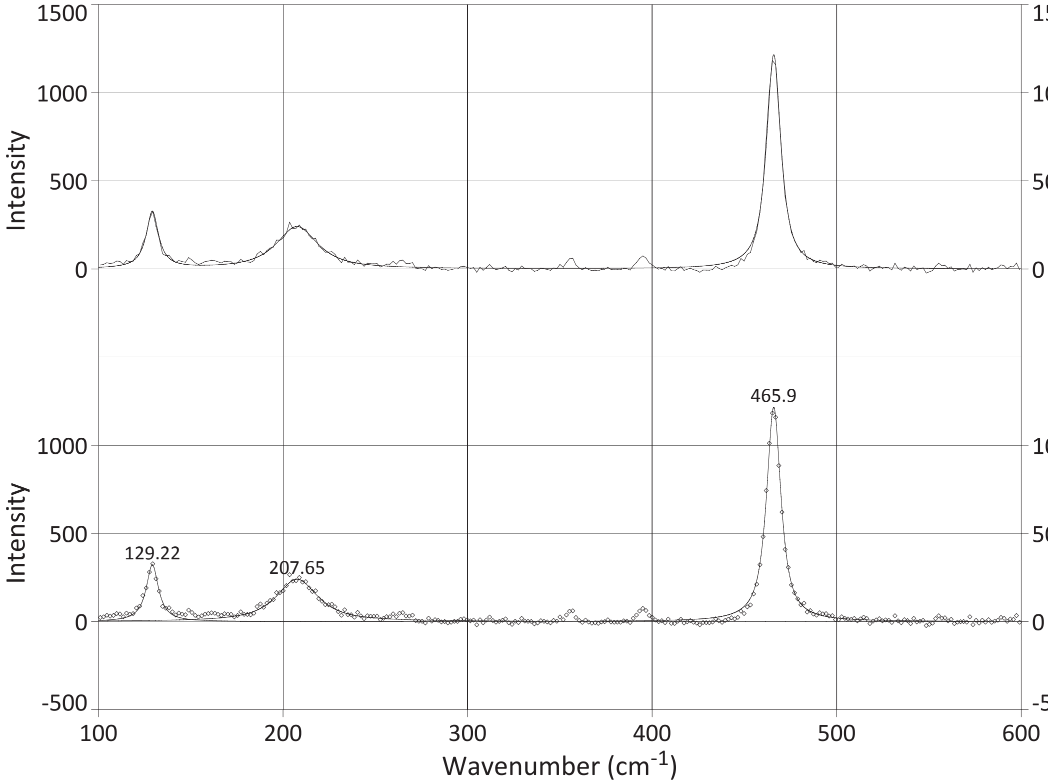

LU 02-8

Garnet K

Locality: Purdy Hill
Collected by William Carlson

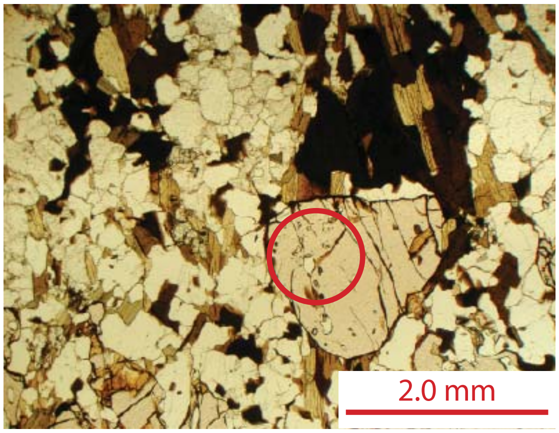

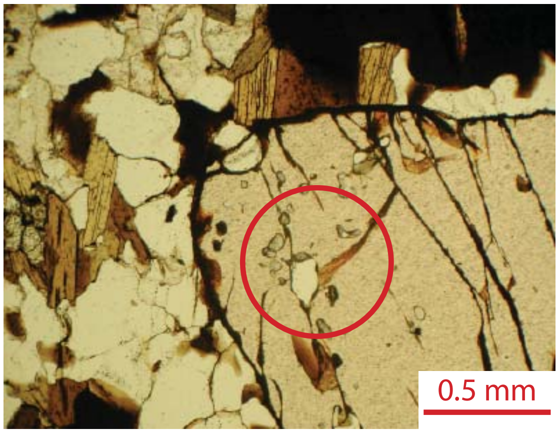

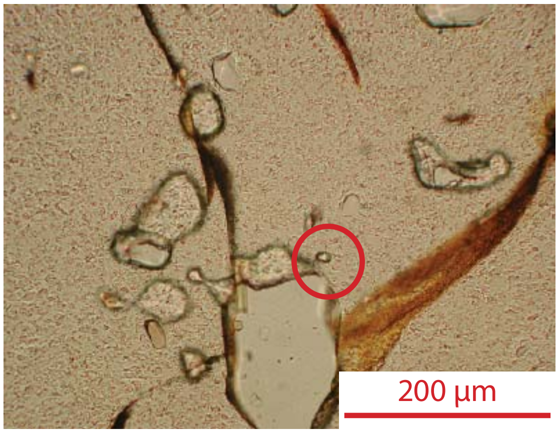

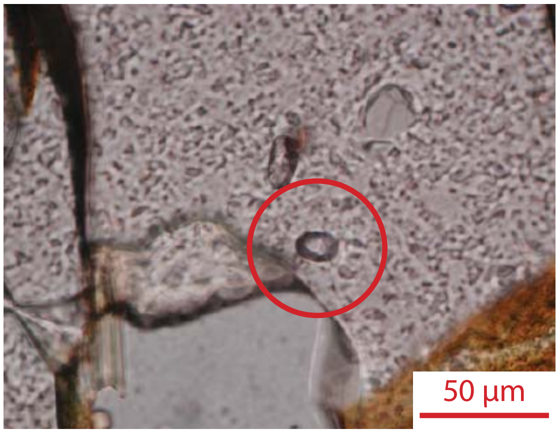

Inclusion Information

Maximum length (X-Y) (μm)	17.4
Minimum length (X-Y) (μm)	11.1
Inclusion thickness (Z) (μm)	10
Location (X-Y coordinates)	(121.9, 1.9)
Description of shape	Ellipsoid
Garnet composition	Alm$_{79.6}$, Prp$_{12.8}$, Grs$_{4.0}$, Sps$_{3.6}$

Data and Pressure Calculation Results

Depth of spectrum (μm)	-10
$\Delta\omega_1$ (cm^{-1})	0.18
$\Delta\omega_2$ (cm^{-1})	0.84
$P_{resid\ [\Delta\omega1]}$ (GPa)	0.011
$P_{resid\ [\Delta\omega2]}$ (GPa)	0.041
$P_{entrap\ [\Delta\omega1]}$ (GPa)	0.43
$P_{entrap\ [\Delta\omega2]}$ (GPa)	0.51

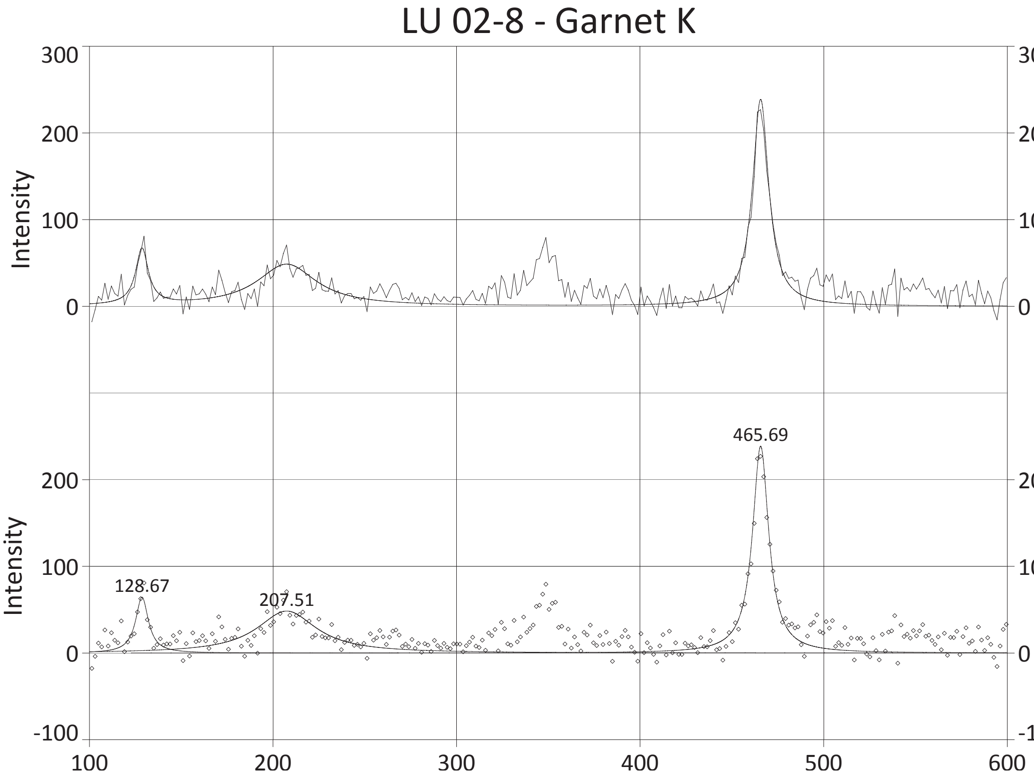
LU 02-8 - Garnet K
Intensity
300
200
100
0
465.69
128.67
207.51
-100
100
200
300
400
500
600

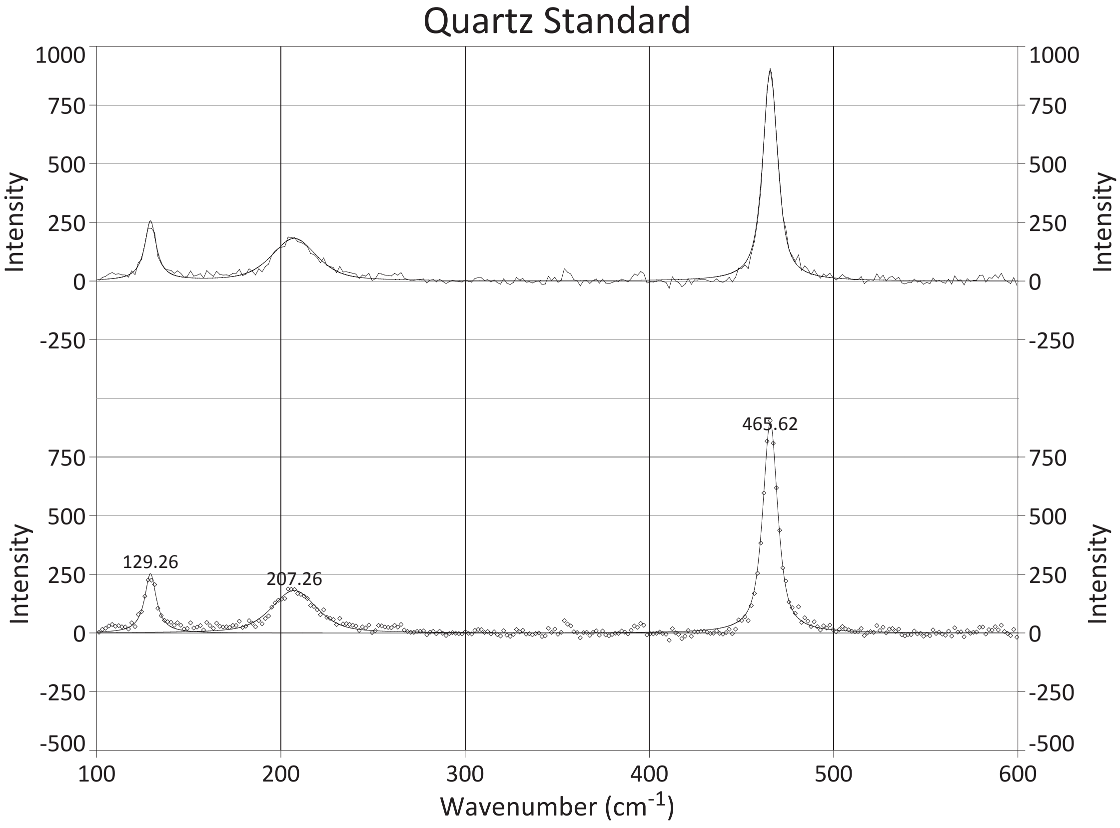
Quartz Standard
Intensity
1000
750
500
250
0
-250
-500
465.62
129.26
207.26
100
200
300
400
500
600
Wavenumber (cm-1)

LU 02-8

Garnet L

Locality: Purdy Hill
Collected by William Carlson

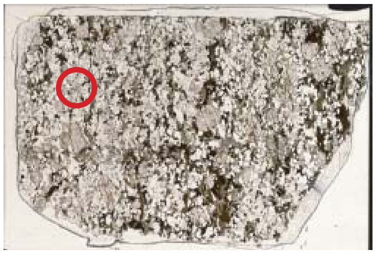

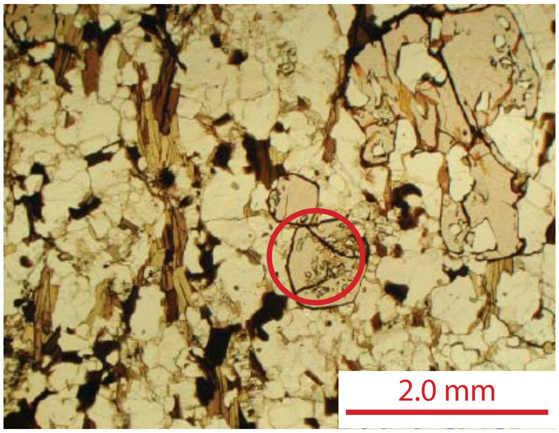

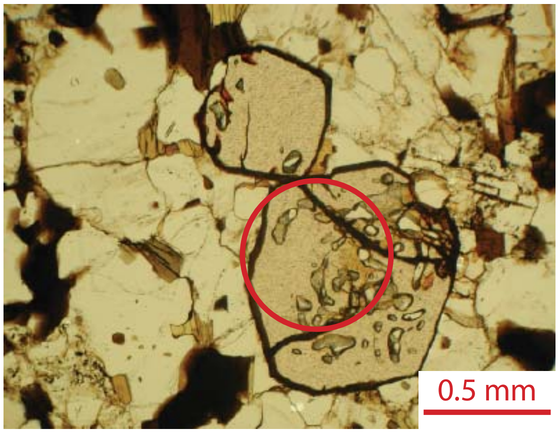

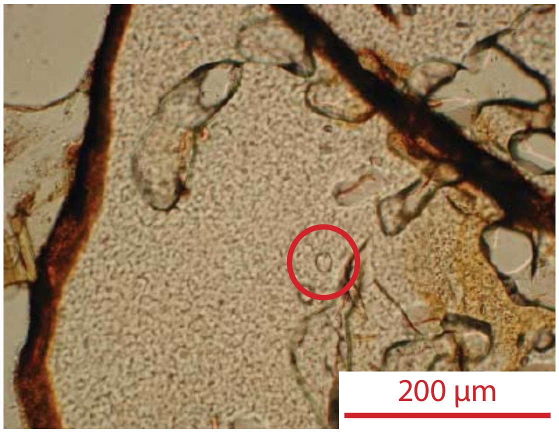

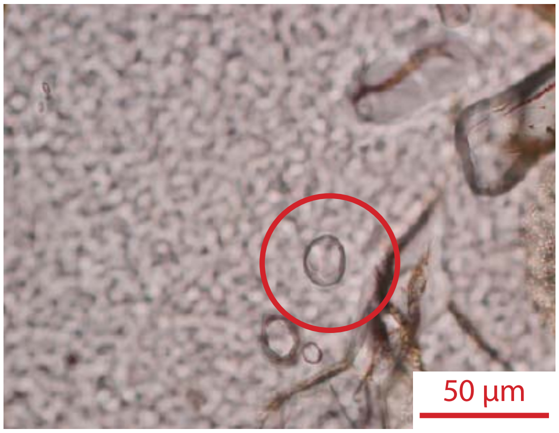

Inclusion Information

Maximum length (X-Y) (µm)	22.1
Minimum length (X-Y) (µm)	17.4
Inclusion thickness (Z) (µm)	11
Location (X-Y coordinates)	-(119.1, 12.6)
Description of shape	Subspherical
Garnet composition	$Alm_{79.6}$, $Prp_{12.8}$, $Grs_{4.0}$, $Sps_{3.6}$

Data and Pressure Calculation Results

Depth of spectrum (µm)	-8
$\Delta\omega_1$ (cm^{-1})	-3.31
$\Delta\omega_2$ (cm^{-1})	-3.78
$P_{resid\ [\Delta\omega1]}$ (GPa)	-0.222
$P_{resid\ [\Delta\omega2]}$ (GPa)	-0.183
$P_{entrap\ [\Delta\omega1]}$ (GPa)	-0.15
$P_{entrap\ [\Delta\omega2]}$ (GPa)	-0.05

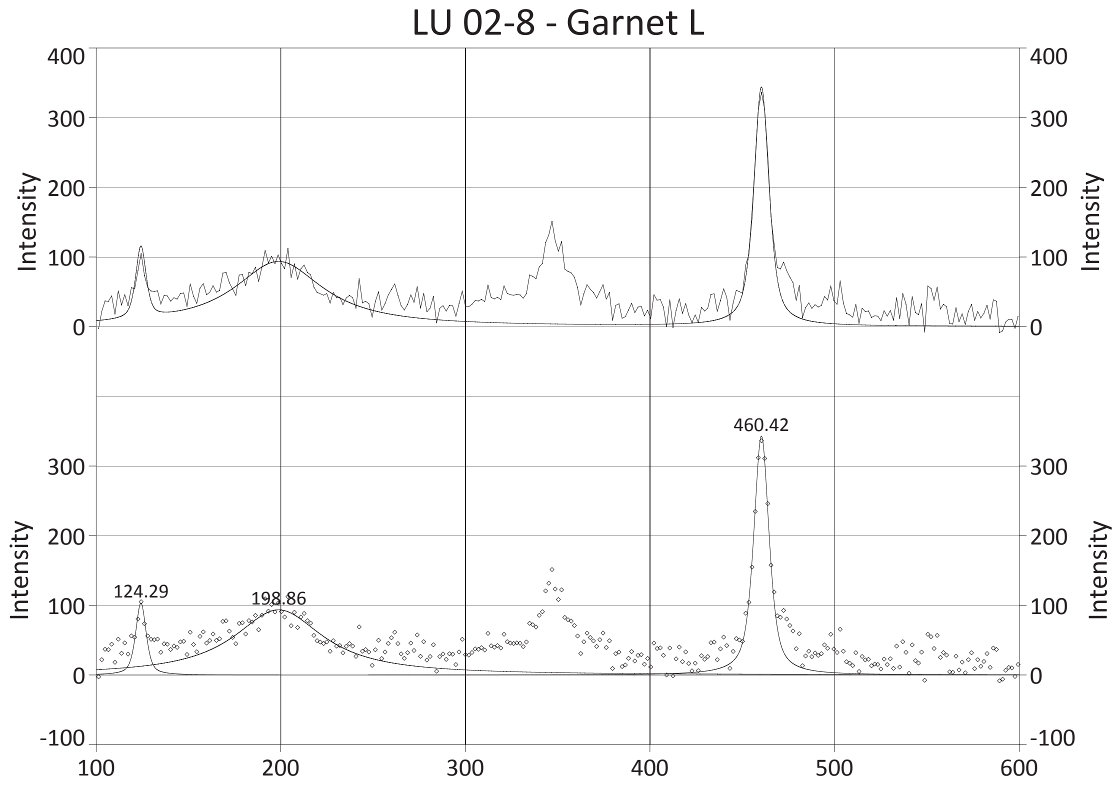
LU 02-8 - Garnet L
Intensity
400
300
200
100
0
460.42
124.29
198.86
-100
100
200
300
400
500
600

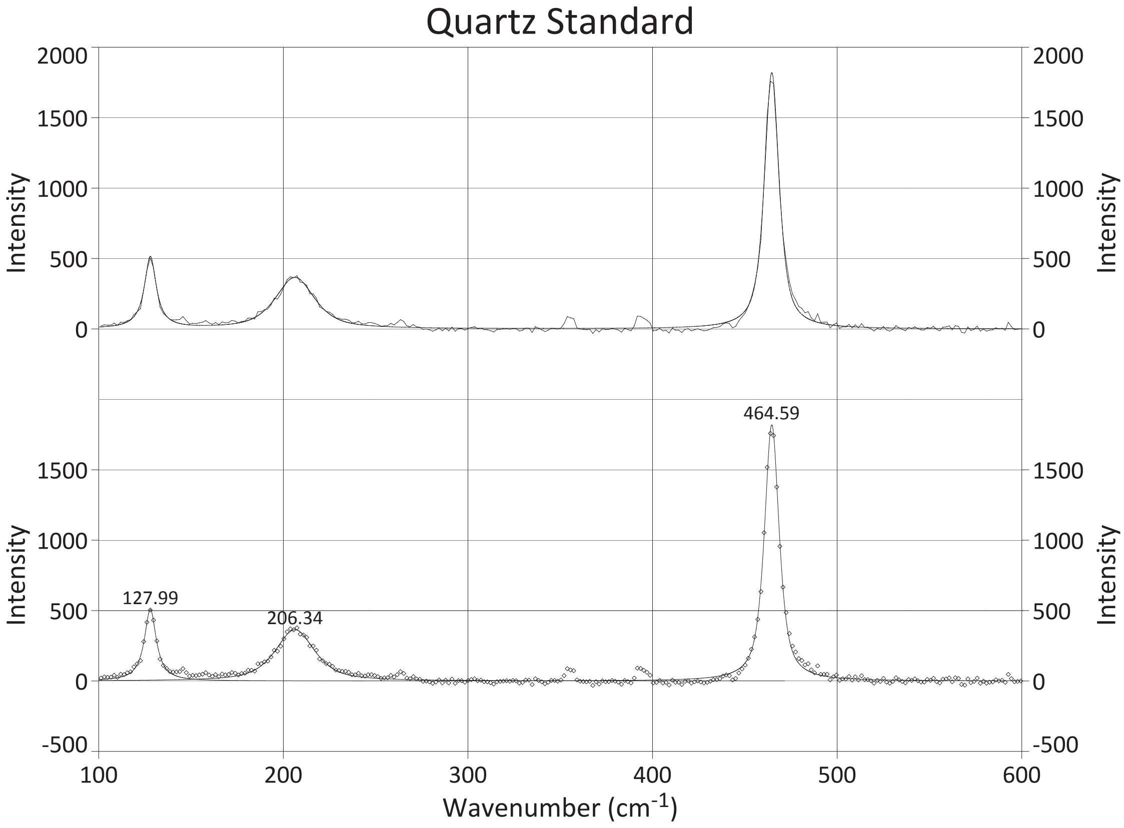
Quartz Standard
Intensity
2000
1500
1000
500
0
464.59
127.99
206.34
-500
100
200
300
400
500
600
Wavenumber (cm-1)

LU 02-9

Garnet D

Locality: Purdy Hill
Collected by William Carlson

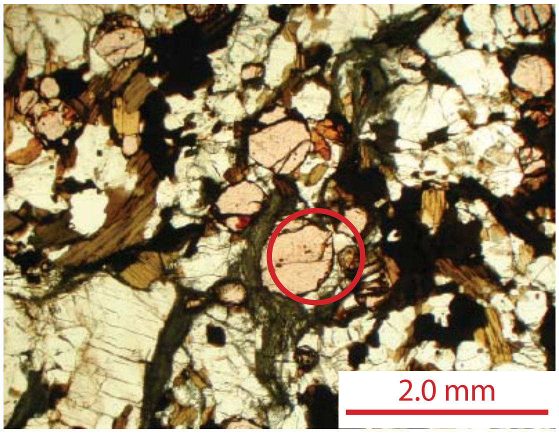

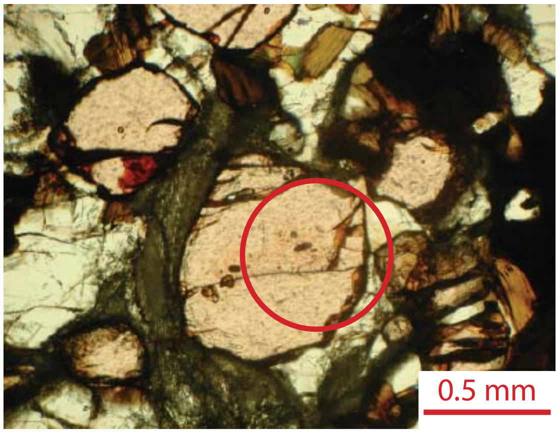

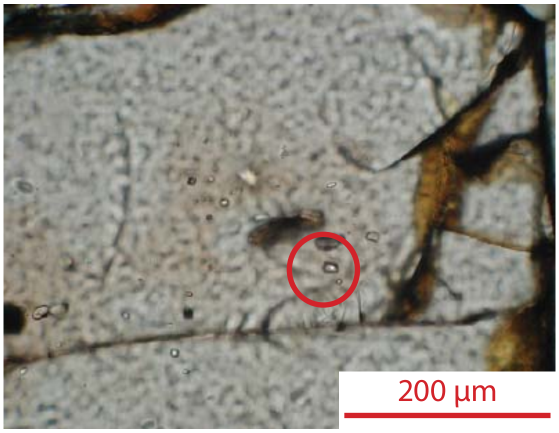

Inclusion Information

Maximum length (X-Y) (µm)	15.8
Minimum length (X-Y) (µm)	11.1
Inclusion thickness (Z) (µm)	14
Location (X-Y coordinates)	(104.6, 5.8)
Description of shape	Ellipsoid
Garnet composition	$Alm_{79.6}$, $Prp_{12.8}$, $Grs_{4.0}$, $Sps_{3.6}$

Data and Pressure Calculation Results

Depth of spectrum (µm)	-10
$\Delta\omega_1$ (cm^{-1})	-3.56
$\Delta\omega_2$ (cm^{-1})	-3.83
$P_{resid\ [\Delta\omega1]}$ (GPa)	-0.241
$P_{resid\ [\Delta\omega2]}$ (GPa)	-0.185
$P_{entrap\ [\Delta\omega1]}$ (GPa)	-0.19
$P_{entrap\ [\Delta\omega2]}$ (GPa)	-0.06

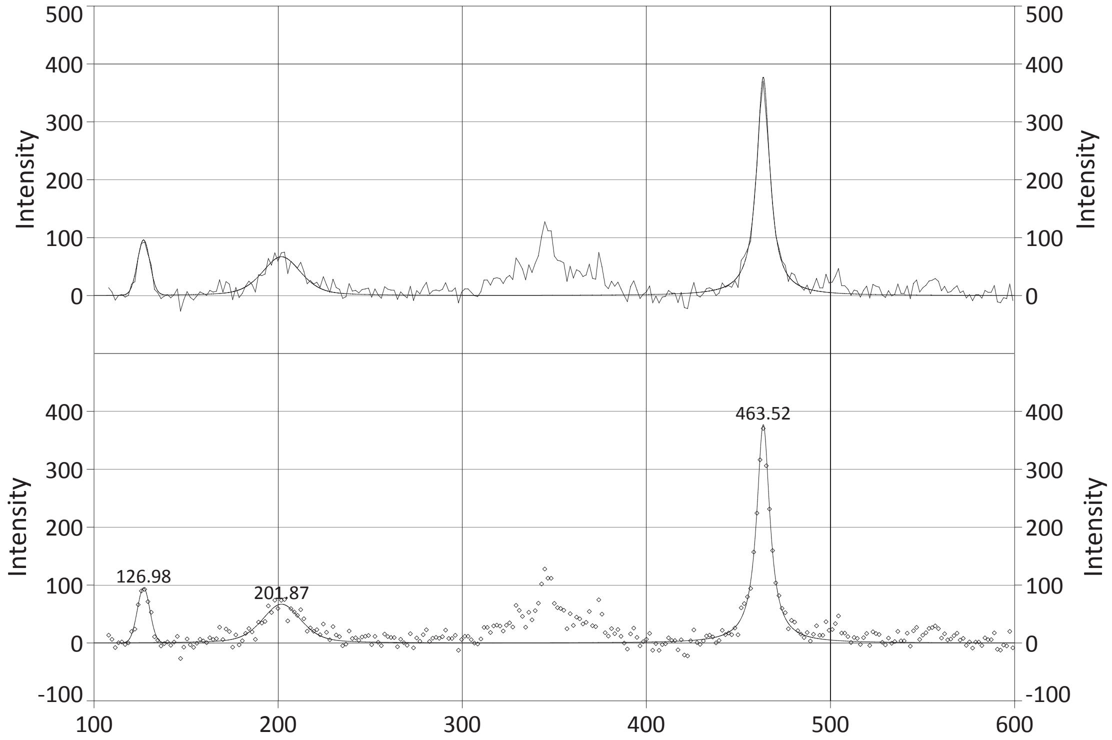

LU 02-9 - Garnet D

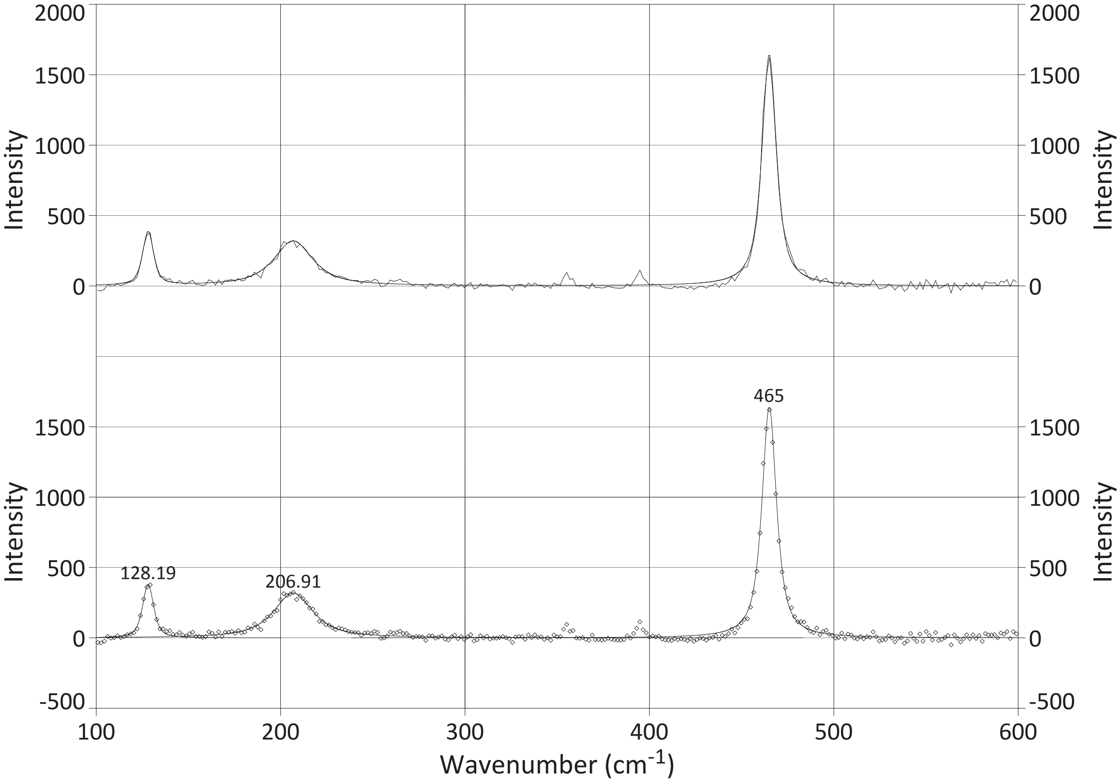

Quartz Standard

LU 02-9

Garnet F

Locality: Purdy Hill
Collected by William Carlson

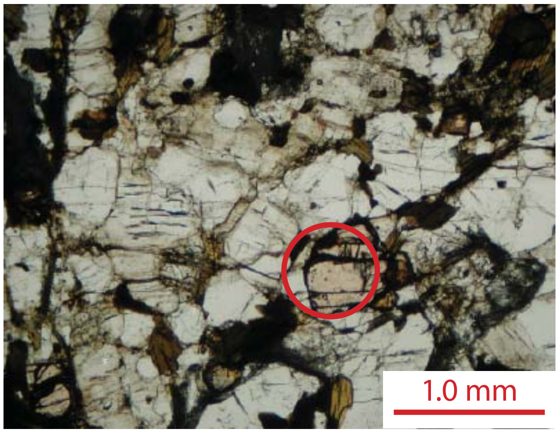

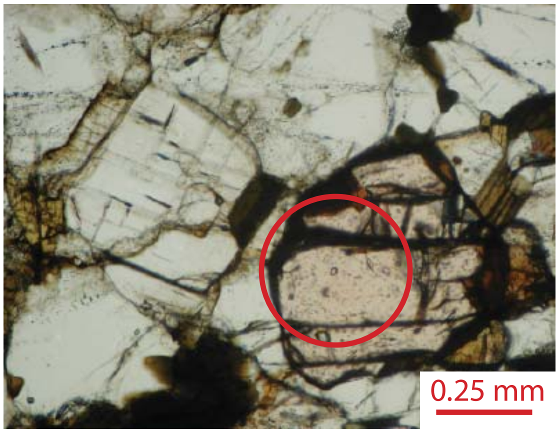

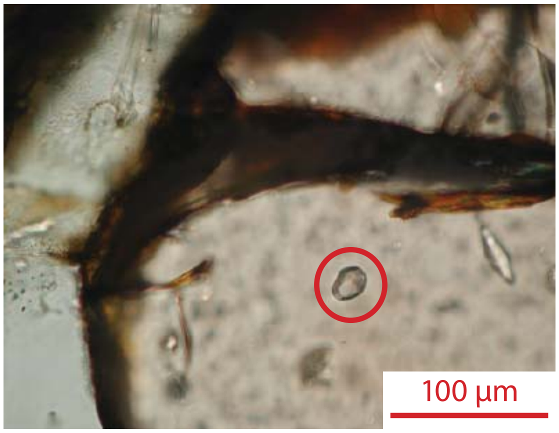

Inclusion Information

Maximum length (X-Y) (µm)	25.3
Minimum length (X-Y) (µm)	18.9
Inclusion thickness (Z) (µm)	15
Location (X-Y coordinates)	(112.7, 18.7)
Description of shape	Ellipsoid
Garnet composition	$Alm_{79.6}$, $Prp_{12.8}$, $Grs_{4.0}$, $Sps_{3.6}$

Data and Pressure Calculation Results

Depth of spectrum (µm)	-15
$\Delta\omega_1$ (cm^{-1})	1.74
$\Delta\omega_2$ (cm^{-1})	1.15
$P_{resid\ [\Delta\omega 1]}$ (GPa)	0.105
$P_{resid\ [\Delta\omega 2]}$ (GPa)	0.057
$P_{entrap\ [\Delta\omega 1]}$ (GPa)	0.67
$P_{entrap\ [\Delta\omega 2]}$ (GPa)	0.55

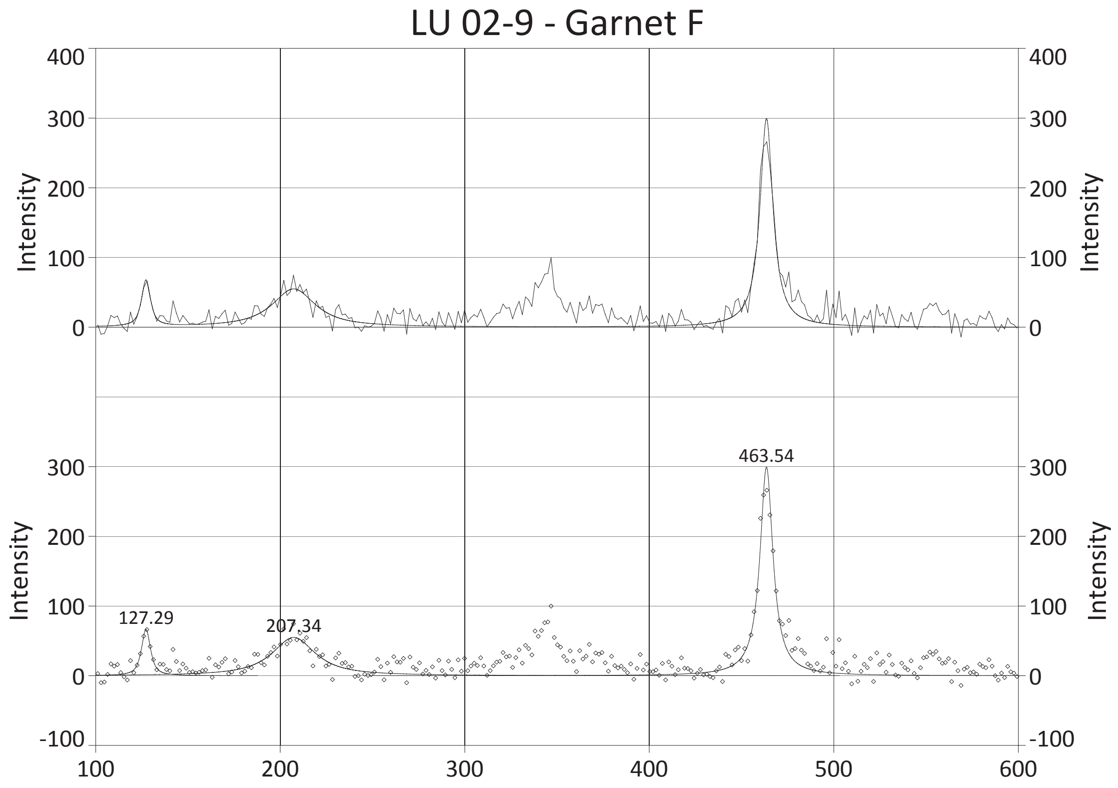
LU 02-9 - Garnet F
Intensity
400
300
200
100
0
-100
127.29
207.34
463.54
100
200
300
400
500
600

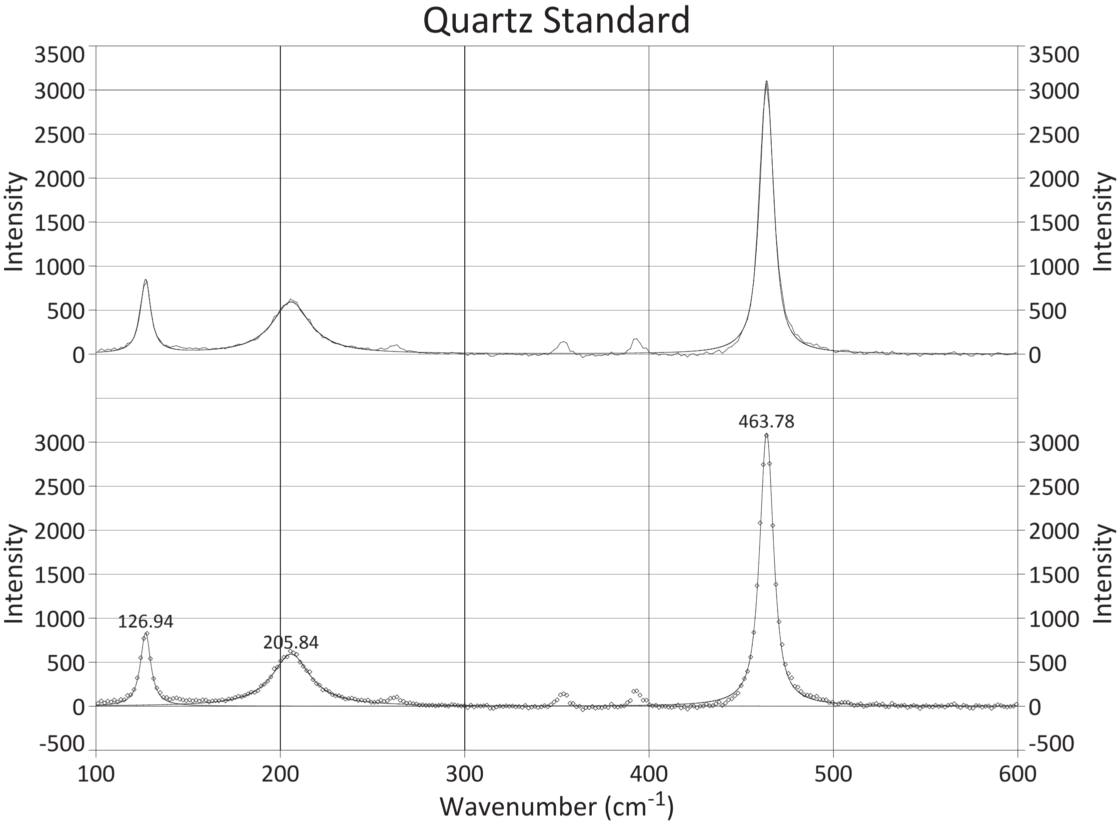
Quartz Standard
Intensity
3500
3000
2500
2000
1500
1000
500
0
-500
126.94
205.84
463.78
100
200
300
400
500
600
Wavenumber (cm-1)

LU 02-9

Garnet G

Locality: Purdy Hill
Collected by William Carlson

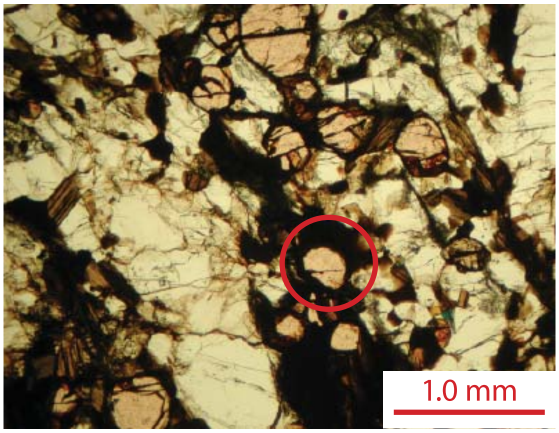

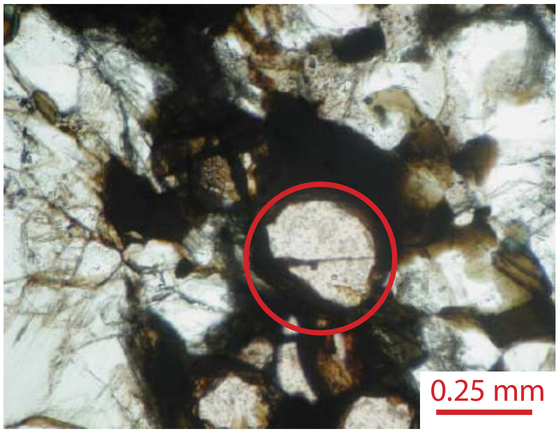

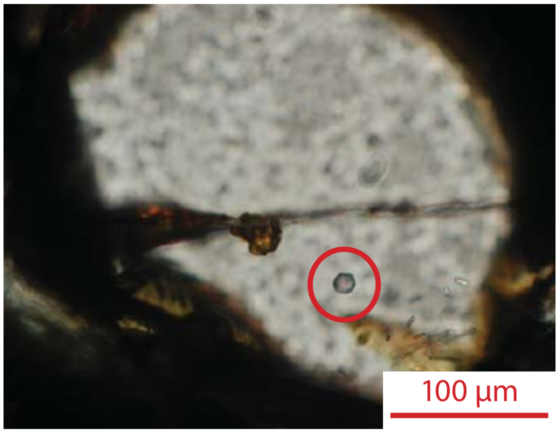

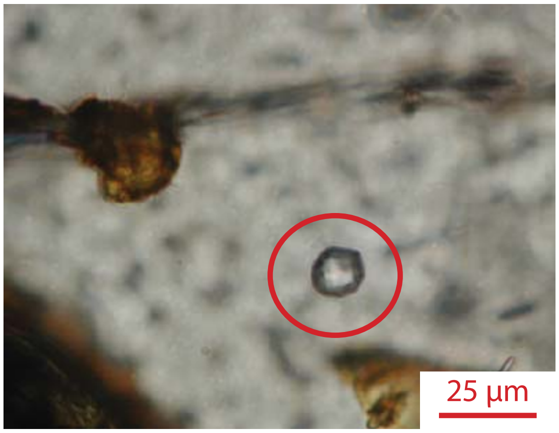

Inclusion Information

Maximum length (X-Y) (µm)	15.8
Minimum length (X-Y) (µm)	11.1
Inclusion thickness (Z) (µm)	24
Location (X-Y coordinates)	(124.9, 7.6)
Description of shape	Spherical
Garnet composition	$Alm_{79.6}$, $Prp_{12.8}$, $Grs_{4.0}$, $Sps_{3.6}$

Data and Pressure Calculation Results

Depth of spectrum (µm)	-21
$\Delta\omega_1$ (cm^{-1})	1.45
$\Delta\omega_2$ (cm^{-1})	1.41
$P_{resid\ [\Delta\omega1]}$ (GPa)	0.088
$P_{resid\ [\Delta\omega2]}$ (GPa)	0.070
$P_{entrap\ [\Delta\omega1]}$ (GPa)	0.62
$P_{entrap\ [\Delta\omega2]}$ (GPa)	0.58

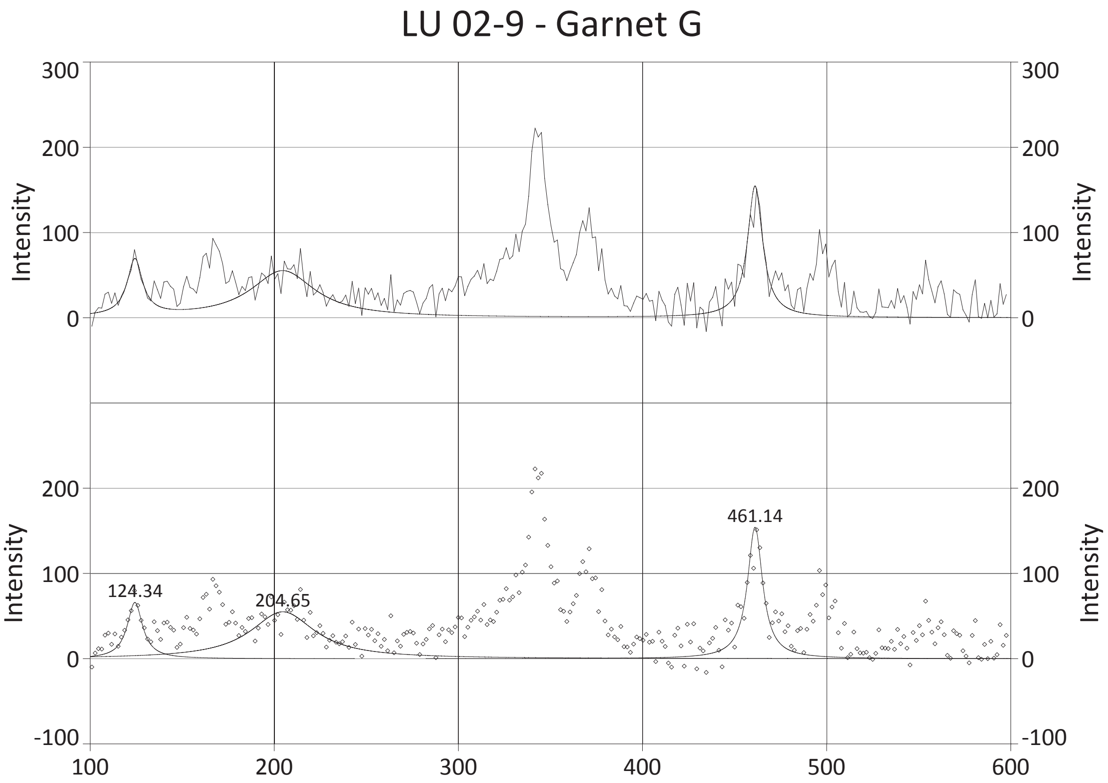
LU 02-9 - Garnet G

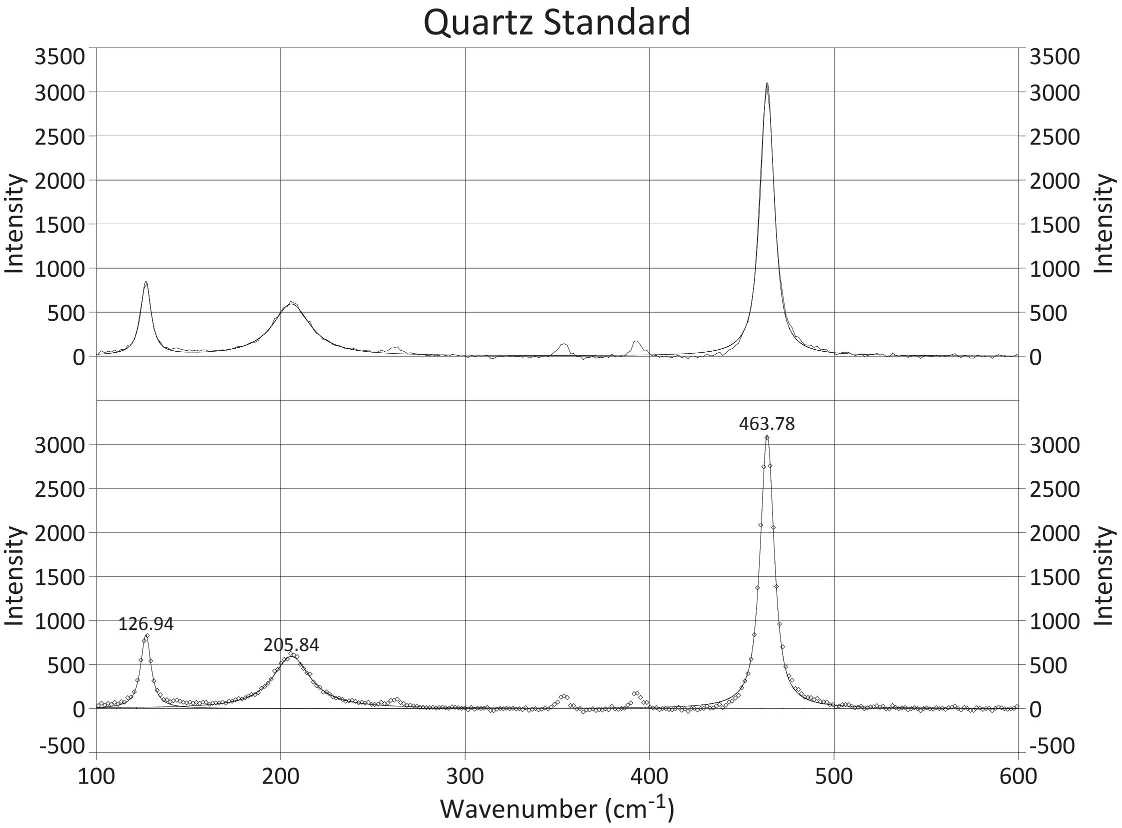
Quartz Standard

LU 02-9

Garnet H

Locality: Purdy Hill
Collected by William Carlson

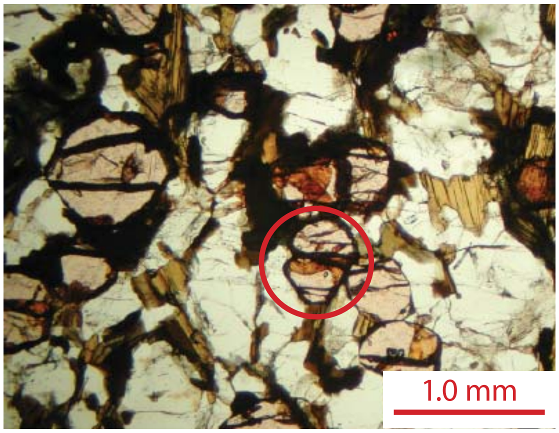

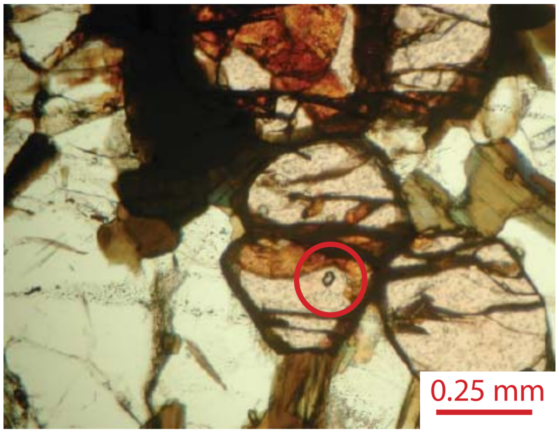

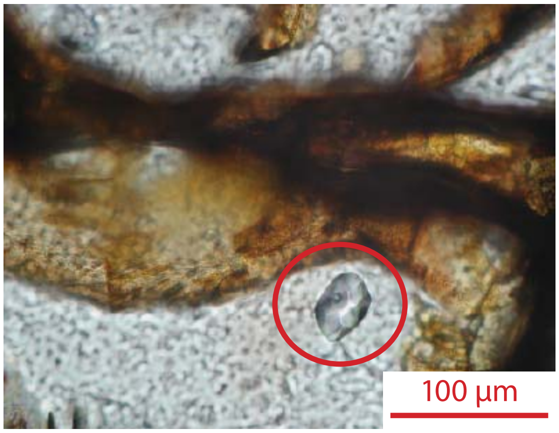

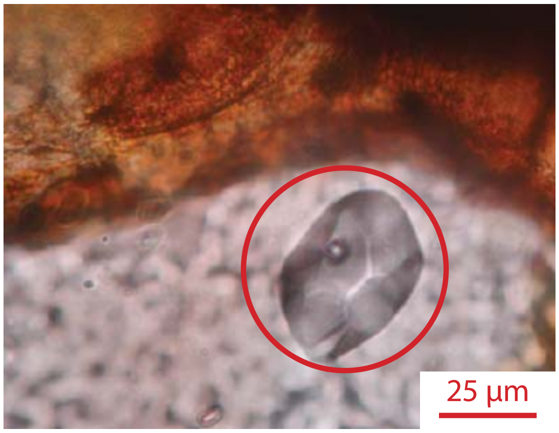

Inclusion Information

Maximum length (X-Y) (µm)	47.4
Minimum length (X-Y) (µm)	31.6
Inclusion thickness (Z) (µm)	23
Location (X-Y coordinates)	-(120.3, 9.3)
Description of shape	Spherical
Garnet composition	$Alm_{79.6}$, $Prp_{12.8}$, $Grs_{4.0}$, $Sps_{3.6}$

Data and Pressure Calculation Results

Depth of spectrum (µm)	-30
$\Delta\omega_1$ (cm^{-1})	-0.92
$\Delta\omega_2$ (cm^{-1})	-0.51
$P_{\text{resid }[\Delta\omega 1]}$ (GPa)	-0.058
$P_{\text{resid }[\Delta\omega 2]}$ (GPa)	-0.025
$P_{\text{entrap }[\Delta\omega 1]}$ (GPa)	0.26
$P_{\text{entrap }[\Delta\omega 2]}$ (GPa)	0.34

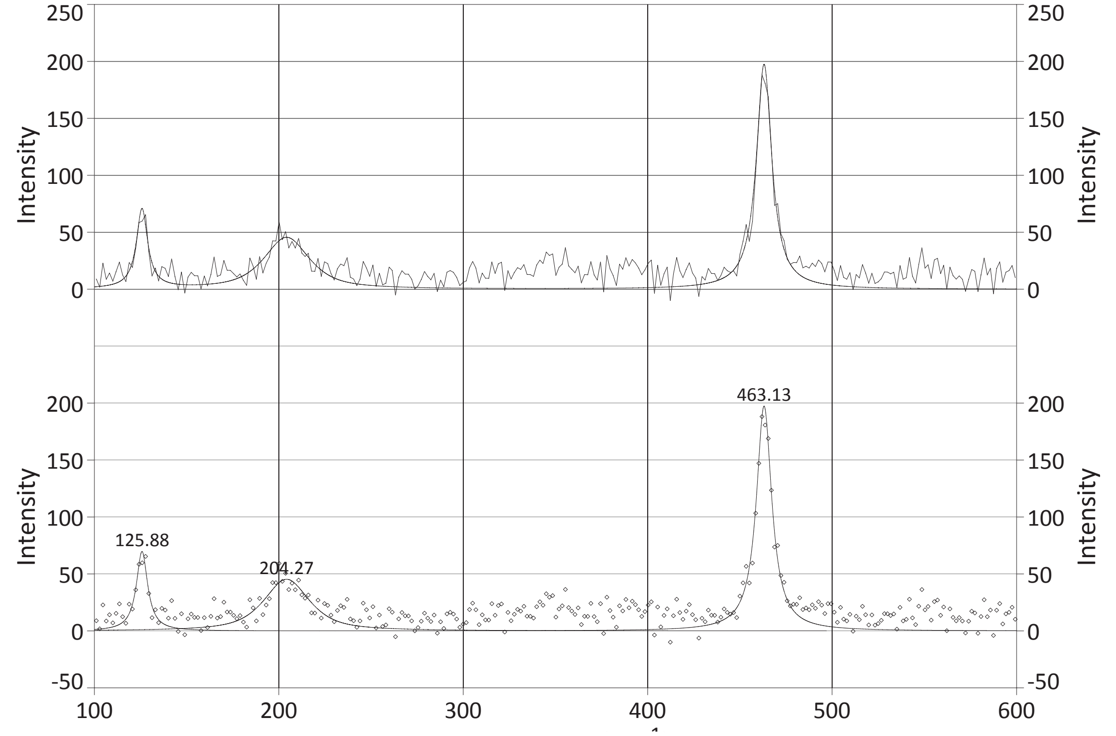
LU 02-9 - Garnet H

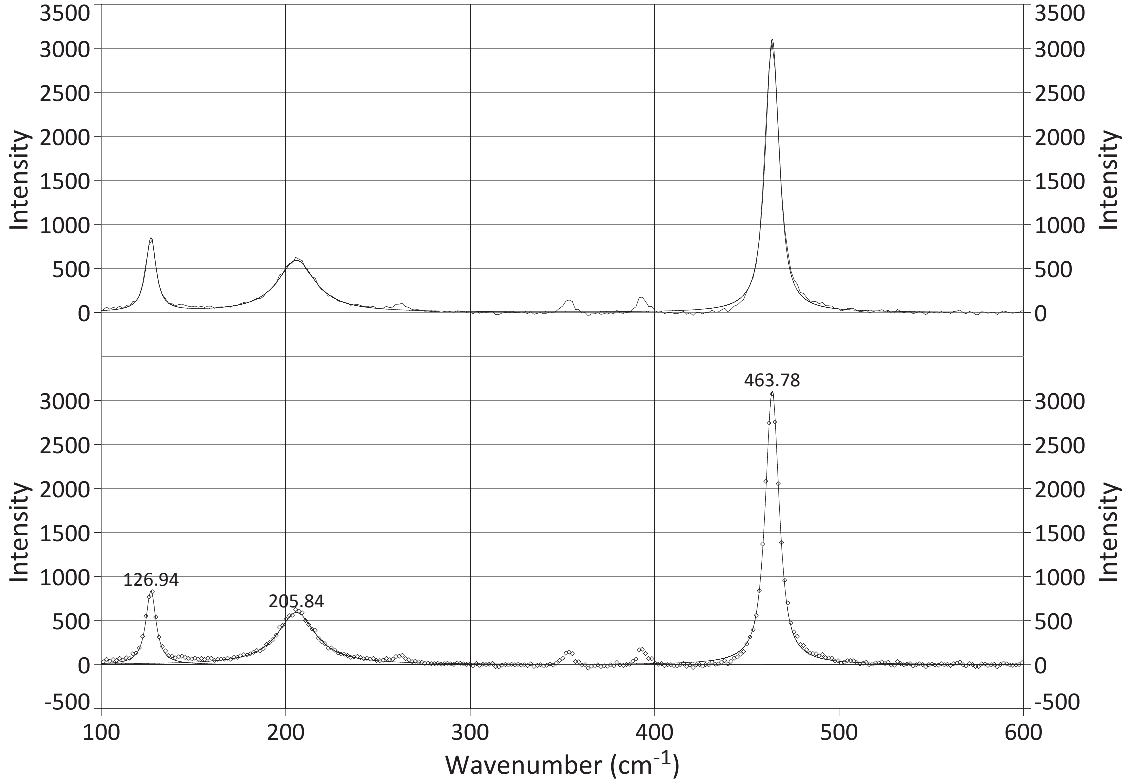
Quartz Standard

LU 02-9

Garnet I

Locality: Purdy Hill
Collected by William Carlson

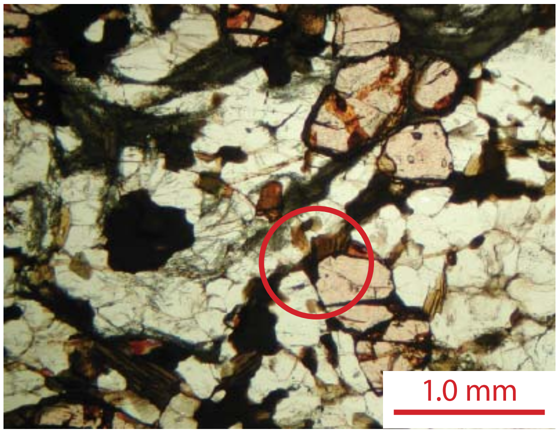

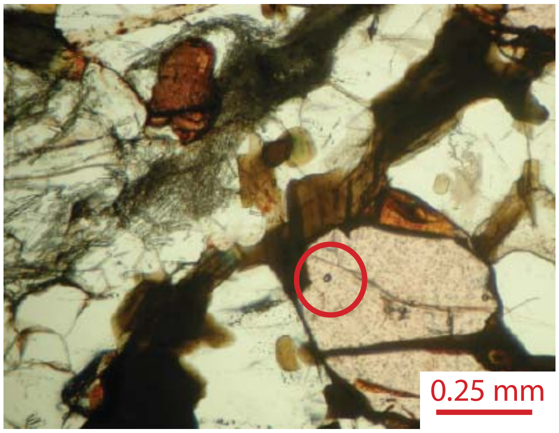

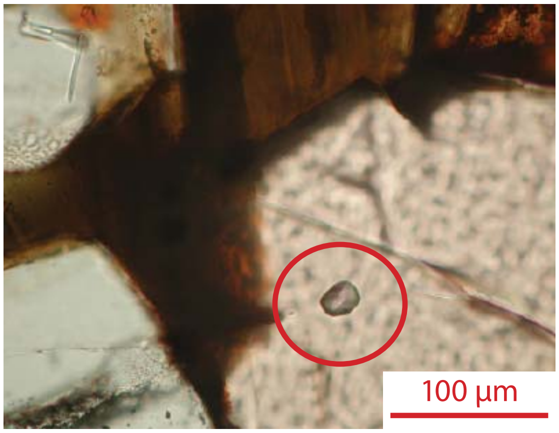

Inclusion Information

Maximum length (X-Y) (μm)	25.3
Minimum length (X-Y) (μm)	19.0
Inclusion thickness (Z) (μm)	20
Location (X-Y coordinates)	-(123.4, 4.9)
Description of shape	Ellipsoid
Garnet composition	$Alm_{79.6}$, $Prp_{12.8}$, $Grs_{4.0}$, $Sps_{3.6}$

Data and Pressure Calculation Results

Depth of spectrum (μm)	-18
$\Delta\omega_1$ (cm^{-1})	3.20
$\Delta\omega_2$ (cm^{-1})	5.07
$P_{resid\ [\Delta\omega1]}$ (GPa)	0.190
$P_{resid\ [\Delta\omega2]}$ (GPa)	0.257
$P_{entrap\ [\Delta\omega1]}$ (GPa)	0.88
$P_{entrap\ [\Delta\omega2]}$ (GPa)	1.04

LU 02-9 - Garnet I

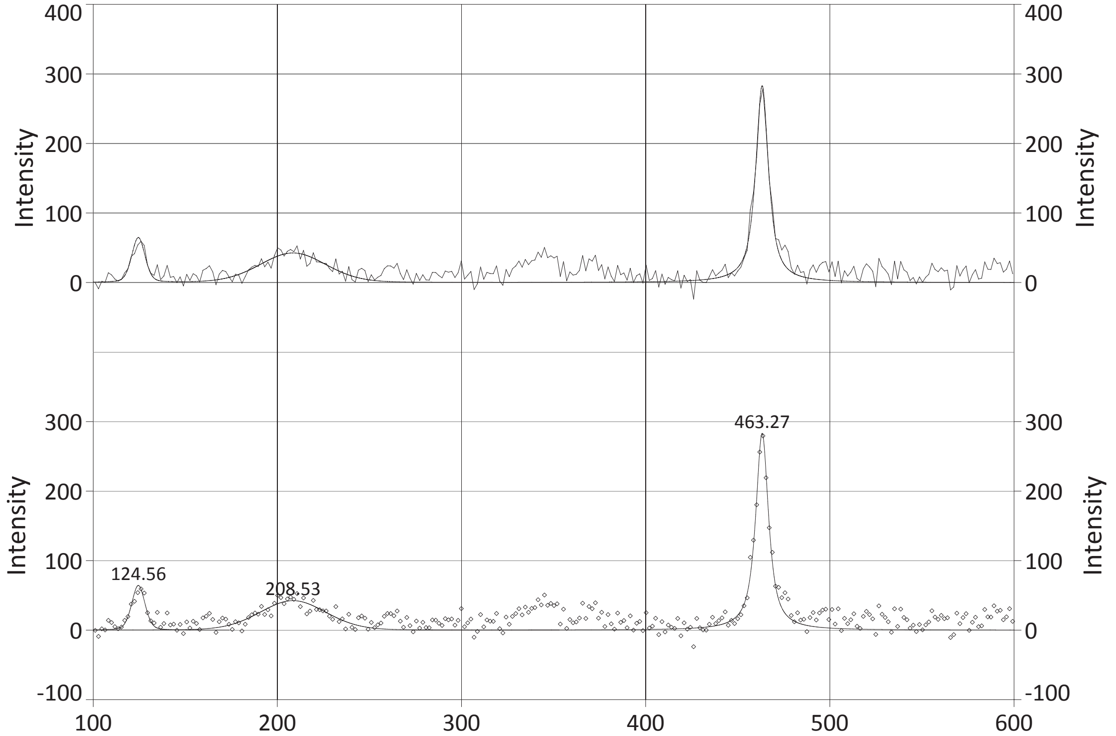

Quartz Standard

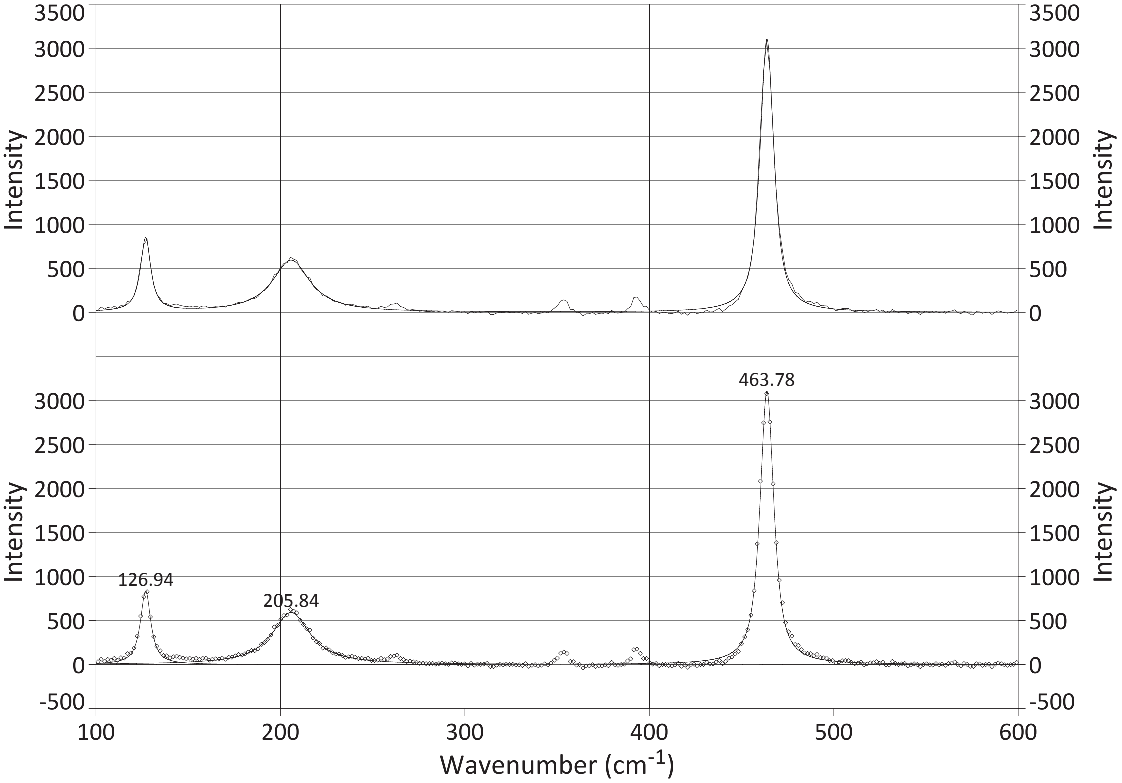

LU 02-10

Garnet B

Locality: Purdy Hill
Collected by William Carlson

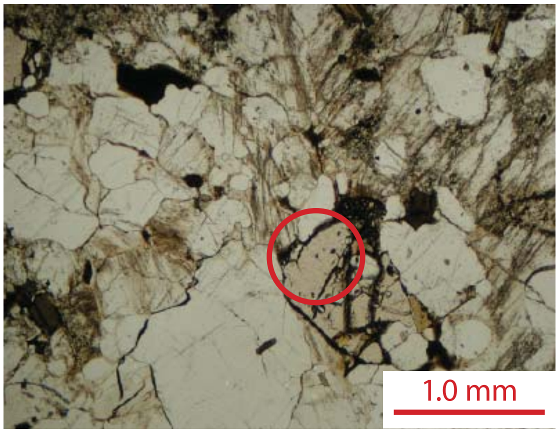

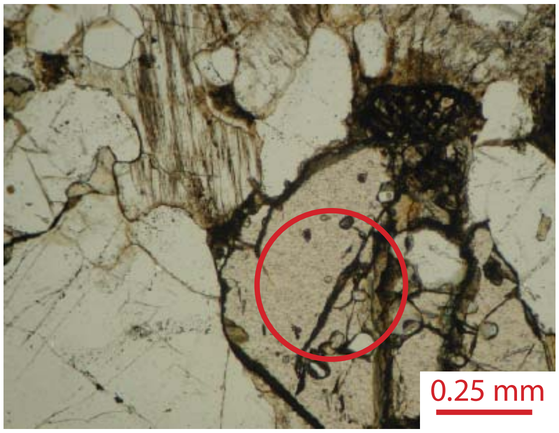

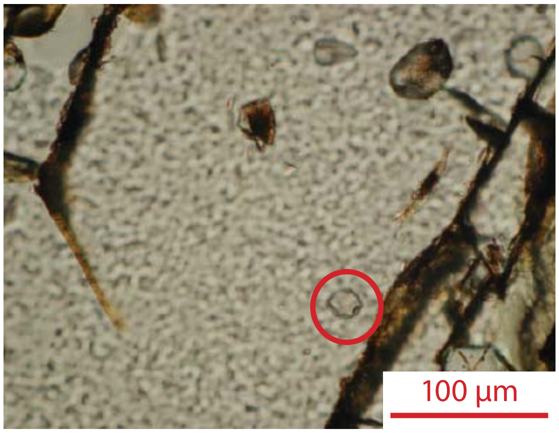

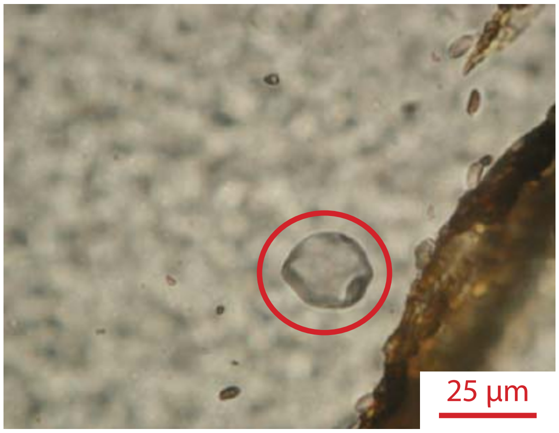

Inclusion Information

Maximum length (X-Y) (μm)	23.7
Minimum length (X-Y) (μm)	22.1
Inclusion thickness (Z) (μm)	9
Location (X-Y coordinates)	-(123.5, 5.0)
Description of shape	Elongate
Garnet composition	$Alm_{81.5}$, $Prp_{13.9}$, $Grs_{2.8}$, $Sps_{1.8}$

Data and Pressure Calculation Results

Depth of spectrum (μm)	-6
$\Delta\omega_1$ (cm^{-1})	2.23
$\Delta\omega_2$ (cm^{-1})	2.12
$P_{resid\ [\Delta\omega1]}$ (GPa)	0.134
$P_{resid\ [\Delta\omega2]}$ (GPa)	0.105
$P_{entrap\ [\Delta\omega1]}$ (GPa)	0.74
$P_{entrap\ [\Delta\omega2]}$ (GPa)	0.67

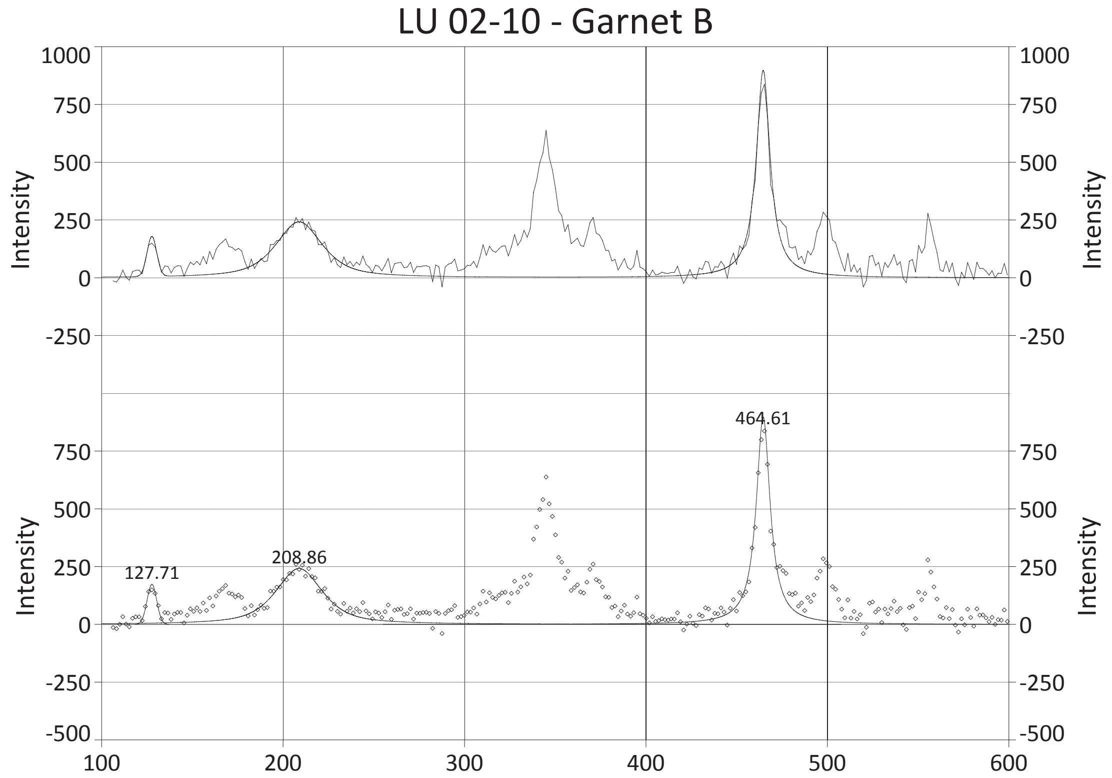

LU 02-10 - Garnet B

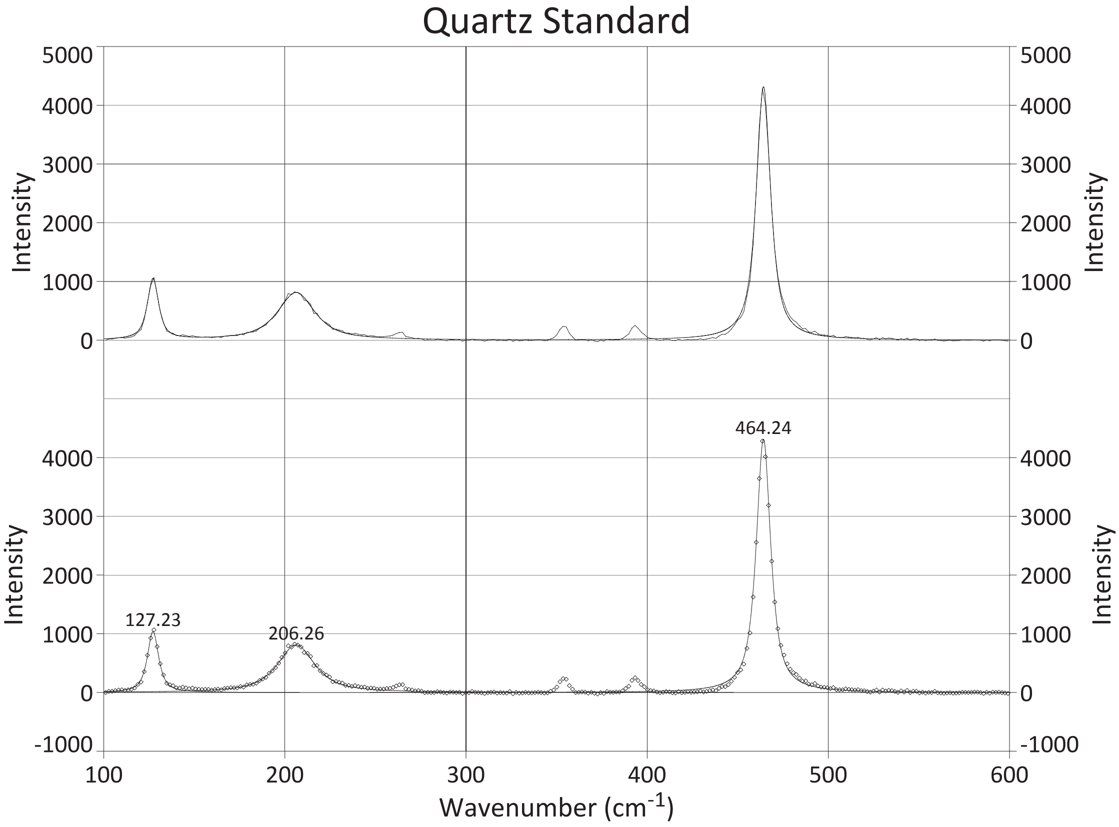

Quartz Standard

LU 02-10

Garnet D

Locality: Purdy Hill
Collected by William Carlson

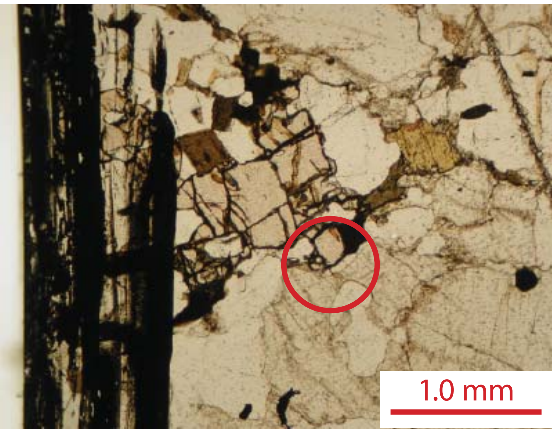

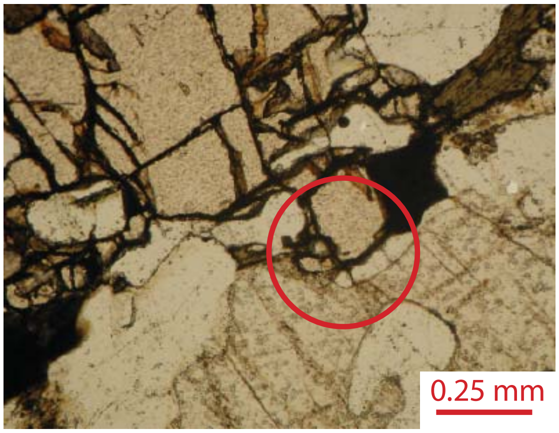

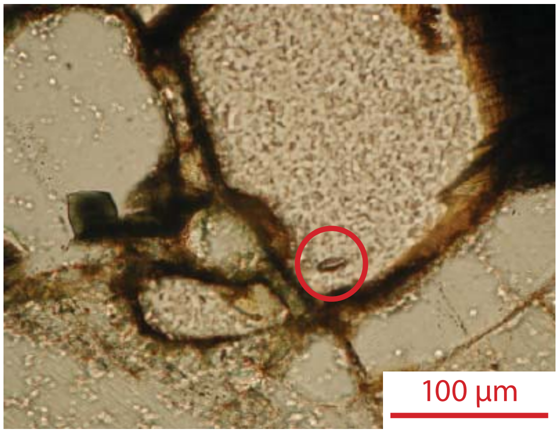

Inclusion Information

Maximum length (X-Y) (µm)	22.1
Minimum length (X-Y) (µm)	11.1
Inclusion thickness (Z) (µm)	15
Location (X-Y coordinates)	--(106.5, 10.6)
Description of shape	Elongate
Garnet composition	$Alm_{82.2}$, $Prp_{12.7}$, $Grs_{3.5}$, $Sps_{1.6}$

Data and Pressure Calculation Results

Depth of spectrum (µm)	-5
$\Delta\omega_1$ (cm^{-1})	-4.22
$\Delta\omega_2$ (cm^{-1})	-4.50
$P_{resid\ [\Delta\omega1]}$ (GPa)	-0.291
$P_{resid\ [\Delta\omega2]}$ (GPa)	-0.217
$P_{entrap\ [\Delta\omega1]}$ (GPa)	-0.32
$P_{entrap\ [\Delta\omega2]}$ (GPa)	-0.13

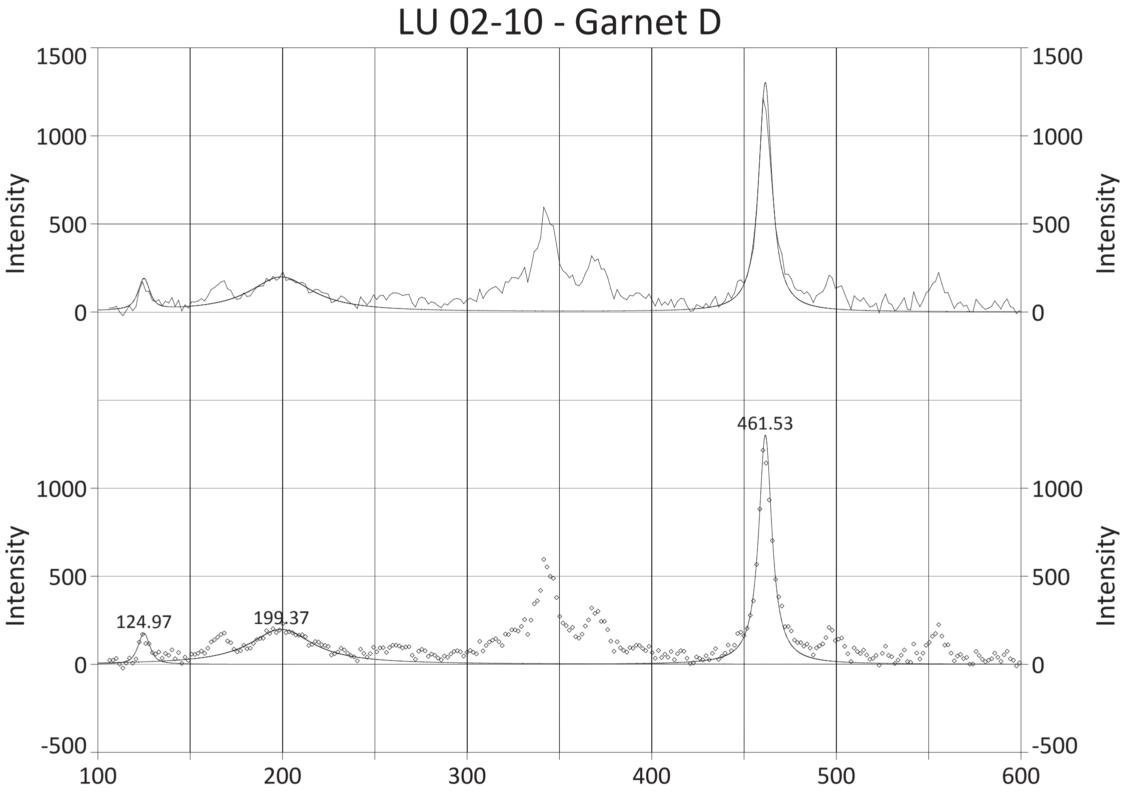
LU 02-10 - Garnet D
Intensity
1500
1000
500
0
-500
461.53
124.97
199.37
100
200
300
400
500
600

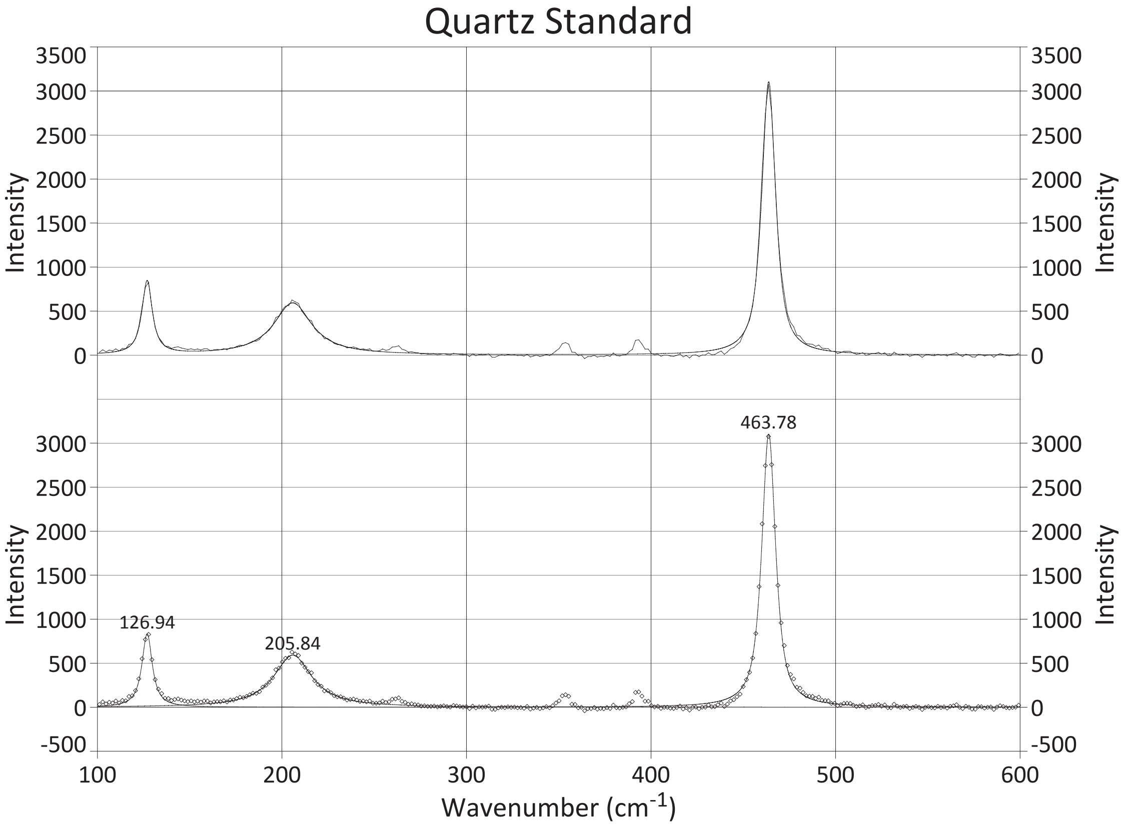
Quartz Standard
Intensity
3500
3000
2500
2000
1500
1000
500
0
-500
463.78
126.94
205.84
100
200
300
400
500
600
Wavenumber (cm^{-1})

LU 02-10

Garnet E

Locality: Purdy Hill
Collected by William Carlson

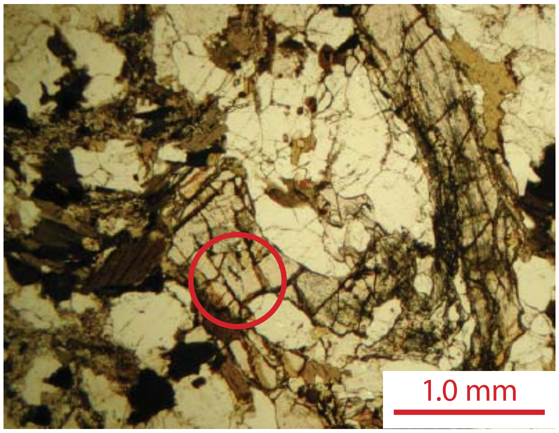

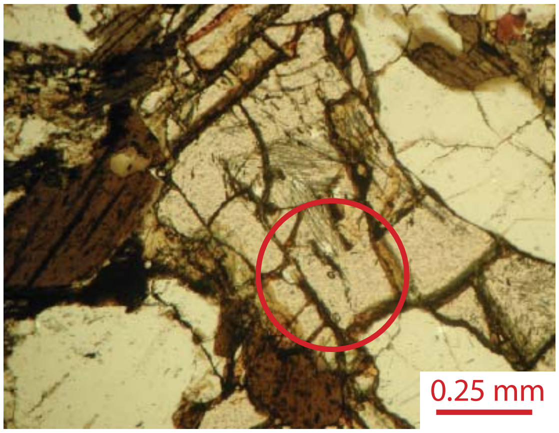

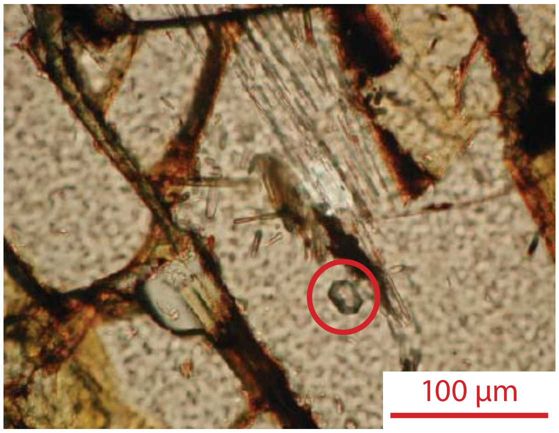

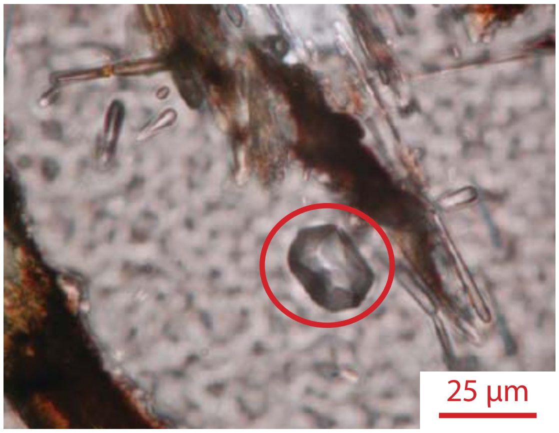

Inclusion Information

Maximum length (X-Y) (µm)	23.7
Minimum length (X-Y) (µm)	22.1
Inclusion thickness (Z) (µm)	9
Location (X-Y coordinates)	-(123.5, 5.0)
Description of shape	Hexagonal
Garnet composition	$Alm_{85.0}$, $Prp_{11.5}$, $Grs_{2.0}$, $Sps_{1.5}$

Data and Pressure Calculation Results

Depth of spectrum (µm)	-6
$\Delta\omega_1$ (cm^{-1})	-0.58
$\Delta\omega_2$ (cm^{-1})	-0.17
$P_{resid\ [\Delta\omega1]}$ (GPa)	-0.036
$P_{resid\ [\Delta\omega2]}$ (GPa)	-0.008
$P_{entrap\ [\Delta\omega1]}$ (GPa)	0.32
$P_{entrap\ [\Delta\omega2]}$ (GPa)	0.39

LU 02-10 - Garnet E

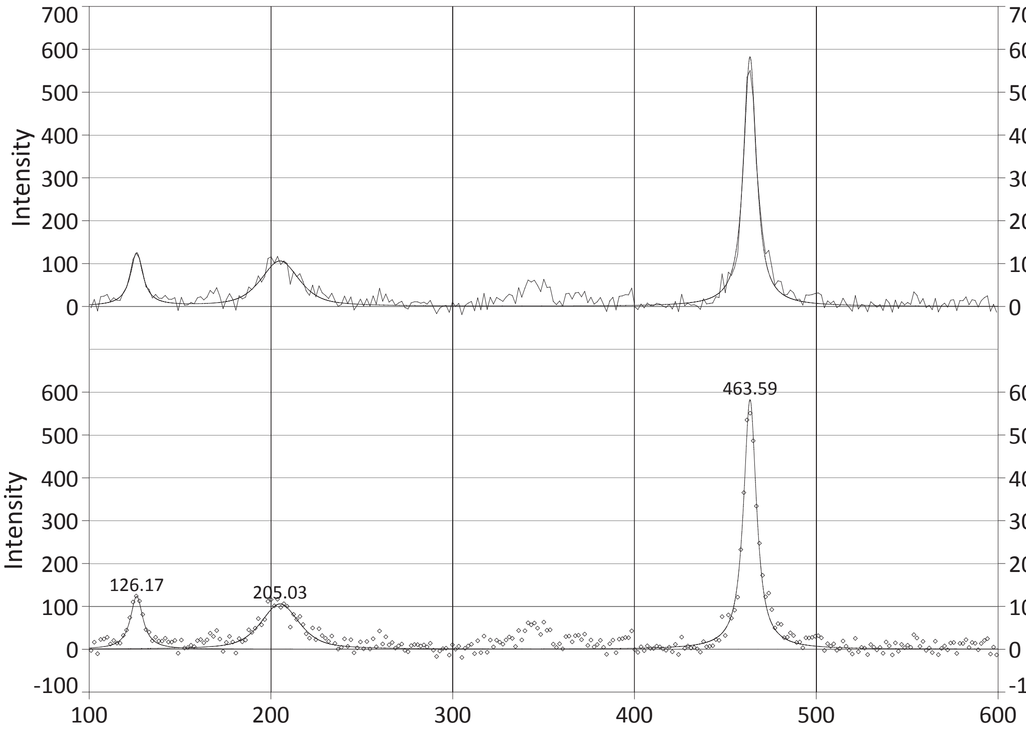

Quartz Standard

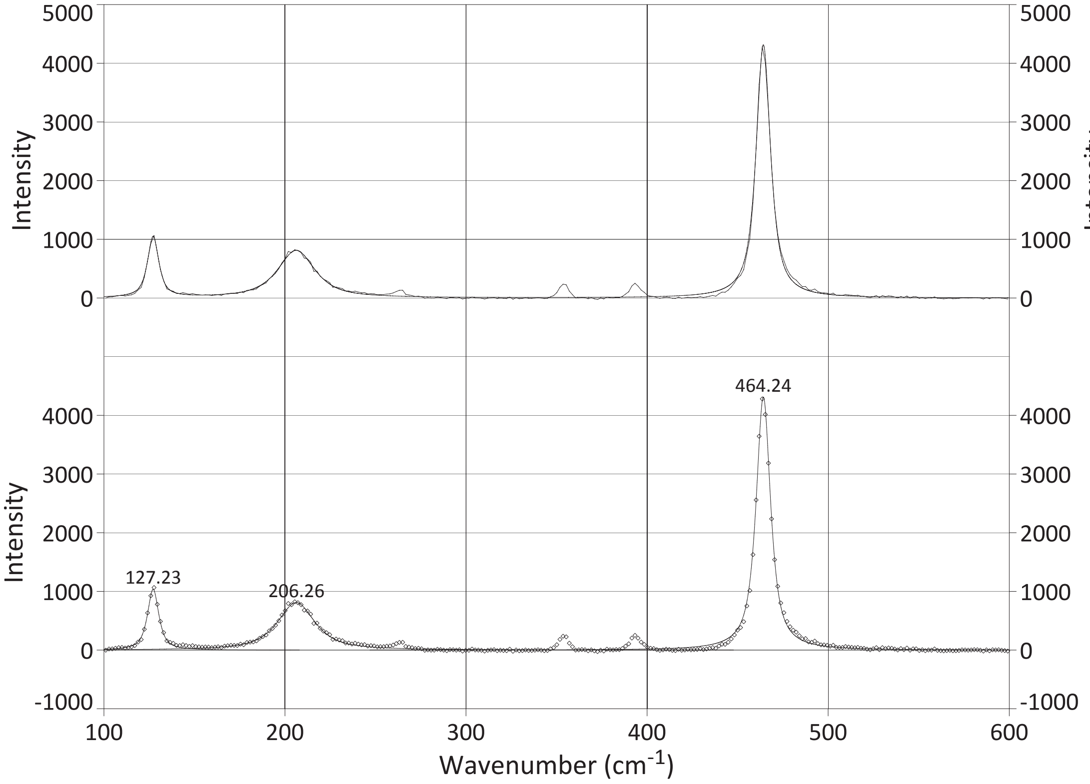

LU 02-10

Garnet G

Locality: Purdy Hill
Collected by William Carlson

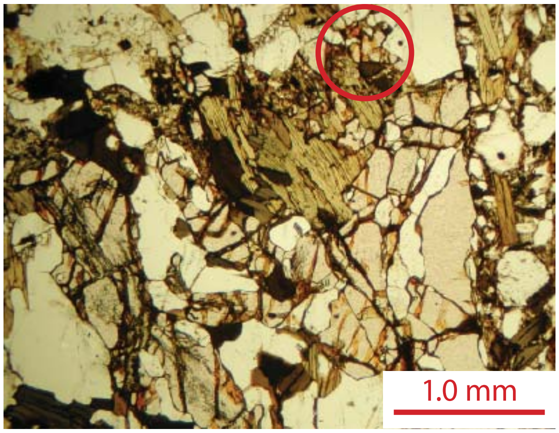

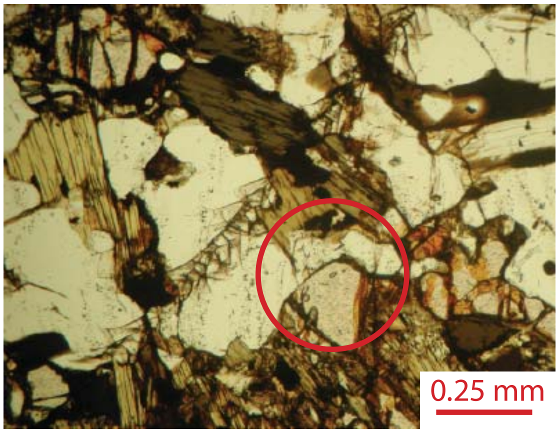

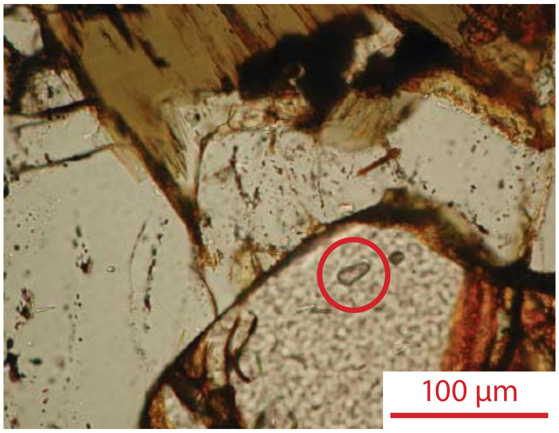

Inclusion Information

Maximum length (X-Y) (µm)	25.3
Minimum length (X-Y) (µm)	15.8
Inclusion thickness (Z) (µm)	17
Location (X-Y coordinates)	(122.5, 10.1)
Description of shape	Elongate
Garnet composition	$Alm_{83.4}$, $Prp_{12.3}$, $Grs_{2.5}$, $Sps_{1.8}$

Data and Pressure Calculation Results

Depth of spectrum (µm)	-7
$\Delta\omega_1$ (cm^{-1})	-4.85
$\Delta\omega_2$ (cm^{-1})	-5.61
$P_{resid\ [\Delta\omega1]}$ (GPa)	-0.341
$P_{resid\ [\Delta\omega2]}$ (GPa)	-0.270
$P_{entrap\ [\Delta\omega1]}$ (GPa)	-0.44
$P_{entrap\ [\Delta\omega2]}$ (GPa)	-0.27

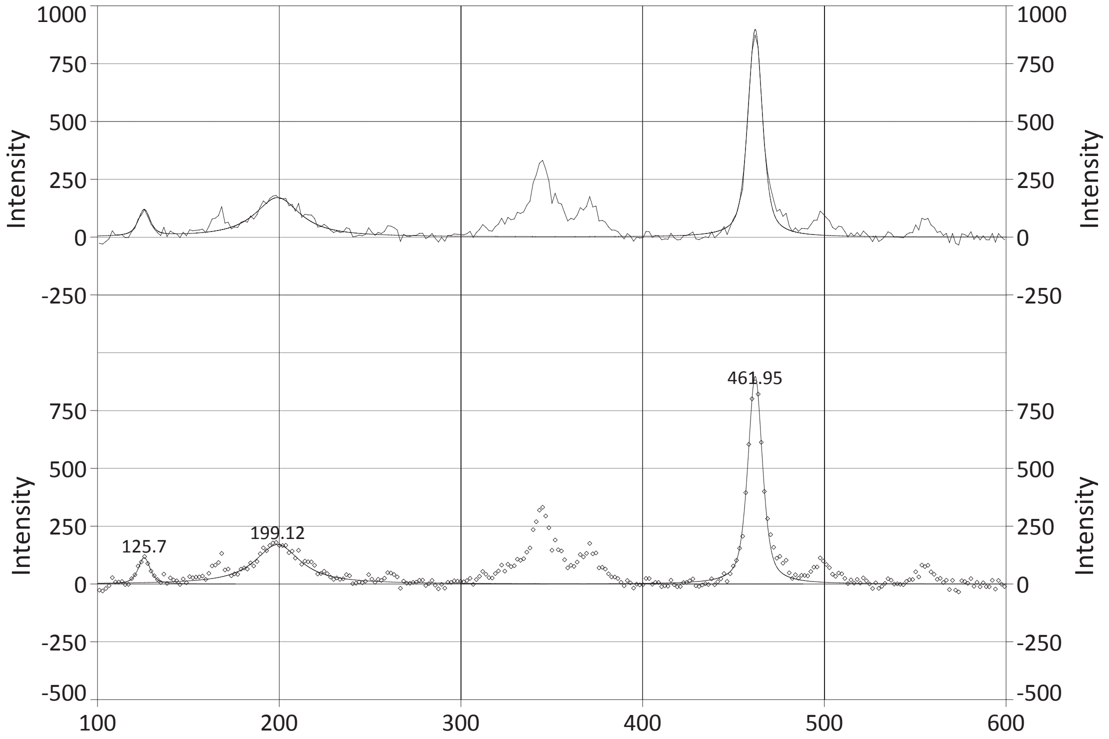
LU 02-10 - Garnet G

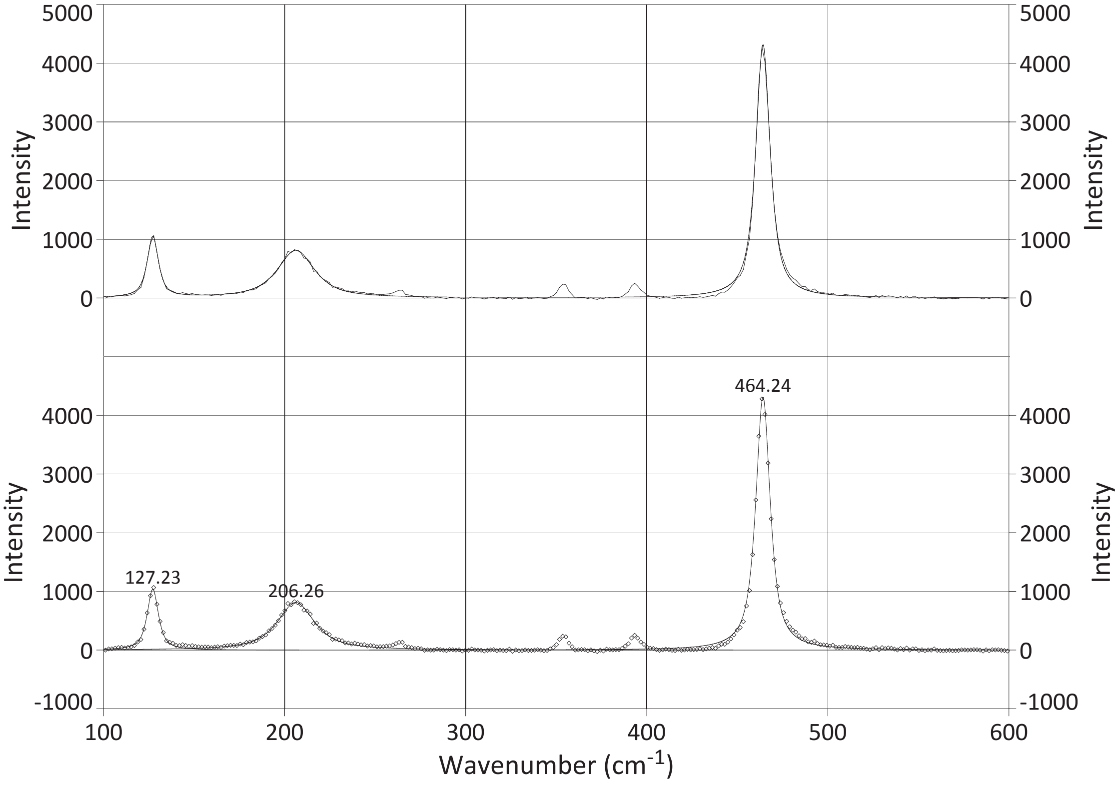
Quartz Standard

REFERENCES

Anderson, S.D., 2001, High-pressure metamorphism in the western Llano Uplift recorded by garnet-clinopyroxenites in Mason County, Texas: Unpubl. M.S. thesis, University of Texas at Austin, 221 p.

Bass, J.D., 1995, Elasticity of minerals, glasses and metals., *in* Ahrens, T.J., ed., Mineral physics and crystallography: A handbook of physical constants, Volume 2: Washington, D.C., American Geophysical Union, p. 45-63.

Barnes, V.E., 1981, Geologic Atlas of Texas—Llano Sheet: Austin, TX, University of Texas at Austin, Bureau of Economic Geology, scale 1:250,000.

Bebout, G.E., and Carlson, W.D., 1986, Fluid evolution and transport during metamorphism: Evidence from the Llano Uplift, Texas: Contributions to Mineralogy and Petrology, 92, 518-529.

Carlson, W.D., and Johnson, C.D., 1991, Coronal reaction textures in garnet amphibolites of the Llano Uplift: American Mineralogist, v. 76, p. 756-772.

Carlson, W.D., and Schwarze, E.T., 1997, Petrological significance of prograde homogenization of growth zoning in garnet: an example from the Llano Uplift: Journal of Metamorphic Geology, v. 15, p. 631-644.

Carlson, W.D., Anderson, S.D., Mosher, S., Davidow, J.S., Crawford, W.D., and Lane, E.D., 2007, High-Pressure Metamorphism in the Texas Grenville Orogen: Mesoproterozoic Subduction of the Southern Laurentian Continental Margin: International Geology Review, v. 49, p. 99-119.

Carlson, W.D., McDowell, E.A., Enami, M., Nishiyama, T., and Mouri, T., 2009, Laser Raman microspectrometry of metamorphic quartz: A simple method for comparison of metamorphic pressures—Corrigendum: American Mineralogist, v. 94, 1291-1292.

Corbin, C, 2010, Geobarometry from Raman microspectrometry of quartz inclusions in garnet: an evaluation: Unpubl. B.S. thesis, University of Texas at Austin, 110 p.

Crawford, W.D., 2004, Comparative study of eclogitic remnants from the Llano Uplift, central Texas: Unpubl. B.S. thesis, University of Texas at Austin, 36 p.

Dean, K.J., Sherman, W.F., and Wilkinson, G.R., 1982, Temperature and pressure dependence of the Raman active modes of vibration of α-quartz: Spectrochimica Acta A, v. 38, p. 1105-1108.

Enami, M., Nishiyama, T., and Mouri, T., 2007, Laser Raman microspectrometry of metamorphic quartz: A simple method for comparison of metamorphic pressures: American Mineralogist, v. 92, p. 1303-1315.

Ernst, W.G., 2001, Subduction, ultrahigh-pressure metamorphism, and regurgitation of buoyant crustal slices—implications for arcs and continental growth: Physics of the Earth and Planetary Interiors, v. 127, p. 253-275.

Ernst, W.G., and Liou, J.G., 2008, High- and ultrahigh-pressure metamorphism: Past results and future prospects: American Mineralogist, v. 93, p. 1771-1786.

Etchepare, J., Merian, M., and Smetankine, L., 1974, Vibrational normal modes of SiO_2. I. α and β quartz: Journal of Chemical Physics, v. 60, p. 1873-1876.

Fei, Y., 1995, Thermal expansion, *in* Ahrens, T.J., ed., Mineral Physics and Crystallography: A Handbook of Physical Constants, Volume 2: Washington, D.C., American Geophysical Union, p. 29-44.

Kretz, R., 1983, Symbols for rock-forming minerals: American Mineralogist, v. 68, p. 277-279.

Liu, L.-g., and Mernagh, T.P., 1992, High-pressure Raman study of the α-quartz forms of SiO_2 and GeO_2 at room temperature: High Temperatures - High Pressures, v. 24, p. 13-21.

Mosher, S., 1998, Tectonic evolution of the southern Laurentian Grenville orogenic belt: Geological Society of America Bulletin, v. 110, p. 1357-1375.

Mosher, S., Levine, J.S.F., and Carlson, W.D., 2008, Mezoproterozoic plate tectonics: A collisional model for the Grenville-aged orogenic belt in the Llano uplift, central Texas: Geology, v. 36, p. 55-58.

Mouri, T., and Enami, M., 2008, Areal extent of eclogite facies metamorphism in the Sanbagawa belt, Japan: New evidence from a Raman microprobe study of quartz residual pressure: Geology, v. 36, p. 503-506.

Peterman, E.M., Hacker, B.R., and Baxter, E.F., 2009, Phase transformations of continental crust during subduction and exhumation: Western Gneiss Region, Norway: European Journal of Mineralogy, v. 21, p. 1097-1118.

Schmidt, C., and Ziemann, M.A., 2000, In-situ Raman spectroscopy of quartz; a pressure sensor for hydrothermal diamond-anvil cell experiments at elevated temperatures: American Mineralogist, v. 85, p. 1725-1734.

Van der Molen, I., 1981, The shift of the α-β transition temperature of quartz associated with the thermal expansion of granite at high pressure: Tectonophysics, v. 73, p. 323-342.

Wang, Z., and Ji, S., 2001, Elasticity of six polycrystalline silicate garnets at pressure up to 3.0 GPa: American Mineralogist, v. 86, p. 1209-1218.

VITA

Emily Allen McDowell, a native of Dallas, Texas attended high school at the Hockaday School. During her sophomore year, she participated in a study abroad program in Zermatt, Switzerland, where she first learned about metamorphic rocks amidst the Swiss Alps. At Washington and Lee University, in Lexington, Virginia, she majored in Geology and graduated with the degree of Bachelor of Science in June, 2007. For her undergraduate Honor's thesis she studied knickpoint migration under Dr. David J. Harbor. Her studies continued with post-graduate work at the Jackson School of Geosciences at the University of Texas at Austin, focusing on metamorphic petrology under the tutelage of Dr. William D. Carlson.

Permanent Address: 4302 Enfield Drive

Dallas, Texas 75220

This thesis was typed by the author.